Modélisation de Processus Photo induits du Photosystem II

Christian Herrero Moreno

Université Paris XI

Ecole Doctorale de Chimie de Paris-Sud

THESE

Présentée en vue de l'obtention du

GRADE DE DOCTEUR DES SCIENCES DE L'UNIVERSITE PARIS XI

par

Christian Herrero Moreno

SYNTHESIS AND CHARACTERISATION OF ARTIFICIAL MIMICS OF PHOTOSYSTEM II

Soutenance prévue le 14 décembre 2007

Composition du jury

Pr Thomas Moore	*rapporteur*
Pr Rene Bensasson	*rapporteur*
Pr Ana Moore	*examinateur*
Dr William Rutherford	*examinateur*
Pr Edmond Amouyal	*examinateur*
Pr Jean Jaques Girerd	*examinateur*
Pr Ally Aukauloo	*examinateur*

Table of Contents

Acknowledgments

All together it has been two countries, three labs, several projects, about six of bosses, and lots of friends. For those which I left behind without saying goodbye, those who welcomed and helped me when I was a bit lost, and those who have, for some reason, stayed behind me all the way I'd like to express all my gratitude and wish that everyone in this world would get to meet such a gang.

Thanks

List of Figures and Tables.

Tables

List of Abbreviations

A	Acceptor
Ant	Antenna
bpy	2,2'-bipyridine
Car	Carotenoid
Cat_{ox}	Catalyst for oxidation
Cat_{red}^-	Catalyst for reduction
Chl	Chlorophyll
Co	Cobalt
D	Donor
db	Double bond
e^-	Electron
EPR	Electron paramagnetic resonance
ET	Electron transfer
eV	Electronvolt
HOMO	Highest occupied molecular orbital
ICT	Internal charge transfer
LH-I	Light-harvesting complex I
LH-II	Light-harvesting complex II
LUMO	Lowest unoccupied molecular orbital
MLCT	Metal to ligand charge transfer
Mn	Manganese
µs	Microsecond
Nm	Nanometer
ns	Nanosecond
OEC	Oxygen Evolving Complex
PCET	Proton coupled electron transfer
Pheo	Pheophytin
Pc	Phthalocyanin
ps	Picosecond
PSII	Photosystem II
P_{680}	Pigment absorbing at 680 nm
Q	Quinone
Ru	Ruthenium
Rc	Reaction centre
S	Sensitiser
SCE	Standard Calamel Electrode
$S_0 - S_4$	Storage states in the Kok cycle
Terpy	2,2':6',2''- terpyridine
THF	Tetrahydrofuran
TiO_2	Titanium dioxide
TW	Terawatt
Tyr_Z	Tyrisine Z
V	Volt

1. Abstract

In natural photosynthesis, light energy is converted into chemical energy by photosynthetic reaction centers. This energy is stored in the form of high energy substances synthesized in the reductive branch of the photosynthetic process. The electrons needed for these processes are furnished by water upon its oxidation by the Oxygen Evolving Complex (OEC) in PSII.

Artificial photosynthesis aims to replicate the reactions that take place in natural organisms in order to i) gain a better understanding of the chemical processes taking place in the natural systems, and ii) strive towards the harnessing of sunlight in order to have access to clean, sustainable fuels. Processes undergone in nature such as light capture, energy transfer, electron transfer, charge separation, activation of catalyst, and reaction at the catalytic site must be accomplished within the framework of artificial systems.

With these concepts in mind we have designed, synthesized and characterized molecules that mimic the reactions performed by antennas and reaction centers present in Photosystem II. These molecules are able to undergo light-induced charge separation, electron transfer, and accumulation of oxidizing/reducing equivalents that mimic the processes occurring in natural systems. The artificial anntenas are composed of carotenoid and phthalocyanin groups. These molecules show large absoption profiles with high extinction coefficients, and are capable of ultra-fast energy transfer processes which lead up to charge separation states. Varying the conjugation length of the carotenoid molecules from 9 double bonds to 11 double bonds, we can show how these molecules may act as energy donors as well as energy dissipators, a process akin to the Non Photochemical Quenching (NPQ) processes which happen during the xanthophyll cycle. The donor side mimics of Photosystem II have also been studied. These supramolecular systems contain a photoactive component covalently linked through a spacer to a cavity where a

metal ion or cluster is located. The photosensitizer used is a $[Ru(bpy)_3]^{2+}$ (bpy = 2,2'-bipyridine) analogue, a counterpart to P_{680}, which absorbs light in the visible region and triggers an electron transfer process. The resulting Ru^{III} species has a reversible oxidation potential of 1.30 V vs. SCE, similar to that of P_{680} (1.25 V vs NHE),[17,18] and is, in theory, capable of oxidizing a Manganese cluster and an electron source. Among the molecules mimicking the donor side of PSII we have synthesized ruthenium-phenol pairs, as well as bimetallic Ruthenium-Manganese systems. Among the latter we have studied those with terpyridine coordination cavities since Mn-di-μ-oxo-Mn dimers of this kind have been reported to catalyze the oxidation of water into molecular oxygen. Other catalytic groups such as salens and salophens have also been studied. These have been reported to perform the two electron oxidation of organic substrates following the same oxygen atom transfer mechanism as the one thought to be responsible for the oxidation of water, and could therefore be useful in achieving our goal. Following the work on synthesis and characterization of molecules capable of harnessing light and using it to drive reduction/oxidation reactions will be presented.

1. Résumé

La photosynthèse est un processus biologique naturel qui convertit l'énergie lumineuse en énergie chimique par l'action de centres réactionnels photosynthétiques. L'énergie convertie est stockée sous forme de produits de haute énergie synthétisés par la branche réductive du processus photosynthétique. Les électrons nécessaires à ces réactions sont fournis par des molécules d'eau lors de leur oxydation par le centre de dégagement de l'oxygène (Oxygen Evolving Complex: OEC) pour le système de photosynthèse II (PSII). La photosynthèse artificielle cherche à

reproduire les réactions qui se produisent dans les organismes naturels afin de i) de mieux comprendre les processus chimiques qui se déroulent dans les systèmes naturels, et ii) de parvenir à exploiter l'énergie solaire pour le développement de carburants propres et renouvelables. Chaque étape qui survient dans le processus de photosynthèse naturelle, telle que la capture de lumière, le transfert d'énergie, le transfert d'électron, la séparation de charge, l'activation du catalyseur et la réaction catalytique doit se produire au sein du système artificiel. La photosynthèse artificielle cherche à reproduire les réactions qui se produisent dans les organismes naturels afin de i) de mieux comprendre les processus chimiques qui se déroulent dans les systèmes naturels, et ii) de parvenir à exploiter l'énergie solaire pour le développement de carburants propres et renouvelables. Chaque étape qui survient dans le processus de photosynthèse naturelle, telle que la capture de lumière, le transfert d'énergie, le transfert d'électron, la séparation de charge, l'activation du catalyseur et la réaction catalytique doit se produire au sein du système artificiel. Avec ces concepts en vue, nous avons conçu, synthétisé et caractérisé des molécules qui imitent les réactions réalisées par les antennes et les centres réactionnels présents dans le photosystème II. Ces molécules sont capables de reproduire la séparation de charges induite par la lumière, le transfert d'électrons et l'accumulation d'équivalents oxydo-réducteurs observés pendant la photosynthèse naturelle. Les antennes artificielles se constituent de caroténoïdes et phthalocyanines. Ces molécules présentent des profiles d'absorption large avec des coefficients d'extinction élevés, et sont capables de supporter des transferts d'énergie ultra rapides qui permettent l'état de séparation de charges. En faisant varier la longueur de la chaine conjuguée des caroténoïdes de neuf à onze liaisons doubles, nous avons pu mettre en évidence comment ces molécules peuvent agir aussi bien comme donneurs que comme agents dissipateurs d'énergie, effet caractéristique qui s'apparente au processus de trempe non-photochimique (Non Photochemical Quenching: NPQ) qui se produit dans le cycle

de la zéaxanthine. Les mimiques des agents donneurs du photosystème II ont aussi été étudiées. Ces systèmes supramoléculaires contiennent une partie photoactive liée de façon covalente par un intermédiaire à une cavité contenant un ion ou un agrégat d'ions métalliques. La photosensibilisateur utilisé est un complexe du ruthénium $[Ru(bipy)_3]^{2+}$ (bpy = 2,2'-bipyridine), homologue du P_{680}, qui absorbe la lumière dans le spectre visible et déclenche le transfert d'électron. Les espèces Ru^{III} résultantes ont un potentiel d'oxydation réversible de 1.3 V vs SCE, comparables à celui de P_{680} (1.25 V vs NHE) et présentent donc la possibilité d'oxyder à la fois un complexe manganèse ainsi qu'une source d'électron. Concernant les molécules imitant le coté donneur du PSII, nous avons synthétisé des paires ruthénium-phénol, ainsi que des systèmes ruthénium-manganèse bimétalliques. Parmi ces dernières, nous avons étudié celles présentant des cavités de coordination constituées de terpyridines, vu qu'il a déjà été montré que les dimères Mn-di-μ-oxo-Mn de ce type peuvent catalyser l'oxydation de l'eau en oxygène moléculaire. Des salènes et salophènes ont aussi été examinés étant donné que de tels groupes peuvent accomplir l'oxydation à deux électrons de substrats organique. Dans la littérature, ces réactions sont toutes conduites par l'action d'oxydants chimiques externes, tandis que nous avons pour but d'utiliser des espèces oxydantes induites par l'action de la lumière.

2. Introduction

One of the most pressing challenges society is facing today is the transition to a new energy scenario. Increases in world population and the rise of emerging economies have projected an increase in energy consumption from 13 TW today to 30 TW by 2050.[1] If we couple the fact that 86 % of this energy comes from fossil fuels to the fact that CO_2 levels are the highest they have

been for the past 650 000 years, it is clear that the burn rate that will be needed in 40 year's time is unacceptable. In order to fill the gap of needed energy we must look for complementary sources that will be reliable enough to fill in the huge gap of demand and sustainable enough so their use will not be deleterious to life on earth. Amongst the possible alternate energy sources, solar power presents itself as the most promising source of renewable energy available. The goal of artificial photosynthesis is to harness this energy to drive the production of high energy chemicals from low energy source compounds.

Nature has given us the guidelines for such a process. During photosynthesis, absorption of light by phototrophic organisms initiates a series of energy and electron transfer processes that conclude with the oxidation of water (eq. 1) to reducing equivalents that can then drive the reduction of CO_2 into higher carbohydrates (eq. 2).

$$2\ H_2O + 4\ h\nu \rightarrow O_2 + 4\ H^+ + 4\ e^- \qquad (1)$$

$$nCO_2 + 2n\ e^- + 2n\ H^+ \rightarrow (CH_2O)_n \qquad (2)$$

$$2\ H^+ + 2\ e^- \rightarrow H_2 \qquad (3)$$

Artificial photosynthesis, thus, aims to imitate the above mentioned processes of light absorption, catalysis, and energy conversion. Photo-driven water oxidation, thus, would act as a source of electrons and protons that could be used to drive the production of high energetic fuels such as H_2 (eq.3), or reduce carbon dioxide to valuable organic compounds (eq.2). Over the last two decades several advances have been made in this field. Examples of light induced long-lived charge separated states,[2-5] electron transfer from chromophores to catalytic sites[6,7] and water oxidation catalysis by chemical or electrochemical means[8-15] have been reported in the literature. Nevertheless, little success has been achieved when trying to combine all these required processes into one complex. In the following, the work done up to date in our laboratory spanning from artificial antennas to light driven electron transfer systems will be presented.

2.1. Natural photosynthesis

Life on earth can be thought of being, almost entirely solar powered. Oxygenic photosynthetic organisms translate this kind of energy into chemical energy in the form of carbohydrates and oxygen, with the former serving as a source of high energy electrons and the latter as a low energy destination. Photosynthesis begins with the absorption of light. In purple bacteria this process is performed by light-harvesting complexes which are intricate assemblies of low molecular weight proteins and pigments housed within the membrane proteins. These moieties mainly include chlorophylls, quinones and carotenoids.

Most purple bacteria have two types of light-harvesting complexes, designated LH-I and LH-II (Fig 1). LH-I complexes are closely associated with the reaction center and form a so-called 'core' complex, while LH-II complexes are peripheral to this core. When light is absorbed by the peripheral antenna LH-II complexes, energy is transferred to LH-I, which then passes it onto the reaction center, in which a redox reaction causes charge separation across the membrane. All these components interact by three basic photochemical processes:

1) singlet-singlet energy transfer, as is the case in antenna systems consisting of chlorophylls, and carotenoids, which collect light and conduct excitation energy to the reaction center,

$$\mathrm{Car} + h\nu \rightarrow {}^{1}\mathrm{Car} \qquad (4)$$

$${}^{1}\mathrm{Car} + \mathrm{Chl} \rightarrow \mathrm{Car} + {}^{1}\mathrm{Chl} \qquad (5)$$

2) triplet-triplet energy transfer, as in the cases of formation of highly reactive singlet oxygen by triplet chlorophylls, and the consequent quenching of these dangerous species by carotenoids,

$${}^{3}\mathrm{Chl} + \mathrm{Car} \rightarrow \mathrm{Chl} + {}^{3}\mathrm{Car} \qquad (6)$$

$${}^{3}\mathrm{Chl} + {}^{3}\mathrm{O_2} \rightarrow \mathrm{Chl} + {}^{1}\mathrm{O_2} \qquad (7)$$

$$^1O_2 + Car \rightarrow {}^3O_2 + {}^3Car \qquad (8)$$

3) Photo-initiated electron transfer, involving chlorophylls and quinones which transform excitation energy into chemical potential in the form of long-lived, trans-membrane charge separation.

$$^1Ant + D\text{-}A \rightarrow Ant + {}^1D\text{-}A \rightarrow D^+\text{-}A^- \qquad (9)$$

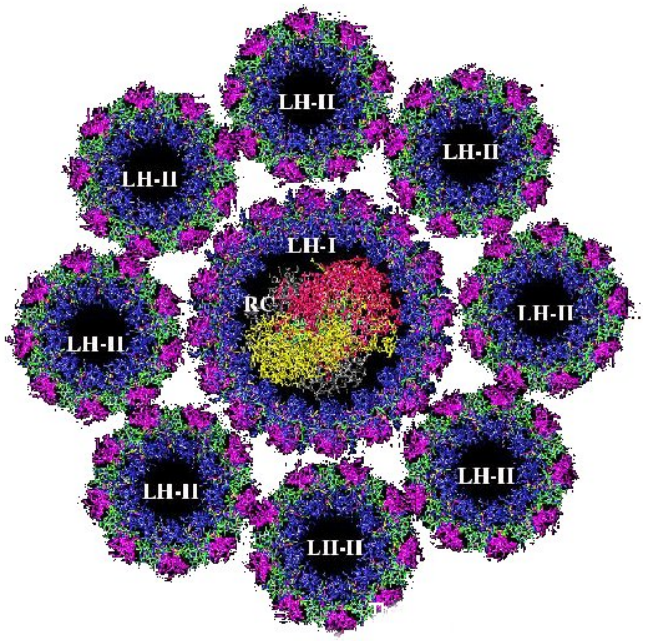

Figure 1: Antenna and reaction center assembly.

The core complex of PS-II, the reaction centre (RC), contains in itself six chlorophyll *a*'s and 2 β-carotene pigments[2,16]. When light is collected by the reaction centre, or the surrounding antennae systems, the absorbed photon energy is funneled through a series of energy transfer steps to the primary electron donor P_{680} which is probably made up by the four excitonically coupled chlorophyll molecules of the PSII core (P_{D1}, P_{D2}, Chl_{D1}, Chl_{D2} in Fig. 2).

This water oxidizing enzyme is a membrane-spanning, pigment-containing protein made up of several subunits. On one side of the membrane, it performs the two electron reduction of

plastoquinone to plastoquinol ($PQ + 2e^- + 2H^+ \rightarrow PQH_2$) while on the other side it catalyses the four electron oxidation of water, producing molecular oxygen and protons as by products ($2H_2O \rightarrow 4e^- + 4H^+ + O_2$). The enzyme is thought of as being composed of i) a photochemical part which upon light absorption, is capable of forming and stabilizing a large charge separated state, thus forming a reductant and a oxidant and ii) a catalytic device made up by a cluster of manganese ions and a redox active tyrosine residue capable of storing oxidizing equivalents, in order to split water.

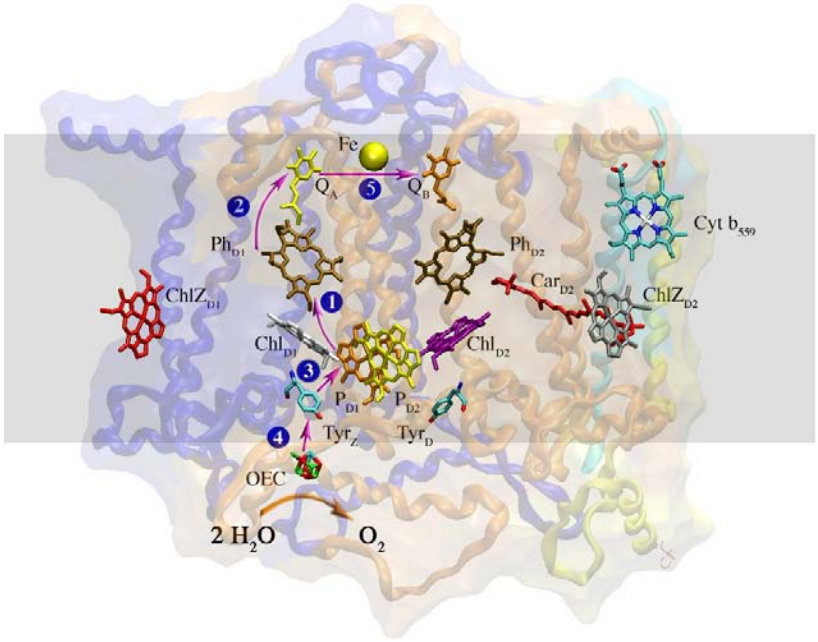

Figure 2: Cofactors of electron transport chain in PSII.

Upon absorption of harnessed light energy, the sequence of electron transfer reactions can be described as follows:

1. The resulting excited P_{680} is capable of reducing a nearby pheophytin to produce the initial charge separation (step 1, figure 2). This yields a cation radical P_{680}^+, and a pheophytin anion radical ($Pheo^-$). P_{680}^+ is the most oxidizing species known in biology with a potential around 1.25 V vs NHE.[17,18]

2. The pheophytin anion radical donates an electron to a quinone (Q_A). By this time (200 ps) the electron is 26 Å away from the oxidized P_{680}, thereby stabilizing the charge separated state (step 2).
3. The highly oxidizing P_{680}^+ extracts an electron from a nearby tyrosine residue (Tyr_Z) (Step 3). Concomitant with this oxidation, proton loss from the tyrosine's phenolic hydroxyl group occurs and the neutral tyrosyl radical is formed.
4. The neutral tyrosyl radical oxidizes the Mn ions of the oxygen evolving complex (designated OEC in Fig. 1).
5. The semiquinone anion formed is further stabilized by a lateral electron transfer step to a second quinone, Q_B.

The resulting state is stable for seconds and contains a semiquinone (Q_B^-) and a high valence form of the Mn cluster (S_1). In order to complete the cycle, the semiquinone will need a second reduction process while the manganese cluster will need three additional ones, with each one resulting in an increase in valence (S_2 to S_0) and the final release of oxygen.

The reaction centre can thus be thought of as a device for generating positive charge equivalents, at the rate of one equivalent per photon. By contrast, as stated above, oxidation of water is a four electron process, and thus this one electron process must be coupled to a multi-electron reaction.

2.2. Water oxidizing complex

In nature, PSII is assembled in the membrane without the presence of the manganese cluster. Subsequent formation of the OEC requires of Mn^{II}, Ca^{2+}, Cl^- as "reagents",[19,20] light as the energy source, and Tyr_Z as the oxidant needed to bring the cluster into its high oxidation states. In its functioning state, the OEC is composed of four high valence manganese ions, calcium, and

chloride. The structure of the manganese cluster is not clear yet, but it is responsible for charge accumulation and substrate binding. Each absorption of a photon is corresponded by an increase in oxidation state of the cluster. This mechanism must also include the removal of four protons and is known as the Kok cycle, where each step, S_0 (most reduced) through S_4 (most oxidized), denotes a storage state of the system. Calcium is required for water oxidation, and its removal from the OEC inhibits the formation of the S_3 state. It has been postulated that calcium might be a substrate for water activation. The function of chloride is less understood, it binds near the water splitting site and its removal slows down the S_3 to S_4 to S_0 water splitting step.

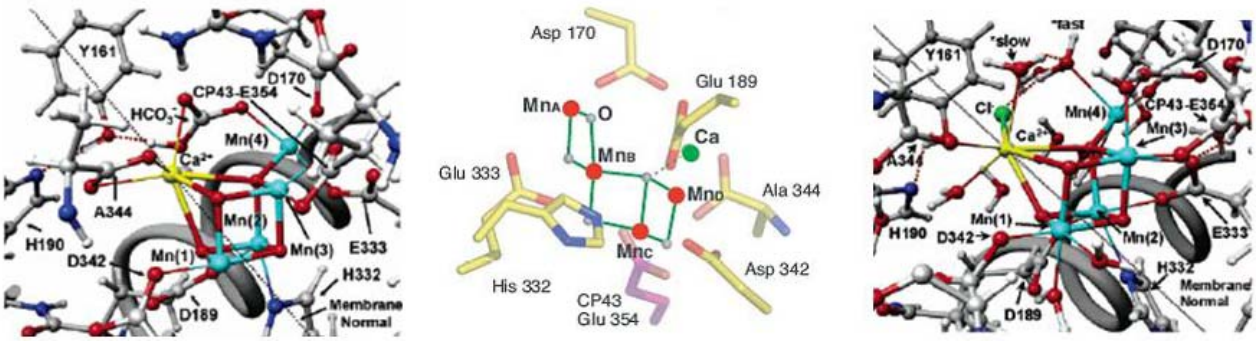

Figure 3: Different models proposed for the structure of the OEC from the groups of Barber[21] (left), Yachandra[22] (middle), Batista[23] (right).

The mechanism for the removal of four electrons and four protons from two substrate water molecules is still subject to speculation.[24] While the electronic structure of the different S-states, substrate binding, calcium/chloride binding, and function of amino acid side chains are still a matter of debate, it is widely admitted that i) the two substrate waters of the OEC are bound, one to Ca^{2+} and the other to one of the Mn ions, ii) the water-bearing Mn ion undergoes oxidation up to the formal +5 oxidation state in the S_4 state, iii) the Mn bound water is deprotonated twice

after the S_2 state, and iv) that the resulting Mn^V=O species in the S_4 state undergoes a nucleophilic attack by the calcium bound water producing dioxygen.[19,25]

3. Artificial photosynthetic devices

Nature thus, has provided us with the inspiration and the basic concepts that should be followed in order to achieve an artificial photosynthetic device. Processes such as light capture, efficient energy transfer coupled to electron transfer, generation of charge separated states, and finally catalytic reaction processes must happen in a concerted fashion. Therefore, in order to achieve these processes when constructing an artificial system one must attend to some basic principles such as architecture of the system, ability to undergo the different and successive processes required for activation (light absorption, electron transfer, charge compensation, charge storage) and use of a suitable catalyst.

The most basic device that could parallel these processes would be composed of a photosensitiser linked to an electron donor on one side and to an electron acceptor on another side. Such a triad would be designed to undergo the following steps:

1. Light absorption by a chromophore (S), or an antenna system followed by energy transfer to the chromophore (S*). $D - S - A \rightarrow D - S^* - A$

2. Quenching of excited chromophore states by e^- transfer $D - S^* - A \rightarrow D - S^+ - A^-$ or, $D - S^* - A \rightarrow D^+ - S^- - A$

3. Electron transfer from donor or sensitizer to form the charge separated state. $D - S^+ - A^-$ (or $D^+ - S^- - A$) $\rightarrow D^+ - S - A^-$.

Studies on triads have been published which show long lifetimes for a charge separated state and multi-electron cascades have been observed.[26,27] These examples show that transformation of

light energy into chemical energy in the form of a charge separated state can be achieved. The next step towards water oxidation would require the coupling of pertinent reduction and oxidation catalysts to a triad. The basic requirements for such a particular photo-catalytic system to work are the following: (i) activation by sequential $1e^-$ transfers, including directionality of these processes for each individual charge separation step (ii) resulting redox potentials energetic enough to carry out the final reactions (iii) reaction rates fast enough so as to make photon absorption the rate limiting step.

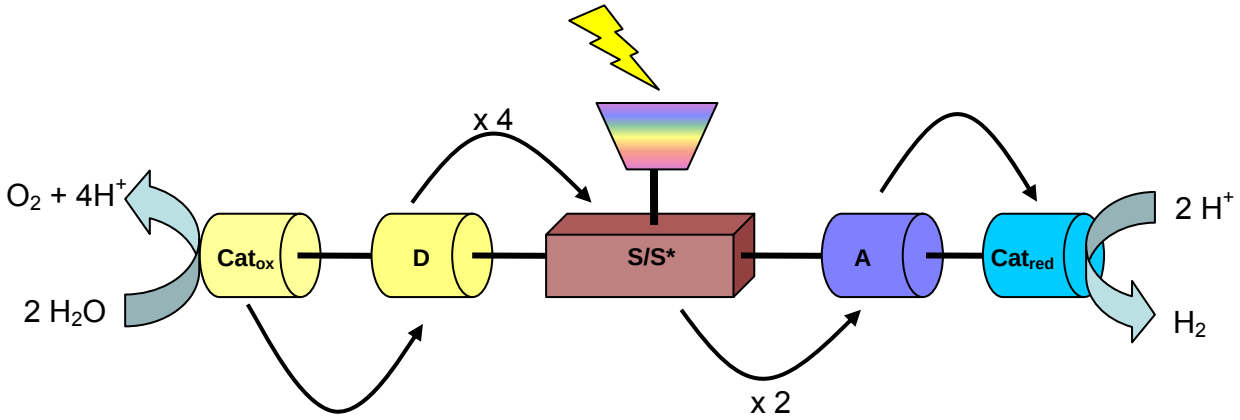

Figure 4: Model of a light absorbing triad for oxidation/reduction processes.

In any photo-activated process, electron transfer quenching of the chromophore, whether oxidative or reductive is always in competition with its excited state decay. It is therefore very important to be able to maximize excited lifetimes and tune electronic couplings in order for these processes to happen. Once the electron transfer has happened and the charge separated state has formed $–D^+ – C – A^–$, electron transfer activation to the catalyst must compete with charge recombination between D^+ and A^- to form the activated species $Cat_{ox}^+ – D – C – A – Cat_{red}^-$. For a second e^- transfer, absorption of a photon must be followed by all the above processes with the added difficulty of higher driving forces for electron transfer, and additional recombination steps.

The $4e^-$ process involving water oxidation adds even more competitive pathways which make the process more difficult.

In order to prevent large increases in activation energies due to charge accumulation, alternatives for compensation should be included in the device. Activation of substrate waters is achieved by coupling proton transfer reactions to multi-electron transfer chemistry. Sequential one electron oxidations of the manganese cluster are matched to Mn-aqua $\rightarrow$ hydroxy $\rightarrow$ oxo changes in the substrate by the simultaneous release of electrons and protons. In this manner the overall charge of the complex stays fairly constant during the S_0 to S_4 states and P_{680}^+ is capable of inducing the four oxidation processes.

The last point to mention is the final formation of the O–O bond. In nature this step is believed to be via a nucleophilic attack of a hydroxide bound to a Ca^{2+} on an electrophilic oxygen from a Mn-oxo bond. The role of Ca^{2+} is believed to decrease the pK_a of the water molecule, producing a nucleophilic hydroxide that can attack the electrophilic oxo group bound to the manganese ion. Following this example, different models have and could be tried in artificial systems. Different metal-oxo bonds have been studied and are reported to act catalytically in the oxidation of water,[60, 68-73] and the epoxidation of olefins.[28] Also, activation of the second water molecule could be accomplished by inserting coordinating basic groups which could lower the pK_a of the water molecule and therefore increase its nucleophilicity.

The overall catalytic system could also be tuned by addition of the pertinent electron withdrawing groups in order to make its high oxidation state neither too reactive so as to undergo self-oxidation, nor too stable so that the reactivity will be hindered.

The architecture of the overall system could be changed from solution based to solid state. A system of this kind would result in a more asymmetric system which could be envisaged to help in the overall directionality of the different processes, something akin to the natural enzyme.

In such systems, the oxidation catalyst (Cat_{ox}) would be linked by a photosensitiser to an anode and the reduction catalyst (Cat_{red}) grafted to a cathode[29] (see Figure 2). Electrons from the oxidation half-cell would be transferred to the reduction half-cell, while protons would move in the same direction through a selective membrane. Recent advances in the field of large bandgap semiconductor surfaces such as TiO_2, SnO_2, or ZnO have opened the way for new approaches in light sensitized devices. Amongst the advantages of Graetzel cell type devices are, i) very fast electron injection rates from the excited state of attached chromophores into the conduction band[30] of the semiconductor, contributing to the necessary control of directionality of electron transfer, ii) high surface areas up to 1000 times more than those offered by monolayers, iii) efficiency of electron collection in external circuits, iv) ability to tune the electron acceptor states in order to maximize light to electrical energy conversion and, v) high transparency in the visible and infrared regions.

Examples of such devices have been developed with porphyrin-sensitised photoanodes,[31,32] which drive oxidation of sugar via a natural enzyme, delivering sufficient reducing potential for H_2 production at a platinum electrode,[33] as well as ruthenium based oxidation of alcohols.[34]

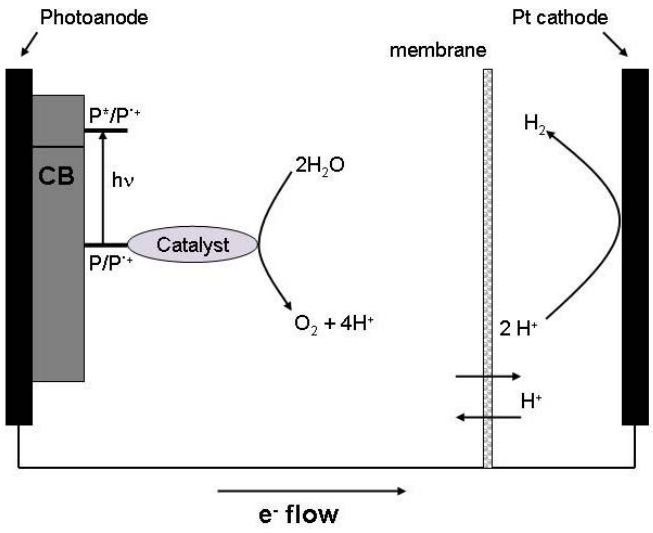

Figure 5: Diagram of a water splitting photochemical cell.

The following chapters present the work carried out in relation to the various components used in artificial photosynthesis devices: antennas, photoactive chromophores, and donor groups including manganese complexes.

3.1. Antennas

The role of an antenna is to increase the absorption cross section of the complex and, through a series of energy transfer steps, funnel that energy to a reaction centre where a charge separated state is formed. The solar spectrum has a maximum intensity just below 500 nm[35] and extends well into the infrared region where a photon with λ = 1000 nm still has 1.2 eV energy. In nature, the efficient geometrical arrangement of the pigments is related to the tertiary structure of the PS-II antenna subunits (light-harvesting complexes).[36] In artificial photosynthesis this spatial arrangement is not easily achievable. The distance between the pigments to be used, their respective angle, and electronic coupling, must be dictated by the covalent bonds that unite them. Two mechanisms are responsible for energy transfer processes. Förster energy transfer occurs in

cases where the distance between the chromophores is larger than their transition dipole strength, the dipoles have sufficient strength, and the lifetime of the emitting chromophore is sufficiently long. Dexter energy transfer takes place when the chromophores are brought into van der Waals contact and there is orbital overlap between them. Systems such as carotenoid-tetrapyrrole triad[37] and dyads,[38,39] and (Phenylethynyl) anthracene-porphyrin-fullerene heptads[40] have been shown to combine large absorption spectral range (350 nm-700 nm), high extinction coefficients (10^5 M^{-1} cm^{-1}), and quantum yields for energy transfer close to 100%.[41] Different approaches, such as the use of dendrimers[42] or self assembled π-stacked arrays[43,44] have also been reported in the literature.

Work on artificial antennas in the laboratory was carried out by linking carotenoids with phthalocyanins. These pigments are porphyrin-like compounds with extended π-systems and strong absorption in the red to infrared region of the spectrum.

Carotenoids play several roles in the photosynthetic process and are also crucial to the photoprotection of the photosynthetic membranes. As accessory light-harvesting pigments, carotenoids (Car) are found in the chlorophyll-binding antenna proteins of photosynthetic organisms where they absorb light in the blue-green spectral region and efficiently transfer energy to nearby chlorophylls (Chl), as depicted in eqs 4 and 5.

It is well established that carotenoids have two low-lying excited singlet states from which energy transfer to chlorophylls (eq. 5) could occur. Two of the possible singlet-singlet energy transfer pathways are shown schematically in figure 6. Following absorption of light and internal conversion from the S_2 ($1^1B_u^+$) state, the S_1 ($2^1A_g^-$) state of the carotenoid is populated. Energy transfer from this state to the Q_y (S_1) level of the chlorophyll is one possible pathway. Energy

transfer from the S_2 state of the carotenoid to the Q_x (S_2) state of the chlorophyll, in competition with the ultrafast internal conversion from the S_2 to S_1 state of the carotenoid, is another one.

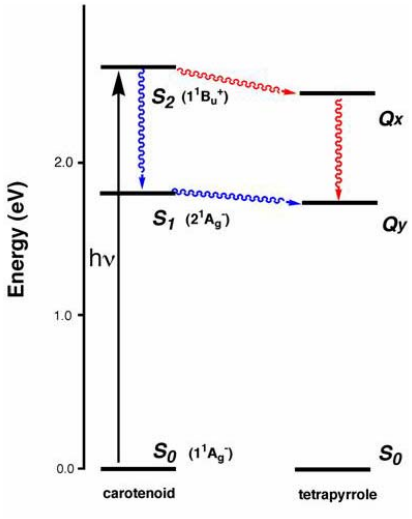

Figure 6: Pathways for energy transfer from a carotenoid to a phthalocyanine.

The extremely short lifetime of the S_2 state of the carotenoid (~ 200 fs) does not exclude this second possible pathway. Indeed, spectroscopic studies on the sub-picosecond time scale of some antenna protein complexes of photosynthetic organisms suggest that some energy transfer to the chlorophyll or bacteriochlorophyll energy acceptors occurs from the carotenoid S_2 state.[45,46] However, the complexity of these natural antenna systems containing multiple chromophores, compounded with the ultrafast time scale, inevitably makes detailed pathway assignments very difficult. Nevertheless, recent results indicate that in some antenna complexes energy transfer proceeds predominantly from the carotenoid S_2 state, rather than from the lower energy excited S_1 state as predicted by Kasha's Rule. Mimicking these unusual photophysics in simple, well defined model systems offers the opportunity to study the energy transfer pathways and to explore, and perhaps control, the nature of the carotenoid-tetrapyrrole electronic interactions affecting the rates and efficiency of energy transfer. Compounds **1** and **2** are examples of

molecular dyads which were designed to help understand the mechanism(s) of the carotenoid to chlorophyll singlet-singlet energy transfer processes in natural systems.

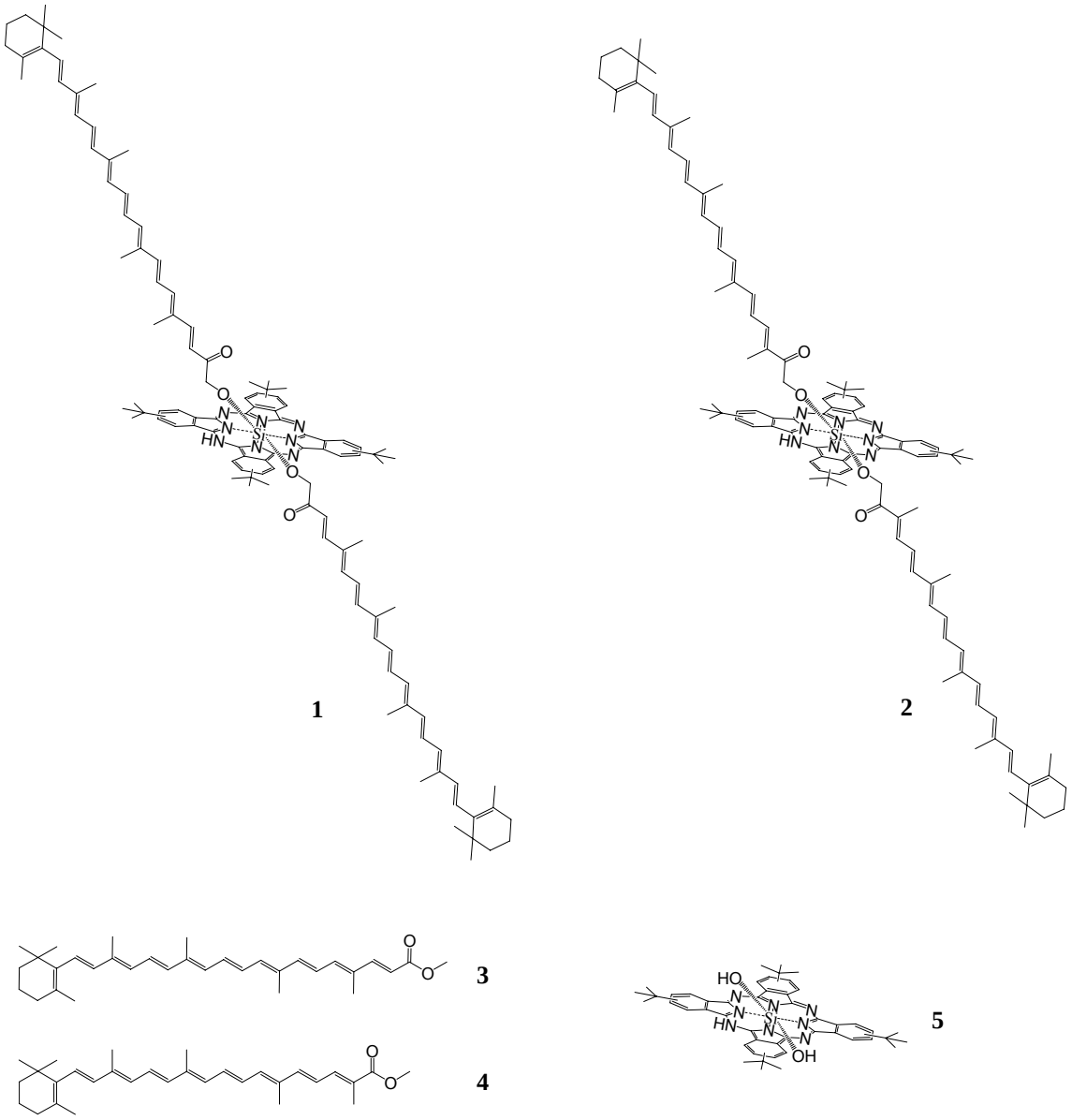

Figure 7: Structures of carotenoid-phthalocyanin triads and model compounds.

Synthesis of triad **1** was accomplished by coupling of silicon-tetra-tert-butyl-phthalocyanin **5** to the acid chloride derivative of carotenoid **3**. This carotenoid was formed by reaction of the

commercially available, 8'-apo-carotenal with phosphonium salt via a Wittig reaction in order to obtain the 10 double bond (db) ester carotenoid, which was further oxidized to its carboxylic acid analogue, and then prepared into its acid chloride synthon.

These molecules show very broad spectral absorptions spanning most of the visible region (300-700 nm). Though their chemical structure is basically the same, and differs only in the extra double bond in each of the carotenoids, their behavior is strikingly different **(**Figure 9). Triad **2** exhibits near complete light harvesting efficiency (92%) from the carotenoid to the phthalocyanin through three of the available electronic states of the carotenoid, namely S_2, S_1, and S* as calculated from the increase in Qy bleaching of Pc.

Triad **1** performs singlet energy transfer at a much lower yield (30%), and it is only the S_2 state which is active in this process, while the S_1 shows very little energy transfer, and there is no evidence for energy transfer from S*. In polar solvents, both triads **1** and **2** exhibit light induced electron transfer from either of the carotenoid molecules to the excited singlet phthalocyanin species with a rise time of about 2 ps. Charge recombination to the singlet ground state occurs in 10 ps for triad **2** and 17 ps for triad **1**.

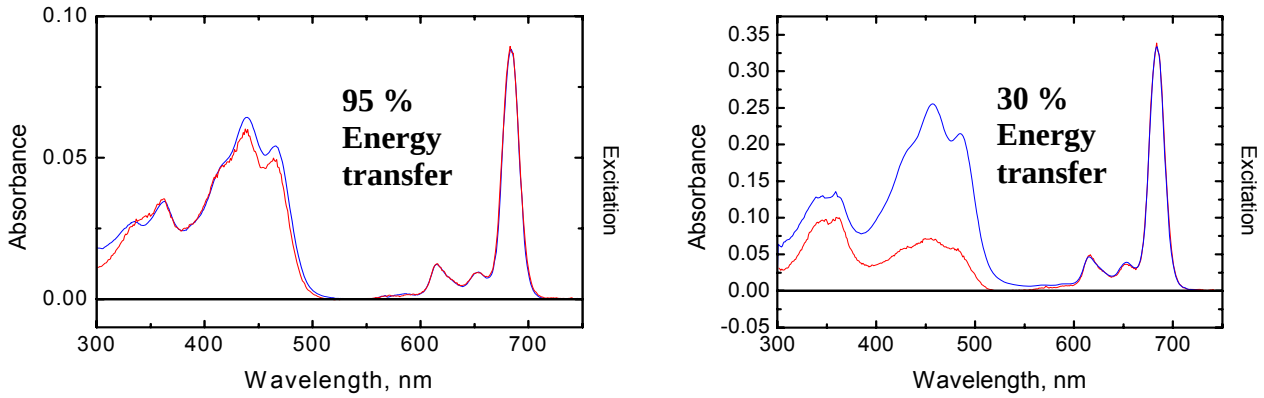

Figure 8: Absorption and excitation spectra for dyads **2** (left) and **1** (right).

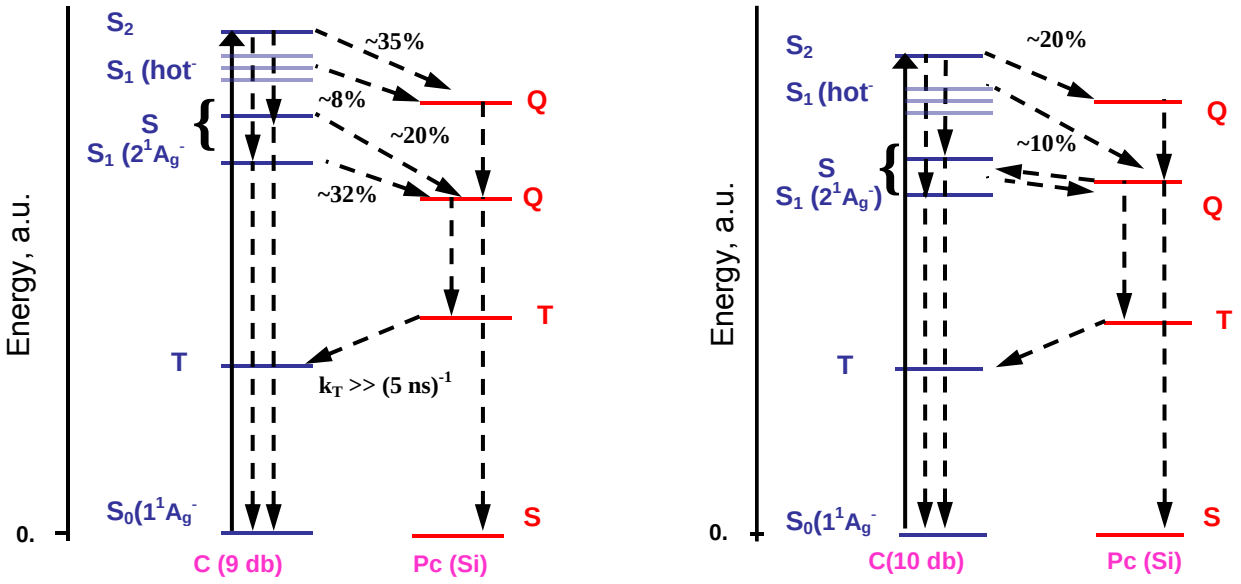

Figure 9: Different energy transfer pathways for dyad **2** (left) and **1** (right).

It can thus be concluded that singlet energy transfer from the S_2 carotenoid state to the phthalocyanin molecule can be extremely fast. When the components of the triad are in good spectral overlap and electronic coupling, both upper and lower excited states of the carotenoid can participate in the energy transfer process. Depending on the energetics, electron transfer or back energy transfer from the Pc to the carotenoid can happen, and also important, when in polar solvents carotenoids are efficient electron donors to the tetrapyrrole groups. More results about these molecules are presented in publications I and IV.

3.1.1. Non-photochemical Quenching

Another important function of carotenoids is that of photoprotection. Their mechanism of action here is two-fold. First, they can scavenge singlet oxygen as well as prevent its formation by quenching the triplet state of Chl. Secondly, they can quench the singlet excited state of Chl

under high illumination periods (eg 6-8). This process is known as nonphotochemical quenching and allows the plant to adjust to different light intensity.

The mechanism is triggered enzymatically at high light intensities, when, upon dropping of thylakoid lumen pH, violaxanthin (9 db) converts into antheraxanthin (10 db), which in turn converts into zeaxanthin (11 db). Conversely, under conditions of dim light the cycle is reversed and zeaxanthin is transformed back into violaxanthin.[47]

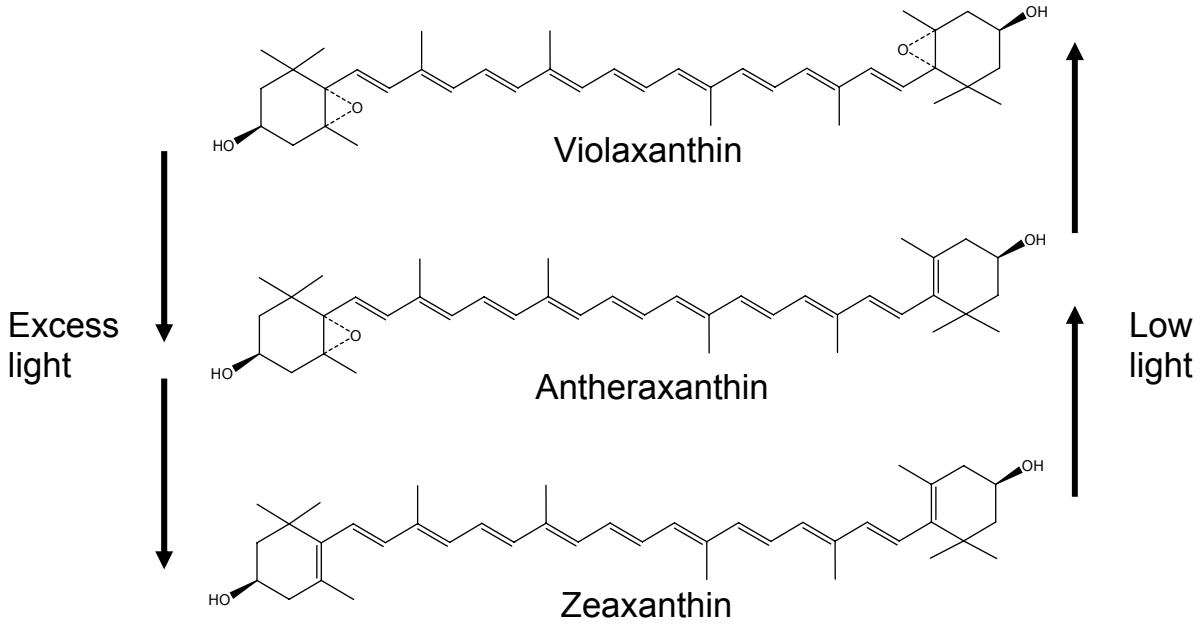

Figure 10: Carotenoids involved in xanthophyll cycle.

The mechanism is still unclear, although there are three proposed hypotheses. The first invokes quenching of the Chl excited state by energy transfer.[48] Upon expansion of the polyene chain, the HOMO-LUMO gap would decrease bringing the S_1 state of the carotenoid under the Q_y of the Chl and thus allowing back energy transfer from Chl to Car. The second hypothesis involves an electron transfer mechanism.[49] As the conjugation of the carotenoid is increased, its first oxidation potential would be lowered and electron transfer from Chl to Car would quench excess energy. The third involves a change in pigment organization.[50,51] As violaxanthin is converted

into zeaxanthin, their structural differences could change the way in which the pigment interacts with the protein complex, and this change in pigment organization could trigger the quenching process.

In order to study this process we decided to synthesize three different artificial antennas made up of zinc phthalocyanins covalently linked to three different carotenoids varying in conjugation length from 9 to 11 double bonds.

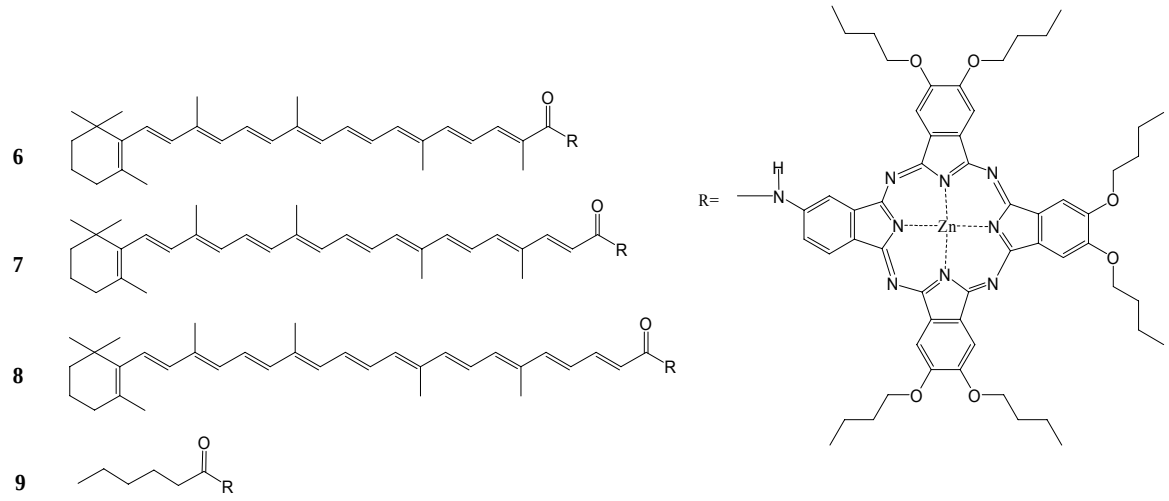

Figure 11: Structures of different length caroteno-phthalocyanin dyads and corresponding model compounds.

Synthesis of triad **8** was performed by reacting the acid chloride equivalent of carotenoid **8**, with the amino phthalocyanin in order to form an amide linkage. The **AB_3** type zinc phthalocyanin had to be synthesized by reacting a statistical mixture of di-butoxy phthalonitrile and amino phthalonitrile. The 11 double bond (db) carotenoid was obtained by a Wittig reaction of 8'-apo-carotenal (9 db) to yield the corresponding 10 db ester. Reduction to the 10 db alcohol, and oxidation to the 10 db aldehyde allowed for the next Wittig reaction to yield the 11 db ester,

which was further oxidized to the corresponding acid, transformed into its acid chloride derivative and coupled to the amino end of the phthalocyanin.

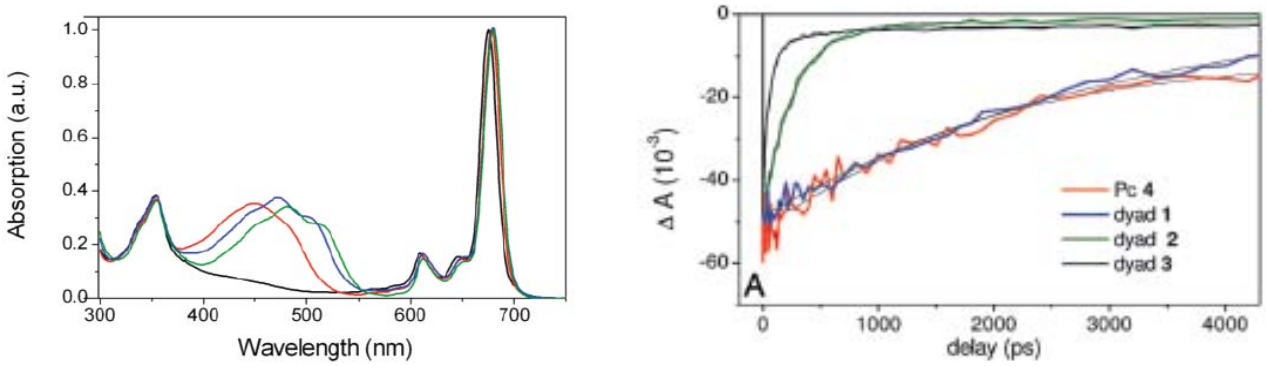

Figure 12: (Left) absorption spectra of dyads **6** (red), **7** (blue), **8** (green), and model phthalocyanin (black). (Right) Emission decays for same compounds.

UV/Vis results of the individual triads (6-8) are shown on Figure 9 (left). The spectra show that upon complexation of the carotenoid to the phthalocyanin the resulting compound shows broad absorption across the visible region which combines features of both individual components. i.e. bands at 350, 610, and 680 nm due to the phthalocyanin moiety and a broad absorption from 400 to 550 nm due to the carotenoid molecule. It can clearly be seen how upon elongation of the polyene chain by one double bond, the absorption spectrum undergoes a bathochromic shift as conjugation increases (9 db-red, 10 db-blue, 11 db-green).

Figure 12 (right) shows kinetic traces with excitation and detection at 680 nm in THF. The difference in behaviour as one double bond is added from a 9 db polyene chain to a 10 db chain is clearly visible in the shortened recovery time of the Q_y state. For model phthalocyanin **9** and 9 db dyad **1**, the recovery time is equal at about 3 ns. On the other hand, the lifetime for 10 db dyad 7, decreases by an order of magnitude to 300 ps, while 11 db dyad **8**, becomes even a stronger quencher with a Q_y lifetime of 56 ps.

Substitution of THF by a more polar solvent makes this effect more pronounced and results in acetone yielded Qy decays of 600 ps for dyad **6**, 30 ps (75%) and 120 ps (25%) for dyad **7**, and 16 ps (65%) and 90 ps (35%) for dyad **8**. This dependence on polarity could suggest an electron transfer process, but no spectral proof for a carotenoid radical cation was found. Instead, the quenching process seems to stem from the S_1 state of the carotenoid in combination with an ICT state which is though to arise from the presence of the carbonyl group in the polyene chain.

These results prove that conjugation changes in the polyene backbone of carotenoids are key to thermal dissipation of excess light energy. In this manner it can be observed how a carotenoid of the right length can dissipate Qy energy by shortening its excited state lifetime, and how an increase/decrease of a double bond can turn a carotenoid from a nonquencher into a quencher. The mechanism seems to be through a carotenoid ICT/S_1 state. The Qy state of the phthalocyanin transfers energy to the ICT state, which in turn transfers energy to the S_1 state. This state is capable of thermal relaxation into the ground state. The effect of the polar solvent seems to be to lower the ICT state making it more available to the Qy state and therefore improving the quenching process. The lowering of the ICT state could be also brought about by conformational changes in the carotenoid, and is a hypothesis that can not be discarded by the experiments presented here. More information about this project is listed in publications III and V.

3.2. Ruthenium based constructs

3.2.1. Photoactive chromophores

A suitable chromophore should replicate the mechanism performed by P_{680}. Energy absorption in the form of a photon or an energy transfer process, formation of an excited state, and consequent photo-initiated electron transfer.

Several types of molecules have been used as photosensitisers in artificial systems, going from tetrapyrrole[4,5,52] systems to transition metal complexes (Ru, Re, Ir, Os)[42,53,54].

Another well-known chromophore is the $[Ru(bpy)_3]^{2+}$ complex[55-57]. This family of molecules has raised a lot of interest in the last decades in the development of photochemistry, photophysiscs, and photocatalysis.[56,58-60]

These complexes present an absorption band in the region around 450 nm corresponding to a Metal to Ligand Charge Transfer (MLCT) process with an extinction coefficient of about 13000 $M^{-1}.cm^{-1}$ [61]. Upon irradiation in the MLCT band, the input light energy is converted into a $1(d\pi^6) \rightarrow 1(d\pi^5\pi^*)$ excited state, which in turn relaxes to form the lowest triplet state (^{3}MLCT) in less than a picosecond[62-64] with a quantum yield of unity.

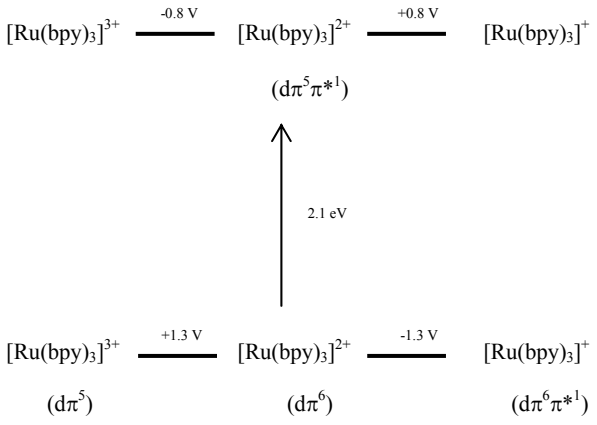

Figure 13: Physical properties of ground and excited state ruthenium $[Ru(bpy)_3]^{3+}$. Potentials vs. SCE.

This state is sufficiently long-lived (1 μs) to encounter other solute molecules and allow energy transfer, as well as reductive or oxidative electron transfer processes to occur before regeneration of the ground state[65]. As shown in figure 13, $*[Ru(bpy)_3]^{2+}$ has 2.12 eV available for energy transfer processes and its reduction and oxidation potentials are around 0.80 V vs SCE. In its ground state, the oxidation potential of $[Ru(bpy)_3]^{3+}$ species is around 1.30 V[56,63] which is close to that of the primary donor of PSII, P_{680}^{+},[17,18,66] (1.25 V vs. NHE) therefore making it a suitable candidate to reproduce the oxidation reactions performed by the natural system.

Synthetic methods are available[57,67] for the modification of the bipyridine ligands surrounding the ruthenium atom. In this manner it is possible to obtain mono and di-substituded ligands with either electron donating or withdrawing groups,[61,67,68] as well as synthetic handles either for further synthesis[53,57,69,70] or for grafting[63,70-72] onto surfaces. Oxidation potentials for this group of molecules range from 1.20 to 1.40 V *vs* SCE, depending on the nature and number of substitutions[61,63,67].

These structural changes on the ligand allow the modulation of the photophysical properties of the complex. For instance, direct changes in the relative energies of the dπ and π* orbital levels observed as bathochromic shifts of up to 50 nm[54,61,67,73] are achieved by the addition of ester or carboxylate groups to the bipyridine ligands. The emission lifetimes of these compounds are also affected by substitution patterns on the bipyridines[61,67,74,75]. Electron withdrawing substituents diminish the fluorescence lifetimes and intensities by up to 70% compared to the parent $[Ru(bpy)_3]^{2+}$ [63,67].

The chromophores used in the molecules that will be presented in the following sections are shown in figure 13.

The simplest of these, $[Ru(bpy)_2Cl_2]^{2+}$ **13**, has been extensively shown in the literature. It is synthesized by reaction $RuCl_3$ and bipyridine. Coordination into a suitable target molecule is done by first replacing the two chloride groups by the more labile nitrate groups, and further reaction with a pertinent synthon.

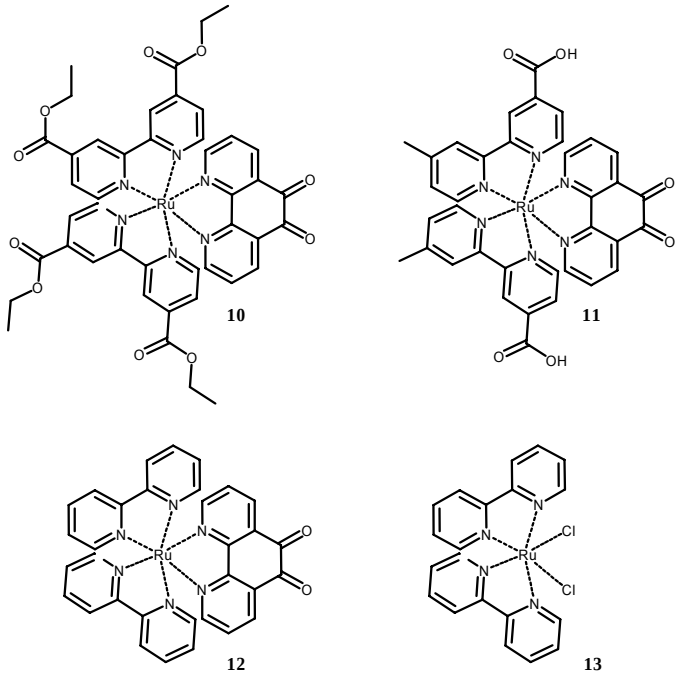

Figure 14: Structure of different chromophores.

Compounds **10**-**12** are heteroleptic ruthenium compounds that were designed in order to function as precursors in cases where the target molecules would present more than one coordination site for insertion of a metal ion. In these cases, instead of coordinating ruthenium in the latter steps, the chromophore would be added as part of an organic substructure. In these situations the synthetic handle used to build up from was the phendione moiety.

Compound **12** shows the basic bipyridine motif, while compounds **10** and **11** show ligand substitution in the form of ethyl esters and carboxylic acids respectively. As mentioned above,

and shown in later sections, the inclusion of these groups changes both the spectral, and electrochemical properties of the resulting molecules. In the case of compounds **10** and **11**, as will be shown in later sections, these modifications will serve as anchoring groups for grafting into TiO_2 surfaces as well as potential synthetic handles from which larger molecules could be constructed.

3.2.2. Donor side

In the "donor" side of PSII, after excitation by light, the oxidized P_{680}^{+} is reduced by Tyr_z, which in turn oxidizes the OEC, with the ultimate source of electrons being water. This branch, which ultimately leads to one of the most important reactions in nature, is of utmost interest to scientists yet remains poorly understood. Processes such as PCET, and its direct implication in electron transfer and charge compensation, charge accumulation, and the oxidative splitting of water have been studied in the last decade by several groups.[76-78] In these cases, the use of simpler artificial systems could allow for the elucidation of pathways which are more complicated to study in natural systems. The following sections, will give an overview of the progress made into ruthenium systems linked to Tyr_z synthetic equivalents and manganese complexes.

3.2.2.1. Phenol group

Proton/electron transfer processes in PSII are initiated at Tyr_Z. It reduces the photoxidised P_{680}, is involved in PCET processes[79] that prevent excessive charge accumulation from making the reaction too endergonic, and has even been thought to intervene in the abstraction of protons from the substrate water molecules.[80,81]

In PSII, initial charge separation between P_{680}^{+} and the reduced quinone is preserved by inserting a tyrosine group between P_{680} and the manganese cluster. As the OEC undergoes the 4 electron oxidation, inner reorganization processes, such as changes in bond lengths, might increase the reorganization energy of the cluster and make the electron transfer processes sluggish. A slow electron transfer rate between the OEC and P_{680}^{+} would favor recombination of the initially formed $P680^{+}$-Q_A^{-} couple, with the consequent loss in efficiency for the overall process. Insertion of a tyrosine group between the chromophore and the manganese cluster induces fast reduction of P_{680}^{+} and therefore prevents the recombination of the charge separated pair.

In natural systems, electron transfer processes are often accompanied by proton transfer processes. In the PSII system where a $4e^{-}$ oxidation is coupled to a 4 proton transfer in order to produce molecular oxygen this process acquires even more importance. This charge compensation process allows the OEC to rock within 300 mV between its four oxidation states, therefore avoiding oxidation potentials that could not be reachable by P_{680}[66,82,123]. The chemical basis for this proton/electron transfer lies within the chemical properties of the phenol moiety. In aqueous solution, the pK_a of a phenol changes from 10 to -2 upon oxidation, with the corollary that these processes will happen concurrently.

In order to study these processes we have synthesized different ligands sharing a common feature. A ruthenium chromophore attached to a hydrogen-bonded imidazole-phenol couple. By varying the structure of the ligand we intended to change the distance of the couple from the chromophore **15**, as well as the angle between the phenol and the imidazole **16** in order to induce some torsional strain between the phenol and imidazole groups, and thus weaken the hydrogen bond between them, and be able to study the differences these structural modifications would cause.

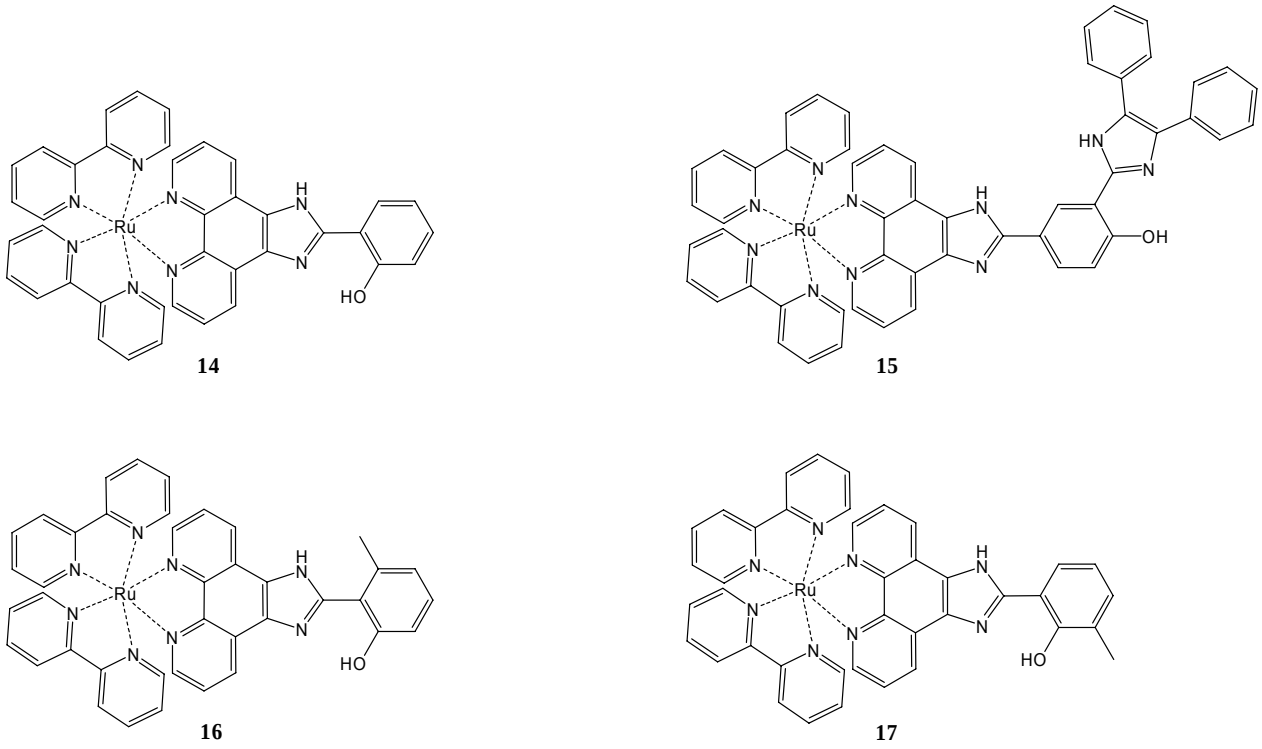

Figure 15: Structure of different Ruthenium-imidazole-phenol compounds.

The UV/Vis absorption of compounds **14**, **16**, **17,** and $[Ru(bpy)_3]^{2+}$ are shown in Figure 16. The absorption spectrum of these molecules is characteristic of ruthenium compounds and exhibits a strong π-π* transition at 280 nm, an increased absorption at 320 nm due to symmetry breaking around the ruthenium metal, and strong MLCT absorption band at 450 nm which in all cases is red shifted by about 5 nm with respect to $[Ru(bpy)_3]^{2+}$. The emission experiments show bands with maxima around 610 nm, with lifetimes of 930 ns for compound **16**, 1.23 μs for **14**, and 1.10 μs for **17**.

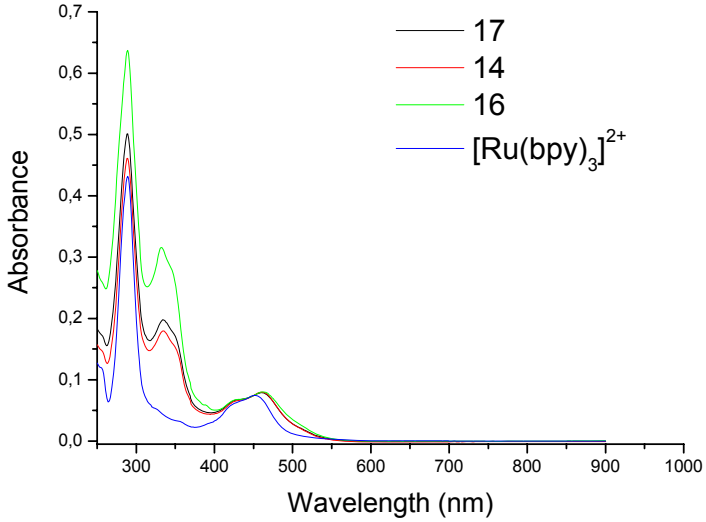

Figure 16: Absorption spectra of compounds $Ru(bpy)_3^{2+}$ (blue), **16** (green), **17** (black), and **14** (red). In acetonitrile.

Cyclic voltammetry studies in acetonitrile show typical ruthenium behavior (Table 1). The ruthenium moiety undergoes oxidation around 1.30 V for all compounds, while on the reduction side, three-one electron processes can be observed for each of the reductions around the ruthenium. The one difference to note is the appearance of a small shoulder in the oxidation of compound **17**, which is assigned to the oxidation of the phenol group.

Compound	$E_{1/2}$ $Ru^{III/II}$	$E_{1/2}$ $OH/OH^{+\cdot}$	$E_{1/2}$ Ligands
14	1.31	N/O	-1.36, -1.58, -1.92
16	1.28	N/O	-1.35, -1.58, -1.92
17	1.39	1.12	-1.26, -1.47, -1.82

Table 1: Electrochemical data for 1 mM solutions of Ruthenium-Phenol compounds **14**, **16-17** containing .1 M TBAP as supporting electrolyte.In acetonitrile vs. SCE. v = 100 mVs^{-1}. (N/O) Not observed.

.

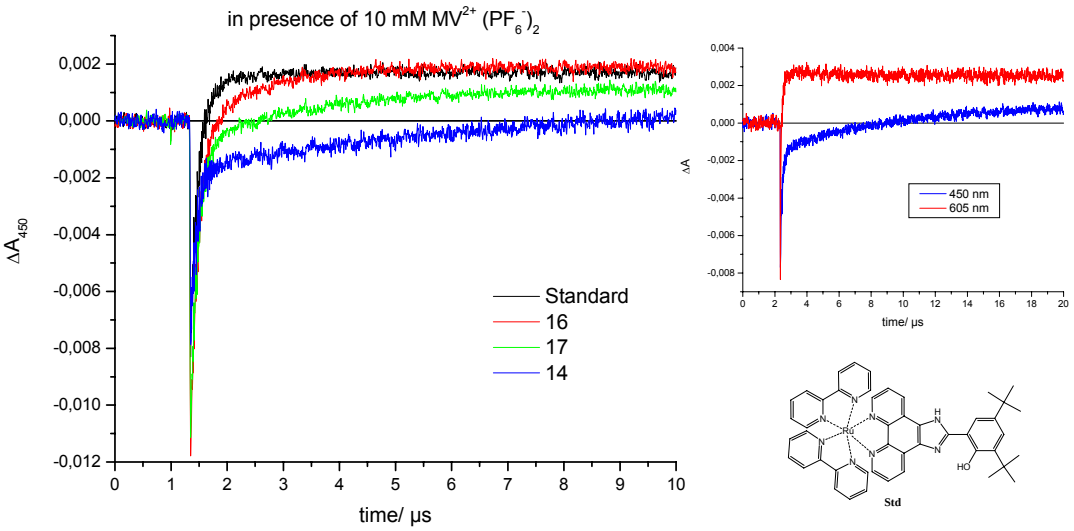

Figure 17: Left: Transient absorption changes at 450 nm for compounds: **Std** (black), 16 (red), 17 (green), and 14 (blue). Right: Example of transient absorption spectrum monitoring for $MV^{\cdot+}$ (red line), and **Std** (blue line). Right bottom: Structure of reference compound **(Std)**.

Photoinduced electron transfer studies in presence of methyl viologen (fig 17 right) were conducted monitoring the signals at 450 nm arising from Ru(II) and the phenoxyl radical, and 610 nm for reduced methyl viologen. These experiments show that in all cases, upon illumination of the compounds and initial bleaching of the absorption at 450 nm [Ru(II) → Ru(III)], the chromophore is reduced at a faster rate than the decay of the reduced methyl viologen. These results confirm that the Ru(II) is formed by electron transfer from the phenol group and not from the recombination reaction. When comparing between molecules **14**, **16**, **17**, and a previously published molecule bearing two tert-butyl groups ortho and para to the phenol group, it was found, as somewhat expected, that the oxidation of the phenol occurs fastest (black trace) and slowest (blue trace) for the molecules **Std** and **14** respectively. In the fast case, the more electron rich character of the phenol lowers its oxidation potential and therefore increases the driving force for the reaction. In the case of compound **14** the effect is the opposite and, while formation of the phenoxy radical is observed, the rate is slowest. As usual, it is in the middle of things

where the results are not the most clear. Molecules **16** and **17** were designed to have the same electron density in the phenol group, but vary in the strength of the hydrogen bond between the two groups, and as such it was expected that molecule **17**, with a stronger hydrogen bond, would undergo oxidation at a faster rate, a process that was also suggested by cyclic voltammetry which showed that there might be a slightly bigger driving force to do the reaction. Experimentally this was not the case, and it was molecule **16**, the twisted molecule, which underwent photo-oxidation faster. Reasons for this behaviour are not clear, and obtaining crystal structures in order to find a value for the degree of twisting as well as NMR experiments in order to try to find a value for the energy of rotation, and therefore the strength of the hydrogen bond, might help elucidate the reasons for these results. Work on the synthesis of molecules containing a phenol group between the chromophore and the catalytic site are currently under progress in the laboratory.

3.2.2.2. Manganese complexes

The ultimate challenge in artificial photosynthesis research is to power a water oxidation catalyst by a photoactive chromophore. Several complexes have been reported to catalyse the oxidation of water chemically. These include manganese cubanes[82,83], di μ-oxo manganese terpyridines[84,85], di-manganese polypyridil complexes[86], face to face Mn-oxo porphyrins[87], and Ruthenium dimers[88]. All these molecules have the need for large amounts of external oxidizing agents and except for the latter, which have shown truly catalytic behaviour albeit their low rates of turnover, the results for the rest of these molecules have been questioned[89] as their mechanisms, as well as the origin of the oxygen atoms involved in the reaction are unknown. Therefore, it would be very interesting from the point of view of artificial photosynthesis to link any of these putative

catalysts to a chromophore that could provide the oxidative power needed to drive these reactions. There have been several attempts at linking ruthenium choromophores to different manganese containing ligands[90-94]. To date, none of these experiments have yielded results towards the oxidation of water.

In this section, we will discuss our first attempts at building a molecular system bearing a ruthenium (II) chromophore and a mono- or polinuclear manganese complex as the donor component.

3.2.2.2.1. Terpyridine complexes

Of all the above mentioned manganese catalysts[79-84], the compound that has received most attention is that discovered by Brudvig's group[81-82]. It utilizes a terpyridine group as the coordinating site for a manganese (II) metal ion, which after further oxidation is transformed into a bis-terpyridine-Mn_2-di-μ-oxo complex (cpd **21**). Further oxidation of this molecule in a water/acetonitrile mixture in the presence of oxone was reported to accomplish the catalytic oxidation of water[85,95]. The mechanism involves the initial formation of a Mn^{III}-Mn^{IV} dimer which undergoes oxidation to a Mn^{IV}-Mn^{V} oxo complex which is thought of being capable of oxidizing water. Upon the $4e^-$oxidation of water, the metal complex is reduced to the Mn^{II}-Mn^{III} state, which replicates the S_0 to S_4 states in the natural system.

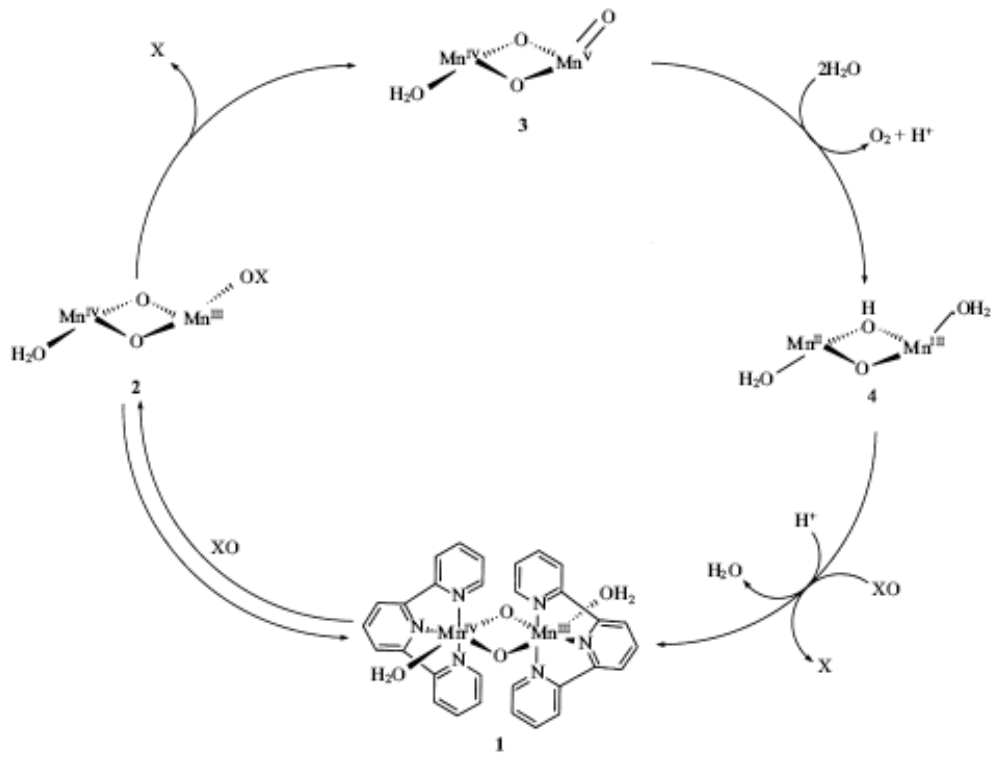

Figure 18: Proposed reaction mechanism for O_2 formation from the reaction of [(terpy)(H_2O)Mn(μ-$O)_2$Mn(H_2O)(terpy)] with an external oxidant. From reference 74.

For this molecule as well as the ones mentioned above there is a caveat. Oxone is a known oxygen transfer reagent, and therefore the origin of the oxygen atoms conforming the resulting molecular oxygen is not clear. It is important to remember that for the water splitting reaction to be catalytic, the O atoms comprising the O_2 molecule must both come from water and not any other reagent. Several studies have been published since trying to prove the origin of oxygen via isotopic labeling and mass spectrometry analyses,[84] although the results are not yet clear. It is with this inspiration that we decided to substitute the external oxidant by a ruthenium chromophore, with the goal being to try to instill the required oxidative power by means of a photogenerated oxidant.

Hence, the molecules used for these studies are composed of a ruthenium based chromophore covalently bound to a terpyridine ligand through an imidazole linkage. The photosensitiser acts

as the P_{680} counterpart, capable of harvesting light and triggering an electron transfer process. The resulting Ru^{III} species has a reversible oxidation wave occurring at 1.3 eV vs. SCE, and is capable of initiating the processes leading to the ultimate oxidation of a Mn^{II} atom which is lodged in the terpyridine cavity.

Photoexcitation: $Ru\ (II) + h\nu \rightarrow [Ru\ (III)(bpy)^{-}(bpy)_2]^{2+}*$

Reduction of electron acceptor: $[Ru\ (III)(bpy)^{-}(bpy)_2]^{2+} + A \rightarrow [Ru\ (III)(bpy)_3]^{3+} + A^{-}$

Oxidation at catalytic site: $Ru\ (III) + Mn\ (II) \rightarrow Ru\ (II) + Mn\ (III)$

Given the two potential coordinating sites of our target ligand, ie. a phenanthroline, and a terpyridine, the synthetic pathway whereby the ligand is prepared prior to metallation was deemed disadvantageous. In this manner it was chosen to start from a ruthenium (II) heteroleptic core containing either bipyridines, or ester modified bipyridines, attached to a phendione ligand which would serve a synthetic handle. The $[Ru(bpy)_2(phendione)]^{2+}$, and [Ru(ethyl ester $(bpy)_2(phendione)]^{2+}$ complexes were prepared following modified literature procedures[72] and were further reacted with 4'-formyl terpyridine or 4'-formyl phenyl terpyridine via a Steck-Day reaction. Insertion of the $Mn^{II}Cl_2$ ion in the terpyridine cavity was performed following modified literature procedures[96].

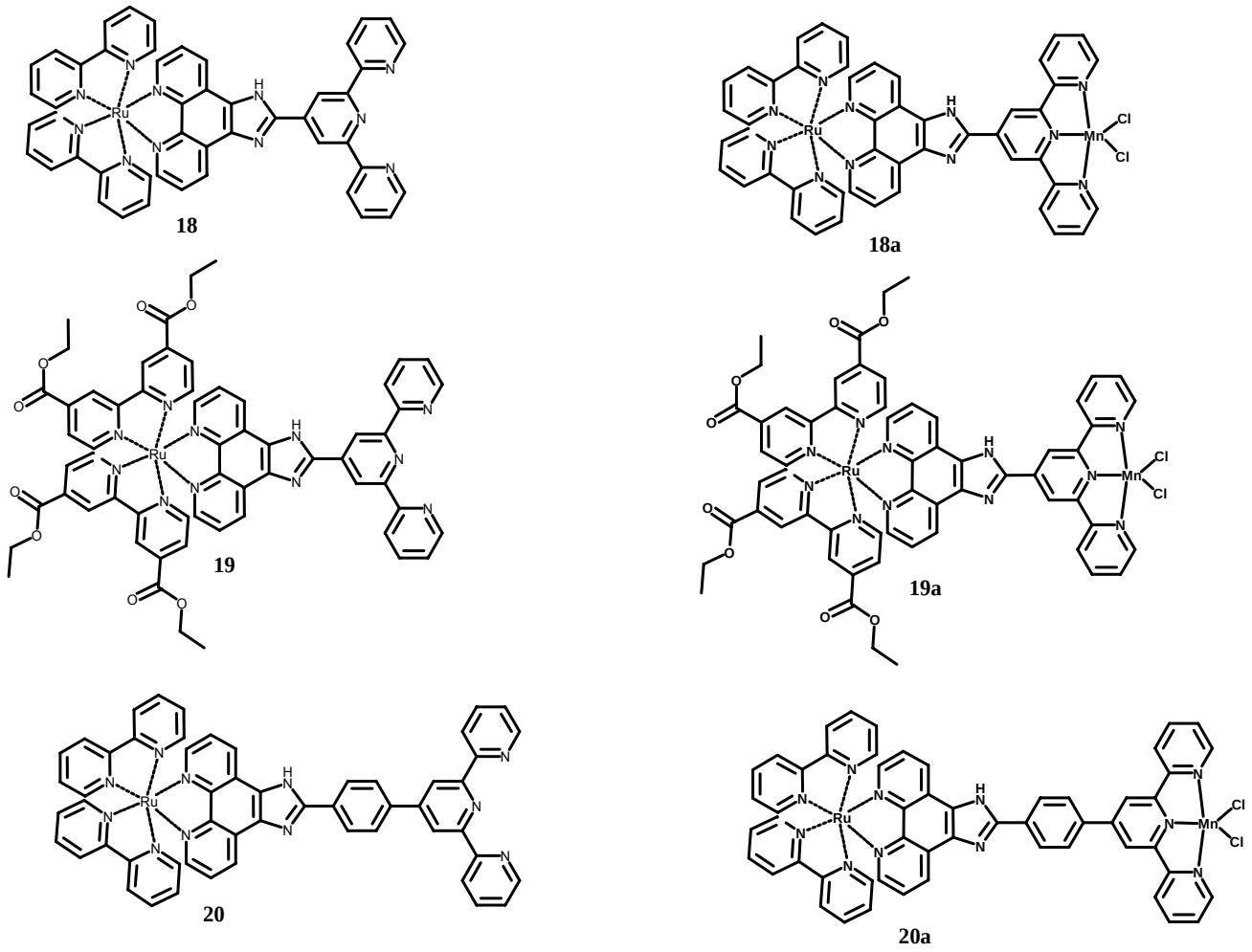

Figure 19: Structure of different Ruthenium-terpyridine compounds.

Cyclic voltammetry of compounds **18** and **20** show a one electron oxidation of around 1.30 V for the Ru^{II} to Ru^{III} step, another around 1.22-.126 attributed to the oxidation of the imidazole group, and three one electron reductions from -1.41 to -1.96 V corresponding to the reduction of the ruthenium ligands (Table 2). Addition of ethyl esters in the bipyridine groups around ruthenium results in positive shifts of about 200 mV for the oxidation process, and between 400 and 200 mV for the reduction processes. These shifts are attributed to the electron withdrawing properties of the four ethyl ester groups in the ruthenium ligands, and the concomitant increase in potential

needed in the oxidation step. Interestingly, in this molecule oxidation of imidazole group was not observed. This effect might be due to the inductive effects of the ester groups on the imidazole moiety. In the bimetallic complexes **18b-20b**, an additional reversible peak around 1.10 V is attributed to the Mn^{II} to Mn^{III} process. Oxidation of Mn^{II} seems to be independent of the substitution pattern of the molecule as the value for its potential only ranges within 50 mV between samples.

Compound	$E_{1/2\ RuIII/II}$	$E_{1/2\ Imid\cdot+/Imid}$	$E_{1/2\ MnIII/II}$	$E_{1/2\ Ligands}$	ΔG (eV)
Ru-Terpy **(18)**	1.27	1.22		-1.41, -1.61, -1.96	
Ru-Terpy-Mn **(18a)**	1.30		1.09		-0.21
Ester-Ru-Terpy **(19)**	1.51			-1.01, -1.24, -1.73	
Ester-Ru-Terpy-Mn **(19a)**	1.54		1.11		-0.43
Ru-Phenyl **(20)**	1.34	1.28		-1.41, -1.66, -1.96	
Ru Phenyl Mn **(20a)**	1.31		1.06		-0.25

Table 2: Electrochemical data for 1mM solutions of Ruthenium(II)-Terpyridine-Manganese(II) complexes containing .1 M TBAP as supporting electrolyte. In acetonitrile vs. SCE. v = 100 mVs^{-1}.

The ground state absorption spectra of $[Ru(bpy)_3]^{2+}$, and complexes **18**, **18a**, **19** and **19a** in acetonitrile are reported in Figure 20.*

The absorption spectrum of the ruthenium complexes exhibits the typical transitions. For Ru-Terpy **(18)**, a strong absorption around 280 nm due to a π-π* transition, another band at 320 nm which results from an intraligand charge transfer, and finally a band at 450 nm, the typical MLCT band of ruthenium complexes. For the ester modified complex the ground state absorption spectrum exhibits a broad and red-shifted peak in the UV (308 nm), an enhanced charge transfer band at 350 nm and a broader and red-shifted MLCT band whose maximum occurs at 475 nm.

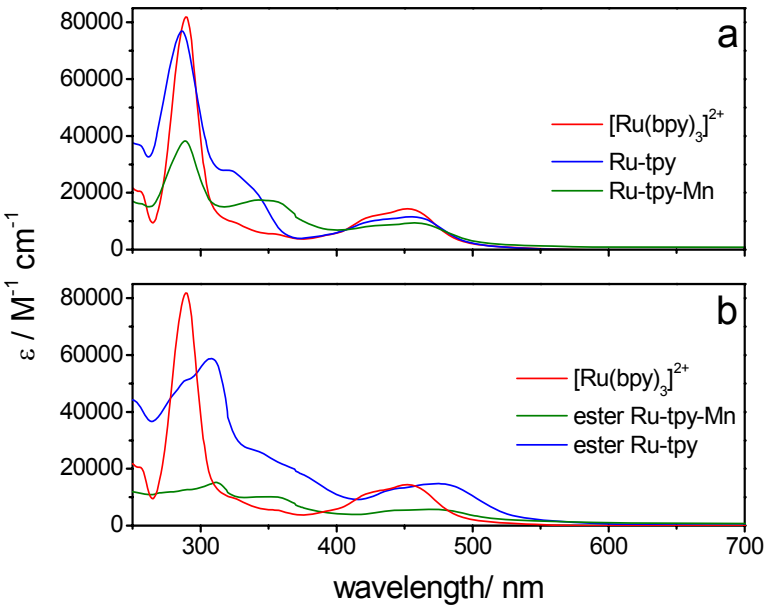

Figure 20: Ground state absorption spectra in acetonitrile for (a) $[Ru(bpy)_3]^{2+}$, Ru-Terpy **18** and Ru-Terpy-Mn **18a**; and (b) $[Ru(bpy)_3]^{2+}$, ester-Ru-Terpy **19** and ester-Ru-Terpy-Mn **19a**.

Insertion of manganese in the second coordination site induces some changes in the absorption spectrum, most notably, a reduction of intensity in the 280 nm band, a new band arising at 350 nm, and a broadening of the MLCT band together with a loss of extinction coefficient.

The strongest changes though are presented in the emission properties of these molecules. Absorption of 450 nm light by the ruthenium complexes induces emission at 610 nm (1.60 μs) for the bipyridine complexes, and 650 nm (1.65 μs) for their ester analogues. The observed red-shift of the optical transitions is a result of a decrease in the HOMO-LUMO gap, due to the electron withdrawing character of ester groups and the greater ease for reduction by the metal. This effect has previously been observed[67].

In the case of the dinuclear complexes Ru-Terpy-Mn **(18a)** and Ester-Ru-Terpy-Mn **(19a)**, the emission is strongly quenched. The lifetimes are biphasic with a main, short living component

(50 and 120 ns respectively) and a small, longer living one (1 μs and 700 ns respectively) in acetonitrile. This quenching process, which has been detected by several groups, has been described as an energy transfer process between ruthenium and manganese. Compounds **20** and **20a** were synthesised in order to try to see the effect of increasing the distance between the two metal centers in this quenching process. Unfortunately, quenching of the emission was just as strong as in the case of molecule **18a.** The reason for this might be the increased conjugation that this molecule offers between the two metal centers, which inhibits the distance effect of the extra phenyl group.

Since the goal of conceiving new Ru-Mn complexes consists of being able to photodrive electron transfer processes so that oxidative equivalents can be stored on the Mn ion, the complexes were studied in presence of light and an irreversible external electron acceptor, $[Co^{III}(NH_3)_5]^{3+}$. The one electron reduction of cobalt pentamine yields ammonia and a Co^{II} ion which is quickly hydrated and renders the reaction irreversible.

For Ru-Terpy **(18)**, these experiments showed that upon illumination of the Ru chromophore, the resulting Ru^{III} species is capable of oxidising the organic ligand around it. Proof for this process is the appearance of an organic radical-like signal around g = 2.01, and the concomitant appearance of a low field band due to the reduced Co (II) species.

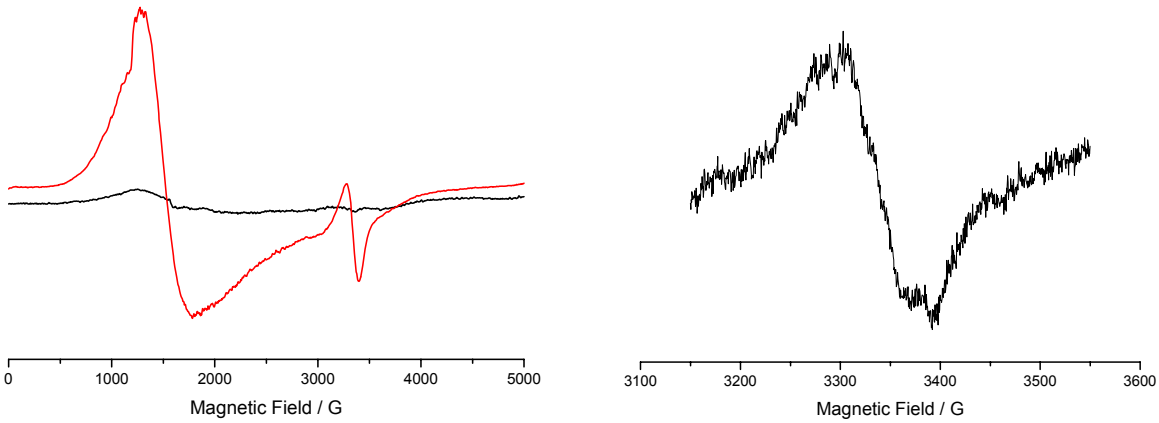

Figure 21: (Left) EPR spectra of a mixture of Ru-Terpy with cobalt pentamine before illumination (black), and after illumination (red). Experimental conditions: microwave frequency 9.415 GHz, microwave power 3.196 mW, modulation amplitude 25.251 G, temperature 5K, time constant 81.92 ms, scan rate 167 s, scan width 5000 G, and modulation frequency 100 kHz. (Right). Closer look at radical region. Experimental conditions same except for: scan width 400 G centered at 3350, time constant 81.92 ms, scan rate 41.93 s. Solvent 5:1 Water : Acetonitrile

Strikingly, the same experiment on the ester analogue did not yield a radical signal, which could imply that the ester groups influence the oxidation potential of not only the ruthenium moiety, but the whole molecule. It must be noted that the electrochemistry of this molecule does not show signs of imidazole oxidation.

EPR measurements (Fig. 22) performed on **18a** and **19a** show the changes undergone by a mixture of $[Co^{III}(NH_3)_5]^{3+}$ and these molecules in the dark (red line), and after exposure to light (black line). Mn^{II} complexes are paramagnetic systems with spins = 5/2 and exhibit characteristic EPR signals around g = 2.00. By contrast, their one electron oxidised products, Mn^{III} complexes, integer spins (S=2) and are therefore silent under standard perpendicular mode EPR conditions. On the contrary, Cobalt(III) compounds are EPR silent while their reduced counterparts exhibit strong transitions at low fields, and it is in this manner that we could follow the changes in the oxidation states of these bi-metallic complexes. The red traces in Figure 22 below show the strong band at g = 2.00 characteristic of Mn^{II} for both compounds. After illumination of these

compounds (black trace), it can be seen that the Mn^{II} signal disappears, with the concomitant appearance of a low field band corresponding to the reduced Co^{II} species. (g = 4.44). These results lead us to believe that upon initial oxidation of Ru^{II} to Ru^{III}, the chromophore is reduced to its original state by the second manganese metal.

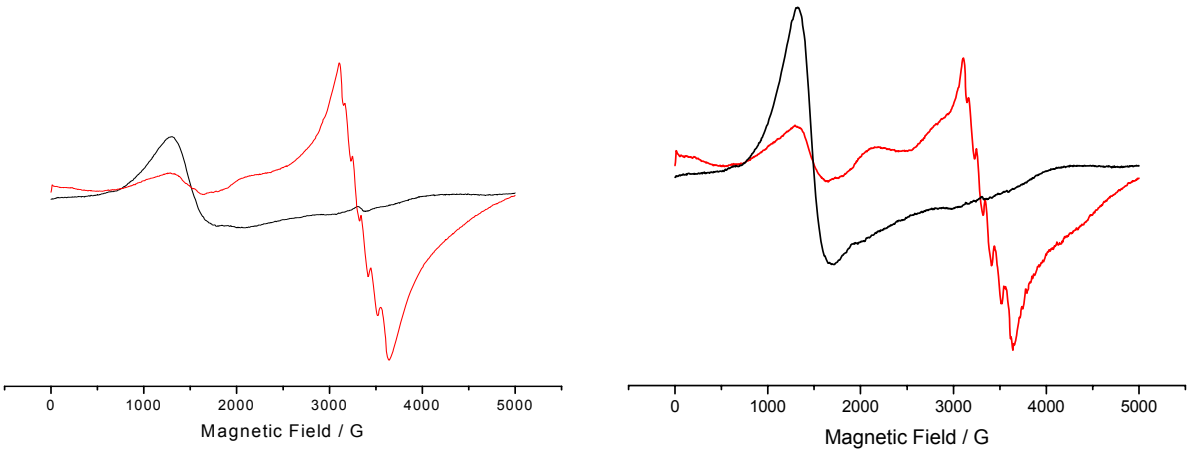

Figure 22: (Left) X band EPR spectra of a mixture of Ru-Terpy-Mn (18a) with cobalt pentamine before illumination (red), and after illumination (black). (Right). X band EPR spectra of a mixture of Ester-Ru-Terpy-Mn (19a) with cobalt pentamine before illumination (red), and after illumination (black). Experimental conditions: microwave frequency 9.415 GHz, microwave power 3.196 mW, modulation amplitude 25.251 G, temperature 5K, time constant 81.92 ms, scan rate 167 s, scan width 5000 G, and modulation frequency 100 kHz.. Solvent 5:1 Water : Acetonitrile.

Separate experiments in which we tried to mimic the formation of the manganese cluster in nature, by trying to achieve the formation of Mn (III-IV) di-μ-oxo dimers starting with Ru-Mn(II) complexes, light, and water was not successful and no multiline signals were observed after prolonged exposure to light in both the presence and absence of base (lutidine).

Preliminary results on the Ester-Ru-Terpy grafted on TiO_2 surfaces working as the electron acceptors showed that these molecules are capable of inserting themselves in high concentrations, as well as keeping the properties of the MLCT band unperturbed as seen by the absorption spectrum in Fig 23 (left). Steady state fluorescence measurements show that upon fixing these

molecules in the TiO_2 surface, their fluorescence emission is almost totally quenched, hinting that the deactivation pathway is electron transfer into the surface rather than the emissive pathway that is normally observed in solution.

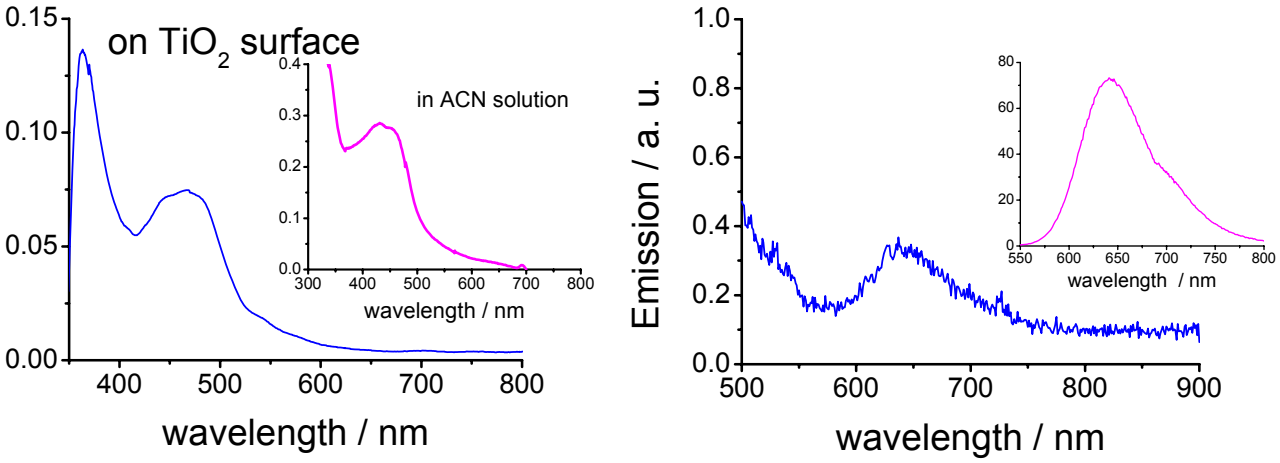

Figure 23: Absorption (left) and emission (right) spectra of compound 19 grafted to a TiO_2 surface. Insets indicate results in solution for comparison.

EPR studies of an illuminated sample of Ester-Ru-Terpy-Mn^{II} complex grafted onto TiO_2 show how the observed characteristic signal of Mn^{II} is reduced by illumination of the powder by white light. Again, this is an indication of light induced electron transfer from the chromophore into TiO_2, and consequent reduction of the ruthenium chromophore by the Mn^{II} group into its oxidized Mn^{III} form. More information on this project can be found in publication VII.

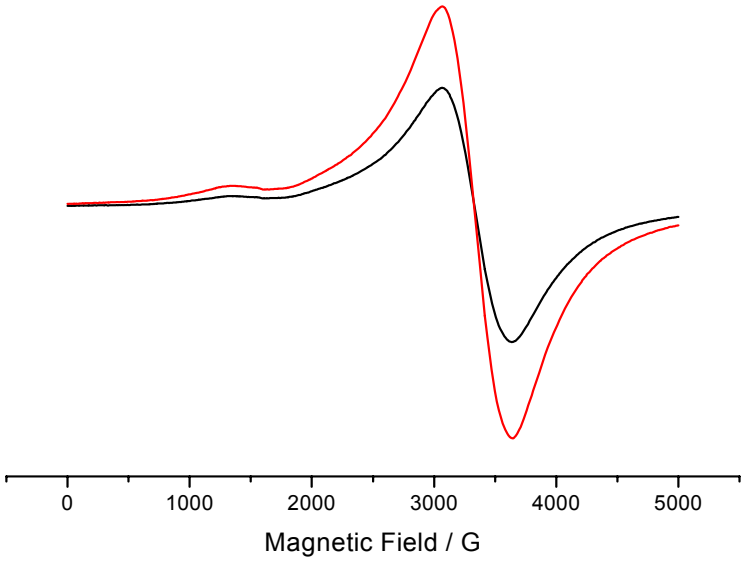

Figure 24: X-band EPR spectrum of compound **19a** grafted onto TiO_2 before (red), and after (black) illumination. Experimental conditions: microwave frequency 9.426 GHz**,** microwave power 3.196 mW, modulation amplitude 25.251 G, temperature 15K, time constant 81.92 ms, scan rate 167 s, scan width 5000 G, and modulation frequency 100 kHz. Samples were scraped from the surface and suspended in an acetonitrile solution prior to insertion in the EPR tube.

3.2.2.2.2. High oxidation state Manganese clusters

The following step towards the target molecule was the coupling of two of the above mentioned molecules in order to produce the desired di-Mn di-μ-oxo (III/IV) complex. Compound **21**, Brudvig's catalyst, has been reported to undergo the 4 e^- of water. Compounds **22** and **23** we synthesised in order to try to have a molecule containing both a catalytic site and a chromophore. This was achieved following literature procedures,[92] and yielded compounds **21-23**. In general

terms, these compounds were synthesised by reaction of oxone with the pertinent Mn-terpyridine complex.

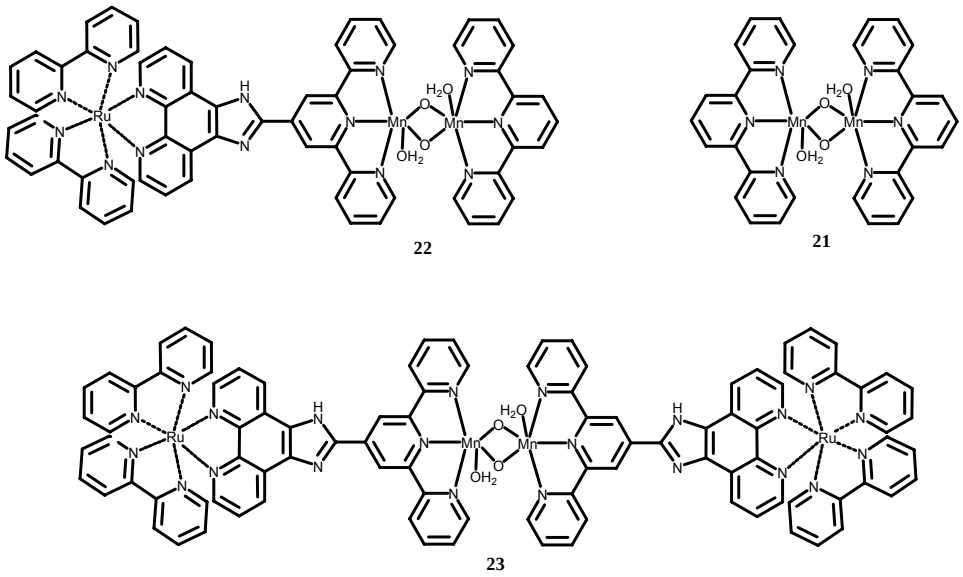

Figure 25: Structures of different Mn_2 di-μ-oxo dimers.

Following the reaction by UV/Vis provided some interesting information. Starting from the yellow terpyridine-Mn-Cl_2 compound which shows no absorption in the visible, addition of oxone and consequent formation of the di-metallic complex **21**, the solution becomes green in colour with three bands in the visible region increasing in intensity (Fig. 26). These are a large band at 420 nm due to a Mn-Mn (III/IV) transition, a small but sharp band at 550 nm, and a very broad and low intensity band at 680 nm that arises because due to a Mn(IV)-oxo charge transfer. For compound **23**, the initial absorption spectrum of its predecessor **18** displays typical ruthenium absorption at 280 nm, 320 nm and 450 nm. Upon addition of oxone there is an increase in absorption from 300 to 500 nm just as in the case of model compound **21**, as well as an increase

in absorption in the red region from 500 to 750-800 nm. The red region features are not as pronounced as in the case of **21**, possibly due to the fact that the absorption of the MLCT band in the starting compound hides their presence.

Results for compound **22** are similar in that, as a mixture of compounds, they display profiles similar to the two cases just mentioned above.

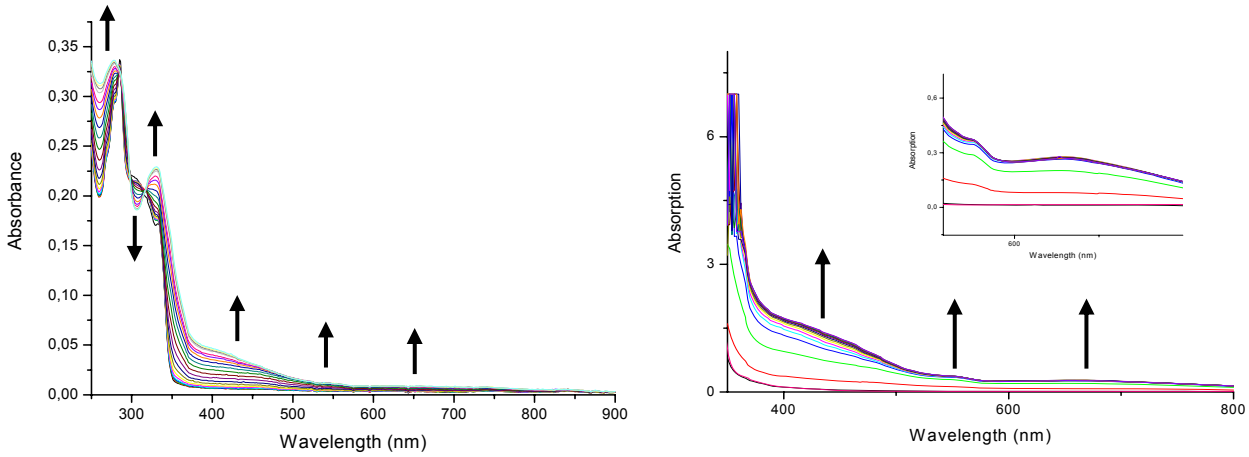

Figure 26: Uv/vis spectra of the formation of compound **21.**

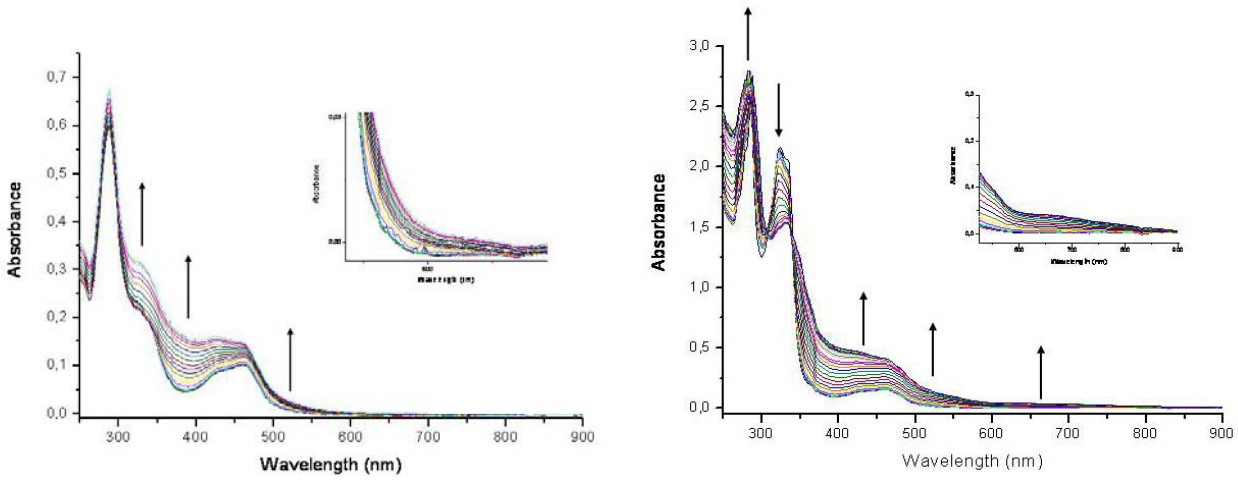

Figure 27: Uv/vis spectra of the formation of compound **23** (left), **and 22** (right).

Cyclic voltammetry experiments on compound **21** show an oxidation wave at 0.83 V vs. SCE for the Mn^{III}-Mn^{IV} to Mn^{IV}-Mn^{IV} process and a very slow reduction process at 0.15 V for the Mn^{III}-Mn^{IV} to Mn^{III}-Mn^{III} process. Compound **23**, for the same processes, yielded values of 0.76 V and 0.11 V vs. SCE and no wave for the oxidation of ruthenium could be observed. The shift of these oxidation processes towards less positive values in the latter case must be due to the presence of the Ru^{2+} moieties, and their value is consistent with published work.[97]

EPR experiments demonstrated the presence of strong 16 line signal centered at g = 2.03 typical of strongly spin coupled Mn^{III}-Mn^{IV} ions, and the absence of any Mn^{II} signal arising from the precursor molecule.

Figure 20 shows the perpendicular mode EPR spectrum of compounds **23** and **22**.

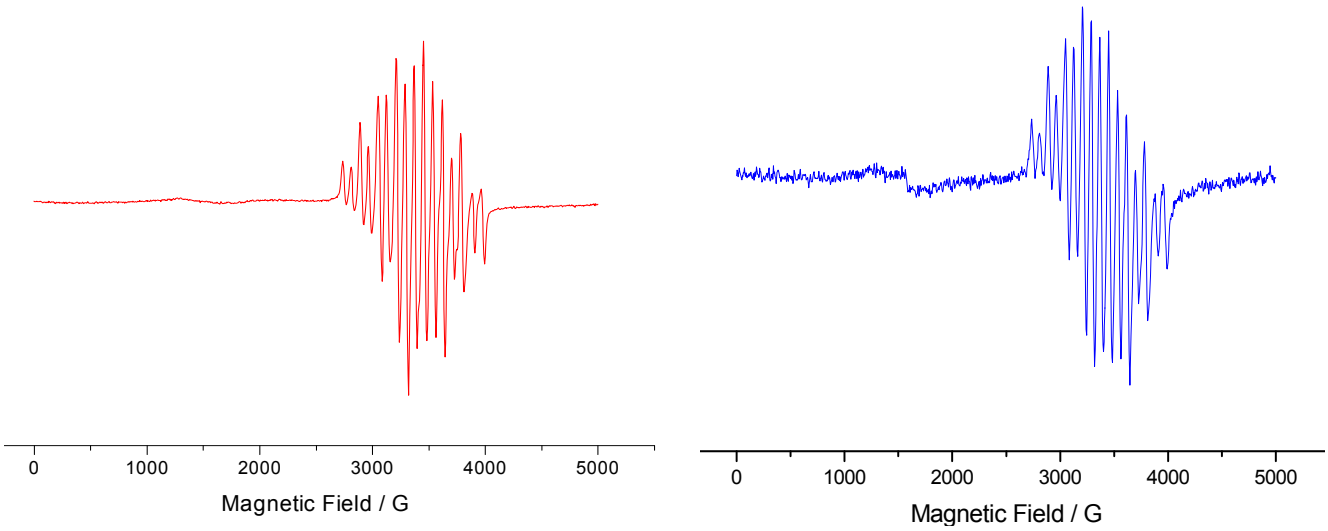

Figure 28: X-band EPR spectra of compounds **23** (left), and **22** (right). Experimental conditions: microwave frequency 9.416 GHz, microwave power 3.196 mW, modulation amplitude 25.251 G, temperature 15K, time constant 81.92 ms, scan rate 167 s, scan width 5000 G, and modulation frequency 100 kHz.. Solvent acetonitrile

Furthermore, when compound **23** was added into a solution with Cobalt pentamine and exposed to constant illumination, the 16 line EPR line disappeared, and evolved into a silent signal.

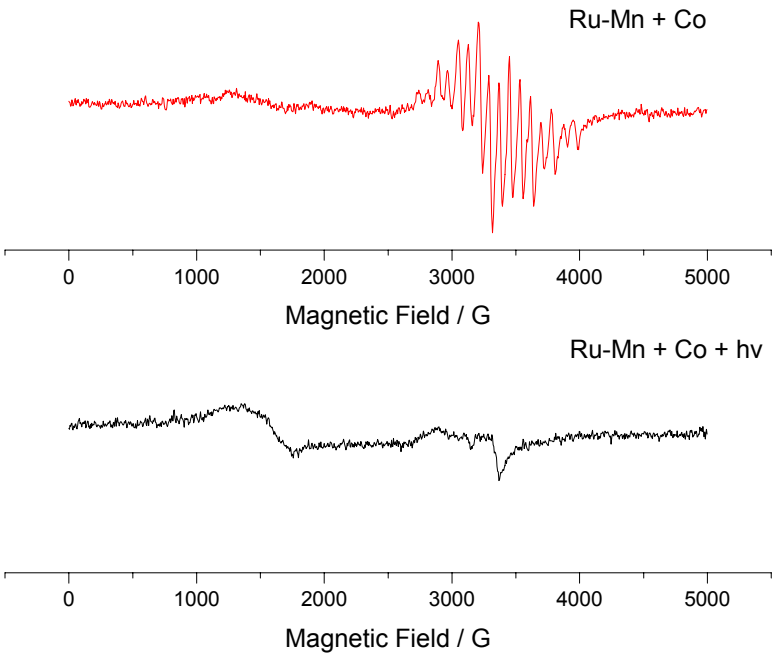

Figure 29: X-band EPR spectra of a mixture of compound 22 with cobalt pentamine before illumination (top) and after illumination (bottom). Experimental conditions: microwave power 3.196 mW, modulation amplitude 25.251 G, temperature 15K, time constant 81.92 ms, scan rate 167 s, scan width 5000 G, and modulation frequency 100 kHz. Solvent 5:1 Water : Acetonitrile

Work on this project is still in progress. Photo-driven oxidation of molecules **22** and **23** in the presence of cobalt pentamine and water have not yet yielded satisfactory results when these were performed in a Clarck electrode. Oxygen production was achieved when these were oxidized by oxone, a process that parallels that of the catalyst designed by the group of Brudvig; There is also interest in the use of an ester/acid modified version of compound **22.** This would allow the use of semiconductor surfaces as the electron acceptor groups instead of the solution based acceptors that have been used in the laboratory until now.

3.2.2.2.3. Salen Compounds

A different approach based on the same principle of inducing oxidative power by means of light energy was developed inspired by Salen chemistry. These kinds of compounds have been widely studied for their use in enantioselective catalytic epoxidations of organic substrates (olefins). Generic salen compounds **(28)** are symmetric molecules containing cavities made up of di-imino, di-phenolic moieties (N_2O_2), where different metals, notably manganese, can be coordinated.

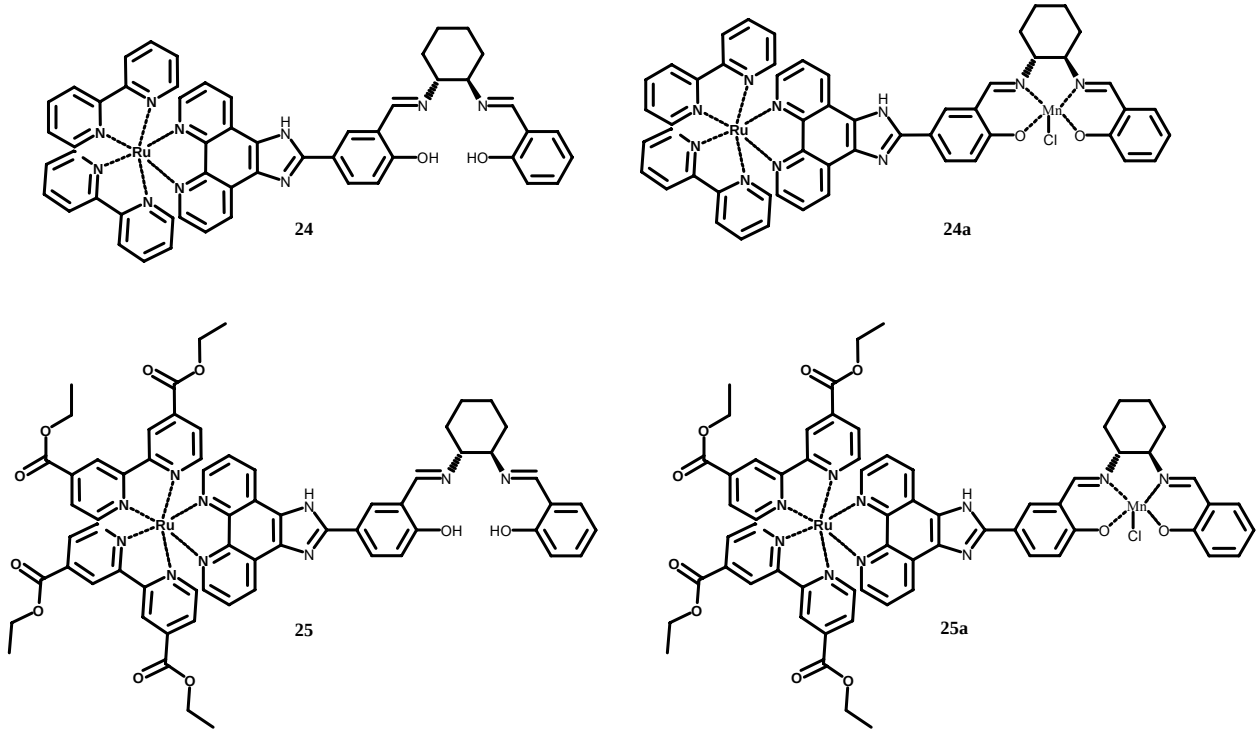

Figure 30: Structures of different salen compounds.

The mechanism of the epoxidation reaction is not completely understood, and some of the postulated processes are i) a two electron oxidation from Mn(III) to form a Mn(V)=O complex. This can undergo electrophilic attack by an electron rich substrate such as an alkene via oxygen atom transfer, ii) an equilibrium between the Mn(V)=O species and a μ-oxomanganese(IV) dimer, or iii) in porphyrins, a mechanism by which two reactive species in the form of Mn(V)=O

and Mn(IV)=O compete for the olefin with the former yielding products with retention of configuration and the latter being nonstereospecific. All these processes, like the ones presented in the previous section are achieved by addition of an external oxidant in order to initiate the reactions.

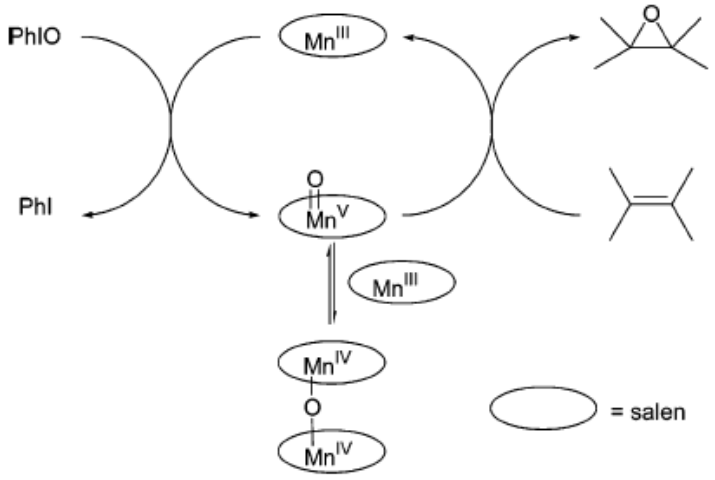

Figure 31: Proposed mechanism for salen epoxidation. From Kochi and coworkers.

Formation of such an epoxide bond would be interesting, not only from a point of view of photo-catalysis, but also as a first learning step towards the oxidation of water. As explained above, the mechanism for the epoxidation is a 2 e^- oxidation of an electron rich olefin with an electron poor metal-oxo group. This mechanism is analogous to the one that has been postulated for the oxidation of water, and therefore reactions of this kind could provide hints about how to maximize the reactivity of the oxo components. Compounds **24-25** were synthesized in order to study whether a ruthenium chromophore was capable of initiating the oxidation processes from a Mn(III) atom lodged in a salen cavity.

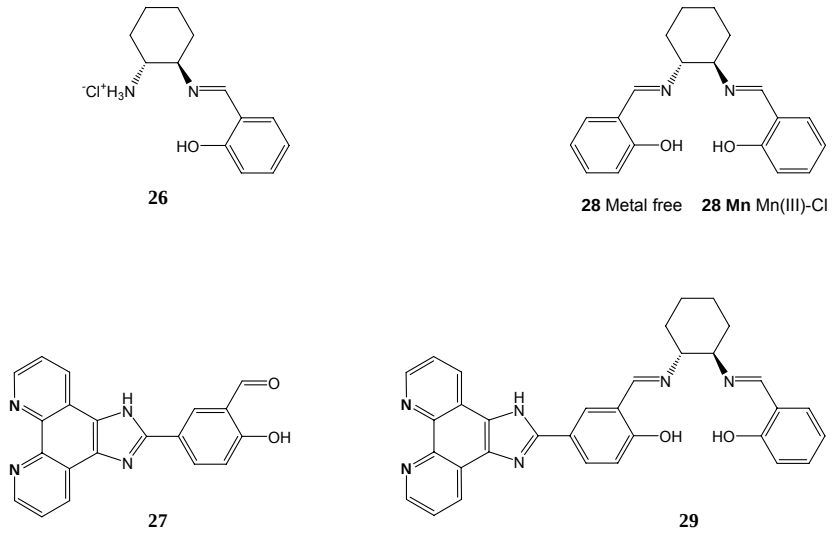

Figure 32: Different synthons required for the preparation of asymmetric salen molecules.

As can be observed from the structure of compounds **24-25** compared with **28**, the salen cavity in the former is asymmetric, and therefore the synthetic pathway is different. In order to arrive to **(29)**, we followed a method developed by Nguyen et al[98] where one of the amino groups of 1,2-cyclohexyldiamine was protected in order to obtain the first mono-imino compound **(26)**, and a second formylated component was reacted with it in order to reach to **(29)**. Insertion of ruthenium, followed by insertion of manganese afforded the desired molecules.

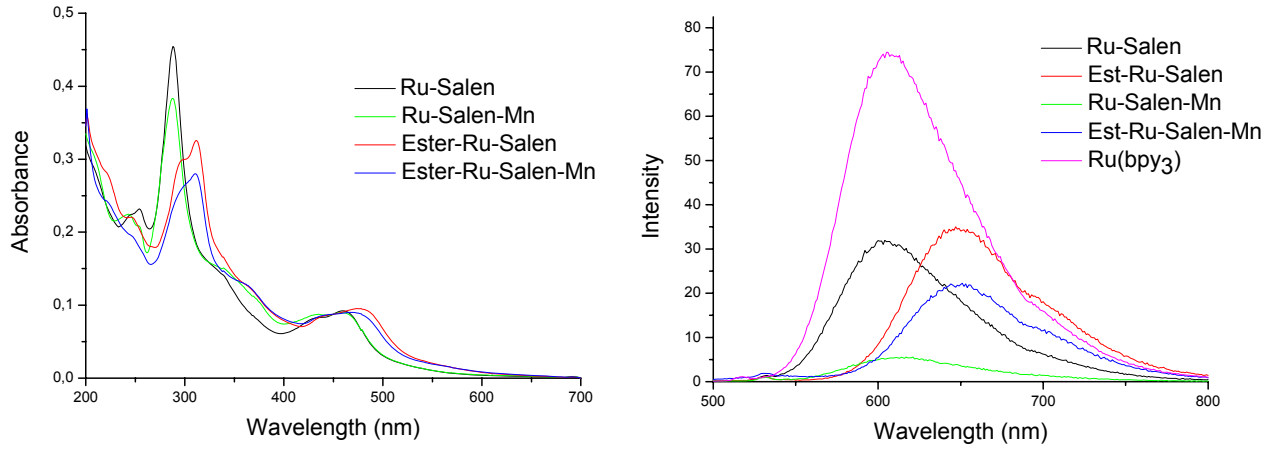

Figure 33: Absorption (left) and emission (right) of compounds Ru Salen **(24)** (black), Ru Salen Mn **(24a)** (green), Ester Ru Salen **(25)** (red), and ester Ru Salen Mn **(25a)** (blue).

The absorption profile is similar to all the ruthenium based molecules previously presented. One striking difference was the large decrease of emission when compared to $Ru(bpy)_3$. This phenomenon has been attributed to reductive quenching, where the electron deficient salen cavity is capable of abstracting one electron from the bipyridine bound to the excited ruthenium atom. Insertion of manganese in the salen cavity, again, as in the previous case of the terpyridine-based molecules quenches the emission of the ruthenium chromophore to a large extent, but insertion of electron withdrawing groups around the ruthenium atom reverse this situation.

	$E_{1/2}Ru^{III/II}$	$E_{1/2}Mn^{IV/III}$	$E_{1/2}$ $Mn^{III/II}$	$E_{1/2}$ **Phenol**
Salen (28)				1.14
Salen Mn (III)		0.76	-0.44	
				$E_{1/2}$ **Bipyridines**
Ru Salen (24)	1.30			-1.27, -1.62, -1.87
Ru-Salen-Mn (III) (24a)	1.36	0.82	-0.20	-1.38, -1.57, -1.78

Table 3: Electrochemical data for 1 mM solutions of complexes **24** and **24a**, **28**, and **salen Mn(III)** containing . .1 M TBAP. In acetonitrile vs. SCE. v = 100 mVs^{-1}.

Cyclic voltammetry studies in acetonitrile are shown in Table 3. The salen compound **28** shows an irreversible wave at 1.14 V vs. SCE which is attributed to the irreversible oxidation of the phenol groups. The Ru-Salen analogue shows a wave at 1.30 V preceded by a shoulder at 0.96 V. These signals are ascribed to the one electron oxidation of Ru(II) to Ru(III), and the oxidation of the phenol groups in the salen cavity. On the reduction side, the three one electron reduction processes observed are attributed to the reduction of each of the bipyridine ligands (-1.27 V to -1.87 V). The model compound Salen-Mn(III) **28-Mn** shows a quasi-reversible oxidation wave at 0.76 V for the Mn(III) to Mn(IV) process, and a reversible reduction wave at -0.44 V for the one electron reduction of Mn(III) to Mn(II). Insertion of Mn(III) in the Ru-salen complex **24** to form

24a exhibits the same features as the parent compound, namely, Ru oxidation and ligand reduction, plus an oxidation (0.82 V) and a reduction wave (-0.20 V) stemming from the coordinated manganese ion. The shift towards more positive values must be due to the presence of the Ru^{2+} ion, and the effect of the induced positive charge in the overall system.

Parallel mode EPR enables us to study integer spin systems such as in the case of the Mn(III) oxidation state. Analysis of the resulting molecules (**25a** and **28-Mn**) in methanol are shown in fig. 34. They exhibit six well resolved hyperfine lines centered at g= 8.144 with these lines split by 42 G. Mn(III) systems have a d^4 electronic configuration with spin (S) = 2. It is important to note that the same analysis performed in an acetonitrile glass did not yield any signal and therefore it can be assumed that the apparition of this signal is strongly dependent on the solvent forming the glassy medium. The shape and displacement of these signals are consistent with published work on Mn(III) systems in both manganese-salen compounds[99] and Mn(III) centers in the Super Oxide Dismutase enzyme.

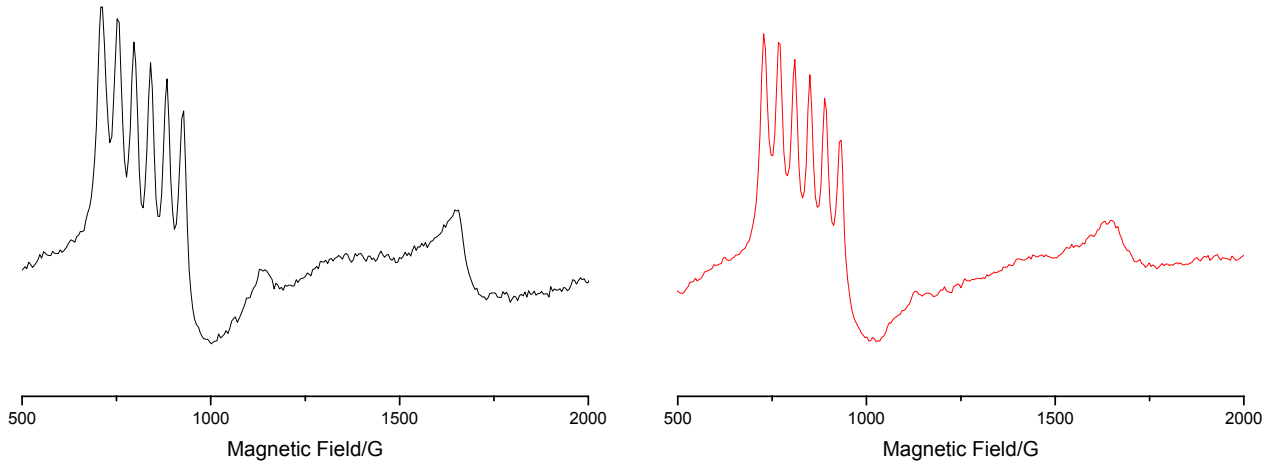

Figure 34: EPR parallel mode spectra in methanol of compounds **28-Mn** (left), and **24a** (right), Experimental conditions: microwave frequency 9.352 GHz**,** microwave power 3.196 mW, modulation amplitude 25.251 G, temperature 5K, time constant 81.92 ms, scan rate 167 s, scan width 5000 G, and modulation frequency 100 kHz.

Light induced oxidation of **(24a)** Ru Salen Mn(III) in aqueous buffer solution at pH 7.8 in the presence of cobalt pentamine was performed in order to try to arrive at the Mn(IV) state. The reaction was monitored by UV/Vis and the results are presented in Fig 35.

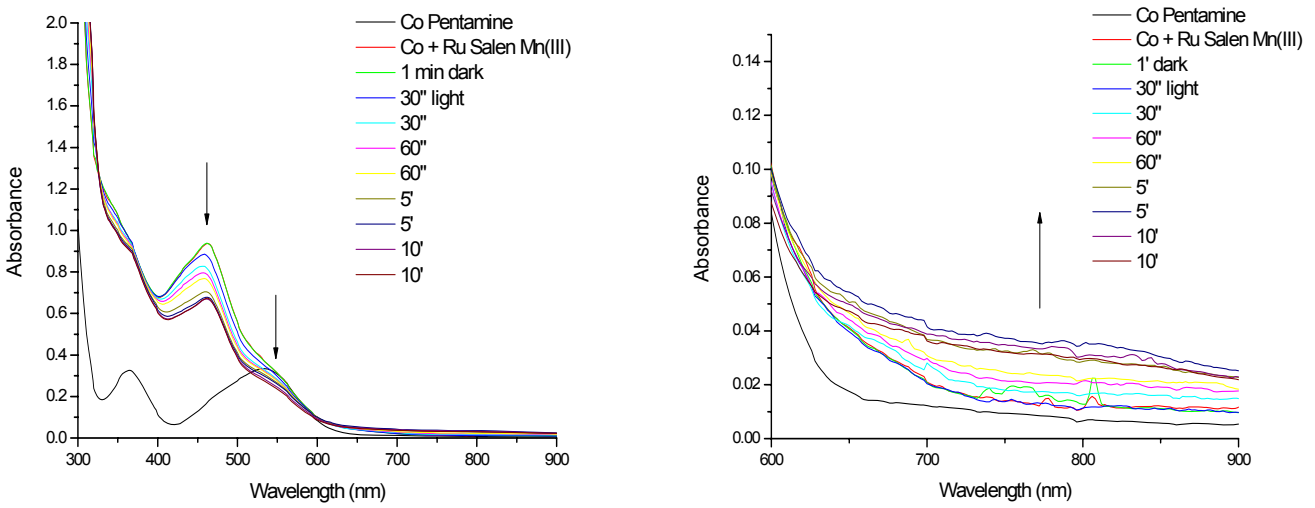

Figure 35: Uv/vis spectra following the reaction of **24a** with cobalt pentamine and light. Solvent 5:1 Acetonitrile : Water.

The absorption spectrum shown is a combination of the initial components making up the mixture. Ru Salen Mn (III) exhibits the typical absorption at 450 nm, with a pronounced shoulder at 550 nm, and a smaller absorption band at 360 nm which are attributed to Cobalt pentamine. Upon illumination it can clearly be seen that these three absorption bands decrease in intensity. This is attributed to reduction of the cobalt pentamine as well as the oxidation process Ru(II) to Ru(III) which bleaches the absorption maxima at 450 nm. Another important change occurs in the region from 700-900 nm where a very broad and low intensity band appears, which is reminiscent of those brought about by Mn-oxo transfer transitions.

EPR analyses of the solution before and after reaction with light were obtained in perpendicular mode. The starting solution shows no signal except for a small indication of residual Co(II) present in the solution. Upon illumination we observe a large signal around g = 4.40 due to

reduction of Co(III) and more interestingly a signal arising centered at g = 2.04. This multi-line signal has not been characterized and could arise from i) reduction of the Mn(III) centre back to Mn(II), or more interestingly, ii) a Mn(III)-O-Mn(IV) dimer of the kind that has been postulated in the mechanism of Salen compounds. Signals of this kind have been observed before, and future work using an electron acceptor that does not interfere with low field signals in the EPR spectrum should be used.

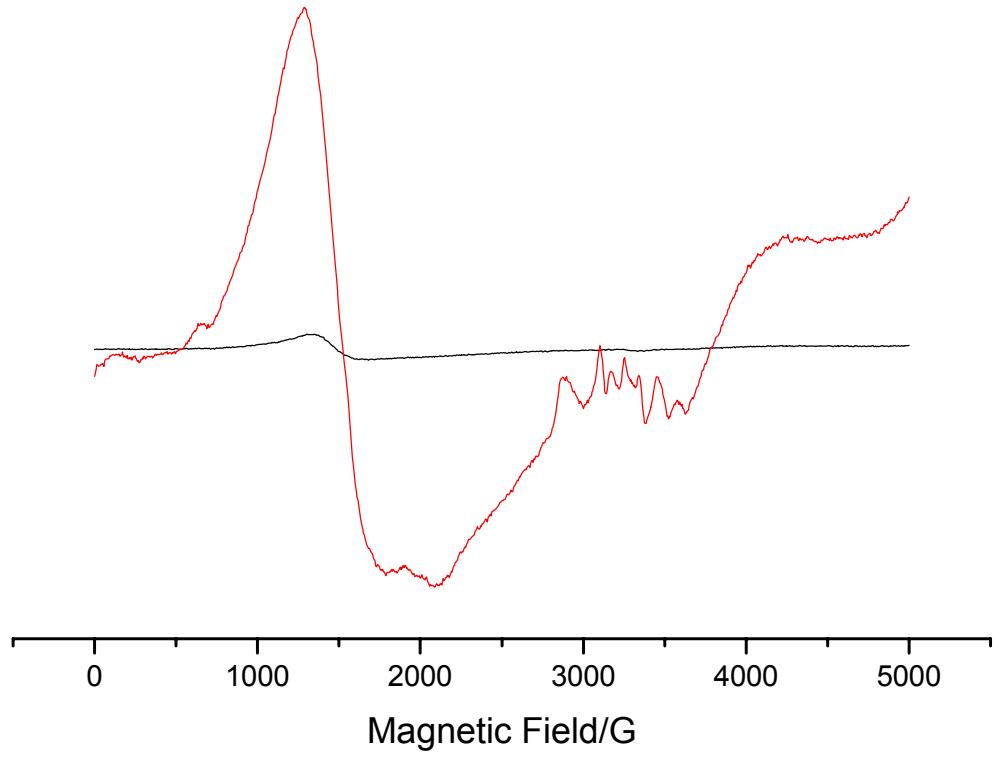

Figure 36: X-band EPR spectra of reactions of **24a** with $[Co^{III}(NH_3)_5]^{3+}$ in the dark (black), and light (red). Experimental conditions: microwave frequency 9.418 GHz**,** microwave power 3.196 mW, modulation amplitude 25.251 G, temperature 5K, time constant 81.92 ms, scan rate 167 s, scan width 5000 G, and modulation frequency 100 kHz. Solvent 5:1 Water : Acetonitrile

Work on this project is currently focused on the light catalysed epoxidation of alkenes, as well as the insertion of these molecules in surfaces as has been explained in previous sections.

3.2.2.2.4. Salophen compounds

Previous work in the laboratory on Ruthenium-salophen compounds[100] with and without copper as second metal in the salophen cavity had shown that in both cases emission of the ruthenium chromophore was totally quenched. The cause of this quenching was attributed, in the case of the copper free molecule, to an electron transfer process from the Ruthenium to the N_2O_2 group of the salophen cavity, yielding a surprisingly long lived charge separated state of 30 μs. In the case of the copper bearing molecule the quenching was even more pronounced, and no electron transfer step was observed. This was attributed to the extremely short lived excited state of the ruthenium chromophore which did not allow for bi-molecular reactions to happen.

With this idea in mind and the previous results obtained when using electron withdrawing groups in the coordination sphere of ruthenium, we decided to introduce tetra-ethyl ester bipyridines in these molecules. The idea being that by changing the electronic configuration of the molecule, electron transfer from ruthenium would be redirected towards the bipyridine ligands rather than towards the salophen cavity.

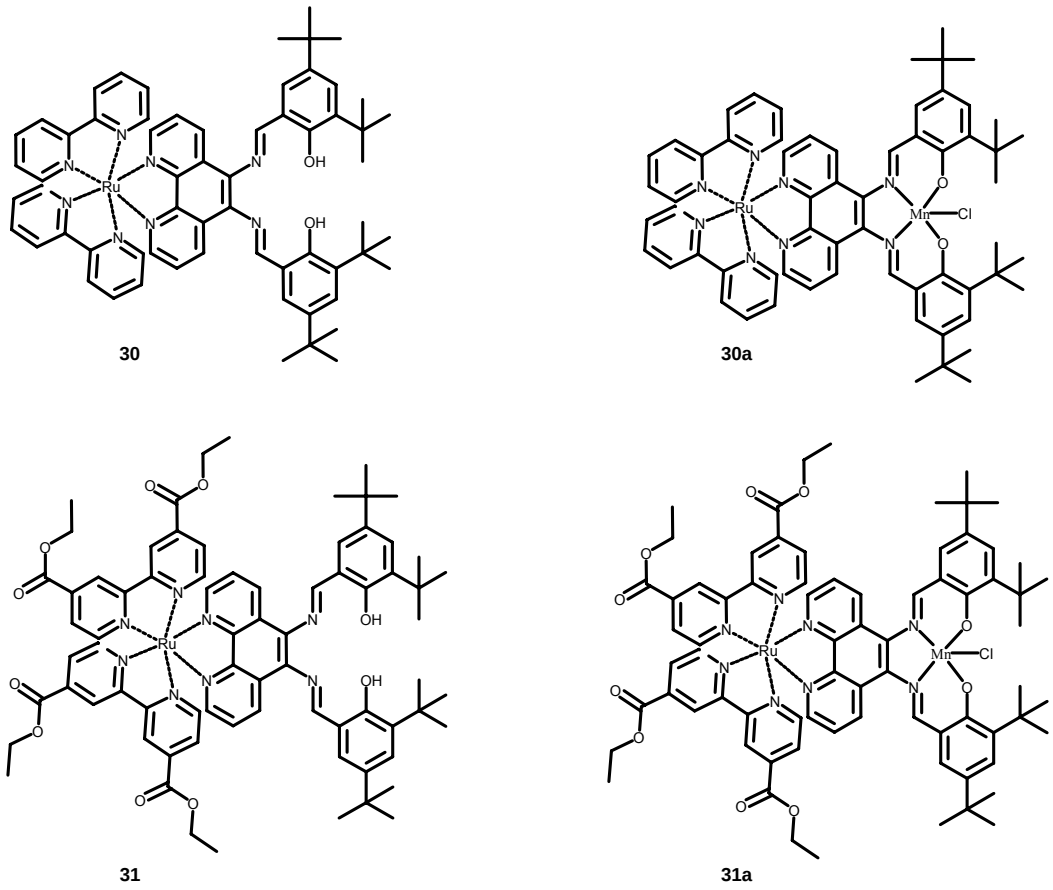

Figure 37: Structures of different salophen compounds.

Absorption spectra of the salophen compounds are presented in figure 37. It follows the same guidelines as with previous complexes. Mainly, small increases in the 350 nm bands for both the Mn and Mn free bipyridne compounds, which become a bit more pronounced for the ester bearing molecules. The latter also exhibit red shifts for the MLCT bands consistent with data shown in previous sections.

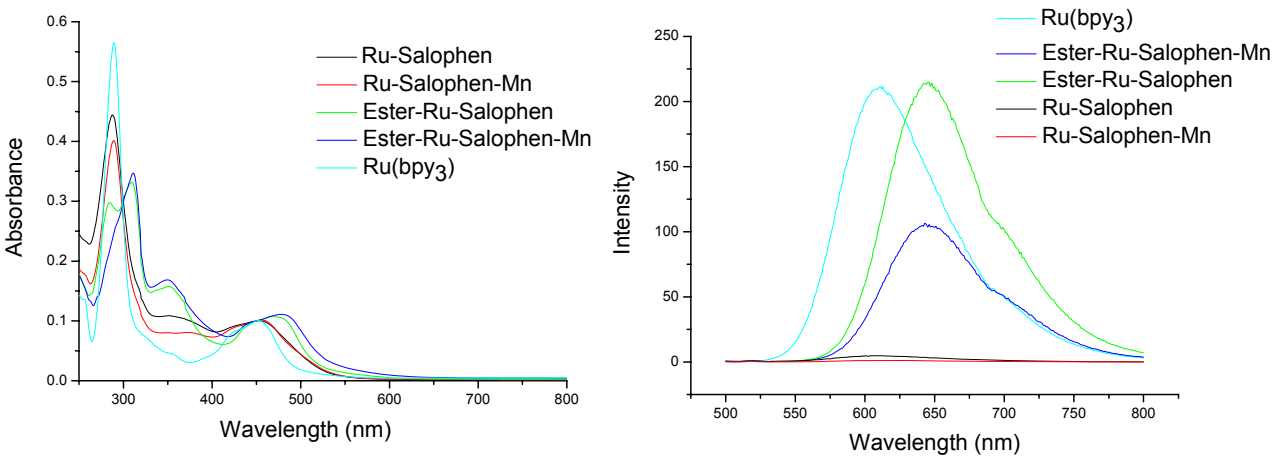

Figure 38: Absorption (left) and emission (right) of compounds Ru Salophen (black), Ru Salophen Mn (red), Ester Ru Salen (green), Ester Ru Salen Mn (blue), and $Ru(bpy)_3$ (light blue).

Steady state emission experiments in methanol yield similar results to those obtained by Pellegrin et al. That is, almost complete quenching of the emission for the ruthenium-salophen compound **(30)** and for the ruthenium-salophen Mn complexes **(30a)**. These results are consistent with the previous work, which characterize this quenching as electron transfer from ruthenium to the salophen cavity. Accordingly, the use of electron withdrawing ligands around the ruthenium yielded the desired results. Emission of ester-ruthenium-salophen has the same intensity as the reference $Ru(bpy)_3$, and the bimetallic compound shows a quenching of about 50% compared to the same reference.

EPR experiments showed that the oxidation state of the Mn ion in the cavity is +2 (S = 5/2).

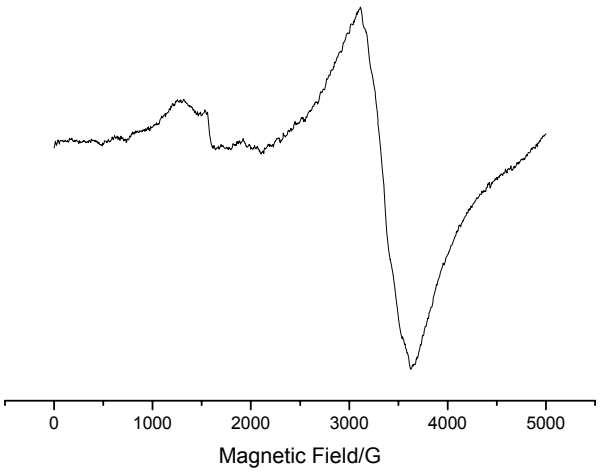

Figure 39: X-band EPR spectrum of compound **30a**. Experimental conditions: microwave frequency 9.415 GHz, microwave power 3.196 mW, modulation amplitude 25.251 G, temperature 5K, time constant 81.92 ms, scan rate 167 s, scan width 5000 G, and modulation frequency 100 kHz. In acetonitrile.

The results presented above show that it is possible to tune the properties of these molecules by modifying their structure. This project is very similar to that in the salen section and similarly future work would consist in achieving higher oxidation states of the manganese ion.

4. Conclusion

20 years after chemists observed the first charge separated state,[55,56] the field of artificial photosynthesis presents itself today as one of the most promising alternatives in our goal to finding clean sources of energy. The challenge is enormous as we are trying to find a system which combines light absorption, energy transfer, 4 electron transfers, and 4 proton transfers, to finally arrive at the oxidation of water by a catalytic center. In addition, this must occur in a sequential process in which the faltering of any one step will short circuit the whole system.

In the previous sections the synthesis, characterization, and properties of different photosynthetic mimics has been presented. The use of organic synthesis combined with coordination chemistry, and different kinds of spectroscopy allow us to study molecules and processes inspired by natural photosynthesis. It is thus possible to synthesize antenna systems and bi-metallic compounds such as the complexes presented here in order to study processes such as light absorption, energy transfer, and photo induced electron transfer processes equivalent to those occurring in nature between P_{680} and the OEC. As has been shown, when trying to assemble an artificial photosynthetic device there are many aspects which must be taken in consideration. i) efficient light absorption both in terms of dipole cross section and spectral width, ii) energy transfer processes which funnel light energy from an antenna or a chromophore but don't quench necessary excited states, iii) vectorial electron transfer with low recombination rates, iv) accumulation of charges that arrive without large increases in oxidation potentials, v) activation of catalytic centers, and iv) final reaction catalytic site must all work in efficient series for the molecule to become a significant candidate. Recent advances in surface chemistry seem to have initiated a movement from solution based chemistry towards solid-state systems. These could prove to be very interesting as it may provide us with better ways to recycle products (electrons and protons) and add a degree of dissymmetry that might be needed in systems of this kind.

Above all it is important to remember that we do not know the actual structure or the mechanism of the natural system. Such information would greatly help towards achieving an artificial working model. On the opposite side, we do not have reliable water splitting catalyst, and obtaining one might be of importance for scientists studying natural photosynthesis. Untill then, the idea of a four photon, four electron, four proton reaction remains distant.

5. References

(1) Lewis, N. S.; Nocera, D. G. *PNAS* **2006**, *103*, 15729 –15735.
(2) Wasielewski, M. R. *Chem. Rev.* **1992**, *92*, 435-461.
(3) Devens Gust; Moore, T. A.; Moore, A. L.; Alisdair N. Macpherson; Lopez, A.; DeGraziano, J. M.; Gouni, I.; Bittersmann, E.; Seely, G. R.; Gao, F.; Nieman, R. A.; Ma, X. C.; Demanche, L. J.; Hung, S.-C.; Luttrull, D. K.; Lee, S.-J.; Kerrigan, P. K. *Journal of the American Chemical Society* **1993**, *115*, 11141-11152.
(4) Guldi, D. M.; Imahori, H.; Tamaki, K.; Kashiwagi, Y.; Yamada, H.; Sakata, Y.; Fukuzumi, S. *Journal of Physical Chemistry A* **2004**, *108*, 541,548.
(5) Imahori, H. *Journal of Physical Chemistry B* **2004**, *108*, 6130-6143.
(6) Rau, S.; Schäfer, B.; Gleich, D.; Anders, E.; Rudolph, M.; Friedrich, M.; Görls, H.; Henry, W.; Vos, J. G. *Angew. Chem. Int. Ed.* **2006**, *45*, 6215-6218.
(7) Ozawa, H.; Haga, M.-a.; Sakai, K. *J. Am. Chem. Soc.* **2006**, *128*, 4926-4927.
(8) Gersten, S. W.; Samuels, G. J.; Meyer, T. J. *J. Am. Chem. Soc.* **1982**, *104*, 4829-4830.
(9) Limburg, J.; Vrettos, J. S.; Liable-Sands, L. M.; Rheingold, A. L.; Crabtree, R. H.; Brudvig, G. W. *Science* **1999**, *283*.
(10) Ruettinger, W.; Yagi, M.; Wolf, K.; Bernasek, S.; Dismukes, G. C. *J. Am. Chem. Soc.* **2000**, *122*, 10353-10357.
(11) Shimazaki, Y.; Nagano, T.; Takesue, H.; Ye, B.-H.; Tani, F.; Naruta, Y. *Angew. Chem. Int. Ed.* **2004**, *43*, 98-100.
(12) Wada, T.; Tsuge, K.; Tanaka, K. *Inorg. Chem.* **2001**, *40*, 329-337.
(13) Yagi, M.; Kaneko, M. *Chem. Rev.* **2001**, *101*, 21-35.
(14) Poulsen, A. K.; Rompel, A.; McKenzie, C. J. *Angew. Chem. Int. Ed.* **2005**, *44*, 6916-6920.
(15) Liu, F.; Cardolaccia, T.; Hornstein, B. J.; Schoonover, J. R.; Meyer, T. J. *J. Am. Chem. Soc.* **2007**, *129*, 2446-2447.
(16) Loll, B.; Kern, J.; Saenger, W.; Zouni, A.; Biesiadka, J. *Nature* **2005**, *438*, 1040-1044.
(17) Ishikita, H.; Loll, B.; Biesiadka, J.; Saenger, W.; Knapp, E.-W. *Biochemistry* **2005**, *44*, 4118-4124.
(18) Rappaport, F.; Guergova-Kuras, M.; Nixon, P. J.; Diner, B. A.; Lavergne¶, J. *Biochemistry* **2002**, *41*, 8518-8527.
(19) McEvoy, J. P.; Brudvig, G. W. *Chemical Reviews* **2006**, *106*, 4455-4483.
(20) Goussias, C.; Boussac, A.; Rutherford, A. W. *Phil. Trans. R. Soc. Lond. B* **2002**, *357*.
(21) Ferreira, K. N.; Iverson, T. M.; Maghlaoui, K.; Barber, J.; Iwata, S. *Science* **2004**, *303*, 1831-1838.
(22) Yano, J.; Kern, J.; Sauer, K.; Latimer, M. J.; Pushkar, Y.; Biesiadka, J.; Loll, B.; Saenger, W.; Messinger, J.; Zouni, A.; Yachandra, V. K. *Science* **2006**, *314*, 821-825.
(23) Sproviero, E. M.; n, J. A. G.; McEvoy, J. P.; Brudvig, G. W.; Batista*, V. S. *Journal of Chemical Theory and Computation*.
(24) Rutherford, A. W.; Boussac, A. *Science* **2004**, *303*, 1782-1784.
(25) Dempsey, J. L.; Esswein, A. J.; Manke, D. R.; Rosenthal, J.; Soper, J. D.; Nocera, D. G. *Inorganic Chemistry* **2005**, *44*, 6879−6892
(26) Falkenstrom, M.; Johansson, O.; Hammarstrom, L. *Inorganica Chimica Acta* **2007**, *360*, 741-750.

(27) Gust, D.; Moore, T. A.; Lee, S.-J.; Bittersmann, E.; Luttrull, D. K.; Rehms, A. A.; DeGraziano, J. M.; Ma, X. C.; Gao, F.; Belford, R. E.; Trier, T. T. *Science* **1990**, *248*, 199-201.
(28) McGarrigle, E. M.; Gilheany, D. G. *Chemical Reviews* **2005**, *105*, 1564-1598.
(29) Gratzel, M. *Accounts of Chemical Research* **1981**, *14*, 376-384
(30) Gratzel, M. *Inorganic Chemistry* **2005**, *44*, 6841−6851.
(31) Brune, A.; Jeong, G.; Liddell, P. A.; Sotomura, T.; Moore, T. A.; Moore, A. L.; Gust, D. *Langmuir* **2004**, *20*, 8366-8371.
(32) Garza, L. d. l.; Jeong, G.; Liddell, P. A.; Sotomura, T.; Moore, T. A.; Moore, A. L.; Gust, D. *journal of physical Chemistry B* **2003**, *107*, 10252-10260
(33) Hambourger, M.; Brune, A.; Gust, D.; Moore, A. L.; Moore, T. A. *Photochemistry and Photobiology* **2005**, *81*, 1015-1020.
(34) Treadway, J. A.; Moss, J. A.; Meyer, T. J. *Inorg Chem* **1999**, *38*, 4386-4387
(35) Neckel, H.; Labs, D. *Solar Physics* **1984**, *90*, 205-258.
(36) Herek, J. L.; Wohlleben, W.; Cogdell, R. J.; Zeidler, D.; Motzkus, M. *Nature* **2002**, *417*, 533-535.
(37) Gould, S. L.; Kodis, G.; Liddell, P. A.; Palacios, R. E.; Brune, A.; Gust, D.; Moore, T. A.; Moore, A. L. *Tetrahedron* **2006**, *62*, 2074-2096.
(38) Schuster, D. I.; Cheng, P.; Jarowski, P. D.; Guldi, D. M.; Luo, C.; Echegoyen, L.; Pyo, S.; Holzwarth, A. R.; Braslavsky, S. E.; Williams, R. M.; Klihm|, G. *Journal of the American Chemical Society* **2004**, *126*, 7257-7270.
(39) Kuciauskas, D.; Lin, S.; Seely, G. R.; Moore, A. L.; Moore, T. A.; Gust, D.; Drovetskaya, T.; Reed, C. A.; Boyd, P. D. W. *Journal of Physical Chemistry* **1996**, *100*, 15926-15932.
(40) Kodis, G.; Terazono, Y.; Liddell, P. A.; Andreasson, J.; Garg, V.; Hambourger, M.; Moore, T. A.; Moore, A. L.; Gust, D. *Journal of the American Chemical Society* **2006**, *128*, 1818-1827.
(41) Kodis, G.; Herrero, C.; Palacios, R.; o-Ochoa, E. M.; Gould, S.; Garza, L. d. l.; Grondelle, R. v.; Gust, D.; Moore, T. A.; Moore, A. L.; Kennis, J. T. M. *journal of physical Chemistry B* **2004**, *108*, 414-425.
(42) Balzani, V.; Juris, A.; Venturi, M.; Campagna, S.; Serroni, S. *Chemical Reviews* **1996**, *96*, 759-833.
(43) Wasielewski, M. R. *Journal of Organic Chemistry* **2006**, *71*, 5051-5066.
(44) Roger, C.; Muller, M. G.; Lysetska, M.; Miloslavina, Y.; Holzwarth, A. R.; Wurthner, F. *Journal of the American Chemical Society* **2006**, *128*, 6542-6543.
(45) Krueger, B. P.; Scholes, G. D.; Jimenez, R.; Fleming, G. R. *Journal of Physical Chemistry B* **1998**, *102*, 2284-2292.
(46) Ricci, M.; Bradforth, S. E.; Jimenez, R.; Fleming, G. R. *Chemical Physics Letters* **1996**, *259*, 381-390
(47) Frank, H. A.; Bautista, J. A.; Josue, J. S.; Young, A. J. *Biochemistry* **2000**, *39*, 2831-2837
(48) Frank, H. A.; Cua, A.; Chynwat, V.; Young, A.; Gosztola, D.; Wasielewski, M. R. *Photosynthesis Research* **1994**, *41*, 389-395.
(49) Holt, N. E.; Zigmantas, D.; Valkunas, L.; Li, X.-P.; Niyogi, K. K.; Fleming, G. R. *Science* **2005**, *433*, 433-436.
(50) Andrew A. Pascal, Z. L., Koen Broess, Bart van Oort, Herbert van Amerongen, Chao Wang, Peter Horton, Bruno Robert, Wenrui Chang, Alexander Ruban *Nature* **2005**, *436*, 134-137.
(51) Holt, N. E.; Fleming, G. R.; Niyogi, K. K. *Biochemistry* **2004**, *43*, 8281-8289.

(52) Gould, S. L.; Kodis, G.; Palacios, R. E.; Garza, L. d. l.; Brune, A.; Gust, D.; Moore, T. A.; Moore, A. L. *journal of physical Chemistry B* **2004**, *108*, 10566-10580
(53) Keene, F. R. *Coordination Chemistry Reviews* **1997**, *166*, 121-159.
(54) Balzani, V.; Juris, A. *Coordination Chemistry Reviews* **2001**, *211*, 97-115.
(55) Meyer, T. J. *Pure Appl. Chem.* **1988**, *58*, 1193-1206.
(56) Hang, M.; Huynh, V.; Dattelbaum, D. M.; Meyer, T. J. *Coordination Chemistry Reviews* **2005**, *249*, 457–483.
(57) Spiccia, L.; Deacon, G. B.; Kepert, C. M. *Coordination Chemistry Reviews* **2004**, *248*, 1329-1341.
(58) Hoffman, M. Z. *journal of Physical Chemistry* **1988**, *92*, 3458-3464.
(59) Young, R. C.; Meyer, T. J.; Whitten, D. G. *Journal of the American Chemical Society* **1975**, *97*, 4781-4782.
(60) Alstrum-Acevedo, J. H.; Brennaman, M. K.; Meyer, T. J. *Inorg Chem* **2005**, *44*, 6802-6827.
(61) Anderson, P. A.; Keene, F. R.; Meyer, T. J.; Moss, J. A.; Strouse, G. F.; Treadway, J. A. *J. Chem. Soc., Dalton Trans.* **2002**, 3820–3831
(62) Damrauer, N. H.; Cerullo, G.; Yeh, A. T.; Boussie, T. R.; Shank, C. V.; McCusker, J. K. *Science* **1997**, *275*, 54-57.
(63) Rillema, D. P.; Blanton, C. B.; Shaver, R. J.; Jackman, D. C.; Boldaji, M.; Bundy, S.; Worl, L. A.; Meyer, T. J. *Inorganic Chemistry* **1992**, *31*, 1600-1606
(64) Caspar, J. V.; Meyer, T. J. *Journal of the American Chemical Society* **1983**, *105*, 5583-5590.
(65) Gafney, H. D.; Adamson, A. W. *J. Am. Chem. Soc.* **1972**, *94*, 8238-8239.
(66) Vass, I.; Styring, S. *Biochemistry* **1991**, *30*, 830-839.
(67) Shan, B.-Z.; Zhao, Q.; Goswami, N.; Eichhorn, D. M.; Rillema, D. P. *Coordination Chemistry Reviews* **2001**, *211*, 117-144.
(68) Ciana, L. D.; Hamachi, I.; Meyer, T. J. *Journal of Organic chemistry* **1989**, *54*, 1731-1735.
(69) Garelli, N.; Vierling, P. *Journal of Organic Chemistry* **1992**, *57*, 3046-3051.
(70) McCafferty, D. G.; Bishop, B. M.; Wall, C. G.; Hughes, S. G.; Mecklenberg, S. L.; Meyer, T. J.; Erickson, B. W. *Tetrahedron* **1995**, *51*, 1093-1106.
(71) Garcia, C. G.; Lima, J. F. d.; Iha, N. Y. M. *Coordination Chemistry Reviews* **2000**, *196*, 219 – 247
(72) Sprintschnik, G.; Sprintschnik, H. W.; Kirsch, P. P.; Whitten, D. G. *Journal of the American Chemical Society* **1977**, *99*, 4947-4954.
(73) Andenon, P. A.; Strouse, G. F.; Treadway, J. A.; Keene, F. R.; Meyer, T. J. *Inorganic Chemistry* **1994**, *33*, 3863-3864.
(74) Collin, J.-P.; Kayhanian, R.; Sauvage, J.-P.; Calogero, G.; Barigelletti, F.; Ciancand, A. D.; Fischerc, J. *Chemical Communications* **1997**, 775-776.
(75) Fanni, S.; Keyes, T. E.; O'Connor, C. M.; Hughes, H.; Wang, R.; Vos, J. G. *Coordination Chemistry Reviews* **2000**, *208*, 77-86.
(76) Baldwin, M. J.; Pecoraro, V. L. *Journal of the American Chemical Society* **1996**, *118*, 11325-11326.
(77) Carra, C.; Iordanova, N.; Hammes-Schiffer, S. *Journal of the American Chemical Society* **2003**, *125*, 10429-10436.
(78) Sjodin, M.; Styring, S.; Akermark, B.; Sun, L.; Hammarstrom, L. *Phil. Trans. R. Soc. Lond. B* **2002**, *357*, 1471–1479.

(79) Sjödin, M.; Styring, S.; Åkermark, B.; Sun, L.; Hammarström, L. *J. Am. Chem. Soc.* **2000**, *122*, 3932-3936.
(80) Hoganson, C. W.; Babcock, G. T. *Science* **1997**, *277*.
(81) Westphal, K. L.; Tommos, C.; Cukier, R. I.; Babcock, G. T. *Curr. Opin. Plant. Biol.* **2000**, *3*, 236-242.
(82) Ruttinger, W.; Dismukes, G. C. *Chemical Reviews* **1997**, *97*, 1-24.
(83) Ruettinger, W.; Yagi, M.; Wolf, K.; Bernasek, S.; Dismukes, G. C. *Journal of the American Chemical Society* **2000**, *122*, 10353-10357.
(84) Limburg, J.; Vrettos, J. S.; Chen, H.; Paula, J. C. d.; Crabtree, R. H.; Brudvig, G. W. *Journal of the American Chemical Society* **2001**, *123*, 423-430.
(85) Limburg, J.; Vrettos, J. S.; Liable-Sands, L. M.; Rheingold, A. L.; Crabtree, R. H.; Brudvig, G. W. *Science* **1999**, *283*.
(86) Poulsen, A. K.; Rompel, A.; McKenzie, C. J. *Angewandte Chemie. Int. Ed* **2005**, *44*, 2-7.
(87) Shimazaki, Y.; Nagano, T.; Takesue, H.; Ye, B.-H.; Tani, F.; Naruta, Y. *Angewandte Chemie. Int. Ed* **2004**, *43*, 98 –100.
(88) Gersten, S. W.; Samuels, G. J.; Meyer, T. J. *Journal of the American Chemical Society* **1982**, *104*, 4029-4030.
(89) Yagi, M.; Kaneko, M. *Chemical Reviews* **2001**, *101*, 21-35.
(90) Huang, P.; Hogblom, J.; Anderlund, M. F.; Sun, L.; Magnuson, A.; Styring, S. *Journal of Inorganic Biochemistry* **2004**, *98*, 733-745.
(91) Magnuson, A.; Berglund, H.; Korall, P.; Hammarstrom, L.; Akermark, B.; Styring, S.; Sun, L. *Journal of the American Chemical Society* **1997**, *119*.
(92) Sun, L.; Berglund, H.; Davydov, R.; Norrby, T.; Hammarstrom, L.; Korall, P.; Borje, A.; Philouze, C.; Berg, K.; Tran, A.; Andersson, M.; Stenhagen, G.; rtensson, J. M.; Almgren, M.; Styring, S.; Akermark, B. *Journal of the American Chemical Society* **1997**, *119*.
(93) Burdinski, D.; Wieghardt, K.; Steenken, S. *Journal of the American Chemical Society* **1999**, *121*, 10781-10787.
(94) Romain, S.; Lepretre, J.-C.; Chauvin, J.; Deronzier, A.; Collomb, M.-N. *Inorg Chem* **2007**, *46*, 2735−2743.
(95) Vrettos, J. S.; Brudvig, G. W. *Phil. Trans. R. Soc. Lond. B* **2002**, *357*, 1395-1405.
(96) Chen, H.; Tagore, R.; Das, S.; Incarvito, C.; J. W. Faller; Crabtree, R. H.; Brudvig, G. W. *Inorg Chem* **2005**, *44*, 7661-7670.
(97) Romain, S.; Baffert, C.; Dumas, S.; Chauvin, J.; Lepretre, J.-C.; Daveloose, D.; Deronzier, A.; Collomb, M.-N. *Dalton Trans.* **2006**, 5691–5702.
(98) Campbell, E. J.; Nguyen, S. T. *Tetrahedron Letters* **2001**, *42*, 1221-1225.
(99) Campbell, A. K.; Lashley, R. M.; Wyatt, K. J.; Nantz, H. M.; Britt, R. D. *Journal of the American Chemical Society* **2001**, *123*, 5710-5719.
(100) Pellegrin, Y.; Quaranta, A.; Dorlet, P.; Charlot, M. F.; Leibl, W.; Aukauloo, A. *Chemistry A European Journal* **2005**, *11*, 3698 – 3710

6. Experimental Section

6.1. Antennas

6.1.1. Triad

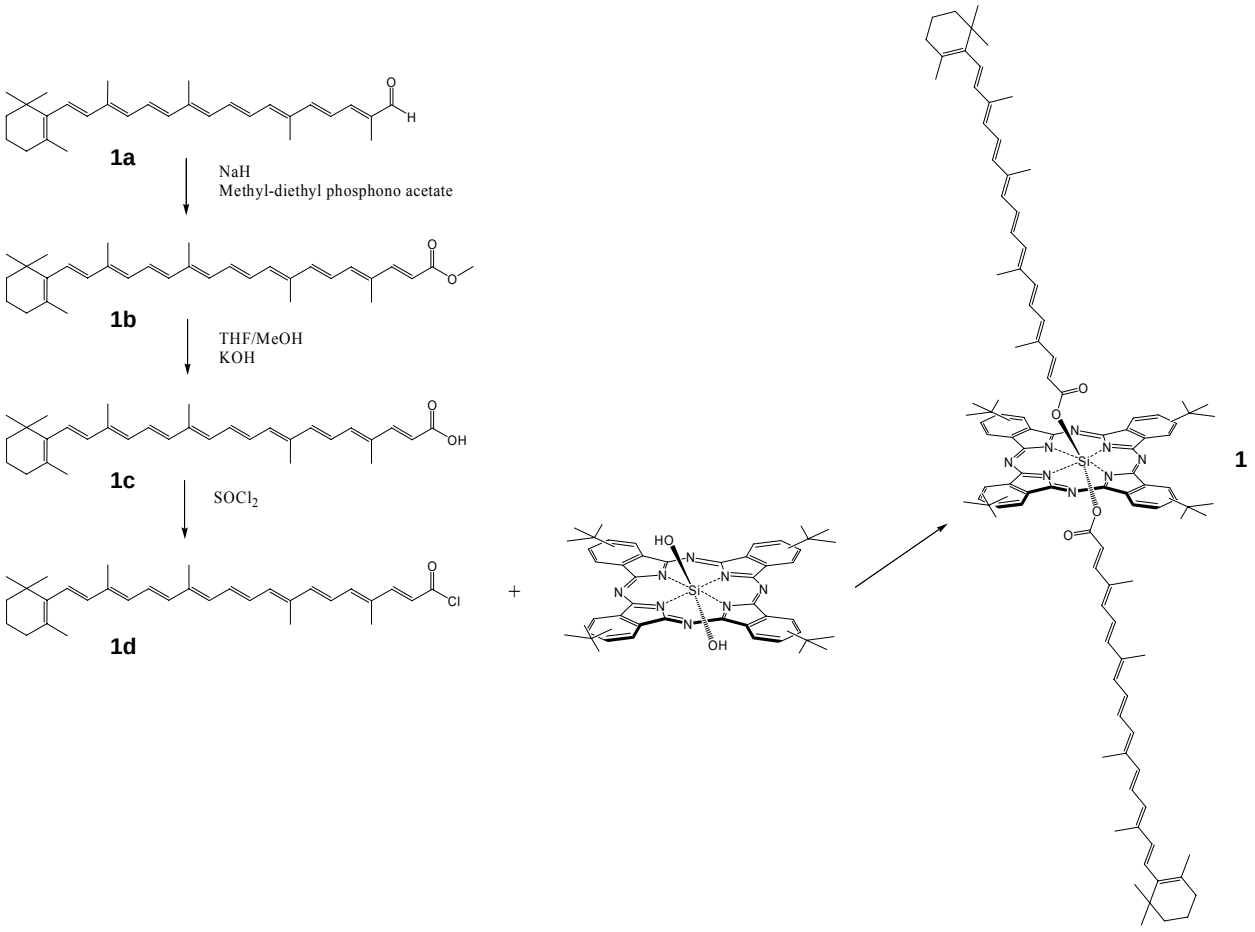

Synthesis of methyl-6'-apo-β-caroten-6'-oate (1b) was performed in 84 % yield by reacting 8'-apo-β-caroten-8'-al (1a) (400 mg, .96 mmol) with methyl-diethyl phosphono acetate (430 mg, 1.92 mmol, 2 eq) in 20 mls THF. To this mixture, 20 mls of sodium methoxide (216 mg, 45 mmol, 2 eq) were added drop wise at room temperature and the solution was allowed to react at until no starting compound was present as shown by TLC. The mixture was extracted with water and methylene chloride. The organic phase dried with $MgSO_4$, filtered, and the solvent removed

by rotary evaporation. The resulting product was recrystallized from a mixture of methanol and dichloromethane to yield 430 mg (90% yield). The resulting ester was transformed into its carboxylic acid derivative by basic hydrolysis (KOH, MeOH). (1c)

The corresponding acid chloride (**1d**) was obtained by dissolving 95 mgs of the carotenoid in 5 mls of a 4:1 toluene:pyridine solution and adding 6 drops of thionyl chloride. The reaction mixture was stirred under a nitrogen atmosphere for 10 min at which time the solvents were evaporated under high vacuum. A solution of Silicon-tetra-tert-butyl-phthalocyanin **4** (20.4 mg .025 mmoles) in 2-picoline (4mL, dried from CaH_2) was added to the carotenoid acid chloride. Stirring continued under a nitrogen atmosphere for 4 hours at 60°C. At this time 30 mg of DMAP was added and the mixture was allowed to continue for another 24 hours. Purification of the mixture was done by column chromatography (6:4 CH_2Cl_2: Hexanes) and yielded 16.2 mg of final product **5** (37.8 % yield). MALDI/TOF mass spectrometry yields a parent peak of 1679 m/z $[M]^+$ and a base peak of 1238 m/z [M-441 (carotene)]$^+$. UV/Vis (CH_2Cl_2) of the triad shows maxima in nm at 684(p), 653(p), 615(p), 486(c), 457 (c), 434(c), 361(p), and 340(p).

6.1.2. Dyad

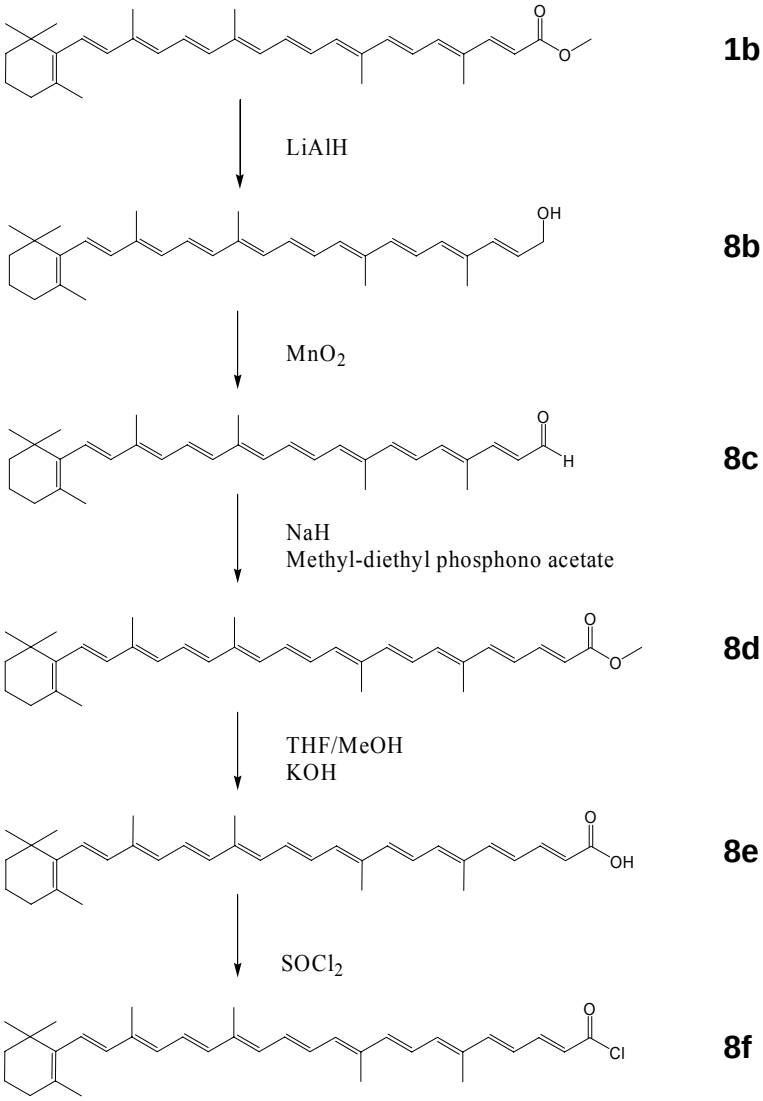

Methyl-6'-apo-β-caroten-6'-oate (1b) was synthesized as previously explained. In order to transform the ester functionality into the desired aldehyde that would allow for the next Wittig reaction, this compound (200 mg, .45 mmol) was reduced into its corresponding alcohol, 6'-apo-β-caroten-6'-ol (8b), by treatment with excess DIBAL-H in hexanes (2.5 mls) at 0°C. The reaction was monitored by TLC until no further starting material was present. The reaction was quenched by extraction with water and dichloromethane.

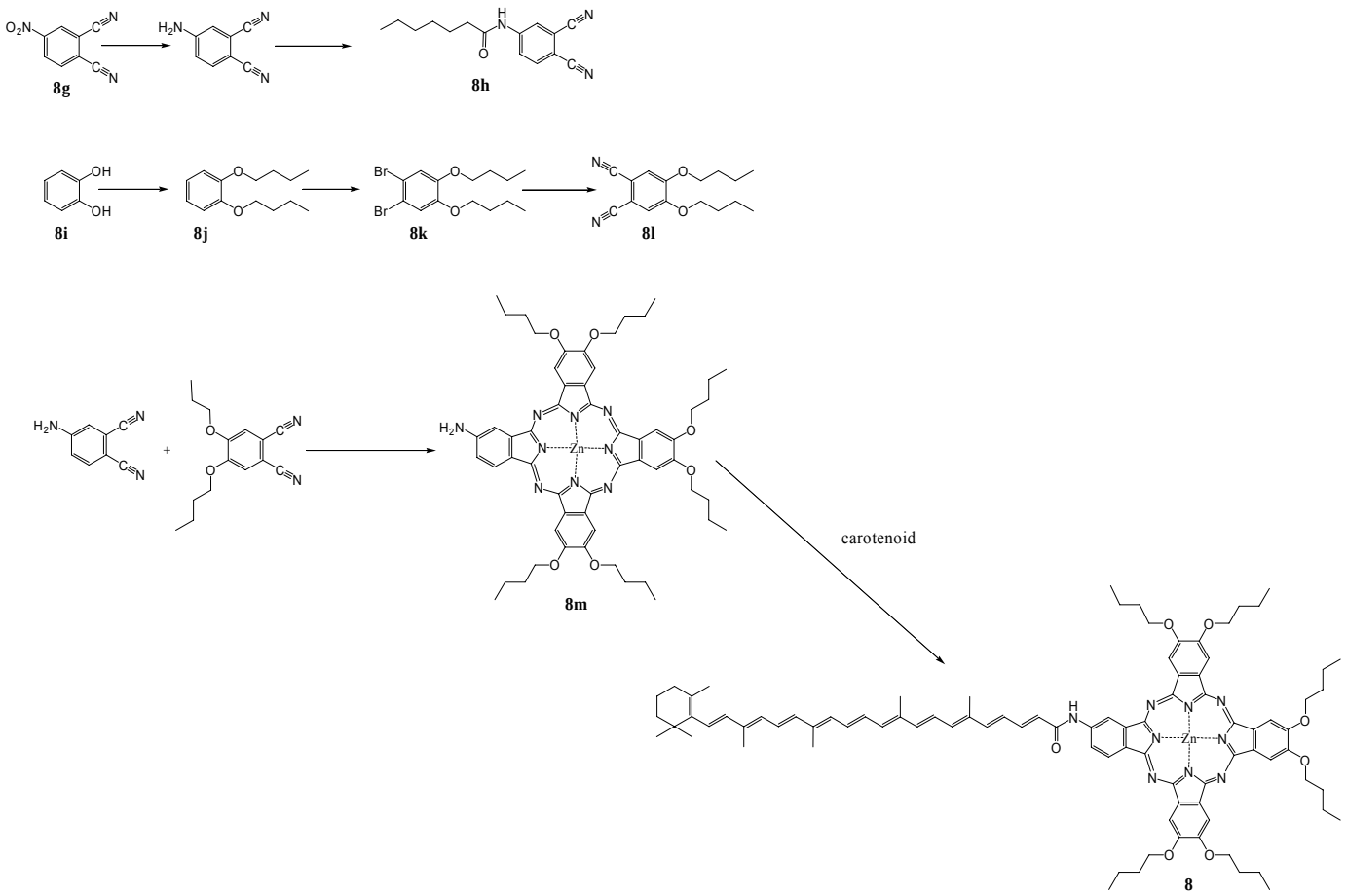

6'-apo-β-caroten-6'-al (8c) was obtained by mixing the alcohol **8b** in 40 mls acetone and 1.50 g MnO_2 and allowing them to react overnight. At this time the reaction was filtered, and put through a silica column with CH_2Cl_2 as eluent.

The following three molecules, methyl-4'-apo-β-caroten-4'-oate (8d), 4'-apo-β-caroten-4'-acid (8e), and 4'-apo-β-caroten-4'-acid chloride (8f) were obtained following the procedures above.

The AB_3 type phthalocyanin was synthesized by reacting a statistical amount of the two different phthalonitriles presented below.

4-Hexanamidophthalonitrile (8h). A solution of 4-nitrophthalonitrile (8g) (5.15 g, 29.77 mmol) in methanol (125 ml) was flushed with N_2, and a portion of 10% Pd/C (0.515 g) was added. This

mixture was then stirred under H_2 (50 psi) for 1 h. The catalyst was removed by filtration through celite, and the solvent was distilled under vacuum to obtain the desired amine (3.66 g, 86% yield). A portion of the amine obtained (3.60 g, 25.17 mmol) was dissolved in pyridine (90 ml), then hexanoyl chloride (8.6 ml, 61.52 mmol) was added. The mixture was stirred under N_2 for 2 h. The solvent was distilled under vacuum, and the mixture was redissolved in CH_2Cl_2, washed with 0.1 M HCl five times, and washed with 5% $NaHCO_3$ three times to neutral pH. The solution was dried over $MgSO_4$ and filtered, and the solvent was distilled under vacuum. The crude product was chromatographed on silica gel (CH_2Cl_2/MeOH 5%) and 4.30 g (71% yield) of the desired nitrile was obtained. ^{1}H-NMR (300 MHz, $CDCl_3$) δ 0.92 (3H, t, -$CO(CH_2)_4CH_3$), 1.36 (4H, m, -$CO(CH_2)_2CH_2CH_2CH_3$), 1.74 (2H, q, -$COCH_2CH_2(CH_2)_2CH_3$), 2.43 (2H, t, -$COCH_2(CH_2)_3CH_3$), 7.62 (1H, s, -NHCO-), 7.74 (1H, d, J = 9 Hz, Bz 3-H), 7.87 (1H, dd, J = 9 Hz, 2Hz Bz 5-H), 8.18 (1H, d, J = 2 Hz, Bz 6-H).

1,2-Dibutoxybenzene (8j). Catechol (technical grade) (13.2 g, 120 mmol) was dissolved in 120 ml of DMF. Potassium carbonate (41.4 g, 300 mmol) and *n*-butylbromide (49.2 g, 360 mmol) were added, and the reaction mixture was stirred at 95°C under N_2 for 24 h. Portions of potassium carbonate (30 g, 217 mmol) and *n*-butylbromide (30 g, 219 mmol) were added, and the stirring continued for 3 h. Potassium carbonate (30 g, 217 mmol) was added, and the reaction was continued overnight. The mixture was allowed to cool down to room temperature and ether (1 liter) was added. The organic layer was washed with water six times. The organic layer was dried over magnesium sulfate, the solvent was distilled under vacuum, and the liquid obtained was fractionally distilled at reduced pressure collecting the fraction between 69°C and 73°C. This fraction consisted of pure 1,2- dibutoxybenzene (19.05 g, 70.8% yield). ^{1}H-NMR (300 MHz,

$CDCl_3$) δ(6H, t, - $OCH_2CH_2CH_2CH_3$), 1.52 (4H, s, -$OCH_2CH_2CH_2CH_3$), 1.81 (4H, q, -$OCH_2CH_2CH_2CH_3$), 4.01 (4H, t, -O-$CH_2CH_2CH_2CH_3$), 6.90 (4H, s, Bz 3,4,5,6-H).

1,2-Dibromo-4,5-dibutoxybenzene (8k). A portion of 1,2-dibutoxybenzene (19.0 g, 86 mmol) was dissolved in CH_2Cl_2 (200 ml) and cooled to 0°C under N_2. Bromine (9.6 ml, 187 mmol) was added slowly, half at 0°C and the other half at room temperature. The reaction mixture was stirred for 2 h. The solution was flushed with N_2 and washed with a 10% $NaHSO_3$ solution and then with 10% $NaHCO_3$ solution. The organic layer was dried over Na_2SO_4, and the solvent was distilled under vacuum to yield 31.71 g (95.6%) of the desired dibromobenzene. ^{1}H-NMR (300 MHz, $CDCl_3$)δ (6H, t, -$OCH_2CH_2CH_2CH_3$), 1.48 (4H, s, -$OCH_2CH_2CH_2CH_3$), 1.78 (4H, q, -$OCH_2CH_2CH_2CH_3$), 3.95 (4H, t, -$OCH_2CH_2CH_2CH_3$), 7.06 (2H, s, Bz 3,6-H).

4,5-Dibutoxyphthalonitrile (8l). A solution of 1,2-dibromo-4,5-dibutoxybenzene (31.7 g, 83.4 mmol) in DMF (400 ml) was stirred and CuCN (22.8 g, 255 mmol) was added. The mixture was heated to reflux under N_2 for 6 h. The mixture was cooled to room temperature and poured into 1.1 liter of concentrated NH_4OH and bubbled with air for 20 h. The mixture was filtered, and the solid obtained was washed with 10% NH_4OH until the filtrate was clear, then with it was washed with water to neutral pH and air-dried. The crude product was extracted with hexanes in a soxhlet for 1 week. The solvent was reduced to 200 ml and filtered. The solid was recrystallized from CH_2Cl_2 and $CHCl_3$/hexanes and decolorized with activated carbon. The desired dinitrile (10.53 g) was obtained in 46% yield. ^{1}HNMR (300 MHz, $CDCl_3$) δ1.00 (6H, t, -$OCH_2CH_2CH_2CH_3$), 1.51 (4H, s, -$OCH_2CH_2CH_2CH_3$), 1.85 (4H, q, -$OCH_2CH_2CH_2CH_3$), 4.06 (4H, t, -O-$CH_2CH_2CH_2CH_3$), 7.12 (2H, s, Bz 3,6-H).

Zinc-2-Amino-9,10,16,17,23,24-Hexabutoxyphthalocyanine (8m). A portion of the hexanamidophthalocyanine obtained in the above reaction (290 mg, 0.258 mmol) was dissolved in 40 ml of THF and 40 ml of a saturated methanolic solution of KOH. The solution was heated to 75°C and stirred overnight under N_2 after the addition of another 10 ml of THF. The reaction mixture was diluted with chloroform and washed with water (three times). The organic layer was dried over Na_2SO_4 and filtered, and the solvent was distilled at reduced pressure. The desired zinc 2-amino-9,10,16,17,23,24- hexabutoxyphthalocyanine (214 mg) was obtained in 81% yield.

Dyad 8. The 4'-apo-β-caroten-4'-oic acid (49 mg, 0.11mmole) was dissolved in 6 ml of toluene and 2 ml of pyridine. One drop of thionyl chloride was added, and the mixture was stirred under N_2 for 15 min. The solvent was distilled under vacuum and the residue kept under vacuum for an extra 15 min. The residue was redissolved in 2.5 ml of pyridine and 6 ml of dry chloroform. The solution of the aminophthalocyanine prepared above (100 mg, 0.1mol) dissolved in 6 ml of chloroform was added to the solution of the acid chloride and the mixture was stirred overnight under N_2. The reaction mixture was diluted with chloroform, washed with water, and dried under vacuum. The product was purified by flash chromatography (silica, chloroform-methanol 0.2%). A second column (silica, $CHCl_3$) was necessary to obtained 73 mg (52% yield) of pure carotenophthalocyanine. ^{1}H-NMR (500 MHz, DMSO/$CDCl_3$) δ 0.96 - 0.98 (6H, m, Car 16-CH_3, Car 17-CH_3), 1.12 - 1.21 (18H, m, -$OCH_2CH_2CH_2CH_3$), 1.41 (2H, m, Car 2-CH_2), 1.56 (2H, m, Car 3-CH_2), 1.65 (3H, s, Car 18-CH_3), 1.75 (12H, s, -$OCH_2CH_2CH_2CH_3$), 1.91 (3H, s, Car 19-CH_3), 1.92 (3H, s, Car 20-CH_3), 1.95 - 2.00 (5H, m, Car-4, Car 20'-CH_3), 2.08 (15H, m, -$OCH_2CH_2CH_2CH_3$, Car 19'-CH_3), 4.53 - 4.57 (12H, m, -O-$CH_2CH_2CH_2CH_3$), 6.05 - 7.32 (16H, m, Car = CH-), 8.29 (1H bs Pc 3-H), 8.65 - 8.73 (6H, m, Pc 8,11,15,18,22,25-H), 9.19 (1H, bs, Pc 4-H), 9.75 (1H, s, Pc 1-H), 10.37 (1H, s, -NHCO-). MS *m/z* 1491.3 $(M)^+$;

6.2. Ruthenium Complexes

6.2.1. Chromophores

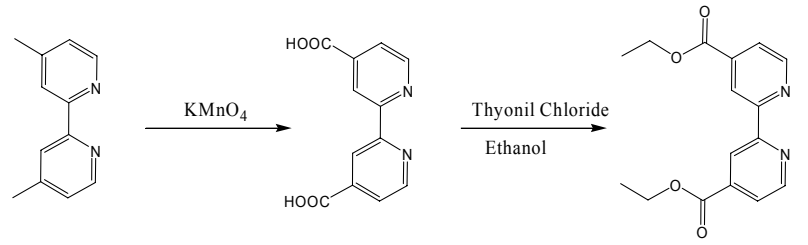

10a **10b**

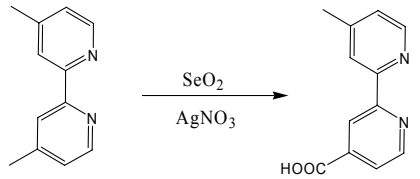

11a

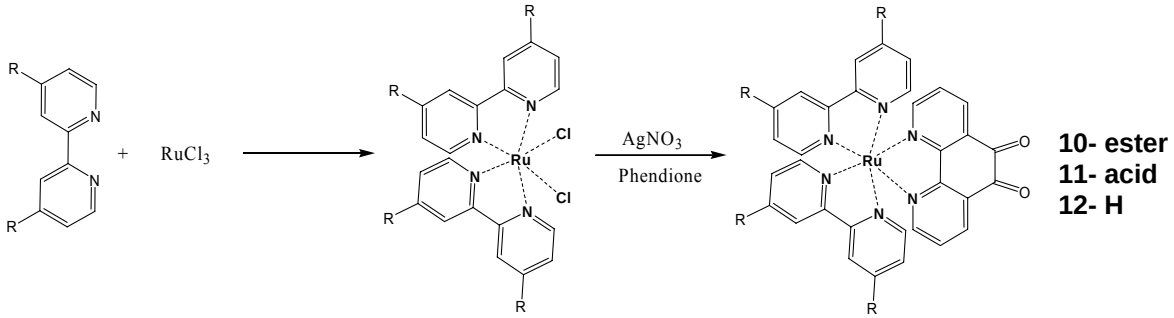

13

4,4'-Dicarboxy-2,2'-bipyridine (10a). 4,4'-Dimethyl-2,2'-bipyridine (4.23 g, 22.98 mmol) was heated to reflux with potassium permanganate (12.69 g, 80.5 mmol, 3.5 eq) in 200 mls water overnight. At this time the solution was filtered to separate a precipitate which had formed. The solution was extracted with ether and the product was obtained by precipitation with hydrochloric acid to yield 1.61 g (29 % yield).

H^1 NMR. (400 MHz, δ, MeOH): H^1 NMR. (400 MHz, δ, DMSO): 8.92 (s, 1H), 8.90 (d, J = 6 Hz, 1H), 7.95 (d, J = 5.6 Hz, 1H).

MS (ESI) = 242 m/z, $[M-H]^+$

4,4'-Diethyl ester-2,2'-bipyridine (10b). 4,4'-Dicarboxy-2,2'-bipyridine (1.27 g, 5.20 mmol) was dissolved in 10 mls thyonil chloride and the reaction was heated to 60°C for 5 hours. Consequently, the solvent was evaporated under vacuum and the resulting solid was redissolved in 10 mls ethanol and .5 mls TEA. The mixture was stirred at reflux for three hour, the solvent evaporated, and the solid suspended in water in order to get rid of the basic salts. Extraction with water and crystallization with ethyl acetate yielded 976 mg of product. (63% yield)

H^1 NMR. (400 MHz, δ, DMSO): 8.95 (s, 1H), 8.88 (d, J = 6 Hz, 1H), 7.92 (d, J = 5.6 Hz, 1H), 4.48 (q, J= 7 Hz, 2H), 1.41 (t, J=7 Hz, 3H).

MS (ESI) = 301 m/z, $[M+H]^+$

4'-Methyl-2,2'-bipyridine-4-carboxylic acid (11a). SeO_2 (2.95 g, 26.04 mmol, 1.2 eq) and 4, 4'-Dimethyl-2,2'-bipyridine (4.00 g, 21.7 mmol) were heated at reflux in 1,4 dioxane for 24 hours. At this time, the solution was allowed to reach room temperature and filtered through a pad of celite. The solvent was removed under reduced pressure and the resulting solid was redissolved in 160 mls ethanol. A solution of $AgNO_3$ (4.00 g, 23.87 mmol, 1.1 eq) in 40 mls H_2O were added. 100 mls of 1M NaOH were added over 20 min and the solution turned black immediately. The mixture was stirred for 12 hours and filtered through a frit in order to get rid of unreacted silver. The solution was extracted with CH_2Cl_2 and the basic solution was adjusted to pH=3.5 with 4 N 1:1 HCl : acetic acid which produced a precipitate. The solution was allowed to sit at -20°C overnight, and then was filtered, vacuum dried and purified by soxhlet extraction with acetone for 72 hours to yield 1.53 g of product. (33% yield)

H^1 NMR. (400 MHz, δ, DMSO): 8.83 (d, J = 6 Hz, 1H), 8.80 (s, 1H), 8.56 (d, J = 6 Hz), 8.25 (s, 1H), 7.84 (d, J = 6 Hz, 1H), 7.31 (d, J = 6 Hz, 1H).

MS (ESI) = 215 m/z, $[M+H]^+$

cis-dichlorobis(bipyridine) Ruthenium (13). In a typical reaction 2.00 g of $RuCl_3$ (9.66 mmol), 2.80 g LiCl (67.63 mmol, 7 eq), and 3.30 g 2,2' bipyridine (21.25 mmol, 2.2 eq) were dissolved in 20 mls dry DMF. The mixture was refluxed overnight under an Ar atmosphere. At this time the reaction was allowed to go to room temperature and 100 mls acetone were added. The solution was placed at -20°C overnight and the resulting precipitate filtered through a frit. The solid was washed with cold acetone.

H^1 NMR. (400 MHz, δ, DMSO):8.90 (d, J= 7 Hz, 2H), 8.10 (t, J=8.0 Hz, 2H), 7.72 (d, J=8.0 Hz, 2H), 7.52 (t, J=8.2 Hz, 2H).

MS (ESI) = 242.2 $[M]^{2+}$, 448.9 $[M-Cl]^+$, 484.1 $[M]^+$.

$(Bipyridine)_2$-Phendione Ruthenium (12). 484 mg of Ru-bipyridine dichloride (1 mmol, 1 eq) were reacted with 338 mg of silver nitrate (2 mmol, 2 eq) in methanol for 2 hours. The solution was filtered in order to remove the silver salt, and the filtrate was evaporated under reduced pressure. The solid was re-dissolved in ethanol and one equivalent of phendione (1) (210 mg, 1 mmol) was added. The solution was refluxed in the dark for three hours. At this time the solvent was evaporated, the remaining solid re-dissolved in a minimum amount of methanol, and the desired compound was precipitated by drop wise addition of a saturated aqueous solution of sodium hexafluorophosphate (275 mg, 44%). H^1 NMR. (400 MHz, δ, DMSO): 8.85 (d, J= 8.0 Hz, 4H, H_4), 8.54 (d, *J*=7.68 Hz, 2H, H_c), 8.21-8.16 (m, 4H, H_3), 7.94 (d, *J*=5.6 Hz, 2H, H_a), 7.75-7.74 (dd, *J*=8.9 Hz, 4H, H_1), 7.70-7.68 (dd, J = 5.7 Hz, 2H, H_B), 7.57-7.52 (m, 4H, H_2).

MS (ESI) = 312.1 $[M]^{2+}$, 624.1 $[M]^{+}$, 769.1 $[M+PF_6]^{+}$.

Tetra ethyl ester (Bipyridine)$_2$-Phendione Ruthenium (10). Synthesis of this compound was done following the above procedure using 4, 4' diethyl ester bipyridine. (65% yield).

H^1 NMR. (400 MHz, δ, DMSO): 9.34 (d, J= 8.0 Hz, 4H, H_4), 8.58 (d, *J*=7.68 Hz, 2H, H_C), 8.00-7.92 (m, 4H, H_1-H_2), 7.80 (d, *J*=5.6 Hz, 2H, H_A), 7.70-7.68 (dd, J = 7.6 Hz, 2H, H_B), 4.45 (q, J = 7.1 Hz, 8 H, CH_2-H), 1.39 (t, J = 7.5 Hz, 12H, CH_3-H).

MS (ESI) = 456.1 $[M]^{2+}$, 912.2 $[M]^{+}$.

6.2.2. Phenols

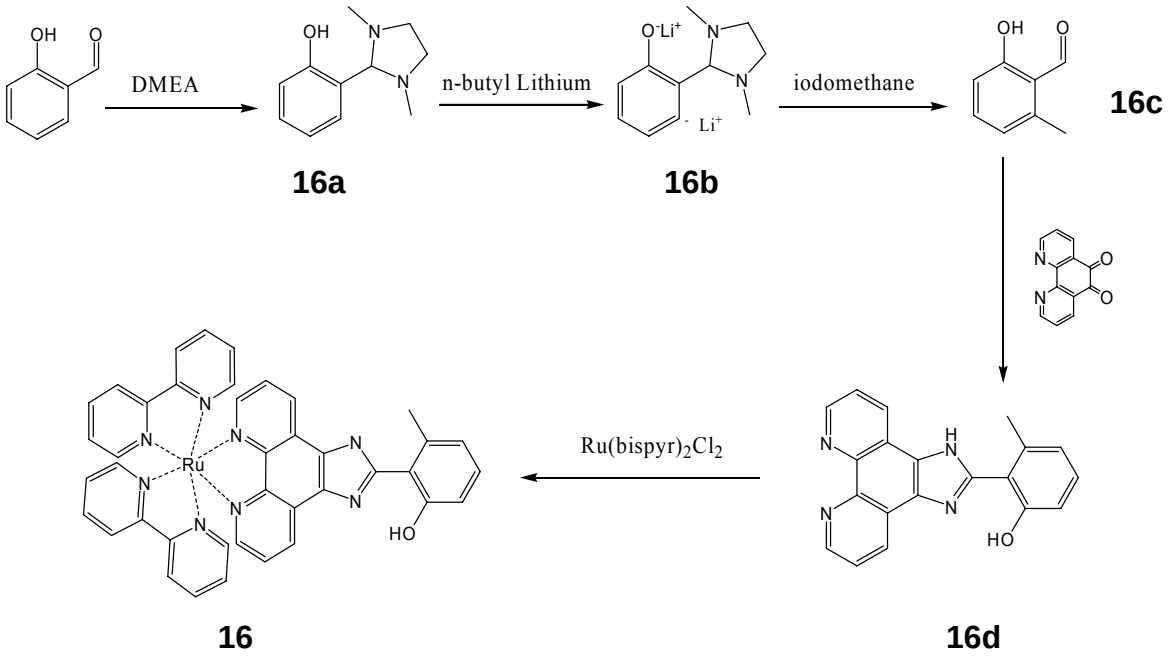

16a. Salicylaldehyde (1.0 g, 8.20 mmol) and DMEDA (1.05 g, 11.8 mmol, 1.2 eq) were mixed in 10 mls dry ethanol and allowed to react overnight at room temperature. The next morning, 5.00 g of sodium sulfate were added and the mixture was stirred for an additional 30 minutes. At this

time the solution was filtered and the solvent evaporated under reduced pressure. The resulting imidazoline product resulted as a yellow oil which yielded 1.57 g. (82 %)

H^1 NMR. (400 MHz, δ, DMSO): 7.21 (t, J = 8 Hz, 1H, Ar H 3), 6.98 (d, J = 7.5 Hz, 1H, Ar H1), 6.85 (d, J= 8 Hz, 1H, Ar H 4), 6.78 (t, J = 7.5, 1 H, Ar H 2), 3.42 (s, 1H, CH), 3.40 (d, J = 4 Hz, 2H, CH_2), 2.57 (d, J = 4 Hz, 2H, CH_2), 2.28 (s, 6H, CH_3).

MS (ESI) = 191 m/z $[M-H]^+$

16b. The resulting imidazoline (1.30 g, 6.77 mmol) was dissolved in 40 mls ether and 2.73 g triethylamine (27.08 mmol, 4 eq) were added. To this mixture n-Butyl Lithium (1.73 g, 27.08 mmol, 4 eq) was added over 2 hours and the reaction was allowed to stir for 3 hours afterwards. 7.8 g of Iodomethane (54.16 mmol, 8 eq) were added over 15 minutes and the reaction was stirred under Ar overnight.

16c. Next morning the reaction was quenched by adding 50 mls of a 2 M HCL solution. The solution was extracted with dichloromethane and purified via column chromatography (silica, CH_2Cl_2) to yield 900 mg of product (87 % yield).

H^1 NMR. (400 MHz, δ, DMSO): 11.26 (s, 1 H Ph-OH), 9.88 (s, 1H, Ph-CHO), 7.41 (m, J = 8 Hz, 2 H, Ar H's 4,6), 6.93 (t, J = 8 Hz, Ar-H 5), 2.27 (s, 3 H, methyl).

MS (ESI) = 137 m/z $[M+H]^+$.

16d. Coupling of compound 2 with phenantroline was done via a Steck Day coupling reaction. In a typical reaction 210 mg of phendione (1 eq, 1.00 mmol) were mixed with 150 mg of methyl salicylaldehyde (1.1 eq, 1.10 mmol) in 3 mls acetic acid. The mixture was stirred at 80^0C for 30 minutes, and 1.54 g of ammonium acetate (20 eq, 20 mmol) were added. The temperature was

raised to 100^0C and the solution was allowed to stir. After one hour a precipitate formed which after cooling was filtered through a frit funnel and washed with copious amounts of acetone and water. The product was collected and dried to yield 120 mg. (37% yield)

H^1 NMR. (400 MHz, δ, DMSO): 9.03 (d, J=8 Hz, 2H,Ar H A), 8.92 (d, J= 8 Hz, 2H, Ar H C), 8.05 (d, J = 8.5 Hz, 1 H, Ar H 6) 7.84 (dd, J=8 Hz, 2 H, Ar H B), 7.52 (d, J=7 Hz, 1 H, Ar H 4), 6.93 (t, J = 8 Hz, 1 H, Ar-H 5), 2.27 (s, 3 H, methyl).

MS (ESI) = 327.1 $[M+H]^+$.

16. Insertion of Ruthenium into the phenanthroline cavity was performed following the procedure for compound **12**. The product was purified by eluting through a short alumina column with acetonitrile as eluent to yield 44 % yield.

H^1 NMR (400 MHz, δ, DMSO): 8.98 (d, J = 7.6 Hz, 2H, Phen-H_c), 8.87 (d, J = 8 Hz, 2H, bpy-H_4), 8.83 (d, J = 8 Hz, 2H, bpy-$H_{4'}$) 8.20 (t, J = 7 Hz, 2H, bpy-H_3), 8.09 (t, J = 7 Hz, 2H, bpy-$H_{3'}$), 8.03 (m, 1H, Ar-H_a), 7.95-7.90 (m, 4H, Phen-H_{A-C}), 7.80 (m, 2H, bpy-H_1), 7.65 (m, 2H, bpy-$H_{1'}$), 7.48 (m, 2H, bpy-H_2), 7.37 (m, 2H, bpy-$H_{2'}$), 7.30 (m, 1H, Ar-H_c), 6.99 (m, 1H, Ar-H_b), 2.29 (s, 3H, H-methyl).

MS (ESI) = 370.1 $[M]^{2+}$, 739.1 $[M-H]^+$

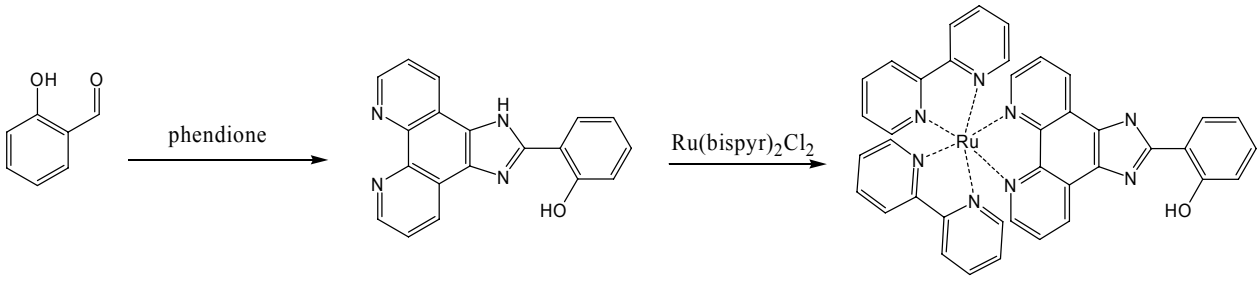

14a **14**

14a. In a typical reaction 210 mg of phendione (1.00 mmol) were and 134 mg of salicylaldehyde (1.1 mmol, 1.1 eq) were dissolved in 3 mls acetic acid. The reaction was heated to 80°C for 30 min and at this time 1.54 g of ammonium acetate (20 mmol, 20 eq) were added. The reaction turned reddish brown immediately and the temperature was raised to 100°C and allowed to stir for three hours. At this time the solution was allowed to return to room temperature and the product was precipitated by drop wise addition of ammonium hydroxide. The resulting product was filtered through a frit, washed repeatedly with water and ether and collected to yield 287 mg (92 % yield)

H^1 NMR (400 MHz, δ, DMSO): 9.03 (d, J=8 Hz, 2H,Phen-H), 8.94 (d, J= 8 Hz, 2H, Phen-H), 8.19 (d, J = 8.5 Hz, 1 H, Ar-H) 7.86 (dd, J=8 Hz, 2 H, Phen-H), 7.40 (t, J=7 Hz, 1 H, Ar-H), 7.09 (m, 2 H, Ar-H).

MS (ESI) = 313.07 $[M+H]^+$

14. Insertion of Ruthenium bipyridine and purification was performed as in the case of compound **16**. Yield (67%)

H^1 NMR (400 MHz, δ, DMSO): 9.18 (d, J=8 Hz, 2H, Phen-H_c), 8.87, 8.84 (d, J=9Hz, 4H, bpy-$H_{4,4'}$), 8.21 (m, 1H, Ar-H_b), 8.20 (m, 2H, bpy-H_3), 8.09 (t, J=7.5 Hz, 2H, bpy-$H_{3'}$), 8.07 (d, J=6.5

Hz, 2H, Phen–H_A), 7.93 (m, 2H, Phen-H_B), 7.83 (d, J=7Hz, 2H, bpy-H_1), 7.59 (m, 4H, bpy-H_2), 7.44 (t, J=8.4 Hz, 1H, Ar-H_d), 7.32 (t, J=8.4 Hz, 2H, bpy-$H_{1'}$), 7.13 (m, 2H, Ar-$H_{a,c}$).

MS (ESI) = 363.1 $[M]^{2+}$, 725.1 $[M-H]^{+}$

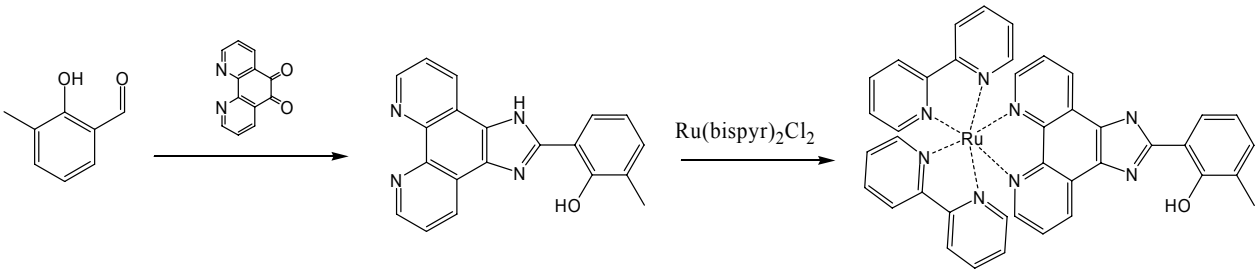

17a **17**

17a. In a typical reaction 210 mg of phendione (1.00 mmol) were and 150 mg of methyl salicylaldehyde (1.1 mmol, 1.1 eq) were dissolved in 3 mls acetic acid. The reaction was heated to 80°C for 30 min, and at this time 1.54 g of ammonium acetate (20 mmol, 20 eq) were added. The reaction turned reddish brown immediately and the temperature was raised to 100°C and allowed to stir for three hours. At this time the solution was allowed to return to room temperature and the product was precipitated by drop wise addition of ammonium hydroxide. The resulting product was filtered through a frit, washed repeatedly with water and ether and collected to yield 230 mg (71 % yield)

H^1 NMR (400 MHz, δ, DMSO): 9.00 (d, J=8 Hz, 2H,Phen-H), 8.83 (d, J= 8 Hz, 2H, Phen-H), 7.96 (d, J = 8.0 Hz, 1 H, Ar-H) 7.79 (dd, J=8 Hz, 2 H, Phen-H), 7.24 (t, J=7 Hz, 1 H, Ar-H), 6.93 (m, 2 H, Ar-H), 2.26 (s, 3H, H-methyl).

MS (ESI) = 327.1 $[M+H]^{+}$, 349.1 $[M+Na]^{+}$

17. Insertion of Ruthenium bipyridine and purification was performed as in the case of compound **16**. Yield 60%.

H^1 NMR (400 MHz, δ, DMSO): 9.13 (d, J=8 Hz, 2H, Phen-H_c), 8.85, 8.81 (d, J=8.5Hz, 4H, bpy-$H_{4,4'}$), 8.19 (m, 2H, bpy-H_3), 8.12 (t, J=7.5 Hz, 2H, bpy-$H_{3'}$), 8.08 (d, J=6.5 Hz, 2H, Phen–H_A), 8.04 (m, 1H, Ar-H_a), 7.92 (m, 2H, Phen-H_B), 7.83 (d, J=7Hz, 2H, bpy-H_1), 7.62 (m, 2H, bpy-$H_{1'}$), 7.57 (m, 2H, bpy-H_2), 7.32 (m, 2H, bpy-2), 7.28 (t,1H, Ar-H_c), 7.02 (t, J=8.3 Hz, 1H, Ar-H_b), 2.28 (s, 3H, H-methyl).

MS (ESI): 370.1 $[M]^{2+}$, 739.1 $[M-H]^+$, 885.0 $[M+PF_6]^+$

6.2.3. Terpyridine Complexes

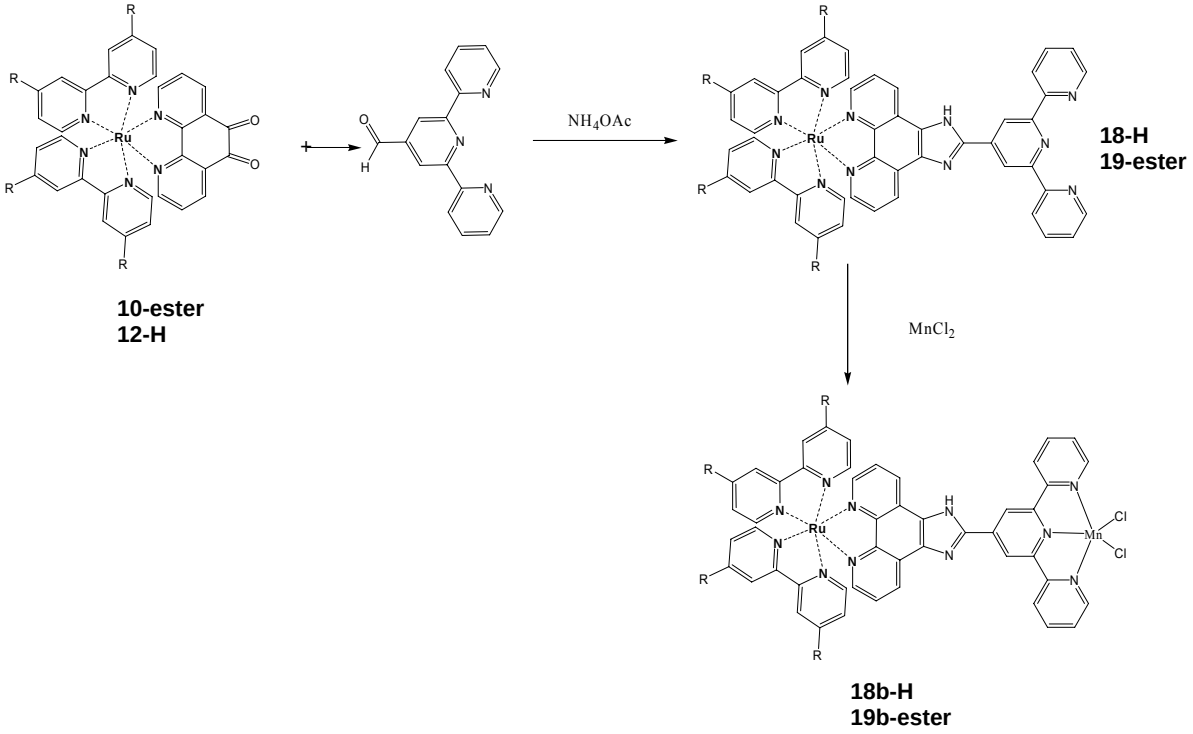

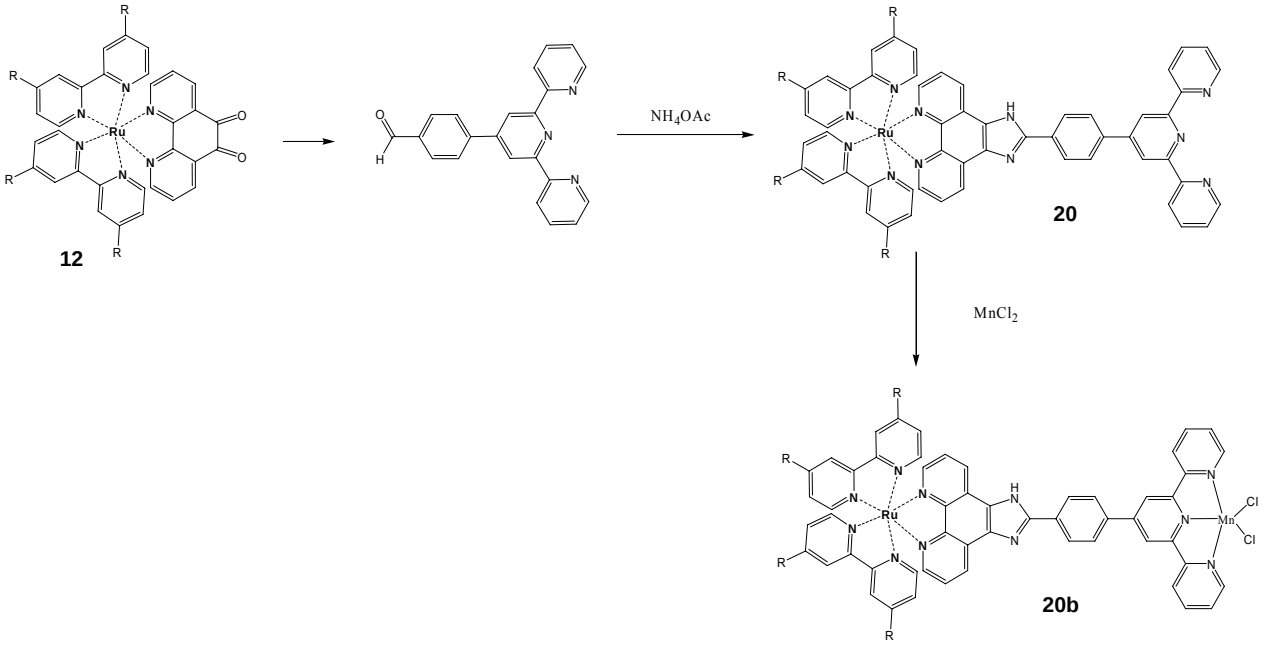

Ruthenium Phendione (12). Synthesis of this compound was performed as described above.

Tetra ethyl ester Ruthenium bipyridine Phendione (10). Synthesis of this compound was performed as described above.

Ru-Terpy (18). 83.78 mg of terpyridine-4' carbaldehyde (.321 mmol, 1 eq) were reacted with 200 mg Ru-phendione (12) (321 mmoles, 1 eq) in 10 mls acetic acid. The mixture was heated to 80°C for thirty minutes. At this time 495 mg of dry ammonium acetate (6.42 mmol, 20 eq) were added and the reaction mixture was heated in the dark at 100°C for 12 hours. The solvent was evaporated under reduced pressure and redisolved in a minimum amount of MeOH. An aqueous solution of NaH_4PF_6 was added drop wise and the resulting precipitate was filtered, washed with cold MeOH and dried under vacuum. The reaction afforded 224 mg of product. (81% yield).

H^1 NMR. (400 MHz, δ, DMSO): 9.39 (s, 2H, terpy-H), 9.27 (d, *J*=8.3 Hz, 2H, terpy-H), 8.91-8.87 (m, 4H, bpy-H), 8.87 (d, *J*=8.0 Hz, 2H, phen-H), 8.76 (d, *J*=7.5 Hz, 2H, terpy-H), 8.26-8.19 (m, 4H, bpy-H), 8.15-8.08 (m, 4H, bpy-H), 8.07 (t, *J*=7.5 Hz, 2H, terpy-H), 8.01 (dd, *J*=8.7, 8.3 Hz, 2H, phen-H), 7.67 (t, *J*=7.2 Hz, 2H, terpy-H), 7.65-7.58 (m, 4H, bpy-H), 7.32 (d, *J*=7.8 Hz, 2H, phen-H). ESI-MS yields mono charged peaks at 1011.1 m/z, $[M\text{-}PF_6^-]^+$, 864.2 m/z, $[M\text{-}H]^+$, and a doubly charged peak at 432.7 m/z, $[M\text{-}H]^{2+}$.

Ru-Terpy-Mn (18b). Compound **18** (52 mg, 0.060 mmol, 1 eq) was dissolved in a minimal amount of acetonitrile. To this solution, 75 mg of $MnCl_2$ (0.60 mmol, 10 eq) dissolved in a minimal amount of MeOH were added and the solution was stirred in the dark under an Ar atmosphere at room temperature. The precipitate formed was filtered, washed with MeOH and ether. The resulting red/orange powder was redissolved in MeOH and precipitated by adding a couple drops of a saturated aqueous NH_4PF_6 solution. This mixture was filtered, washed with MeOH and ether, and dried under vacuum. The reaction yielded 46 mg of product. (77 % yield). ESI-MS = 955 $[M\text{-}Cl]^+$.

Ester-Ru-Terpy (19). Synthesis of this compound was done by reacting terpyridine-4' carbaldehyde and **10** following the same procedure as for **18**.

H^1 NMR. (400 MHz, δ, DMSO):9.34 (m, 4H, bpy-H), 9.20 (m, 2H, terpy-H), 8.84 (d, J= 5.58 Hz, 2H, Phen-H), 8.75 (d, J=7.75 Hz, 2H, terpy-H), 8.65 (m, 4H, bpy-H), 8.26 (d, J= 7.72 Hz, 2H, Terpy-H), 8.11 (m, 2H, terpy-H), 7.97(m, 2H, phen-H), 7.87 (s, 4H, bpy-H), 7.73(t, J = 7.53 Hz, 2H, phen-H), 7.51(m, 2H, terpy-H), 4.45 (q, J = 7.1 Hz, 8 H, CH_2-H), 1.39 (t, J = 7.5 Hz, 12H, CH_3-H). ESI-MS = 576.2 $[M]^{2+}$.

Ester–Ru-Terpy-Mn (19b). This compound was obtained following the same procedure as for compound **18b**. (64 % yield). ESI-MS = 1242.0 $[M\text{-}Cl]^+$.

Ru-Phen-Terpy (20). The synthesis of this molecule was achieved following the same procedure as for (3). 60 mg of terpyridine-4' benzaldehyde (.160 mmol, 1 eq) were reacted with 120 mg Ru-phendione (2) (160 mmoles, 1 eq) in 10 mls acetic acid. The mixture was heated to 80°C for thirty minutes. At this time 275 mg of dry ammonium acetate (3.20 mmol, 20 eq) were added and the reaction mixture was heated in the dark at 100°C for 12 hours. The solvent was evaporated under reduced pressure and redissolved in a minimum amount of MeOH. An aqueous solution of $NaPF_6$ was added drop wise and the resulting precipitate was filtered, washed with cold MeOH and dried under vacuum. The reaction afforded 136 mg of product. (91% yield).

H^1 NMR. (400 MHz, δ, DMSO): 8.98 (m, 2H, phen-H), 8.80 (d, J= 8.0 Hz, 4H, bpy-H), 8.64 (d, J = 8.2 Hz, 2H, benz-H), 8.54-8.48 (dd, J = 8.2 Hz, 4H, bpy-H), 8.44 (d, J = 7.4 Hz, 2H, terpy-H), 8.09 (m, 4H, bpy-H), 8.03 (d, *J*=5.6 Hz, 2H, phen-H), 7.99 (t, J = 7.5 Hz, 2H, terpy-H), 7.92 (t, J = 7.92 Hz, 2H, benz-H), 7.85 (d, J = 5.2 Hz, 2H, terpy-H), 7.78 (dd, J = 8.2 Hz, 2H, phen-H), 7.62 (d, J = 5.9 Hz, 2H, terpy-H), 7.46 (m, 4H, bpy-H), 7.25 (t, J = 5.9 Hz, 2H, terpy-H).

MS (ESI) = 470.7 $[M]^{2+}$, 941.2 $[M]^+$

Ru-Phen-Terpy-Mn (20b). The same procedure as for compound (3b) was used. (84 % yield). MS: 1089.2 $[M+Na]^+$.

6.2.4. Ru-Terpyridine-Mn_2-di-μ-oxo Complexes

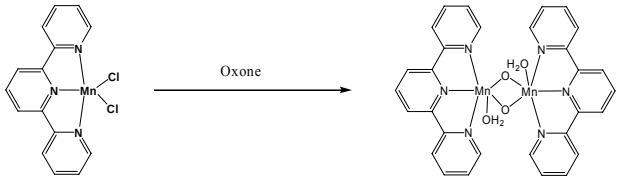

21a **21**

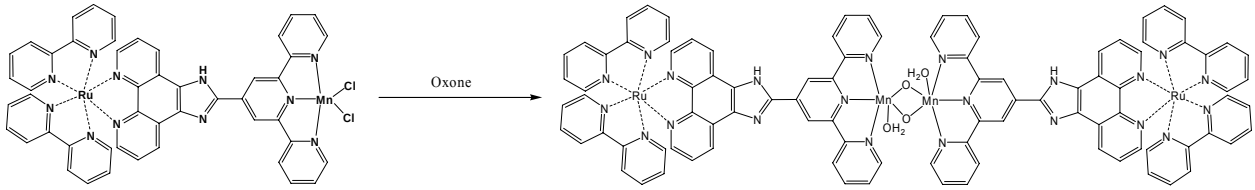

18b **23**

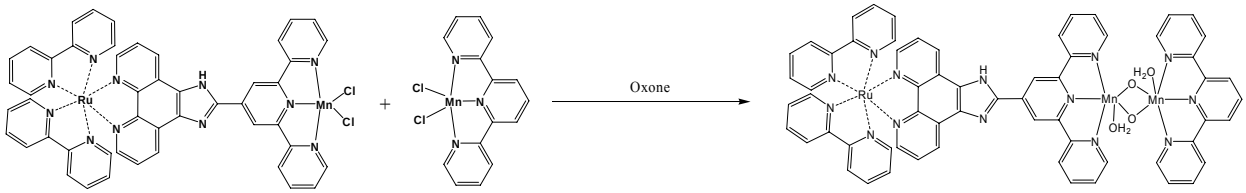

18b **21a** **22**

Terpy$_2$-Mn$_2$-di-μ-oxo (21). Terpy-$MnCl_2$ (**21a**) (50 mg, .140 mmol) was dissolved in 70 mls of 1:1 water:acetonitrile solution and was placed in an ice bath. Oxone (64 mg, .105 mmol, .75 eq) was dissolved in an equal volume of water. The terpyridine solution was allowed to cool to 0°C and the oxone solution was added dropwise. The starting yellow solution turned greenish after a couple minutes. The reaction was allowed to stir for 15 min, at which time the solvent was removed by rotary evaporation. The resulting solid product was isolated without further purification. (65 mg, 89% yield)

Ru_2-$Terpy_2$-Mn_2-di-μ-oxo (23). Ru-Terpy-$MnCl_2$ (20 mg, .020 mmol) was dissolved in 10 mls of 1:1 water : acetonitrile solution and allowed to cool to 0°C in an ice bath. Oxone (9.0 mg, .015 mmol, .75 eq) was dissolved in 10 mls water and added to the terpyridine solution. The solution turned from orange to green, then brown in about 4 minutes and was allowed to react for another 15 min. At this time the reaction was taken out of the ice bath and several drops of a saturated aqueous solution of ammonium hexafluorophosphate were added. A very fine precipitate formed immediately which was isolated by filtration, washed with copious amounts of ether to yield 19 mg of product. (84% yield).

Ru-Terpy-Terpy'-Mn_2-di-μ-oxo (22). A mixture of Ru-Terpy-$MnCl_2$ (37 mg, .037 mmol) and Terpy-$MnCl_2$ (132 mg, .37 mmol, 10 eq) were dissolved in 50 mls of 1:1 water : acetonitrile solution which was allowed to cool to 0°C. 50 mls of an aqueous solution of Oxone (170 mg, .28 mmol, 7.5 eq) was added and the solution, which was allowed to react for an additional 10 min turned from orange to green immediately. At this time the reaction was taken out of the ice bath and several drops of a saturated aqueous solution of ammonium hexafluorophosphate were added. A very fine precipitate formed immediately which was isolated by filtration, washed with copious amounts of ether to yield 17 mg of product. (72% yield).

Characterisation of these compounds was not possible by mass spectroscopy or NMR analysis so the presence of the Mn_2-di-μ-oxo moiety was determined by EPR and in situ UV/Vis methods.

6.2.5. Salen Ligands

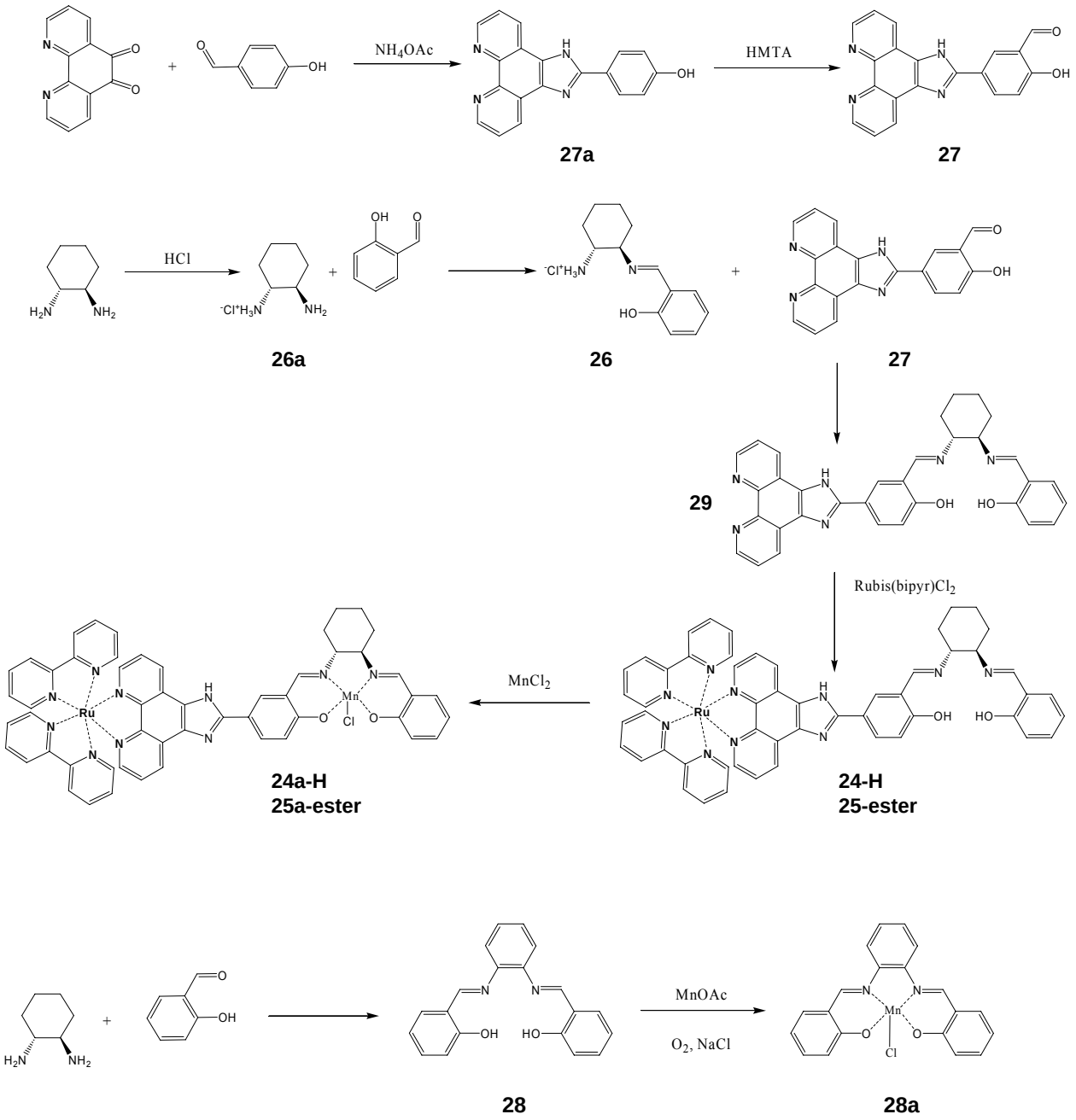

27a. Following a Steck-Day reaction, 500 mg of 1,10 phenanthroline dione (2.4 mmol) were dissolved together with 350 mg 4-hydroxy benzaldehyde (2.8 mmol) in 10 ml acetic acid. The mixture was heated to 80° C and stirred for 30 min. At this time 3.7 g of ammonium acetate were

added and the reaction was stirred at 110° C for three hours. The reaction was taken to room temperature and filtered through a frit funnel and washed with copious amounts of acetone to yield 510 mg of the desired product (68%).

NMR (400 MHz, DMSO): 9.00 (d, J=8.2 Hz, 2H, H-A), 8.90 (d, J=7.0Hz, 2H, H-C), 8.11 (d, J=8.7 Hz, 2H, H-1), 7.82 (dd, J_{A-B}=8.4 Hz, J_{B-C}=7.0 Hz, 2H, H-B), 6.98 (d, J=7.9 Hz, 1H, H-2). ESI-MS= 313.2 $[M+H]^+$.

27. Following a modified Duff reaction, 500 mg (1.6 mmol) of **27a** and 896 mg of hexamethylene tetraamine (6.4 mmol) were dissolved in 10 mls trifluoroacetic acid and refluxed for three days. The reaction was allowed to cool to room temperature and 50 mls of a 4M HCl solution were added and allowed to stir for 1 hour, during which time the reaction became cloudy. The solid was collected by filtration, washed with acetone, and dried in vacuum to yield 452 mg of **27**. (56% yield).

NMR (400 MHz, DMSO): 10.32 (s, 1H, H-5), 9.42 (d, J=8 Hz, 2H, H-A), 9.10 (d, J=7Hz, 2H, H-C), 8.51 (d, J=9Hz, 1H, H-3), 8.46 (s, 1H, H-1), 8.19 (dd, J_{A-B}=8.8 Hz, J_{B-C}=8.4 Hz, 2H, H-B), 7.20 (d, J=8.2 Hz, 1H, H-4). ESI-MS=341.1 $[M+H]^+$.

26a. 2.00 g of the 1,2 diaminocyclohexane (17.5 mmol) were dissolved in ether. 1.40 g of HCl dissolved in ether (36% v/v) was added to the amine solution over a period of 20 min. The reaction turned cloudy and white. The reaction was allowed to stir for 2 hours, filtered and washed with cold ether to yield 2.51 g (95% yield).

NMR (300 MHz, D_2O): 2.72 (m, 2H, H-NH_2), 1.91 (m, 2H, H-$BCH_{2-\beta}$), 1.68 (m, 2H, H-$CH_{2-\beta}$), 1.23 (m, 4H, H-$CH_{2-\gamma}$). ESI-MS = 115 $[M]^+$

26. 510 mg of 1, 2 di-amino cyclohexane (4.43 mmol) and 541 mg of salicylaldehyde (1 eq) were mixed in 20 mls dry MeOH. To this solution 10 drops of triethyl orthoformate and some molecular sieves were added. The solution was allowed to stir for 5 hours under Ar. At this time

the solid that had formed was filtered off and the remaining solution was evaporated under reduced pressure. This solid was redissolved in CH_2Cl_2: 5% MeOH and the solid was collected by filtration to yield 592 mg of product.(61 % yield).

NMR (400 MHz, DMSO): δ 8.58 (s, 1H, C=N-H), 7.42 (d, J= 8 Hz, 1H, H-d), 7.35 (t, J= 8 Hz, 1 H, H-b), 6.91 (t, J= 8 Hz, 1 H, H-c), 6.90 (d, J= 8 Hz, 1 H, H-a), 2.05-1.15 (m, 12 H, Aliph). ESI-MS = 219.1 $[M+H]^+$.

29. Compound **27** (170 mg, .50 mmol) was dissolved in 10 mls dry MeOH to which some molecular sieves, and 100 mgs of triethyl amine (1 mmol) were added. To this mixture 110 mgs of half salen **26** (.5 mmol) were added, and the mixture was stirred under Ar for 2 days. At this time the solution was evaporated under reduced pressure and the resulting solid was washed with plenty of ether in order to get rid of any symmetrical salen.

NMR (400 MHz, DMSO): δ 9.00 (d, J=8 Hz, 2H, H-A), 8.86 (dd, J=9.3 Hz, 2H, H-C), 8.72 (s, 1H, C=N-H), 8.65 (s, 1H, C=N-H), 8.47 (s, 1H, H-1), 8.30 (dd, J=8.5 Hz, 1H, H-3), 7.04 (dd, J=8.5 Hz, 1H, H-4), 7.36 (dd, J=7.9 Hz, 1H, H-d), 7.26 (q, J=7.22 Hz, 1H, H-b), 6.82 (t, J=7.6 Hz, 1H, H-c), 6.79 (d, J=8.1 Hz, 1H, H-a), 2.20-1.27 (m, 10 H, H-aliph). ESI-MS = 541.2 $[M+H]^+$.

24. Ruthenium bipyridine was inserted as previously described

ESI-MS = 477.1 $[M]^{2+}$.

25. Tetra ethyl ester Ruthenium bipyridine was inserted as previously described

ESI-MS = 621.2 $[M]^{2+}$.

24a. 300 mg of compound 6 (.31mmol) and 227 mg Mn(II)OAc were dissolved in 20 mls MeOH. The solution was heated to 60°C for three hours under Ar. After this time, the solution was allowed to return to room temperature and air was bubbled in the solution for one hour. 10 mls of a saturated aqueous solution of NaCl were added and the solution was stirred for an additional hour. The product was precipitated by addition of PF_6^- aqueous solution.

ESI-MS = 1042.1 $[M]^+$.

28. 200 mg of 1,2 cyclohexyl diamine (1.75 mmol) were dissolved in 20 mls ethanol. To this solution 427 mgs, (3.50 mmol, 2 eq) of salicylaldehyde were added and the reaction which turned yellow almost immediately was allowed to stir for two hours. The product was collected as a precipitate, washed with plenty ethanol, and water to yield 382 mg (68%) of product which needed no further purification.

NMR (400 MHz, DMSO): δ 8.59 (s, 2H, C*H*-N), 7.45 (d, J = 6.8 Hz, 2H, H-d), 7.34 (t, J = 8Hz, 2H, H-b), 6.89 (m, 4H, H-a,c), 2.08-1.16 (m, 10H, H-aliph).

ESI-MS = 323.1 $[M+1]^+$.

28a. 300 mg of salen compound 28 (.55 mmol) were dissolved into 10 mls toluene and added to a 10 mls ethanol solution of Mn (II) acetate (404 mg, 1.65 mmol, 3 eq). The reaction was allowed to reflux for one hour. At this time the heat was turned off and air was bubbled through the solution while stirring for another hour. 9 mls of a saturated NaCl solution were added and the reaction was carried on for 45 minutes. At this time the solution was extracted with toluene, dried over magnesium sulfate, and the solvent was evaporated under reduced pressure. The product was recrystilized (80 mg, 40% yield) by dissolving in a minimum amount of a 1/1 pentane/dichloromethane solution and placed in an ice bath.

ESI-MS = 374.4 $[M-Cl]^+$

6.3. Instrumentation

Steady state absorption: Absorption spectra were recorded on Specord 210 (Analytic Jena) spectrophotometer.

Steady state emission: Luminescence spectra were recorded on a Varian Cary Eclipse spectrofluorimeter. Measurements were obtained by exciting diluted ($A(\lambda_{exc})< 0.1$) solutions at 460 (MLCT maximum). $[Ru(bpy)_3]^{2+}$ was always employed as reference. Samples were purged with Argon for 10 minutes prior to measurements

EPR: X-band electron paramagnetic resonance spectra were recorded in a Bruker 300 spectrometer with the following parameters: microwave 3.196 mW, modulation amplitude 25.251 G, time constant 81.92 ms, scan rate 167 s, scan width 5000 G, and modulation frequency 100 kHz.

Electrochemistry: Cyclic voltammetry was performed in a potentiostat-galvanostat using a 3 mm^2 surface glassy carbon electrode. Acetonitrile was distilled prior to each experiment and the solution (1 mM for the complexes, 0.1 M of tetrabutyl ammonium perchlorate introduced in an Argon purged electrochemical cell. The experiments were performed at room temperature using a glassy carbon electrode as the working electrode, a platinum wire as the counter electrode, and a $Ag/AgClO_4$ (0.01 M) electrode in acetonitrile as the reference electrode (+.292 vs. SCE).

Mass Spectrometry: Electrospray mass spectra were recorded on a Finnigan MAT95S in a mixture of CH_2Cl_2/MeOH/H_2O (1/1/1).

NMR: Nuclear magnetic resonance experiments were performed in a myriad of machines.

Photo-induced oxidations: were usually performed by mixing the required Ruthenium compounds (.5 mls, 1mM) with $[Co(NH_3)_5Cl]Cl_2$ (2.5 mls, 20 mM) resulting in solutions .17 mM

in Ruthenium complex and 17 mM in electron acceptor. The samples were degassed with Argon and the solutions were placed under illumination with a 250 W lamp for 10 min with both infrared and 400 nm cut off filters. After this time 100 μl aliquots were transferred in an EPR tube which was immediately immersed into liquid nitrogen for further analysis.

If the reactions were monitored by UV/Vis, an aliquot of the above mentioned solution would be diluted to the desired absorbance value.

7. Publications

I. Kodis, Gerdenis; Herrero, Christian; Palacios, Rodrigo; Marino-Ochoa, Ernesto; Gould, Stephanie; De la Garza, Linda; Van Grondelle, Rienk; Gust, Devens; Moore, Thomas A.; Moore, Ana L.; Kennis, John T. M. **Light Harvesting and Photoprotective Functions of Carotenoids in Compact Artificial Photosynthetic Antenna Designs.** Journal of Physical Chemistry B (2004), 108(1), 414-425.

II. Palacios, Rodrigo E.; Gould, Stephanie L.; Herrero, Christian; Hambourger, Michael; Brune, Alicia; Kodis, Gerdenis; Liddell, Paul A.; Kennis, John; Macpherson, Alisdair N.; Gust, Devens; Moore, Thomas A.; Moore, Ana L. **Bioinspired energy conversion.** Pure and Applied Chemistry (2005), 77(6), 1001-1008.

III. Berera, Rudi; Herrero, Christian; van Stokkum, Ivo H. M.; Vengris, Mikas; Kodis, Gerdenis; Palacios, Rodrigo E.; van Amerongen, Herbert; van Grondelle, Rienk; Gust, Devens; Moore, Thomas A.; Moore, Ana L.; Kennis, John T. M. **A simple artificial light-harvesting dyad as a model for excess energy dissipation in oxygenic photosynthesis.** Proceedings of the National Academy of Sciences of the United States of America (2006), 103(14), 5343-5348.

IV. Palacios, Rodrigo E.; Kodis, Gerdenis; Herrero, Christian; Ochoa, Ernesto Marino; Gervaldo, Miguel; Gould, Stephanie L.; Kennis, John T. M.; Gust, Devens; Moore, Thomas A.; Moore, Ana L. **Tetrapyrrole Singlet Excited State Quenching by Carotenoids in an Artificial Photosynthetic Antenna.** Journal of Physical Chemistry B (2006), 110(50), 25411-25420.

V. Berera, Rudi; van Stokkum, Ivo H. M.; Kodis, Gerdenis; Keirstead, Amy E.; Pillai, Smitha; Herrero, Christian; Palacios, Rodrigo E.; Vengris, Mikas; van Grondelle, Rienk; Gust, Devens; Moore, Thomas A.; Moore, Ana L.; Kennis, John T. M. **Energy transfer, excited-state deactivation and exciplex formation in artificial carotene-phthalocyanine light-harvesting antennas.** Journal of Physical Chemistry B (2007), 111(24), 6868-6877.

VI. Herrero, Christian; Lasalle-Kaiser, Benedikt; Leibl, Winfried; Rutherford, William A.; Aukauloo, Ally. **Artificial systems related to light driven electron transfer processes in PSII**. Coordination Chemistry Reviews. *In press*.

VII. Herrero, Christian; Quaranta, Annamaria; Leibl, Winfried; Fallahpour, Reza; Aukauloo, Ally. **Photoinduced Oxidation of a Manganese Terpyridine Complex. Laser Flash Photolysis and EPR studies.** *In preparation.*

VIII. Quaranta, Annamaria; Lachaud, Fabien; Herrero, Christian; Guillot, Regis; Charlot, Marie-France; Leibl, Winfried Leibl; Aukauloo, Ally. **Influence of the Protonic State of an Imidazole-Containing Ligand and on the Electrochemical and Photophysical Properties of a Ruthenium(II)–Polypyridine-Type Complex.** Chemistry-A European Journal (2007), 13, 8201-8211.

Not included in this thesis

He, Jin; Chen, Fan; Li, Jun; Sankey, Otto F.; Terazono, Yuichi; Herrero, Christian; Gust, Devens; Moore, Thomas A.; Moore, Ana L.; Lindsay, Stuart M. **Electronic Decay Constant of Carotenoid Polyenes from Single-Molecule Measurements.** Journal of the American Chemical Society (2005), 127(5), 1384-1385.

Visoly-Fisher, Iris; Daie, Kayvon; Terazono, Yuichi; Herrero, Christian; Fungo, Fernando; Otero, Luis; Durantini, Edgardo; Silber, Juana J.; Sereno, Leonides; Gust, Devens; Moore, Thomas A.; Moore, Ana L.; Lindsay, Stuart M. **Conductance of a biomolecular wire.** Proceedings of the National Academy of Sciences of the United States of America (2006), 103(23), 8686-8690.

I. Kodis, Gerdenis; Herrero, Christian; Palacios, Rodrigo; Marino-Ochoa, Ernesto; Gould, Stephanie; De la Garza, Linda; Van Grondelle, Rienk; Gust, Devens; Moore, Thomas A.; Moore, Ana L.; Kennis, John T. M. **Light Harvesting and Photoprotective Functions of Carotenoids in Compact Artificial Photosynthetic Antenna Designs.** Journal of Physical Chemistry B (2004), 108(1), 414-425.

Light Harvesting and Photoprotective Functions of Carotenoids in Compact Artificial Photosynthetic Antenna Designs

Gerdenis Kodis,*,†,‡ Christian Herrero,† Rodrigo Palacios,† Ernesto Mariño-Ochoa,† Stephanie Gould,† Linda de la Garza,† Rienk van Grondelle,§ Devens Gust,† Thomas A. Moore,† Ana L. Moore,† and John T. M. Kennis*,§

Department of Chemistry and Biochemistry and the Center for the Study of Early Events in Photosynthesis, Arizona State University, Tempe, Arizona, Department of Biophysics, Division of Physics and Astronomy, Faculty of Sciences, Vrije Universiteit, 1081 HV Amsterdam, The Netherlands, and Institute of Physics, Savanoriu 231, LT-2053 Vilnius, Lithuania

Received: July 22, 2003; In Final Form: October 10, 2003

Artificial light-harvesting constructs were synthesized by covalently linking two carotenoids to the central silicon atom of a phthalocyanine (Pc) derivative. Triad **1** binds two carotenoids having nine conjugated double bonds, whereas triad **2** binds two carotenoids having 10 carbon−carbon double bonds in conjugation. Fluorescence excitation experiments indicated that, in triad **1** dissolved in *n*-hexane, the carotenoid to Pc singlet energy transfer efficiency is ca. 92%, whereas in triad **2**, it is 30%. Results from ultrafast laser spectroscopy indicate that upon population of the optically allowed S_2 state of the carotenoid the optically forbidden states S_1 and S* are rapidly generated in both triad **1** and triad **2**. In triad **1**, S_2, S_1, and S* all contribute singlet electronic energy to Pc. In triad **2**, singlet electronic energy transfer to Pc occurs primarily from the optically allowed S_2 state with little energy transfer to Pc via the S_1 state, and there is no evidence for energy transfer via S*. Instead, in triad **2**, we find a multiphased quenching of the Pc singlet excited state on the picosecond and nanosecond time scales. Upon intersystem crossing from the singlet excited state of Pc to the triplet state in triad **1**, triplet−triplet energy transfer to either of the carotenoids takes place on a time scale significantly shorter than 5 ns. When dissolved in polar solvents, triads **1** and **2** exhibit light-induced electron transfer from either of the carotenoid moieties to the excited singlet Pc species with a time constant of about 2 ps. Charge recombination to the singlet ground state occurs in 10 ps in triad **1** and 17 ps in triad **2**.

1. Introduction

Carotenoids are indispensable in photosynthetic energy conversion, where they function as light harvesters and photoprotectors.[1−3] They exert their light harvesting (LH) function by absorbing sunlight in the blue and green parts of the solar spectrum and transferring the energy to nearby (bacterio)chlorophyll (B)(Chl) molecules. In subsequent steps, the excitation energy is transported to the reaction center, where photochemical conversion takes place.[4] The energy of the photons made available this way accounts for a significant fraction of photosynthetic biomass production on earth. In addition to their light-harvesting function, carotenoids assume a number of photoprotective roles. Essentially all antenna and reaction center complexes bind carotenoids to protect the organism from oxidative damage, primarily by quenching harmful (B)Chl triplet and singlet oxygen species. Recently, it has been discovered that carotenoids can act as electron donors to reduce long-lived $P680^+$, and in such a way prevent damage to reactions centers of oxygenic photosynthetic organisms.[5,6] Moreover, carotenoids appear to play a large and thus far poorly understood role in the direct quenching of Chl singlet states in the xanthophyll cycle in Photosystem II of plants.[7] To perform this variety of functions, carotenoids are incorporated in photosynthetic pigment−protein complexes in close contact with (B)Chl.[8−11]

The main feature in the molecular structure of carotenoids is a polyene chain of alternating carbon−carbon single and double bonds. Until recently, the electronic states involved in the LH function have been described by one high-lying optically allowed singlet excited state (S_2) and a low-lying, optically forbidden singlet excited state (S_1). Upon light absorption, the S_2 state relaxes to the optically forbidden S_1 state in 100−200 fs by internal conversion (IC), after which the S_1 state internally converts to the ground state on the picosecond time scale.[1,2] Recent work has shown that excited-state energy transfer (EET) from both the S_2 and S_1 states is required for efficient LH function.[12−15] The carotenoid to (B)Chl EET processes are thought to be governed by the Coulombic coupling and the spectral overlap between donor and acceptor states,[1,16,17] and the overall efficiency can vary from as low as 35%, for instance in the LH1 complex of *Rhodospirillum (Rs.) rubrum*[18] and the PSII core complex of oxygenic photosynthesis[19] to as much as 80% or more in the LHCII of plants,[14,20] the PSI complex of cyanobacteria[21,22] and various LH2 antennas of purple bacteria.[1,13,15,23]

In recent years, it has become increasingly clear that the traditional description of the excited-state manifold of caro-

* To whom correspondence should be addressed. E-mail: gerdenis@asu.edu (G.K.); john@nat.vu.nl (J.T.M.K.).
† Arizona State University.
‡ Institute of Physics.
§ Vrije Universiteit.

10.1021/jp036139o CCC: $27.50
Published on Web 12/10/2003

tenoids in terms of the S_2 and S_1 states mentioned above is incomplete, and that additional optically dark states need to be considered. Koyama and co-workers presented experimental evidence concerning the existence of the theoretically predicted $^1B_u^-$ state in carotenoids by carrying out Raman excitation profile measurements.[24,25] Subsequent ultrafast studies were interpreted in terms of an internal conversion cascade from S_2, via $^1B_u^-$ to S_1 on the sub-100 fs time scale.[26,27] Using multicolor femtosecond spectroscopy, we (R.v.G. and J. K.) uncovered another new optically forbidden electronic state in carotenoids, which we labeled S*. Surprisingly, in carotenoids bound to the LH complexes of purple photosynthetic bacteria, this new S* state is the precursor on an ultrafast reaction pathway to the carotenoid triplet state.[18] To explain the ultrafast triplet formation, a singlet fission mechanism was invoked by which the S* singlet state separates into a pair of triplet states localized on separate parts of the polyene chain, thereby conserving a total singlet spin. In subsequent work, we obtained clear evidence that S* is active as an excited-state energy donor to BChl in bacterial LH complexes.[23] So far, the only information we have on the new S* state is phenomenological: we know its optical absorption properties and its dynamical behavior. Its nature, identity, and origin have remained elusive. Given its ability to generate triplets, we suggested that S* may correspond to one of the "covalent" optically dark states, like the $^1B_u^-$ state, which exhibits a doubly excited triplet character.[28]

The development and study of simple artificial photosynthetic antennas serve a number of goals. On one hand, technological development of organic photovoltaic devices could greatly benefit from insights and design considerations that derive from artificial systems. As carotenoids constitute an integral part of the natural photosynthetic machinery where they have a multitude of functions, it would appear advantageous to incorporate them into artificial antennas. On the other hand, artificial light-harvesting antennas can be designed in a minimalistic way to exert specific functions, like maximizing absorption cross sections, accessing certain spectral windows, and carrying out efficient energy transport or photoprotection in its various forms. The basic simplicity of artificial antenna systems has important advantages over the invariably far more complex natural photosynthetic systems. Their specific photophysics can be related to unambiguous energetic, electronic, and structural features through the use of advanced spectroscopic methods, and this may yield important insights into many aspects of natural photosynthesis.[29−32]

In this report, we have investigated the light-harvesting and photoprotective function of carotenoids in simple artificial photosynthetic antennas that consist of a phthalocyanine (Pc) moiety, to which a pair of carotenoids have been covalently linked in an axial way (Figure 1). By varying the number of carbon−carbon conjugated double bonds of the carotenoid moieties in the triads, we have studied the influence of the relative energy levels of carotenoid and Pc on their designed functions. Spectroscopic studies show that these simple antennas are capable of performing light harvesting, photoprotective, and electron transfer processes, and the mechanisms, pathways, and electronic states involved are highly reminiscent of those in natural photosynthesis.

2. Materials and Methods

Synthesis. *Dicarotenophthalocyanine **1** (Triad **1**).* Methyl 8′-apo-β-caroten-8′-oate (**3**) was prepared by published procedures,[33] and 8′-apo-β-caroten-8′-oic acid was prepared by base-catalyzed hydrolysis of **3**. The coupling reaction between 8′-apo-β-caroten-8′-oic acid and silicon tetra-*tert*-butylphthalocyanine dihydroxide (**2**, Aldrich, mixture of regioisomers) to generate triad **1** has been described.[29] ^{1}H NMR (500 MHz, $CDCl_3$) δ −0.21 (6H, s, car H-19′), 1.02 (12H, s, car H-16, H-17), 1.41 (6H, s, car H-20′), 1.45−1.47 (4H, m, car H-2), 1.60−1.62 (4H, m, car H-3), 1.71 (6H, s, car H-18), 1.81−1.83 (36H, m, Pc H-1′), 1.98 (6H, s, car H-19), 1.99 (6H, s, car H-20), 2.01 (4H, t, J = 6.0, car H-4), 3.59 (2H, d, J = 11.5, car H-10′), 5.08 (2H, d, J = 14.5, car H-12′), 5.19 (2H, d, d, J = 13.0, 11.5), 5.81 (2H, d, J = 12.0, car H-14′), 6.11 (2H, d, J = 7.0, car H-14), 6.13−6.17 (6H, m, car H-7, H-8, H-10), 6.30 (2H, d, J = 15.5, car H-12), 6.35 (2H, d, d, J = 13.5, 13.5, car H-15′), 6.58 (2H, d, d, J = 13.0, 13.0, car H-15) 6.67 (2H, d, d, J = 13.5, 12.0, car H-11), 8.44 (4H, d, J = 8.0, Pc H-2(3), H-9(10), H-16(17), H-23(24)), 9.58−9.74 (8H, m, Pc H-1, H-4, H-11, H-15, H-18, H-22, H-25); (MALDI-TOF) m/z 1628 $(M)^+$, calc. for C_{108} H_{126} N_8 O_4 1628.3; UV/VIS (Toluene) 693(Pc), 662-(Pc), 622(Pc), 478(C), 452 (C) and 366(Pc) nm.

*Dicarotenophthalocyanine **2** (Triad **2**).* Methyl 6′-apo-β-caroten-6′-oate (**4′**) was synthesized according to previous methods (same as above). The corresponding acid, 6′-apo-β-caroten-6′-oic acid, was obtained by basic hydrolysis. This acid (94.8 mg, 0.21 mmol) was transformed to the corresponding acid chloride by dissolving it in 5 mL of a 4:1 toluene:pyridine solution and adding 6 drops of thionyl chloride. The reaction mixture was stirred under a nitrogen atmosphere for 10 min, and then the solvents were removed under high vacuum. A solution of silicon tetra-t*ert*-butyl-phthalocyanine dihydroxide (**2**, Aldrich, mixture of regioisomers) (20.4 mg, 0.025 mmol) in 2-picoline (4 mL, distilled from CaH_2) was added to the carotenoid acid chloride. Stirring continued under a nitrogen atmosphere for 4 h at 60 °C. At this time, 30 mg of 4-(dimethylamino)pyridine (DMAP) was added, and the mixture was allowed to react for another 24 h. Purification was done by column chromatography (silica, 6:4 CH_2Cl_2:hexanes) to yield 16.2 mg of the final product (37.8% yield). ^{1}H NMR (500 MHz, $CDCl_3$) δ 0.81 (6H, s, car H-19′), 1.01 (12H, s, car H-16, H-17), 1.42−1.45 (4H, m, car H-2), 1.60−1.63 (4H, m, car H-3), 1.68 (6H, s, car H-20′), 1.70 (6H, s, car H-18), 1.81−1.82 (36H, m, Pc H-1′), 1.95 (6H, s, car H-19), 1.96 (6H, s, car H-20), 1.99−2.00 (4H, m, car H-4), 2.92 (2H, d, J = 15.5, car H-7′), 4.44 (2H, d, J = 15.5, car H-8′), 5.19−5.21 (2H, m, car H-10′), 5.97−5.98 (2H, m, car H-11′), 6.09−6.19 (10H, m, car H-7, H-8, H-10, H-12, H-15), 6.31 (2H, d, J = 15.0, car H-14′), 6.57 (2H, d, J = 12.5, car H-12′), 6.61−6.62 (2H, m, car H-11), 6.65 (2H, d,d, J = 13.5, J = 12.0, car H-15′), 8.44 (4H, d, J = 8.5, Pc H-2(3), H-9(10), H-16(17), H-23(24)), 9.58−9.73 (8H, m, Pc H-1, H-4, H-8, H-11, H-15, H-18, H-22, H-25); MALDI/TOF m/z 1679 $(M)^+$, base peak 1238 $(M - 441$ (carotene$))^+$, calc. for C_{112} H_{130} N_8 O_4 Si 1680.4; UV/VIS (CH_2Cl_2) 693-(Pc), 663(Pc), 623(Pc), 468(C), 361(Pc) nm.

Instrumental Techniques. Ultraviolet−visible absorption spectra were measured on a Cary 500 UV−vis−NIR spectrophotometer, and corrected fluorescence excitation and emission spectra were obtained using a Photon Technology International MP-1 spectrofluorometer and optically dilute samples ($A < 0.07$). The excitation spectrum of silicon 1,4,8,11,15,18,22,25-octabutoxyphthalocyanine dihydroxide was used to generate an excitation correction file in the 300−750 nm region by assuming that the absorption and fluorescence excitation spectra were identical.

Femtosecond transient absorption measurements in the visible were carried out with an amplified Ti:sapphire laser system as described earlier.[14] In brief, part of the output of a 1 kHz

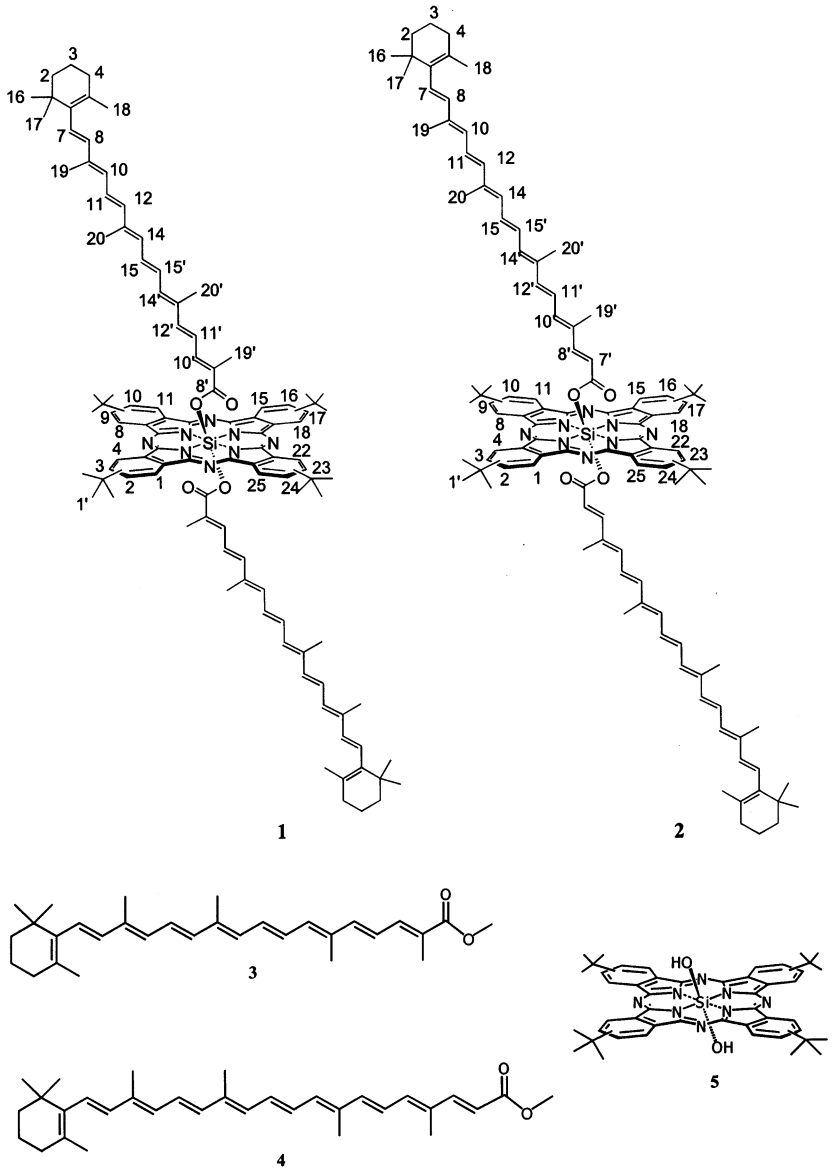

Figure 1. Structures of triads **1** and **2**, model carotenoids **3** and **4**, and phthalocyanine **5**. The three-dimensional structure of **1** and **2** has been inferred by NMR spectroscopy.[29]

amplified Ti:sapphire laser system (Coherent-BMI α1000) was used to drive a home-built noncollinear optical parametric amplifier. In the experiments presented here, the excitation wavelength was tuned to 475 nm (17 nm fwhm) so as to selectively excite the S_2 state of the carotenoid. The pulse duration was 80 fs, and the energy was 300 nJ. A white light continuum generated by focusing amplified 800 nm light on a 1 mm sapphire crystal was split into probe and reference. The beams were focused in a 1 mm path-length quartz cuvette to a 150 μm diameter spot. To avoid sample degradation, the cuvette was mounted on a shaker. The polarization between the pump and the probe was set to the magic angle (54.7°). After passing through the sample, the probe and reference beams were dispersed by a polychromator and projected on a home-built double diode array detector. Femtosecond time delays between pump and probe were controlled by a delay line, covering delays of up to 5 ns.

Femtosecond transient absorption measurements in the IR spectral region were carried out with another amplified Ti:sapphire laser system.[34] The laser pulse train was provided by a Ti:sapphire regenerative amplifier (Clark-MXR, model CPA-1000) pumped by a diode-pumped CW solid-state laser (Spectra Physics, model Millennia V). The typical laser pulse was 100 fs at 790 nm, with a pulse energy of 0.9 mJ at a repetition rate of 1 kHz. Most of the laser energy (80%) was used to pump an optical parametric amplifier (IR−OPA, Clark-MXR). The excitation pulse was sent through a computer controlled optical delay line. The remaining laser output (20%) was focused into a 1.2 cm rotating quartz plate to generate a white light continuum. The continuum beam was further split into two identical parts and used as the probe and reference beams, respectively. The probe and reference signals were focused onto two separated optical fiber bundles coupled to a spectrograph (Acton Research, model SP275). The spectra were acquired on a dual diode array detector (Princeton Instruments, model DPDA-1024).

Data Analysis. The recorded time-resolved spectra were analyzed with a global analysis program using a kinetic model [35] consisting of sequentially interconverting species, e.g., 1 → 2 → 3 → ... The arrows indicate successive monoexponential decays of increasing time constants, which can be regarded as the lifetime of each species. Associated with each species is a

lifetime and a difference spectrum, called a species-associated difference spectrum (SADS). The first SADS corresponds to the time zero difference spectrum. In general, the SADS may well correspond to mixtures of excited states and should not be considered to portray spectra of pure states. This procedure enables us to visualize clearly the evolution of the transient states of the system. The instrument response function was fit to a Gaussian (120 fs fwhm) and the group velocity dispersion of the probing white light was fit to a third order polynomial. To optimally illustrate our observations, the SADS are presented instead of raw time-resolved spectra. For selected detection wavelengths, we present raw data by showing the measured kinetic traces including the fit.

3. Results and Discussion

Figure 1 shows the structures of the compounds under study. These include model carotenoid **3**, which comprises 9 carbon−carbon double bonds in its conjugated π-electron system, model carotenoid **4**, which is similar to model carotenoid **3** except that it has 10 conjugated carbon−carbon double bonds, and model phthalocyanine **5**. Conformational information for **1** has been determined by NMR techniques.[29] The ^{1}H NMR spectra of triads **1** and **2** exhibit upshift fields of many of the carotenoid protons due to the phthalocyanine ring currents. In triad **1**, proton 10′ is shifted up field to 3.59 ppm from 7.29 ppm in model compound **3**. Triad **2** exhibits also large upfield shifts for protons 7′ and 8′ (2.92 and 4.44 ppm, respectively), which appear at 5.85 and 7.37 ppm, respectively, in model compound **4**. Upshift fields were also found for the methyl protons 19′ and 20′ for each triad (in triad **1**, protons 19′ and 20′ are shifted to −0.21 and 1.41 ppm from 1.99 and 1.97 ppm, respectively, in model **3**; in triad **2**, protons 19′ and 20′ are shifted to 0.81 and 1.68 ppm from 1.91 and 1.96 ppm, respectively, in model **4**). These field trends are consistent with the proposed three-dimensional structure of **1** and suggest that **2** has a similar structure in which the two carotenoids are covalently attached to the central silicon atom of the phthalocyanine and are oriented almost perpendicular to the tetrapyrrole plane.

Energy Transfer. *Absorption and Fluorescence-Excitation Spectra.* The absorption spectrum of model phthalocyanine **5** dissolved in *n*-hexane, with an absorption maximum at 671 nm and minor bands at 641, 604, and 355 nm, is shown as the dotted line in Figure 2, parts A and B. This spectrum is typical of a metal phthalocyanine, and only a very weak absorption is observed in the region between 400 and 575 nm. The pattern and spectral positions of the Pc absorption bands very much resemble those of chlorophyll *a*. In triad **1** (solid line, Figure 2A), the addition of the two carotenoid pigments results in a large increase in absorption in the center of the spectrum and a substantial red shift of the phthalocyanine bands, resulting in an absorption maximum of the red-most band at 684 nm instead of 671 nm in model **5**. The absorption of the carotenoid moiety at 466 and 440 nm is slightly blue shifted compared to model carotenoid **3**, which has absorption maxima at 470 and 444 nm (Figure 2A, dashed line). Similar shifts occur in triad **2** (Figure 2B, solid line): the Pc moiety has shifted to the red (684 nm), and the carotenoid moiety has shifted to the blue at 486 and 457 nm, as compared to model carotenoid **4**, which absorbs at 491 and 463 nm (dashed line, Figure 2B).

The fluorescence emission spectrum of the phthalocyanine moiety of triad **1** and **2** (Figure 2, parts A and B, dash−dotted line) has a maximum at 684.7 and a minor band at 759 nm. The figure shows the corrected excitation spectra for the phthalocyanine fluorescence of triad **1** and **2** (solid symbols)

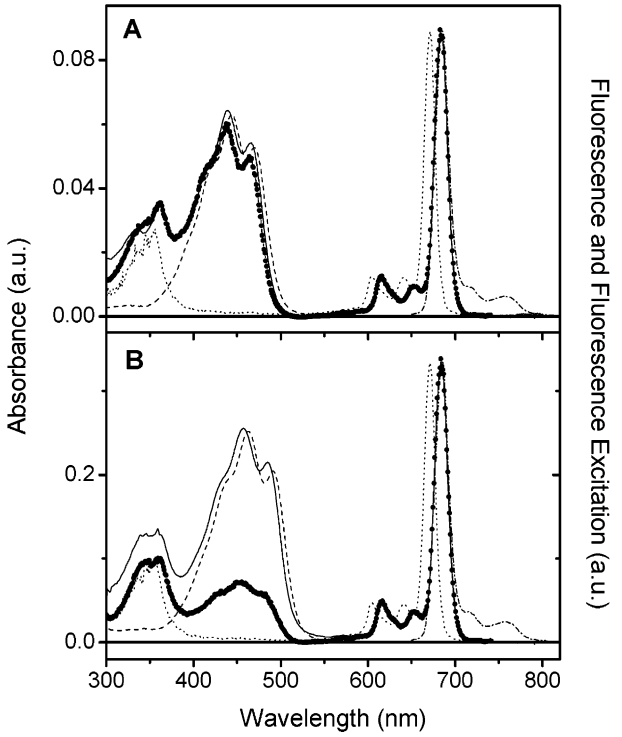

Figure 2. Panel A: absorption spectra of phthalocyanine **5** (dotted line), model carotenoid **3** (dashed line), and triad **1** (solid line); fluorescence spectrum of triad **1** (dash−dotted line); fluorescence excitation spectrum of triad **1** (solid circles). Panel B: absorption spectra of phthalocyanine **5** (dotted line), model carotenoid **4** (dashed line), and triad **2** (solid line); fluorescence spectrum of triad **2** (dash−dotted line); fluorescence excitation spectrum of triad **2** (solid circles).

with emission monitored at 759 nm. The excitation spectrum was normalized to the absorption spectrum at the red-most bands. These spectra clearly indicate a dramatic difference in the singlet−singlet energy transfer efficiency from carotenoid to phthalocyanine: 92% for triad **1** and 30% for triad **2**.

*Model Carotenoids **3** and **4**: Femtosecond Studies.* We first present the femtosecond results from model carotenoid **3** (9 carbon−carbon conjugated double bonds) dissolved in *n*-hexane. We collected time-resolved spectra by exciting the sample with 50 fs flashes at 475 nm and probing with a white-light continuum, with a time range from −3 ps to 200 ps. Rather than presenting the time-resolved spectra themselves, we show the results of a global analysis of these data with a sequential model. Three components were required for an adequate description of the time-resolved data, with lifetimes of 73 fs, 620 fs, and 25 ps (Figure 3A). Each species is characterized by a difference spectrum (so-called SADS) relative to the ground-state absorption, a rise time, and a decay time. The spectrum represents the absorption change, determined from the raw data after correction for the group-velocity chirp in the probe light and deconvolution with the instrument response function. The SADS of the initially created singlet excited S_2 state (red line) shows ground-state bleaching near 480 nm, and a pronounced stimulated emission (SE) at 530 and 570 nm. The lifetime of this state, 73 fs, may be assigned to very rapid internal conversion (IC) from the S_2 to the S_1 state. This S_2 lifetime is almost identical to that reported by Mariño-Ochoa and co-workers[29] on the same carotenoid, and appears to be rather short as compared with those of other carotenoids, which are generally on the order of 100−200 fs.[36−39] The S_2 state evolves into the second SADS (blue line), which has a lifetime of 620 fs. This SADS shows a pronounced excited-state absorption at 545 nm,

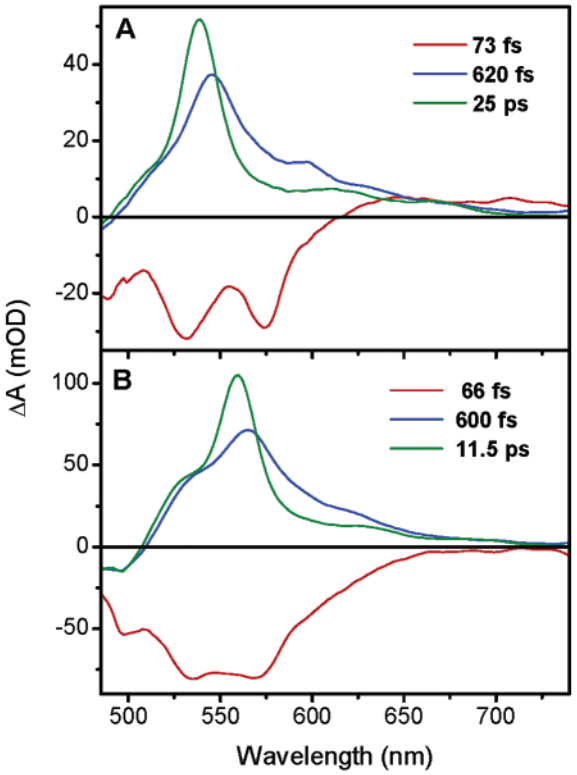

Figure 3. Panel A: Species-associated difference spectra (SADS) that follow from global analysis of the time-resolved experiments on model carotenoid **3** with excitation at 475 nm, with associated lifetimes of 73 fs (red line), 620 fs (blue line), and 25 ps (green line). Panel B: Same as panel A for model carotenoid **4**, with associated lifetimes of 66 fs (red line), 600 fs (blue line), and 11.5 ps (green line).

with shoulders at either side of this maximum, and can be assigned to population of the optically forbidden S_1 state upon IC from S_2. The third SADS (green line) is formed in 620 fs and has a lifetime of 25 ps. This SADS exhibits an overall blue-shifted and sharpened excited-state absorption with a maximum at 540 nm. The lifetime of the final SADS, 25 ps, results from IC of the S_1 state to the ground state and is similar to the lifetime in solution of other carotenoids with 9 conjugated double bonds, like neurosporene[40] and violaxanthin.[41,42]

Figure 3B shows the results of time-resolved measurements on model carotenoid **4** (10 carbon−carbon conjugated double bonds) dissolved in *n*-hexane. As with model carotenoid **3**, three components are required for a satisfactory description of the time-resolved spectra. The first SADS has a lifetime of 66 fs, has a shape very similar to that of the first SADS of model carotenoid **3**, and can be assigned to the S_2 state. The second SADS has a lifetime of 600 fs and exhibits an excited-state absorption near 565 nm with shoulders near 525 and 620 nm. The final SADS has a lifetime of 11.5 ps. It has a blue-shifted absorption with a peak at 560 nm and a shoulder at ∼530 nm, and we assign it to the S_1 state of the carotenoid. The 11.5 ps lifetime of the S_1 state resembles that of other 10-double bond carotenoids such as spheroidene in solution.[43]

The spectral evolution of model carotenoids **3** and **4** is similar to those observed earlier for other carotenoids: an extremely short lifetime for the S_2 state in the order of 100 fs, immediately followed by the appearance of an intense absorption that can be attributed to the appearance of the S_1 state. The dynamic blue-shift of the S_1 absorption on the sub-ps time scale is a well-documented phenomenon and has been assigned to a vibrational cooling process in the S_1 state.[23,44,45]

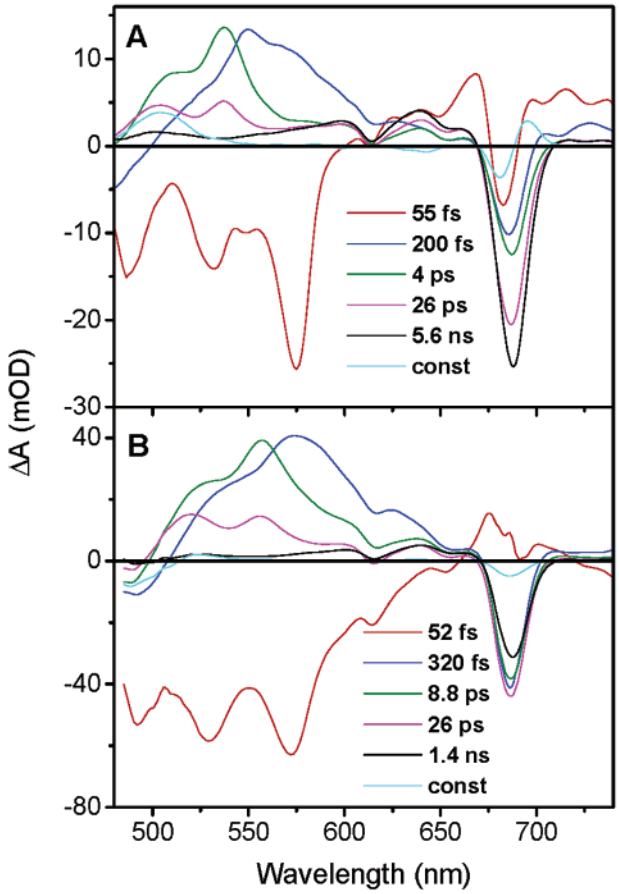

Figure 4. Panel A: Species-associated difference spectra (SADS) that follow from global analysis of time-resolved experiments on triad **1** with excitation at 475 nm, with associated lifetimes of 55 fs (red line), 200 fs (blue line), 4 ps (green line), 26 ps (magenta line), 5.6 ns (black line), and a nondecaying component (cyan line). Panel B: Same as panel A for triad **2**, with associated lifetimes of 52 fs (red line), 320 fs (blue line), 8.8 ps (green line), 26 ps (magenta line), 1.4 ns (black line), and a nondecaying component (cyan line).

*Femtosecond Time-Resolved Studies of Triad **1**.* After dissolving the triads in *n*-hexane, a nonpolar solvent, the light-harvesting function of these systems can be studied in detail, whereas in polar solvents, light-induced electron-transfer processes take place among the carotenoid and Pc moieties of the triads, as we will see below. Figure 4A shows the results of femtosecond time-resolved measurements on triad **1** dissolved in *n*-hexane in the form of a global analysis of the data using a sequential model. In Figure 5, kinetic traces are depicted at selected wavelengths (circles), along with the results of the global analysis procedure (solid lines). To illustrate the quality of the data, a selection of 12 raw time-resolved spectra out of the total of 120 recorded spectra is shown in Figure 9B of the Appendix. After excitation, optically dark states of the carotenoids are rapidly generated, giving rise to absorption features that are red-shifted with respect to that of the ground state of the carotenoid. The various carotenoid electronic excited states exhibit dynamics on a number of time scales and may be involved in IC processes and EET to Pc. The latter process becomes apparent in the spectral evolution by changes in the ground-state bleaching and SE of phthalocyanine near 685 nm. No less than six kinetic components are required for satisfactory description of the time-resolved spectra. The SADS of the initially created excited state (red line) has a lifetime of 55 fs. It exhibits a pronounced negative signal from 480 to 600 nm, arising from ground-state bleaching of the carotenoid near 480

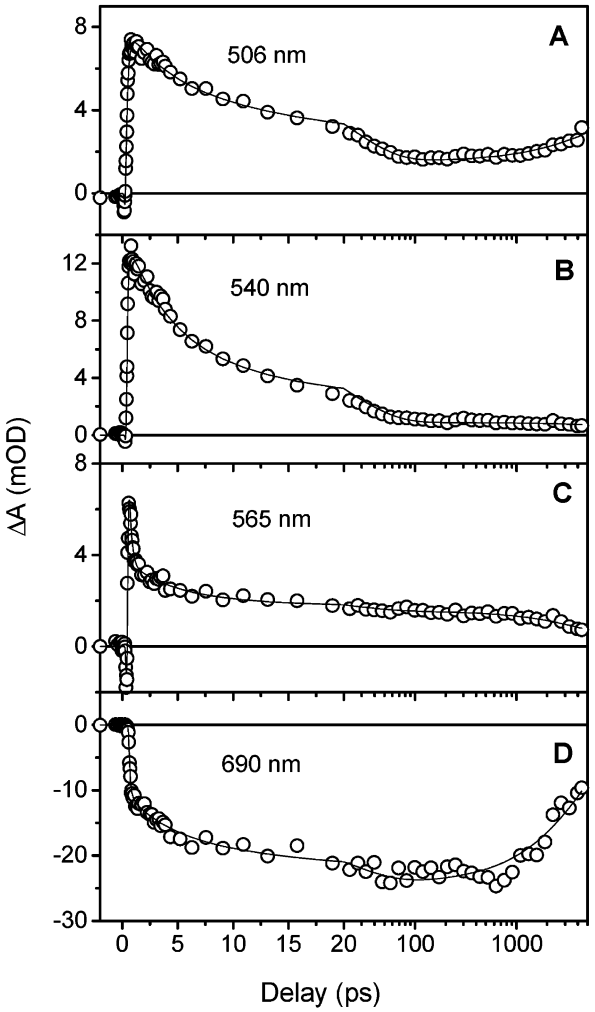

Figure 5. Kinetic traces measured in triad **1** at (A) 506 nm, (B) 540 nm, (C) 565 nm, and (D) 690 nm with excitation at 475 nm. The solid lines denote the fitted curves as determined by the global analysis procedure, of which the SADS are displayed in Figure 4A.

nm and stimulated emission to the ground state from ~520 to 600 nm. In addition, the initial SADS shows a band-shift like signal in the Q_y region of the Pc, which may be assigned to an electric-field effect by the charge redistribution of the excited carotenoid on the absorption spectrum of Pc. We assign this component to the population of the strongly allowed S_2 state of the carotenoid. The second SADS (blue line) has a lifetime of 200 fs. It shows a broad absorption near 550 nm and a negative feature near 685 nm. The negative signal at 685 nm can be attributed to ground-state bleaching and SE of Pc, which indicates that energy transfer has taken place from the S_2 state of the carotenoid to the Pc. This becomes apparent in the kinetic trace at 690 nm in Figure 5D as an almost instantaneous partial rise of the negative bleach/SE signal. The absorption near 550 nm can be assigned to population of the S_1 state of the carotenoid, which is formed through internal conversion from the S_2 state. The spectral maximum and the shape (blue line) are very similar to that of the second SADS of the model carotenoid, indicating that this state corresponds to a vibrationally hot S_1 state of the carotenoid, although its lifetime appears to be significantly shorter (200 vs 600 fs). The 200 fs dynamic process in the S_1 state is manifested in the kinetic trace at 565 nm, where a rapid decay of the absorption signal by about 40% is observed. The third SADS (green line) has a lifetime of 4 ps, and shows an absorption maximum near 540 nm. The spectral characteristics of this SADS encompass a blue shift with respect to the previous SADS (blue line). Importantly, the third SADS shows a pronounced shoulder near 505 nm. This absorption feature is not observed in the 9-double bond model carotenoid in solution (Figure 2). An induced absorption band that is blue-shifted with respect to that of S_1 and coincides with that of the carotenoid triplet state (see also below) is typical for the presence of the S* state.[18,23,46] The fourth SADS (magenta line) has a lifetime of 26 ps. It shows a significant decrease of the S_1 absorption at 540 nm and a concomitant rise of the Pc bleach/SE with respect to the previous SADS (green line). The S* absorption near 505 nm has decayed to a much smaller extent, which indicates that this state has a significantly longer lifetime than the S_1 state, as observed previously in several bacterial LH complexes and in spirilloxanthin in solution.[18,23] The separate lifetimes of S_1 and S* are illustrated in the kinetic traces in Figure 5, parts A and B, where S* (506 nm) clearly decays more slowly than S_1 (540 nm). The fifth SADS (black line) has a lifetime of 5.6 ns and its main feature involves a bleach/SE band near 690 nm. The time range used in this experiment (4.5 ns) is too short to accurately determine this time constant, and the 5.6 ns lifetime has been taken from single-photon timing experiments on the same triad (not shown) and fixed in the global analysis routine. We remark that, if this lifetime is allowed to vary in the global analysis routine, a very similar lifetime of 4.8 ns is obtained. The SADS is relatively flat in the 480−600 nm region, showing that the vast majority of carotenoid singlet states, e.g., S_1 and S*, have disappeared after 26 ps, and only Pc singlet excited states are present with bleaching/SE at 685 nm, a broad, flat absorption at longer wavelengths and a small bleach of the Q_x band at 615 nm. The final, nondecaying SADS (cyan line) shows the rise of a marked absorption band at 505 nm, indicative of formation of the carotenoid triplet state. This is clearly seen in the kinetic trace at 506 nm (Figure 5A), where the signal passes through a minimum near 100 ps and rises thereafter. Concomitantly, the ground-state bleach/SE signal on the Pc near 685 nm in the nondecaying SADS has disappeared completely and has been replaced by a band shift-like signal.

The spectral evolution in triad **1** shows similarities to that of the model carotenoid, but also shows marked differences that can be related to the covalent attachment to the Pc. First of all, the lifetime of the optically allowed S_2 state is shorter in triad **1**, 55 fs, as compared to the model carotenoid, 73 fs. The SADS in Figure 4 show that, in 55 fs, a ground state bleaching/SE band of Pc evolves from the band-shift like signal (red to blue line). These observations indicate that energy transfer to the Pc occurs from the optically allowed S_2 state of the carotenoid.

In competition with the energy transfer process, the S_2 state decays by internal conversion to low-lying optically forbidden carotenoid singlet excited states. Upon decay of the S_2 state, a broad absorption near 550 nm associated with the S_1 state appears, which shifts to the blue with a time constant of 200 fs (blue to green lines, Figure 4A). The spectral evolution is very similar to that arising from the vibrational cooling process in model carotenoid **3**, occurring with a time constant of 600 fs. The increased cooling rate in triad **1** most likely follows from an enhanced vibronic coupling in the triad because of the covalent linkage to the Pc, which opens up more degrees of freedom for intramolecular vibrational relaxation. Concomitant with the blue shift of the carotenoid S_1 absorption, we observe a slight increase and red shift of the bleach/SE signal near 690 nm. The rise of the bleach/SE signal possibly results from energy transfer from the vibrationally excited S_1 state of the carotenoid

to Pc. However, internal conversion from the Q_x to Q_y state of the Pc or a dynamic solvation process of the Pc Q_y states in the hexane solvent may also contribute to these signals.

The induced absorption band near 540 nm, which can be assigned to the relaxed S_1 state, has a lifetime of 4 ps, significantly shorter than that of model carotenoid **3** (25 ps). The concomitant rise of the Pc bleach/SE near 690 nm indicates that this shortening of the S_1 lifetime results from energy transfer to Pc (green to magenta line). Given an IC time constant of 25 ps of the S_1 state, it follows that, upon its formation, the S_1 state transfers its energy to Pc with a rate of $(4.7\ \text{ps})^{-1}$, at an efficiency of 84%.

The induced absorption near 505 nm is a new, unexpected feature that becomes apparent after vibrational relaxation of the S_1 state. We assign the 505 nm ESA to formation of the S* state, a new carotenoid singlet excited state which we have recently characterized in carotenoids bound to bacterial LH complexes and in the long carotenoid spirilloxanthin in hexane solution.[18,23,46] The S* state has a lifetime of 26 ps in triad **1**. The accompanying rise of the phthalocyanine bleaching near 690 nm with this time constant indicates that S* transfers energy to Pc.

The time-resolved data for triad **1** allow for an assessment of the relative contributions by the various carotenoid electronic excited states to the energy transfer process to Pc. From the S_2 lifetimes of model carotenoid **3** and triad **1**, it follows that the S_2 channel accounts for about 30% of the total energy transferred to Pc. This agrees reasonably with the relative bleach/SE signal of the Pc after S_2 relaxation (Figure 4A, blue line), which has an amplitude of 40% compared to that after all energy transfer processes are complete (black line). The rise of the Pc bleach/SE signal furthermore indicates a possible minor contribution of ~8% by the vibrationally excited S_1 state (blue to green line), a major contribution of ~32% by the relaxed S_1 state (green to magenta line), and a significant (20%) contribution by the S* state (magenta to black line). The light harvesting function of carotenoids in triad **1** shows striking similarities to that of the LH2 complex of *Rb. sphaeroides*, where a similar use of S_2, hot S_1, S_1, and S* pathways leads to a 90% total carotenoid−BChl energy transfer efficiency.[23]

With regard to the roles of the S_2 and S_1 states the present results agree quite well with earlier findings on the same compound.[29] Virtually the same S_2 lifetimes were found for triad **1** and model carotenoid **3,** whereas an S_1 lifetime of 2.8 ps was reported, which differs slightly from the number in this study (4 ps). Moreover, Mariño-Ochoa et al. found no evidence for energy transfer processes on time scales longer than 2.8 ps. The reason for this is not entirely clear, but we note that the experiments of Mariño-Ochoa et al. were conducted on triad **1** in a different solvent (toluene) on a short time axis of 20 ps and that, in the present experiment, the 4 ps lifetime is estimated from a full spectral analysis of a broad dataset encompassing carotenoid and Pc excited-state features, rather than from single kinetic traces.

*Femtosecond Time-Resolved Studies of Triad **2**.* The results for triad **1** indicate how the manifold of excited states in carotenoids are involved in singlet energy transfer processes to phthalocyanine. To assess the role of the excited-state energies of carotenoids on energy transfer rates and efficiencies in a similar geometrical configuration, we have performed fs transient absorption experiments on triad **2**, which binds a pair of carotenoids with 10 carbon−carbon double bonds each, as shown in Figure 1. Figure 4B shows the results of a global analysis of the femtosecond time-resolved measurements on triad

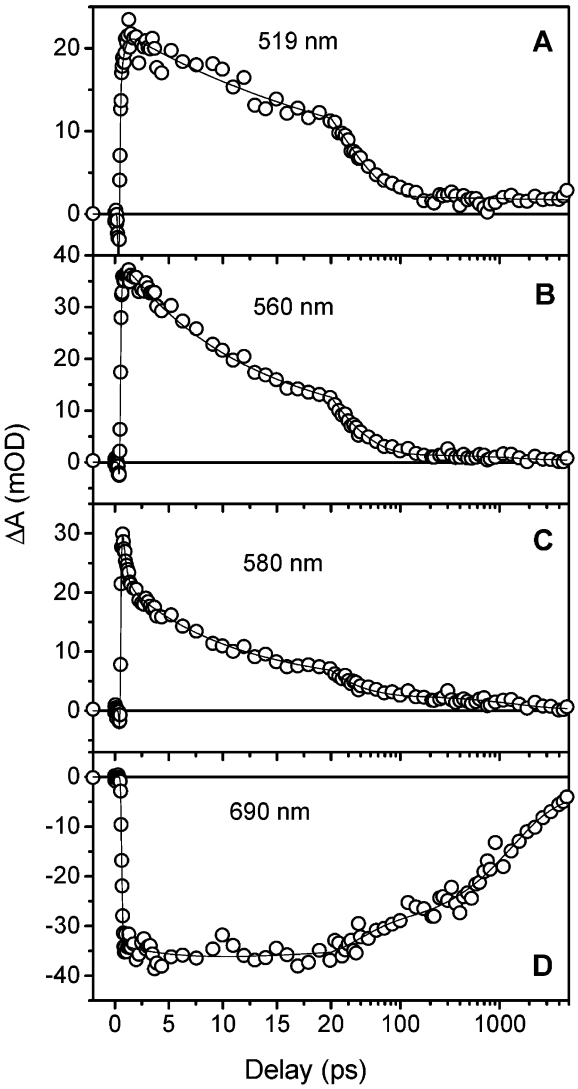

Figure 6. Kinetic traces measured in triad **2** at (A) 519 nm, (B) 560 nm, (C) 580 nm, and (D) 690 nm with excitation at 475 nm. The solid lines denote the fitted curves as determined by the global analysis procedure, of which the SADS are displayed in Figure 4B.

2 in *n*-hexane upon excitation at 475 nm. Kinetic traces at selected wavelengths have been depicted in Figure 6 (circles), along with the result of the global analysis (solid lines). Figure 9A of the Appendix shows a selection of raw time-resolved spectra. As with triad **1**, 6 components are needed for a satisfactory description of the time-resolved data. The first SADS (red line, Figure 4B) has a lifetime of 52 fs and can be assigned to the initially excited S_2 state of the carotenoid and exhibits distinct ground-state bleaching and stimulated emission features from 480 to 620 nm and a band-shift like feature around 680 nm superimposed on an induced absorption. The second SADS (blue line) has a lifetime of 320 fs and shows a pronounced induced absorption at 570 nm, which we attribute to the vibrationally excited S_1 state of the carotenoid. It furthermore shows a bleach/SE signal near 690 nm, which results from very rapid energy transfer to Pc from the carotenoid S_2 state, as evidenced by the rapid rise of a bleach/SE signal of the kinetic trace at 690 nm (Figure 6D). The third SADS (green line) has an associated decay time of 8.8 ps. It shows an induced absorption at 555 nm and pronounced shoulder near 525 nm. In analogy with triad **1**, we assign the former feature to the thermally relaxed S_1 state of the carotenoid and the latter to the S* state. Thus, upon carotenoid excitation, the S* state is

transiently present not only in triad **1** but in triad **2** as well. The system further evolves into the fourth SADS (magenta line), which has a lifetime of 26 ps. As compared to the previous SADS, a slight increase of the bleach/SE signal of Pc takes place in the 690 nm region. Concomitantly, the absorption at 555 has largely disappeared, indicating a decay of the S_1 state. The S* absorption at 520 nm has largely stayed intact, similar to the situation in triad **1**. The distinct lifetimes of S_1 and S* become apparent in the kinetic traces at 519 (Figure 6A) and 560 nm (Figure 6B). The fifth SADS (black line) has a lifetime of 1.4 ns. Given its flat absorption in the 480−600 nm region and the bleach/SE band at 685 nm, we attribute this spectrum solely to the singlet excited state of Pc. Intriguingly, the amplitude of the bleach/SE band of Pc has decreased by about 25% as compared to the previous SADS, denoting a quenching of Pc singlet excited states in the 26 ps evolution to this state.

Moreover, the singlet excited state of Pc, which lives 1.4 ns, appears to be quenched as compared to model Pc **5** (5.23 ns) and to Pc in triad **1** (5.6 ns). The reasons for these Pc singlet state quenchings are not clear, but they hint at direct singlet-state quenching mechanisms by carotenoids. Further experimental study and discussion of this phenomenon will be the subject of a forthcoming paper. The final, nondecaying SADS (cyan line) shows a small negative feature in the Pc bleaching region. This may be assigned to a small residue of singlet excited states of Pc, as single photon timing experiments on triad **2** yielded a biexponential decay of the Pc singlet state with time constants of 1.4 and 4 ns (not shown). In the present experiments, the time axis (4.5 ns) is not sufficient to distinguish the latter lifetime from a nondecaying component. Although the Pc triplet yield in triad **2** will be significantly lower as compared to that of triad **1** as a result of the quenched singlet lifetime, the final SADS may have a contribution by Pc triplet states which have formed through intersystem crossing from the Pc singlet state. It is important to note, however, that the biexponential decay of the Pc excited states precludes an accurate estimate of the final SADS, and it is thus difficult to interpret the data in terms of molecular processes that occur in this time range.

Despite the fact that the carotenoid to Pc energy transfer efficiency is dramatically lower in triad **2** as compared to that for triad **1**, the overall spectral evolution upon carotenoid excitation is very similar in these two systems: the same number of kinetic components is needed, and the difference spectra of the electronic states involved exhibit essentially the same absorption features. The total Pc bleach/SE amplitude near 685 nm in triad **2** remains significantly lower at all times as compared to that of triad **1**, consistent with the lower energy transfer efficiency from the carotenoids to the Pc.

Energy transfer from the optically allowed carotenoid S_2 state to the Pc moiety appears to proceed at a rate similar to that in triad **1**, as the S_2 lifetimes are very similar (55 and 52 fs), as are the S_2 lifetimes of their model compounds (73 and 66 fs). The quantum yields of energy transfer from S_2 in **1** and **2** can be estimated to be approximately 30% and 25%. The difference in energy transfer efficiency between triad **2** and triad **1** finds its origin in the properties of the optically forbidden states S_1 and S*. The lifetime of the S_1 state, 8.8 ps in triad **2**, is only marginally shorter than that of model carotenoid **4**, 11.5 ps. This indicates that only a little energy transfer occurs from the S_1 state in triad **2**. From its lifetime, an energy transfer rate constant of $(37\ \text{ps})^{-1}$ can be deduced, which implies that only 23% of the S_1 states that are formed transfer their energy to Pc. In agreement with this, the bleach/SE signal of Pc increases only slightly upon decay of the S_1 state (Figure 4B, green to magenta line evolution). Thus, energy transfer from the carotenoid to Pc in triad **2** proceeds almost exclusively through the S_2 state. This situation is very reminiscent of photosynthetic antenna systems that show similarly low carotenoid to (B)Chl transfer yields, like the LH1 complex of *Rs. rubrum*[18] and the CP43 and CP47 core antenna proteins of Photosystem II.[19]

*Energy Transfer from the S_1 State in Triads **1** and **2**.* It has become increasingly clear that efficient light harvesting strategies by carotenoids involve the employment of the optically forbidden S_1 state as an excited-state energy donor. Although it was previously believed that an electron exchange mechanism could mediate the energy transfer process, it was recently shown by quantum chemical methods that in natural light-harvesting complexes the exchange term is insignificant compared to the Coulombic interactions.[16,17] Energy transfer from the S_1 state to (B)Chl was, in many cases, found to proceed on the picosecond time scale, which implies a significant electronic coupling of the order of 10's of cm^{-1}.[12−14] How an optically dark state can exhibit such a strong Coulombic coupling is far from clear: it was argued that it follows from higher order terms in the multipole expansion of the transition charge density, and it was suggested that the exact geometric details of donor and acceptor influence this coupling to a great extent.[16,17,47] On the other hand, we have preliminary data on a model carotenoid−gold porphyrin dyad in which triplet−triplet energy transfer from a cyclic tetrapyrrole to an attached carotenoid occurs in ∼1 ps (Kodis et al., unpublished). This indicates that exchange-mediated processes can occur on the ps time scale and therefore should not be ruled out for S_1 transfer in the covalently linked artificial antenna systems.

Triads **1** and **2** show vastly different energy transfer rates from their respective S_1 states to Pc, of $(4.8\ \text{ps})^{-1}$ and $(37.5\ \text{ps})^{-1}$, respectively. Given the similar geometric structures of triads **1** and **2**, this phenomenon is likely associated with the relative energy levels of the S_1 states in these systems. Although we do not know the S_1 energy levels of model carotenoids **3** and **4**, approximate estimates may be made from comparison with carotenoids that have the same number of conjugated double bonds. For neurosporene, which has 9 double bonds, the 0−0 transition of the S_1 state has been estimated to lie around 654 nm (15300 cm^{-1}).[48] For violaxanthin (9 double bonds), estimates range from 672 (14880)[49] to 691 nm (14470 cm^{-1}).[41] For spheroidene (10 conjugated double bonds), estimates of the 0−0 transition of the S_1 state lie between 704 (14200)[48] and 746 nm (13400 cm^{-1}).[50]

To illustrate the effect of a decreasing energy gap (10 vs 9 bond carotenoid) on the spectral overlap of donor and acceptor, in Figure 7, we have depicted the S_1 emission of neurosporene (dashed line) and spheroidene (dotted line), both taken from ref 48, along with the absorption of the Pc moiety in triads (solid line). Obviously, the S_1 emission from the 9-conjugated double bond carotenoid is in much better resonance with Pc than that of the 10-conjugated-double-bond carotenoid, with a 3-fold larger spectral overlap of neurosporene as compared to spheroidene. We note that the carotenoid S_1 energies are somewhat controversial in the sense that near-IR transient absorption spectroscopy systematically yields results that are lower by 400−800 cm^{-1} on the same carotenoids compared to fluorescence spectroscopy.[50] If we assume such a red-shift by 400−800 cm^{-1} of the S_1 emission, the differences in spectral overlap between triad **1** and triad **2** become even larger because the 10-double-bond carotenoid shifts almost completely out of the overlap region with the Pc absorption, whereas the 9-double

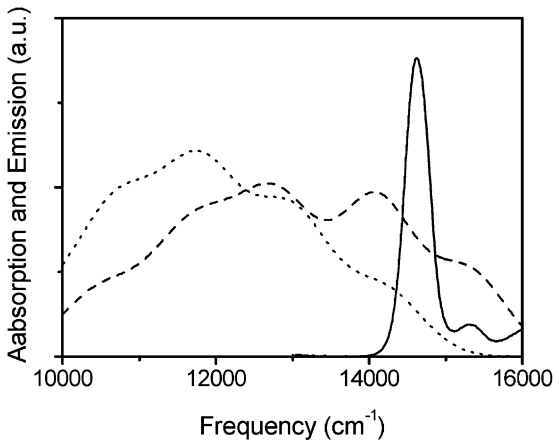

Figure 7. Absorption spectrum of phthalocyanine bound to triad **1** or **2** (solid line), fluorescence from the S_1 state of neurosporene, a 9 conjugated carbon−carbon double bond carotenoid (dashed line), and spheroidene, a 10 conjugated carbon−carbon double bond carotenoid (dotted line), taken from ref 48. The vertical scaling of absorption and emission spectra is arbitrary. See text for details.

bond carotenoid does so to a much smaller extent. Thus, it may be concluded that the spectral overlap of donor and acceptor states is to a significant extent responsible for the large difference in carotenoid light harvesting efficiency from the S_1 state in triad **1** and **2**.

S State in Triads 1 and 2.* The spectral evolution following carotenoid excitation in both triads **1** and **2** clearly indicates that, in addition to S_2 and S_1, the recently characterized S* state is transiently formed. Thus far, the S* state has been observed in spirilloxanthin in solution and in carotenoids bound to bacterial light harvesting complexes.[18,23,46] Gradinaru et al. and Papagiannakis et al. have previously reported that S* is populated in parallel with S_1 through IC from S_2 and have speculated that specific pigment−protein interactions could induce formation of this state in carotenoids shorter than spirilloxanthin.[18,23,46] The present observation of S* in an artificial antenna complex indicates that carotenoid−protein interactions are not necessary for the formation of this state. Moreover, we did not detect transient absorption characteristic of S* in model carotenoids **3** and **4** indicating that either S* is not populated in the model carotenoids or it quickly relaxes to the S_1 state and thereby escapes detection. These observations suggest that formation, or perhaps kinetic stabilization of S*, results from electronic (vibrational) coupling with nearby pigments. The sizable amplitudes of the S* absorption bands at 505 (triad **1**) and 520 nm (triad **2**) indicate that S* is formed in significant amounts. Although the extinction coefficients of these bands are not known, an estimate of the population of S* can be made from the relative energy transfer fraction in triad **1**: S* contributes about 20% of the total energy from the carotenoid to Pc (Figure 4A), and, given the fact that the energy transfer efficiency is almost 100%, about 20% of the photoexcited carotenoids in triad **1** must relax to the S* state. Assuming that the extinction coefficients of the S* bands in triads **1** and **2** are similar, we conclude from the amplitude of the S* bands (magenta lines in Figure 4A and B) that the transient S* concentration in triad **2** is similar, i.e., about 20%.

Strikingly, S* has identical lifetimes in triads **1** and **2** of 26 ps, suggesting that, in contrast to the S_1 state, the lifetime of S* does not depend strongly on the conjugation length of the carotenoid by an energy-gap law dependence. However, in triad **1**, the decay of S* is associated with a rise of the Pc bleach/SE signal (Figure 4A). In the absence of other carotenoid excited states on this time scale, this observation strongly indicates that S* transfers energy to Pc. The situation in triad **2** is completely different. The Pc bleach/SE signal does not rise concomitantly with the decay of S* in 26 ps but, instead, shows a marked decay by about 25% (Figure 4B).

Our results are consistent with the previous interpretation that S* corresponds to one of the theoretically predicted optically forbidden covalent states $^1B_u^-$ or $^3A_g^-$.[18,23,46] Another possibility, if the simultaneous decay of S* and the singlet excited state of Pc in triad **2** is not fortuitous, is that this new transient feature corresponds to a collective excited state of the triad. If this is the case, in triad **1**, the composite state relaxes to populate the singlet excited state of Pc, whereas in triad **2**, presumably for thermodynamic reasons, it does not and decays by IC to the ground state. Interestingly, Polivka et al. reported the transient formation of carotenoid radicals in the LH2 complex of *Rb. sphaeroides* with a lifetime identical to that of S* in the same complex[51] which suggests that S* could possess a certain degree of charge-transfer character and might represent a state that is more complex than previously thought.

Andersson and Gillbro[52] and Yoshizawa et al.[53] reported transient absorption features similar to the S* state in polyenes homologous with all-*trans*-β-carotene having 13, 15, and 19 conjugated double bonds and assigned these features to the hot carotenoid ground state. However, the shape of the difference spectrum of S* and its role in ultrafast triplet formation and light harvesting rules out this possibility.[18,23] Moreover, as a result of the differences in light-harvesting efficiencies, significantly more excited-state energy is dissipated to the carotenoid ground state in triad **2** as compared to triad **1** on the picosecond time scale. Despite this, the amplitude of the S* signals in triads **1** and **2** are very similar, which provides another argument against the interpretation of S* as a hot carotenoid ground state.

Recent femtosecond stimulated Raman experiments have suggested that, in short carotenoids (<12 conjugated double bonds), incomplete vibrational relaxation takes place during the S_1 lifetime, whereas in long carotenoids (>12 double bonds), the S_1 state may rapidly relax to its 0−0 level.[53,54] In this scenario, S* could be identified with the fully relaxed S_1 state. In shorter carotenoids, the S* or fully relaxed S_1 state is only observed when the carotenoid is interacting with chlorophylls in LH systems or with Pc in the artificial systems. In this view, the tetrapyrrole states could act as mediator states allowing the carotenoid to reach the zero vibration level of S_1. Slow relaxation in the lower vibrational states of the singlet manifold could explain why different spectroscopic methods give different values for the 0−0 transition of the S_1 state in carotenoids.[41,48−50] However, picosecond time-resolved anti-Stokes Raman experiments have shown that complete vibrational relaxation in β-carotene is complete in less than 2 ps, arguing against the picture painted above.[55] Moreover, application of femtosecond stimulated Raman spectroscopy on carotenoids by several research groups has not yet given mutually consistent results[53,54,56,57] and the validity of Yoshizawa's results remains to be demonstrated.

In triads **1** and **2**, the SADS that represents the absorbance changes after S* has decayed show a relatively flat absorption in the 480−550 nm region (Figure 4, parts A and B, black line), arising from the Pc singlet excited state. This indicates that no detectable carotenoid triplet states are directly generated from S*, in contrast to the case of the LH complexes of photosynthetic bacteria, where the S* state is a precursor to the picosecond formation of carotenoid triplet states. These carotenoid triplets may be formed with a yield of up to 30% by a singlet fission

mechanism.[18,23,46] It thus appears that in triads **1** and **2** the singlet fission mechanism is either not active or so slow that it cannot compete with other relaxation processes from S* including energy transfer to Pc in triad **1**. Quantum-chemical calculations by Tavan and Schulten[24,28] have shown that the "covalent", optically dark excited singlet states in carotenoids exhibit a doubly excited triplet character, and they suggested that dissociation, or fission, of such states into pairs of spin-correlated triplet states could be induced by lattice distortions, i.e., structural deformations of the polyene backbone. In full agreement with this, recent experiments on carotenoid-reconstituted LH complexes *Rb. sphaeroides R.26* and *Rs. rubrum* have demonstrated that the extent of triplet generation from S* depends on the degree of protein-imposed structural distortion of the polyene backbone in the LH complex.[46] In the triads, the carotenoids assume a relaxed, planar conformation (Figure 1), which minimizes the fission probability and suppresses triplet formation.

*Triplet Energy Transfer in Triads **1** and **2**.* In triad **1**, formation of the carotenoid triplet state immediately follows decay of the Pc singlet excited state with a time constant of 5.6 ns, as indicated by the rise of the triplet absorption at 505 nm (Figure 4A, sixth SADS, cyan line). The Pc triplet state, which is formed through intersystem crossing from the Pc singlet excited state, is not observed at any time in the spectral evolution. This implies that triplet−triplet energy transfer from the Pc to the carotenoid takes place very rapidly, and proceeds at a rate that is much faster than the rate of Pc singlet state decay, $(5.6\ \text{ns})^{-1}$, which itself is the sum of the radiative rate, the ISC rate, and the IC rate. This observation is consistent with recent experiments on a carotenoid−goldporphyrin (C−AuP) dyad alluded above, where it was shown that the AuP triplet excited state, formed from the singlet excited state in 560 fs, was quenched from 2.4 ns to 1.5 ps by triplet−triplet energy transfer to yield the carotenoid triplet excited state [Kodis et al., unpublished results]. Time constants on the order of 10 ns have been reported for BChl to carotenoid triplet transfer in bacterial light harvesting complexes.[58] It thus appears that the triplet−triplet energy transfer process in triad **1** is orders of magnitude faster than in natural photosynthetic systems. This may be related to the covalent linkage between the carotenoid and Pc moieties in the triad, which provides closer contacts for exchange mediated processes between the π orbitals of the donor and acceptor than the van der Waals contacts between (B)Chls and carotenoids in the natural photosynthetic systems.

Our experiments do not give clear-cut information on the triplet energy transfer processes in triad **2**; the Pc singlet state is quenched as compared to triad **1**, which accordingly lowers the Pc triplet yield. Moreover, the multiexponential decay of Pc on the nanosecond time scale severely hampers an assessment of late-time spectra, which contain the dynamic information regarding formation of the carotenoid triplet state.

Electron Transfer. *Cyclic Voltammetry.* Upon dissolving triads **1** and **2** in polar solvents, light-induced electron-transfer events occur among the carotenoid and Pc moieties. Electrochemical measurements were undertaken to investigate the redox properties of phthalocyanine and carotenoid moieties in triads **1** and **2**. These were necessary in order to estimate the energies of the charge-separated states. The measurements were carried out with a Pine Instrument Co. model AFRDE4 potentiostat at ambient temperatures with a glassy carbon or platinum wire working electrode, a Ag/Ag^+ reference electrode, and a platinum wire counter electrode. Measurements were performed in benzonitrile containing 0.1 M tetra-*n*-butylammonium hexafluorophosphate and ferrocene as an internal standard (oxidation at 0.46 V vs SCE). Phthalocyanine model **5** featured an oxidation wave at 1.04 V vs SCE and reduction at −0.76 V vs SCE. Model carotenoid **3** (9 double bonds) showed an oxidation wave at 0.68 V vs SCE, and 10 double bond carotenoid model **4** showed an oxidation wave at 0.60 V vs SCE, both irreversible. Triads **1** and **2** were found to exhibit a ∼0.02 V higher oxidation potential of their carotenoid moieties (0.7 and 0.62 V vs SCE) and ∼0.04 V lower reduction potential of phthalocyanine (−0.72 V vs SCE). The energies of the $C^{\bullet+}-Pc^{\bullet-}$ charge-separated states in triads **1** and **2** were estimated as 1.42 and 1.34 eV, respectively, based on the electrochemically determined oxidation and reduction potentials of the triads.

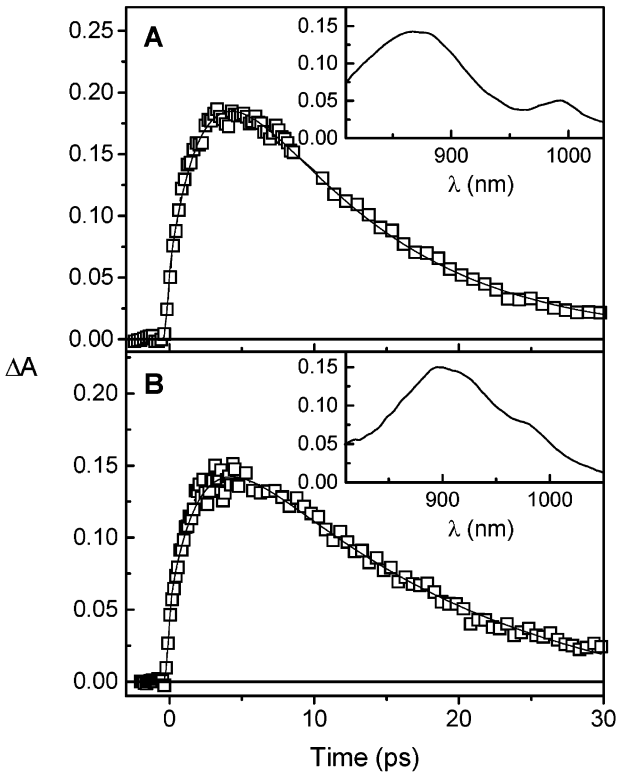

Figure 8. A: Kinetic trace recorded in triad **1** dissolved in benzonitrile upon excitation at 680 nm, and detection at 870 nm. The inset shows the absorbance difference spectrum at a delay of 2 ps under the same conditions. B: Same as A for triad **2**, with detection at 900 nm. The inset shows the absorbance difference spectrum at a delay of 3 ps under the same conditions.

Femtosecond Transient Absorption. The formation of a $C^{\bullet+}-Pc^{\bullet-}$ charge separated state by photoinduced electron transfer was probed by a fs transient absorption spectroscopic investigation of the triads in benzonitrile solution. In both triad **1** and triad **2,** $C^{\bullet+}-Pc^{\bullet-}$ charge separation was observed. This state can be readily identified by the phthalocyanine radical anion near 580 and 990 nm and/or by the carotenoid radical cation absorption at 820−950 nm (see Figure 8A,B inset). Figure 8A shows the kinetic trace of triad **1** with excitation at 680 nm and detection at 870 nm and the time-resolved difference spectrum obtained after 2 ps (inset). At 680 nm, the excitation light is absorbed exclusively by the Pc moiety generating the singlet excited state which decays with a time constant of 2.5 ps to yield the $C^{\bullet+}-Pc^{\bullet-}$ charge-separated state, observed as a rise/formation of the carotenoid radical band at 870 nm. The charge-separated state decays to the ground state with a lifetime of 10.5 ps.

Figure 8B shows the corresponding kinetic trace for triad **2**, with detection at 900 nm. The time-resolved spectrum, obtained

after 3 ps, is shown in the inset. In this case, the $C^{\bullet+}-Pc^{\bullet-}$ charge-separated state is formed with a time constant of 2.2 ps and decays to the ground state in 17 ps. Electrochemical measurements gives a value of the $C^{\bullet+}-Pc^{\bullet-}$ charge-separated state energy that is ~0.1 eV higher for triad **1.** Therefore, there is less driving force for electron transfer in this case and charge separation is slower, whereas charge recombination is faster compared to triad **2**. The induced absorption due to the carotenoid radical cation in triad **2** is shifted to the red relative to that in **1**, as is expected.

In *n*-hexane, charge separation was not observed, most likely due to lack of charge stabilization in the nonpolar solvent.

4. Conclusions

The application of time-resolved spectroscopy to triads **1** and **2** has revealed that carotenoids and tetrapyrroles can be designed in a compact architecture to closely mimic light-harvesting and photoprotective functions as they exist in natural photosynthesis. Triad **1**, which binds a pair of carotenoids with 9 carbon−carbon conjugated double bonds, is a most appealing example because it exhibits near complete light-harvesting through three of the available electronic states of the carotenoid: the optically allowed S_2 state, the optically forbidden S_1 state, and the newly discovered S* state. In contrast to many photosynthetic light harvesting complexes, formation of the S* state does not lead to a loss of light harvesting efficiency by generating carotenoid triplet states on the ultrafast time scale, which may be related to the relaxed, planar, conformation of the triad-bound carotenoid in hexane solution. Upon completion of the light harvesting function, the carotenoids in triad **1** efficiently accept energy from phthalocyanine triplet states that have been formed through intersystem crossing, and do so at a rate that is much faster than the phthalocyanine singlet-state decay rate, $(5.6\ \text{ns})^{-1}$.

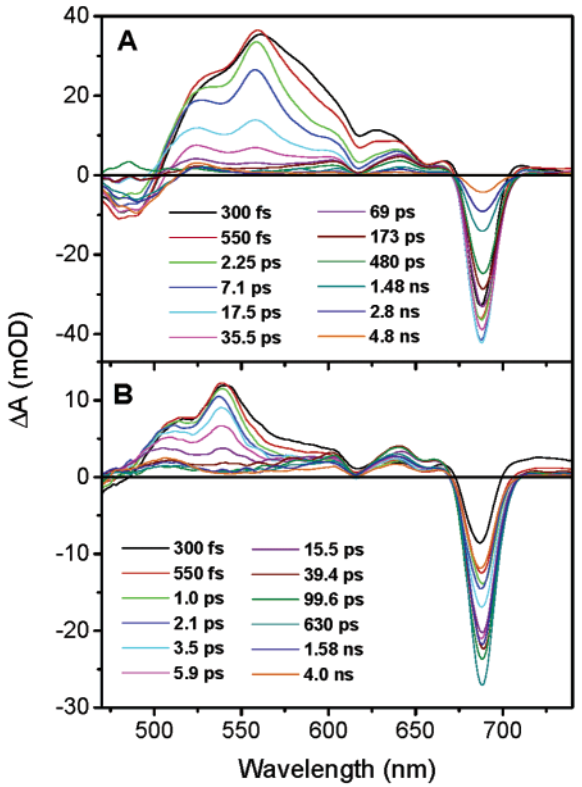

Figure 9. A: raw time-resolved spectra in triad **2** dissolved in *n*-hexane upon excitation at 475 nm, recorded at the time delays indicated. B: Same as A for triad **1**.

Our studies on triad **2**, which binds carotenoids with 10 conjugated carbon−carbon double bonds, have shown that accurate tuning of the energies of the optically forbidden states of the carotenoid relative to the states of the acceptor molecule are crucial for an efficient light harvesting function. We found that lowering of the S_1 state energy leads to a loss of overall energy transfer efficiency, which can be traced back to a decreased spectral overlap between donor and acceptor. The light-harvesting role of the S* state could not unambiguously be elucidated for triad **2**, nor could the multiple quenching processes that govern the singlet state decay of the Pc. These will be the subject of further studies.

Finally, we have shown that the carotenoids serve as excellent electron donors to phthalocyanine in triads **1** and **2** when the molecules are dissolved in a polar solvent.

5. Appendix

To indicate the quality of the time-resolved spectra taken on triads **1** and **2** and illustrate their complex spectral evolutions in time, raw time-resolved spectra are shown in Figure 9, parts A (triad **2**) and B (triad **1**), at time delays indicated. Twelve out of a total of 120 spectra are shown for each triad. The SADS shown in Figure 4, parts A and B are derived from the complete datasets of 120 spectra.

Acknowledgment. This work was supported by the European Union − access to Research Infrastructures action of the Improving Human Potential Program (HPRI-CT-1999-00064), the U. S. Department of Energy (DE-FG02-03ER15393), the Earth and Life Sciences Council of The Netherlands Organization for Scientific Research (NWO-ALW), and The Netherlands Organization for Fundamental Research on Matter (FOM). We thank Roche for the generous gift of carotenoid samples. This is publication 579 from the ASU Center for the Study of Early Events in Photosynthesis.

References and Notes

(1) Ritz, T.; Damjanovic, A.; Schulten, K.; Zhang, J.-P.; Koyama, Y. *Photosynth. Res.* **2000**, *66*, 125.
(2) Koyama, Y.; Kuki, M.; Andersson, P. O.; Gillbro, T. *Photochem. Photobiol.* **1996**, *63*, 243.
(3) Frank, H. A.; Cogdell, R. J. In *Carotenoids in Photosynthesis*; Young, A., Britton, G., Eds.; Chapmann & Hall: London, 1993; p 252.
(4) van Grondelle, R.; Dekker: J. P.; Gillbro, T.; Sundström, V. *Biochim. Biophys. Acta (Bioeng.)* **1994**, *1187*, 1.
(5) Tracewell, C. A.; Vrettos, J. S.; Bautista, J. A.; Frank, H. A.; Brudvig, G. W. *Arch. Biochem. Biophys.* **2001**, *385*, 61.
(6) Hanley, J.; Deligiannakis, Y.; Pascal, A.; Faller, P.; Rutherford, A. W. *Biochemistry* **1999**, *38*, 8189.
(7) Horton, P.; Ruban, A. V.; Young, A. J. In *The Photochemistry of Carotenoids*; Frank, H. A., Britton, A. J. Y. G., Cogdell, R. J., Eds.; Kluwer Academic Publishers: Dordrecht, The Netherlands, 1999; p 271.
(8) McDermott, G.; Prince, S. M.; Freer, A. A.; Hawthornthwaite-Lawless, A. M.; Papiz, M. Z.; Cogdell, R. J.; Isaacs, N. W. *Nature* **1995**, *374*, 517.
(9) Jordan, P.; Fromme, P.; Witt, H. T.; Klukas, O.; Saenger, W.; Krauss, N. *Nature* **2001**, *411*, 909.
(10) Kuhlbrandt, W.; Wang, D. N.; Fujiyoshi, Y. *Nature* **1994**, *367*, 614.
(11) Koepke, J.; Hu, X. C.; Muenke, C.; Schulten, K.; Michel, H. *Structure* **1996**, *4*, 581.
(12) Walla, P. J.; Linden, P. A.; Hsu, C. P.; Scholes, G. D.; Fleming, G. R. *Proc. Natl. Acad. Sci. (U.S.A.)* **2000**, *97*, 10808.
(13) Zhang, J.-P.; Fujii, R.; Qian, P.; Inaba, T.; Mizoguchi, T.; Koyama, Y.; Onaka, K.; Watanabe, Y. *J. Phys. Chem. B* **2000**, *104*, 3683.
(14) Gradinaru, C. C.; van Stokkum, I. H. M.; Pascal, A. A.; van Grondelle, R.; van Amerongen, H. *J. Phys. Chem. B* **2000**, *104*, 9330.
(15) Shreve, A. P.; Trautman, J. K.; Frank, H. A.; Owens, T. G.; Albrecht, A. C. *Biochim. Biophys. Acta* **1991**, *1058*, 280.
(16) Damjanovic, A.; Ritz, T.; Schulten, K. *Phys. Rev. E* **1999**, *59*, 3293.
(17) Krueger, B. P.; Scholes, G. D.; Fleming, G. R. *J. Phys. Chem. B* **1998**, *102*, 5378.

(18) Gradinaru, C. C.; Kennis, J. T. M.; Papagiannakis, E.; van Stokkum, I. H. M.; Cogdell, R. J.; Fleming, G. R.; Niederman, R. A.; van Grondelle, R. *Proc. Natl. Acad. Sci. (U.S.A.)* **2001**, *98*, 2364.
(19) de Weerd, F. L.; Dekker: J. P.; van Grondelle, R. *J. Phys. Chem. B* **2003**, *107*, 6214.
(20) Croce, R.; Muller, M. G.; Bassi, R.; Holzwarth, A. R. *Biophys. J.* **2001**, *80*, 901.
(21) Kennis, J. T. M.; Gobets, B.; van Stokkum, I. H. M.; Dekker: J. P.; van Grondelle, R.; Fleming, G. R. *J. Phys. Chem. B* **2001**, *105*, 4485.
(22) de Weerd, F. L.; Kennis, J. T. M.; Dekker: J. P.; van Grondelle, R. *J. Phys. Chem. B* **2003**, *107*, 5995.
(23) Papagiannakis, E.; Kennis, J. T. M.; van Stokkum, I. H. M.; Cogdell, R. J.; van Grondelle, R. *Proc. Natl. Acad. Sci. (U.S.A.)* **2002**, *99*, 6017.
(24) Tavan, P.; Schulten, K. *J. Chem. Phys.* **1986**, *85*, 6602.
(25) Sashima, T.; Nagae, H.; Kuki, M.; Koyama, Y. *Chem. Phys. Lett.* **1999**, *299*, 187.
(26) Zhang, J.-P.; Inaba, T.; Watanabe, Y.; Koyama, Y. *Chem. Phys. Lett.* **2000**, *332*, 351.
(27) Cerullo, G.; Polli, D.; Lanzani, G.; De Silvestri, S.; Hashimoto, H.; Cogdell, R. J. *Science* **2002**, *298*, 2395.
(28) Tavan, P.; Schulten, K. *Phys. Rev. B* **1987**, *36*, 4337.
(29) Marino-Ochoa, E.; Palacios, R.; Kodis, G.; Macpherson, A. N.; Gillbro, T.; Gust, D.; Moore, T. A.; Moore, A. L. *Photochem. Photobiol.* **2002**, *76*, 116.
(30) Macpherson, A. N.; Liddell, P. A.; Kuciauskas, D.; Tatman, D.; Gillbro, T.; Gust, D.; Moore, T. A.; Moore, A. L. *J. Phys. Chem. B* **2002**, *106*, 9424.
(31) Gust, D.; Moore, T. A.; Moore, A. L. *Acc. Chem. Res.* **2001**, *34*, 40.
(32) Liddell, P. A.; Kuciauskas, D.; Sumida, J. P.; Nash, B.; Nguyen, D.; Moore, A. L.; Moore, T. A.; Gust, D. *J. Am. Chem. Soc.* **1997**, *119*, 1400.
(33) Cardoso, S. L.; Nicodem, D. E.; Moore, T. A.; Moore, A. L.; Gust, D. *J. Am. Chem. Soc.* **1996**, *7*, 19.
(34) Freiberg, A.; Timpmann, K.; Lin, S.; Woodbury, N. W. *J. Phys. Chem. B* **1998**, *102*, 10974.
(35) van Stokkum, I. H. M.; Scherer, T.; Brouwer, A. M.; Verhoeven, J. W. *J. Phys. Chem. B* **1994**, *98*, 852.
(36) Macpherson, A. N.; Gillbro, T. *J. Phys. Chem. A* **1998**, *102*, 5049.
(37) Ricci, M.; Bradforth, S. E.; Jimenez, R.; Fleming, G. R. *Chem. Phys. Lett.* **1996**, *259*, 381.
(38) Macpherson, A. N.; Arellano, J. B.; Fraser, N. J.; Cogdell, R. J.; Gillbro, T. *Biophys. J.* **2001**, *80*, 923.
(39) Holt, N. E.; Kennis, J. T. M.; Dall'Osto, L.; Bassi, R.; Fleming, G. R. *Chem. Phys. Lett.* **2003**, *379*, 305.
(40) Zhang, J.-P.; T., I.; Watanabe, Y.; Koyama, Y. *Chem. Phys. Lett.* **2000**, *331*, 154.
(41) Polivka, T.; Herek, J. L.; Zigmantas, D.; Akerlund, H. E.; Sundstrom, V. *Proc. Natl. Acad. Sci. (U.S.A.)* **1999**, 4914.
(42) Frank, H. A.; Cua, A.; Chynwat, V.; Young, A.; Gosztola, D.; Wasielewski, M. R. *Photosynth. Res.* **1994**, *41*, 389.
(43) Desamero, R. Z. B.; Chynwat, V.; van der Hoef, I.; Jansen, F. J.; Lugtenburg, J.; Gosztola, D.; Wasielewski, M. R.; Cua, A.; Bocian, D. F.; Frank, H. A. *J. Phys. Chem. B* **1998**, *102*, 8151.
(44) de Weerd, F. L.; van Stokkum, I. H. M.; van Grondelle, R. *Chem. Phys. Lett.* **2002**, *354*, 38.
(45) Billsten, H. H.; Zigmantas, D.; Sundstrom, V.; Polivka, T. *Chem. Phys. Lett.* **2002**, *355*, 465.
(46) Papagiannakis, E.; Das, S. K.; Gall, A.; van Stokkum, I. H. M.; Robert, B.; van Grondelle, R.; Frank, H. A.; Kennis, J. T. M. *J. Phys. Chem. B* **2003**, *107*, 5642.
(47) Hsu, C. P.; Walla, P. J.; Head-Gordon, M.; Fleming, G. R. *J. Phys. Chem. B* **2001**, *105*, 11016.
(48) Fujii, R.; Onaka, K.; Kuki, M.; Koyama, Y.; Watanabe, Y. *Chem. Phys. Lett.* **1998**, *288*, 847.
(49) Frank, H. A.; Bautista, J. A.; Josue, J. S.; Young, A. J. *Biochemistry* **2000**, *39*, 2831.
(50) Polivka, T.; Zigmantas, D.; Frank, H. A.; Bautista, J. A.; Herek, J. L.; Koyama, Y.; Fujii, R.; Sundstrom, V. *J. Phys. Chem. B* **2001**, *105*, 1072.
(51) Polivka, T.; Zigmantas, D.; Herek, J. L.; He, Z.; Pascher, T.; Pullerits, T.; Cogdell, R. J.; Frank, H. A.; Sundstrom, V. *J. Phys. Chem. B* **2002**, *106*, 11016.
(52) Andersson, P. O.; Gillbro, T. *J. Chem. Phys.* **1995**, *103*, 2509.
(53) Yoshizawa, M.; Aoki, H.; Ue, M.; Hashimoto, H. *Phys. Rev. B* **2003**, *67*, 174302.
(54) Yoshizawa, M.; Aoki, H.; Hashimoto, H. *Phys. Rev. B* **2001**, *63*, 180301.
(55) McCamant, D. W.; Kim, J. E.; Mathies, R. A. *J. Phys. Chem. A* **2002**, *106*, 6030.
(56) Rondonuwu, F. S.; Watanabe, Y.; Zhang, J. P.; Furuichi, K.; Koyama, Y. *Chem. Phys. Lett.* **2002**, *357*, 376.
(57) McCamant, D. W.; Kukura, P.; Mathies, R. A. *J. Phys. Chem. A* **2003**, *107*, 8208.
(58) Bittl, R.; Schlodder, E.; Geisenheimer, I.; Lubitz, W.; Cogdell, R. J. *J. Phys. Chem. B* **2001**, *105*, 5525.

II. Palacios, Rodrigo E.; Gould, Stephanie L.; Herrero, Christian; Hambourger, Michael; Brune, Alicia; Kodis, Gerdenis; Liddell, Paul A.; Kennis, John; Macpherson, Alisdair N.; Gust, Devens; Moore, Thomas A.; Moore, Ana L. **Bioinspired energy conversion.** Pure and Applied Chemistry (2005), 77(6), 1001-1008.

Pure Appl. Chem., Vol. 77, No. 6, pp. 1001–1008, 2005.
DOI: 10.1351/pac200577061001

Bioinspired energy conversion*

Rodrigo E. Palacios[1], Stephanie L. Gould[1], Christian Herrero[1], Michael Hambourger[1], Alicia Brune[1], Gerdenis Kodis[1], Paul A. Liddell[1], John Kennis[2], Alisdair N. Macpherson[3], Devens Gust[1,‡], Thomas A. Moore[1,‡], and Ana L. Moore[1,‡]

[1]The Center for the Study of Early Events in Photosynthesis, Department of Chemistry and Biochemistry, Arizona State University, Tempe, AZ 85287, USA; [2]Department of Biophysics, Division of Physics and Astronomy, Faculty of Sciences, Vrije Universiteit, 1081 HV Amsterdam, The Netherlands; [3]Department of Chemistry, University of York, Heslington, York, YO10 5DD, UK

Abstract: Artificial photosynthetic antenna systems have been synthesized based on carotenoid polyenes and polymer-polyenes covalently attached to tetrapyrroles. Absorption of light in the blue/green region of the spectra excites the polyenes to their S_2 state, and ultrafast singlet energy transfer to the tetrapyrroles occurs when the chromophores are in partial conjugation. The additional participation of other excited states of the polyene in the energy-transfer process is a requirement for perfect antenna function. Analogs of photosynthetic reaction centers consisting of tetrapyrrole chromophores covalently linked to electron acceptors and donors have been prepared. Excitation of these constructs results in a cascade of energy transfer/electron transfer which, in selected cases, forms a final charge-separated state characterized by a giant dipole moment (>150 D), a quantum yield approaching unity, a significant fraction of the photon energy stored as chemical potential, and a lifetime sufficient for reaction with secondary electron donors and acceptors. A new antenna-reaction center complex is described in which a carotenoid moiety is located in partial conjugation with the tetrapyrrole π-system allowing fast energy transfer (<100 fs) between the chromophores. In this assembly, the energy transduction process can be initiated by light absorbed by the polyene.

Keywords: bioinspired; energy conversion; photosynthesis; carotenoid polyenes; antenna systems.

INTRODUCTION

Energy security is an issue facing humanity that is no less significant than war, famine, disease, the plight of refugees, and the guarantee of human rights across the lands. Indeed, providing energy security is a necessary step that societies must take to resolve conflicts. Nature's photosynthetic process provides paradigms for sustainable global energy production and efficient energy transformations, which are conditions that underpin energy security. The combination of mechanistic and structural informa-

*Paper based on a presentation at the XX[th] IUPAC Symposium on Photochemistry, 17–22 July 2004, Granada, Spain. Other presentations are published in this issue, pp. 925–1085.
‡Corresponding authors

tion available for energy-transducing biological structures serves to guide organic, inorganic, and materials chemists in their efforts to abstract and mimic the active elements of nature's energy-processing constructs and press them into human-directed service. Toward these ends, in our laboratory we have designed a number of artificial photosynthetic constructs and assembled them into energy-converting systems [1].

LIGHT HARVESTING

Effective absorption of light by chromophores in photosynthetic membranes is achieved by complex arrays of tetrapyrrole macrocycles, carotenoids, and other pigments. In many biomimetic systems, the conversion of excitation energy to electrical or chemical energy by electron- or proton-transfer reactions must occur at a phase boundary. This can limit the useful absorption of light to a monolayer of chromophores at or near the surfaces of membranes or of semiconductors. Therefore, in these constructs there is a fundamental problem due to the limited light capture cross-section of dye molecules. One successful strategy has been the use of high-surface-area materials consisting of nanocrystalline wide band-gap semiconducting oxide particles with a mesoporous architecture over which a monolayer of dye is deposited [2,3]. Other approaches include the use of covalently linked arrays of porphyrins and other chromophores as well as self-assembled constructs to form compact structures with high-absorption cross-sections which could be positioned at an interface for charge separation [4–7]. An example of a porphyrin array linked to a free-base porphyrin-fullerene artificial reaction center is illustrated by **1** [8,9].

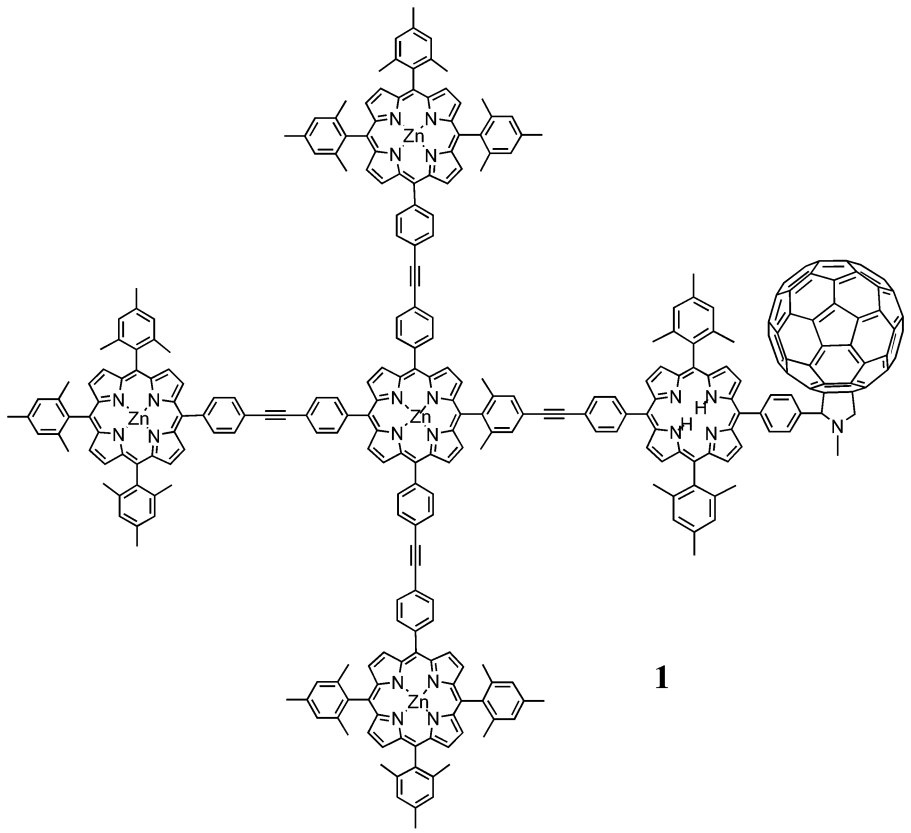

1

Time-resolved absorption and emission studies revealed that excitation of a peripheral zinc porphyrin in **1** is followed by singlet–singlet energy transfer among the four porphyrins of the antenna array, with final trap of the excitation by the free-base porphyrin, which acts as an energy sink. The excited state of the free-base porphyrin decays by electron transfer to the fullerene with a time constant of 25 ps and generates the $(P_{zn})_4$–$P^{\bullet+}$–$C_{60}^{\bullet-}$ state with a quantum yield of 0.98, based on light absorbed by the antenna zinc porphyrins. Thermodynamically favorable migration of the positive charge into the zinc porphyrin array transforms the initial state into a long-lived $(P_{zn})_4^{\bullet+}$–P–$C_{60}^{\bullet-}$ charge-separated state with a quantum yield of ~0.90 and lifetime of 25 μs in benzonitrile. In this process, the light-gathering power of the system is increased tremendously at many wavelengths, as four zinc porphyrin moieties feed excitation energy to the reaction center. However, by inspection of the absorption spectrum of **1** shown in Fig. 1, it is evident that there is little absorption of light in the vicinity of 500 nm, the region of maximum solar irradiance, by the array of antenna porphyrins. In order to ameliorate this deficiency, typical of porphyrin-based antennas, we have designed artificial antennas with carotenoid pigments to "fill in" absorption in regions where tetrapyrrole absorption is low.

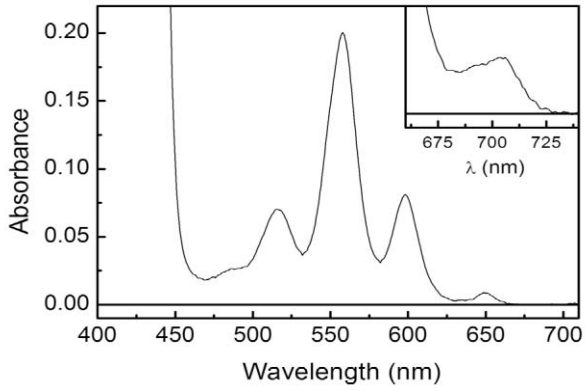

Fig. 1 Absorption spectra of **1** in 2-methyltetrahydrofuran. The inset is an expansion of the fullerene long-wavelength absorption region.

Carotenoid polyenes are found in essentially all the chlorophyll-binding antennas of photosynthetic organisms where, among other vital photoprotective functions, they absorb light in the blue/green region of the spectrum, and efficiently transfer energy to chlorophylls, which are located in van der Waals contact with them. Carotenoid antenna function is perplexing in that although antenna function requires singlet–singlet energy transfer among chromophores, carotenoids in solution do not undergo singlet energy transfer to other chromophores. Artificial antennas containing a carotenoid moiety must have covalent bonds between the carotenoid and the cyclic tetrapyrrole in order to display efficient carotenoid-to-tetrapyrrole singlet energy transfer. This is due to the extremely short lifetime of the carotenoid excited states, which requires relatively strong electronic coupling for rapid energy transfer. An example of a covalently bonded system that does show energy transfer is **2**, in which a carotenoid is covalently attached to a purpurin through an amide linkage, which leads to partial conjugation between the chromophores [10].

Ultrafast fluorescence upconversion measurements on the carotenopurpurin dyad **2** and an unlinked model carotenoid demonstrate that the fluorescent (optically allowed) S_2 excited state of the carotenoid model compound has a lifetime of 150 fs, while the corresponding excited state of the carotenoid in **2** is quenched to 40 fs. This quenching is assigned to energy transfer from the S_2 state of the carotenoid to the purpurin with 73 % efficiency, which is in accord with the quantum yield obtained by steady-state fluorescence excitation measurements. The lifetime of the optically forbidden S_1 state of the carotenoid (7.8 ps), which is populated by internal conversion from the S_2 state, is the same in

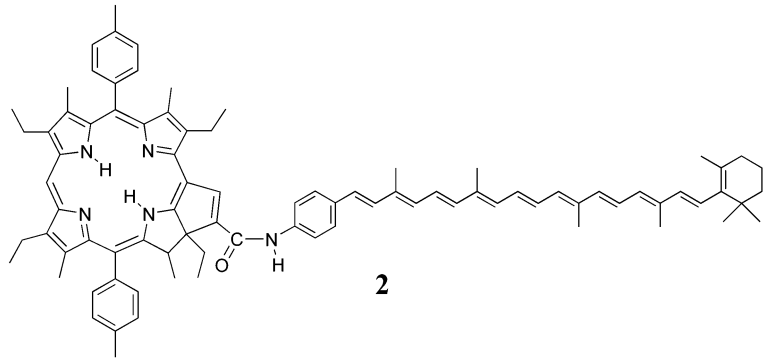

2

both the carotenoid model and dyad **2**. Thus, in this case, it is unequivocal that the S_2 state of the carotenoid moiety is the sole donor state in the observed singlet energy-transfer process. The efficiency is limited by the extremely short lifetime of this state, the spectral overlap term, and the requirement for even stronger electronic coupling than provided by the amide linkage.

In a different architecture, light-harvesting constructs were synthesized by covalently linking two carotenoids to the central silicon atom of a phthalocyanine (Pc) (see triads **3** and **4**) [11,12]. Triad **3** binds two carotenoids having nine conjugated carbon–carbon double bonds, whereas triad **4** binds two carotenoids having ten carbon–carbon double bonds in conjugation. Fluorescence excitation experiments indicated that in triad **3** dissolved in *n*-hexane, the carotenoid-to-Pc singlet energy-transfer efficiency is ca. 92 %, whereas in triad **4** it is 30 %. This is a striking difference in the antenna function of the carotenoids resulting from addition of a carbon–carbon double bond. In order to identify the basis

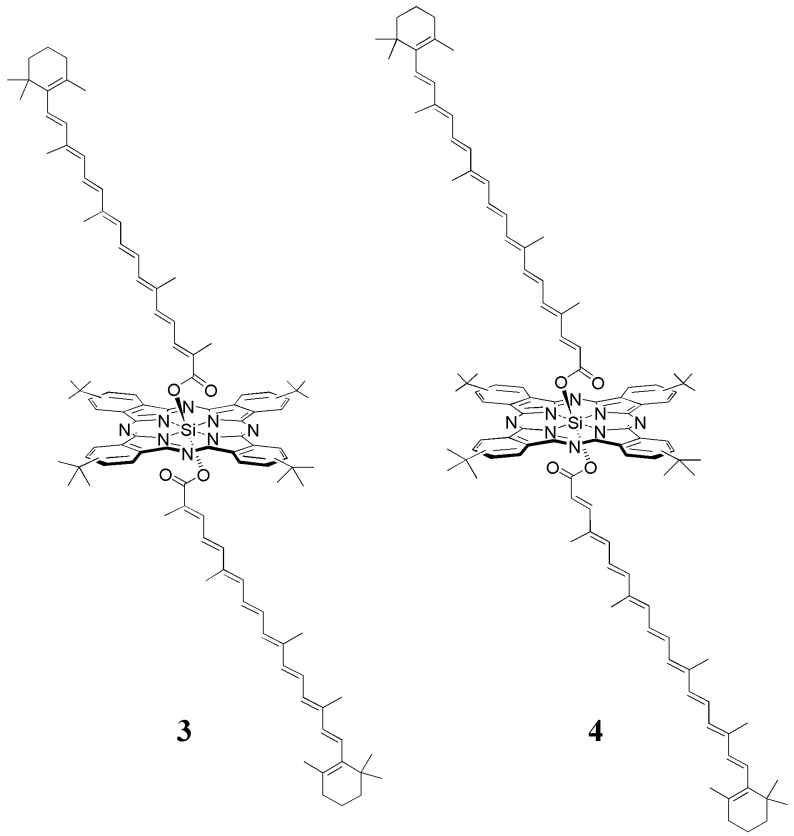

3 **4**

for this behavior, time-resolved absorption studies were performed. Results from ultrafast laser spectroscopy indicate that upon population of the optically allowed S_2 state of the carotenoid, the optically forbidden states including S_1, vibronically excited S_1, and a recently described S*, are rapidly generated in both triads **3** and **4**. In triad **3**, all of these states contribute singlet energy to Pc. As was the case in **2**, in triad **4** singlet energy transfer to Pc occurs primarily from the S_2 state with little energy transfer to Pc via the S_1 state, and there is no evidence for energy transfer via S*. Moreover, in triad **4** we find a multiphased quenching of the Pc singlet excited state on the picosecond and nanosecond time scales, indicating a back energy transfer and/or electron transfer from the excited singlet state of Pc to the carotenoid moiety.

Triad **3** is a remarkable example of an artificial antenna with nearly complete light harvesting through the participation of all the known excited states of the carotenoid. Upon completion of the light-harvesting function, the carotenoids in triad **3** efficiently carry out their photoprotective function by accepting energy from the triplet state of Pc that is formed by normal intersystem crossing; the triplet–triplet energy transfer takes place at a rate much faster than the Pc singlet state decay rate of $(5.6\ \text{ns})^{-1}$ and is, therefore, not measured directly by flash spectroscopy.

Conjugated-polyene-polymers are, in principle, attractive building blocks for the construction of artificial antennas. A living polymerization of dipropargyl malonate using Schrock's procedure [13,14] was terminated with 4-formyltetraphenylporphyrin, resulting in a polymer-polyene-porphyrin antenna system **5**. The crude reaction mixture exhibits extended absorption that covers the entire visible spectrum, making it a nearly ideal antenna for sunlight. It was expected that conformational disorder would limit the effective conjugation length of the polymer, providing a distribution of shorter effective conjugation lengths necessary for energy transfer to the tetrapyrrole. However, only limited energy transfer from the polyene-polymer to the porphyrin was detected by fluorescence excitation measurements in fractions enriched in polyene moieties containing pentamers and hexamers (11 and 13 carbon double bonds, respectively). Triplet–triplet energy transfer from the porphyrin to the polymeric-polyene was detected by flash-photolysis experiments which indicated the transient formation of polyene triplet(s) having a maximum at ~620 nm and a lifetime of 6 μs (in argon-purged solutions). The lifetime was quenched to ~200 ns by the addition of oxygen.

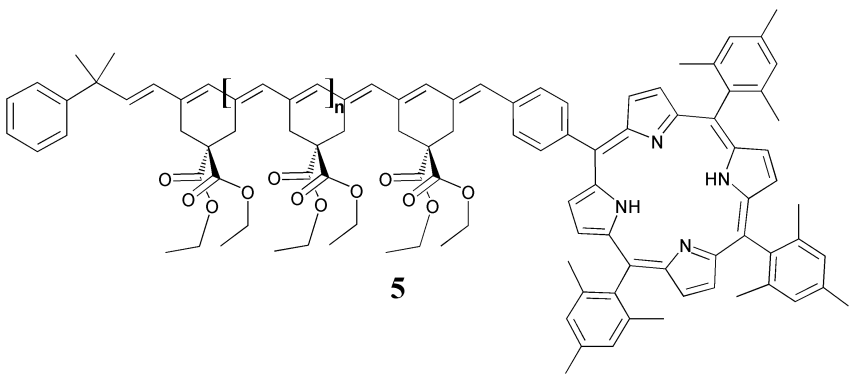

5

ARTIFICIAL REACTION CENTERS

A number of analogs of photosynthetic reaction centers consisting of tetrapyrrole chromophores covalently linked to electron acceptors and donors have been designed and synthesized. An example is triad **6** [1,15]. Excitation of these artificial reaction centers results in a cascade of energy transfer/electron transfer processes which, in selected cases, form a final charge-separated state characterized by a giant dipole moment (>150 D), a quantum yield approaching unity, a significant fraction of the photon energy stored as chemical potential, and a lifetime sufficient for reaction with secondary electron donors

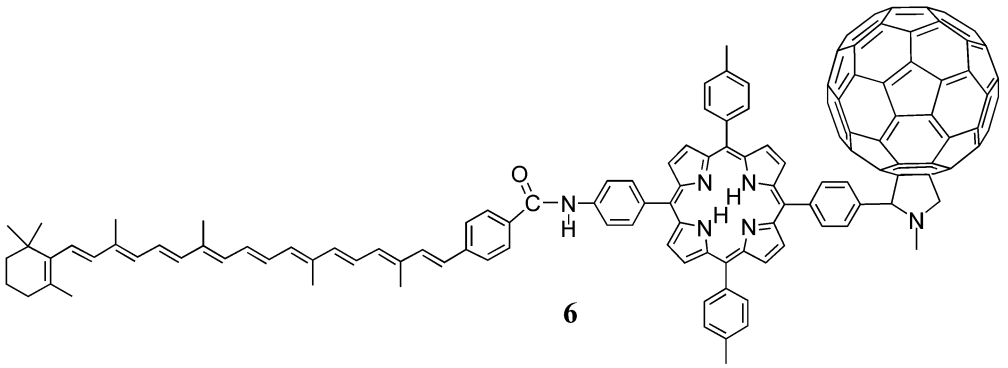

6

and acceptors. Reaction with secondary electron/hole transfer species may occur in solution, in membranes, or through interactions with conductive surfaces [16,17].

In artificial reaction centers such as **6**, light harvesting is carried out mainly by the porphyrin moiety. The carotenoid moiety does not act as an effective antenna, but rather as secondary electron donor, resulting in the formation of a final charge-separated state with the hole delocalized in the polyene chain.

A new antenna reaction center, structure **7**, in which a carotenoid moiety has been located in partial conjugation with the tetrapyrrole π-system, allowing fast energy transfer (<100 fs) between the chromophores has recently been synthesized. In this assembly, the energy transduction process can be initiated by light absorbed by the polyene. As expected, because of the structural similarity with antenna model **2**, singlet energy transfer from the carotenoid to the tetrapyrrole is ~70 % efficient [10]. Once the excitation arrives at the tetrapyrrole (purpurin), fast electron transfer to C_{60} is observed in 10 ps to form C–Pur$^{\bullet+}$–$C_{60}^{\bullet-}$, followed by a slower charge shift reaction involving the carotenoid moiety in 30 ps to form the final charge-separated state C$^{\bullet+}$–Pur–$C_{60}^{\bullet-}$, which recombines to a triplet state localized on the carotenoid in 1600 ps.

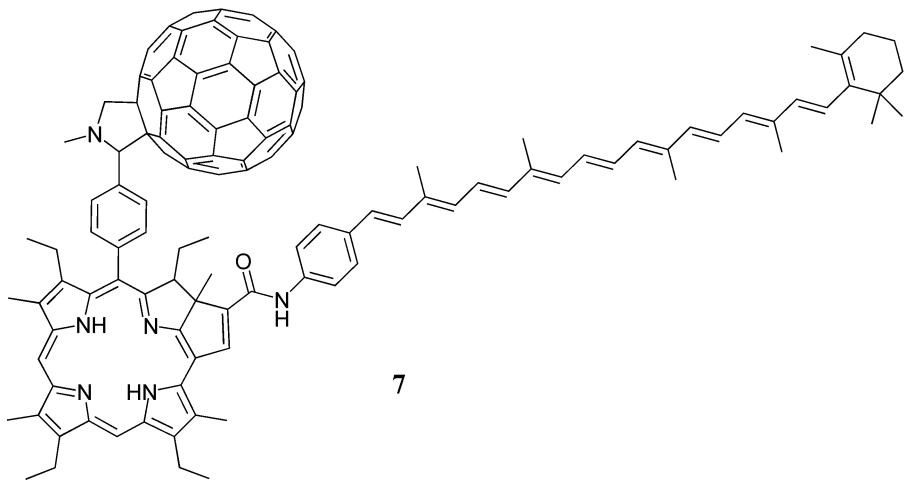

7

The results obtained with this antenna-reaction center system point to several areas for optimization. For example, the rate of recombination of the initial charge-separated state C–Pur$^{\bullet+}$–$C_{60}^{\bullet-}$ is extremely fast (70 ps), resulting in a relatively low yield of the final charge-separated state (~50 %). The fast rate of recombination can be traced to the excessive driving force for photoinduced electron trans-

fer (0.56 eV), which locates the initial charge-separated state (C–Pur$^{\bullet+}$–$C_{60}^{\bullet-}$) lower in energy than optimal to take advantage of the Marcus inverted region effect to slow recombination. Tuning the redox potential of the purpurin moiety by introducing electron-withdrawing groups and thereby increasing the energy of C–Pur$^{\bullet+}$–$C_{60}^{\bullet-}$ should slow recombination. Of course, a balance must be found that preserves sufficient driving force for photoinduced electron transfer to ensure a good quantum yield. Also, the relatively short-lived final charge-separated state could be traced to, among other factors, the proximity of the C_{60} to the carotenoid in compound **7**. Different architectures with the carotenoid moiety located at the 15-meso position of the macrocycle (opposite to the C_{60} moiety) are being considered.

FUTURE DEVELOPMENTS

A photoelectrochemical biofuel cell

We are developing a hybrid cell that consists of a dye-sensitized nanoparticulate semiconductor photoanode working in combination with an enzyme-catalyzed biofuel cell. The anodic half-cell can be coupled to various cathodic half-cell reactions through an ion-permeable membrane in a two-compartment electrochemical cell. The photoanode consists of a Grätzel-type nanoparticulate TiO_2 electrode coated with a porphyrin sensitizer [18]. Upon visible light excitation of the porphyrin (**P**), electrons are injected from the S_1 state of the porphyrin into the TiO_2 conduction band. Glucose or other reduced carbon compounds in the anode aqueous solution are oxidized by the appropriate NAD-linked dehydrogenase enzyme reducing NAD^+ to NADH. NADH is in turn oxidized by the porphyrin radical cation, regenerating **P** for subsequent rounds of photoexcitation. Key to the operation of the cell is the coupling of the anode photoreactions to the oxidation of biological fuels by the NADH/NAD^+ coenzyme and NAD-linked dehydrogenase enzyme and the facile and cyclical electron donation to the oxidized sensitizer $P^{\bullet+}$ by NADH, generating NAD^+, which is not reduced by charge recombination reactions at the photoanode.

When the photanode is coupled to a Hg/Hg_2SO_4 cathode (for evaluation purposes), theoretical values for open-circuit voltage (1.25 V) are produced with fill factors of ~0.6. These hybrid cells are nonregenerative systems; the reduced carbon compounds are the source of electrons and the photosensitizer/NADH/enzyme constitute a catalytic cycle. Thus, the electrons produced by the photoanode are available to carry out useful reductions in the cathode compartment.

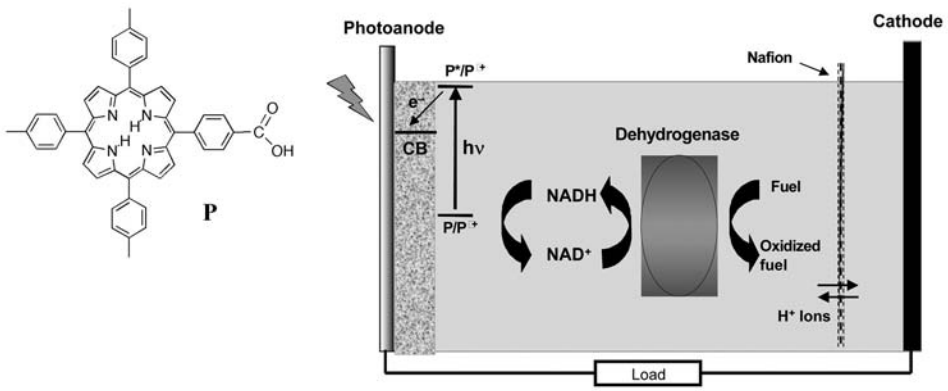

Fig. 2 Schematic diagram of a hybrid photoelectrochemical biofuel cell.

ACKNOWLEDGMENTS

This work was supported by grants from by the U.S. Department of Energy (DE-FG02-03ER15393), the National Science Foundation (CHE-0352599), and The Matsushita Industrial Co., Ltd. This is publication 603 from the ASU Center for the Study of Early Events in Photosynthesis.

REFERENCES

1. D. Gust, T. A. Moore, A. L. Moore. *Acc. Chem. Res.* **34**, 40–48 (2001).
2. B. O'Regan and M. Grätzel. *Nature* **335**, 737–739 (1991).
3. A. Hagfeldt and M. Grätzel. *Acc. Chem. Res.* **33**, 269–277 (2000).
4. X. B. Peng, N. Aratani, A. Takagi, T. Matsumoto, T. Kawai, I. W. Hwang, T. K. Ahn, D. Kim, A. Osuka. *J. Am. Chem. Soc.* **126**, 4468–4469 (2004).
5. N. Aratani, H. S. Cho, T. K. Ahn, S. Cho, D. Kim, H. Sumi, A. Osuka. *J. Am. Chem. Soc.* **125**, 9668–9681 (2003).
6. K. Muthukumaran, R. S. Loewe, C. Kirmaier, E. Hindin, J. K. Schwartz, I. V. Sazanovich, J. R. Diers, D. F. Bocian, D. Holten, J. S. Lindsey. *J. Phys. Chem. B* **107**, 3431–3442 (2003).
7. K. Y. Tomizaki, L. H. Yu, L. Y. Wei, D. F. Bocian, J. S. Lindsey. *J. Org. Chem.* **68**, 8199–8207 (2003).
8. G. Kodis, P. A. Liddell, L. de la Garza, P. C. Clausen, J. S. Lindsey, A. L. Moore, T. A. Moore, D. Gust. *J. Phys. Chem. A* **106**, 2036–2048 (2002).
9. D. Kuciauskas, P. A. Liddell, S. Lin, T. E. Johnson, S. J. Weghorn, J. S. Lindsey, A. L. Moore, T. A. Moore, D. Gust. *J. Am. Chem. Soc.* **121**, 8604–8614 (1999).
10. A. N. Macpherson, P. A. Liddell, D. Kuciauskas, D. Tatman, T. Gillbro, D. Gust, T. A. Moore, A. L. Moore. *J. Phys. Chem. B* **106**, 9424–9433 (2002).
11. G. Kodis, C. Herrero, R. Palacios, E. Marino-Ochoa, S. Gould, L. de la Garza, R. van Grondelle, D. Gust, T. A. Moore, A. L. Moore, J. T. M. Kennis. *J. Phys. Chem. B* **108**, 414–425 (2004).
12. E. Marino-Ochoa, R. Palacios, G. Kodis, A. N. Macpherson, T. Gillbro, D. Gust, T. A. Moore, A. L. Moore. *Photochem. Photobiol.* **76**, 116–121 (2002).
13. P. Wood, I. D. W. Samuel, R. Schrock, R. L. Christensen. *J. Chem. Phys.* **115**, 10955–10963 (2001).
14. H. H. Fox, M. O. Wolf, R. Odell, B. L. Lin, R. R. Schrock, M. S. Wrighton. *J. Am. Chem. Soc.* **116**, 2827–2843 (1994).
15. J. L. Bahr, D. Kuciauskas, P. A. Liddell, A. L. Moore, T. A. Moore, D. Gust. *Photochem. Photobiol.* **72**, 598–611 (2000).
16. G. SteinbergYfrach, P. A. Liddell, S. C. Hung, A. L. Moore, D. Gust, T. A. Moore. *Nature* **385**, 239–241 (1997).
17. I. M. Bennett, H. M. V. Farfano, F. Bogani, A. Primak, P. A. Liddell, L. Otero, L. Sereno, J. J. Silber, A. L. Moore, T. A. Moore, D. Gust. *Nature* **420**, 398–401 (2002).
18. L. de la Garza, G. Jeong, P. A. Liddell, T. Sotomura, T. A. Moore, A. L. Moore, D. Gust. *J. Phys. Chem. B* **107**, 10252–10260 (2003).

III. Berera, Rudi; Herrero, Christian; van Stokkum, Ivo H. M.; Vengris, Mikas; Kodis, Gerdenis; Palacios, Rodrigo E.; van Amerongen, Herbert; van Grondelle, Rienk; Gust, Devens; Moore, Thomas A.; Moore, Ana L.; Kennis, John T. M. **A simple artificial light-harvesting dyad as a model for excess energy dissipation in oxygenic photosynthesis.** Proceedings of the National Academy of Sciences of the United States of America (2006), 103(14), 5343-5348.

A simple artificial light-harvesting dyad as a model for excess energy dissipation in oxygenic photosynthesis

Rudi Berera, Christian Herrero, Ivo H. M. van Stokkum, Mikas Vengris, Gerdenis Kodis, Rodrigo E. Palacios, Herbert van Amerongen, Rienk van Grondelle, Devens Gust, Thomas A. Moore, Ana L. Moore, and John T. M. Kennis

PNAS 2006;103;5343-5348; originally published online Mar 28, 2006;
doi:10.1073/pnas.0508530103

A simple artificial light-harvesting dyad as a model for excess energy dissipation in oxygenic photosynthesis

Rudi Berera[†], Christian Herrero[‡], Ivo H. M. van Stokkum[†], Mikas Vengris[†], Gerdenis Kodis[‡], Rodrigo E. Palacios[‡], Herbert van Amerongen[§], Rienk van Grondelle[†], Devens Gust[‡], Thomas A. Moore[‡], Ana L. Moore[‡], and John T. M. Kennis[†¶]

[†]Department of Biophysics, Division of Physics and Astronomy, Faculty of Sciences, Vrije Universiteit, 1081 HV, Amsterdam, The Netherlands; [‡]Department of Chemistry and Biochemistry and Center for the Study of Early Events in Photosynthesis, Arizona State University, Tempe, AZ 85287; and [§]Laboratory for Biophysics, Wageningen University, 6703 HA, Wageningen, The Netherlands

Edited by Robin M. Hochstrasser, University of Pennsylvania, Philadelphia, PA, and approved February 10, 2006 (received for review September 29, 2005)

Under excess illumination, plant photosystem II dissipates excess energy through the quenching of chlorophyll fluorescence, a process known as nonphotochemical quenching. Activation of nonphotochemical quenching has been linked to the conversion of a carotenoid with a conjugation length of nine double bonds (violaxanthin) into an 11-double-bond carotenoid (zeaxanthin). It has been suggested that the increase in the conjugation length turns the carotenoid from a nonquencher into a quencher of chlorophyll singlet excited states, but unequivocal evidence is lacking. Here, we present a transient absorption spectroscopic study on a model system made up of a zinc phthalocyanine (Pc) molecule covalently linked to carotenoids with 9, 10, or 11 conjugated carbon–carbon double bonds. We show that a carotenoid can act as an acceptor of Pc excitation energy, thereby shortening its singlet excited-state lifetime. The conjugation length of the carotenoid is critical to the quenching process. Remarkably, the addition of only one double bond can turn the carotenoid from a nonquencher into a very strong quencher. By studying the solvent polarity dependence of the quenching using target analysis of the time-resolved data, we show that the quenching proceeds through energy transfer from the excited Pc to the optically forbidden S_1 state of the carotenoid, coupled to an intramolecular charge-transfer state. The mechanism for excess energy dissipation in photosystem II is discussed in view of the insights obtained on this simple model system.

artificial photosynthesis | carotenoid | nonphotochemical quenching | photoprotection | xanthophyll cycle

The ubiquity of carotenoids in nature reflects the crucial roles they play. In photosynthesis, carotenoids act mainly as light harvesters and photoprotectors. They absorb light in the blue-green region, where chlorophylls (Chls) display little absorption and transfer the energy to neighboring Chls (1, 2), thus increasing the absorption cross section for photosynthesis. Their role in the photoprotection of the photosynthetic apparatus is of vital importance; carotenoids can both scavenge injurious singlet oxygen and prevent its sensitization by quenching the Chl triplet state (3). Another crucial function of carotenoids, extensively studied yet poorly understood at the molecular level, is their role in the quenching of Chl singlet excited states in photosystem II (PSII) under excess illumination (4–7). This process, known as nonphotochemical quenching, allows the plant to adapt to different light levels by preventing photoinduced damage (8). Feedback deexcitation is the main component of nonphotochemical quenching (7, 9). Its activation and regulation is linked to an enzymatic, rapidly reversible process known as the xanthophyll cycle. Under high light illumination a drop in the thylakoid lumen pH triggers the cycle: violaxanthin, a 9-double-bond carotenoid, is converted into zeaxanthin, an 11-double-bond carotenoid (7). As the intensity of light decreases, or under conditions of dim light, the process is reversed. Besides activating the xanthophyll cycle, the drop in luminal pH leads to protonation of PsbS (10), a PSII subunit thought to have a central role in feedback deexcitation (11).

The question of whether zeaxanthin plays a direct role in the quenching process remains unsettled. It has been proposed that expanding the conjugation length from 9 to 11 double bonds brings the energy level of the carotenoid S_1 state below that of the Q_y state of Chl, rendering the carotenoid capable of quenching the Chl excited state by energy transfer (12). The expansion of the conjugation length would lower the first oxidation potential of the carotenoid as well (13, 14), and thus quenching could also proceed by electron transfer (5, 12, 15, 16). Alternatively, it was suggested that structural differences between violaxanthin and zeaxanthin change the way the carotenoid interacts with the surrounding pigment–protein complex, leading to a change in the pigment organization that induces quenching (4, 5, 17). Even with the emergence of new crystallographic structures of the PSII antenna (18, 19), the role of zeaxanthin in nonphotochemical quenching remains unresolved.

Artificial light-harvesting antennae are used for the study of light harvesting, energy transfer, electron transfer, and photoprotective functions of carotenoids (20, 21). These minimalist constructs are capable of performing the specific functions carried out by their natural counterparts; their simplicity allows one to establish the basic photophysical and photochemical mechanisms underlying the behavior of the natural systems. Here, we present results from transient absorption spectroscopy on dyads consisting of a zinc phthalocyanine (Pc), acting as a mimick for Chl *a*, covalently linked to a series of carotenoids having 9, 10, or 11 conjugated carbon–carbon double bonds. These dyads have previously been shown to exhibit an efficient carotenoid-to-Pc light-harvesting function (22). We define the conditions under which a carotenoid molecule quenches the excited state of a Pc-based tetrapyrrole, identify the quenching mechanism, and determine to what extent the quenching depends on the conjugation length. The implications for the mechanism of excess energy dissipation in PSII are discussed.

Results

The structures of dyads **1**, **2**, and **3**, are shown in Fig. 1 *Upper*, and their absorption spectra along with that of model Pc **4** dissolved

Conflict of interest statement: No conflicts declared.

This paper was submitted directly (Track II) to the PNAS office.

Freely available online through the PNAS open access option.

Abbreviations: EADS, evolution-associated difference spectrum; SADS, species-associated difference spectrum; Pc, phthalocyanine; ICT intramolecular charge transfer; Chl, chlorophyll; PSII, photosystem II; THF, tetrahydrofuran; LHC, light-harvesting complex.

¶To whom correspondence should be addressed. E-mail: j.kennis@few.vu.nl.

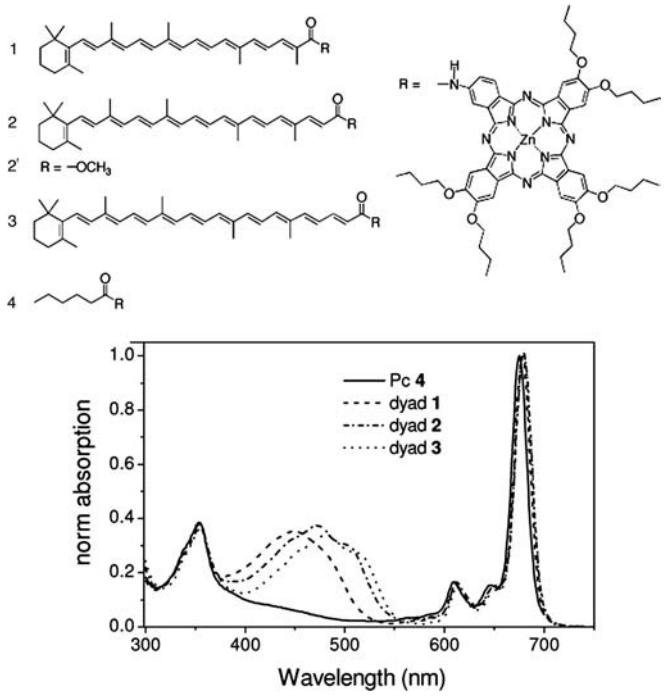

Fig. 1. Molecular structures and absorption spectra of the compounds. (*Upper*) Molecular structures of the dyads. A zinc-Pc is covalently linked to a carotenoid with 9 conjugated carbon–carbon double bonds (dyad **1**), 10 carbon–carbon double bonds (dyad **2**), and 11 carbon–carbon double bonds (dyad **3**). Model Pc **4** bears a hexanoyl group instead of a polyene. Model carotenoid **2**′ has a terminal ester instead of a Pc. (*Lower*) Absorption spectrum in THF for dyad **1** (dashed line), dyad **2** (dashed-dotted line), dyad **3** (dotted line), and model Pc **4** (solid line).

in tetrahydrofuran (THF) are shown in Fig. 1 *Lower*. The carotenoids of dyad **1**, **2**, and **3** have 9, 10, and 11 conjugated carbon–carbon double bonds, respectively, and a carbonyl group terminating the conjugated system. The carbonyl group is in an s-*cis* conformation, which only partly adds to π-conjugation of the system (1, 23). The lifetimes of the optically forbidden S_1 state of the model carotenoids of dyads **1** and **2**, determined previously to be 25 and 11.5 ps, respectively (21), are similar to those typically observed for other carotenoids with 9 and 10 conjugated carbon–carbon double bonds (1).

Fig. 2*A* shows kinetic traces with excitation and detection at 680 nm, corresponding to the maximum of Pc Q_y absorption, for dyads **1**–**3** and model Pc **4** dissolved in THF. The switch from nonquenching to quenching upon an increase in the conjugation length by one double bond is clearly seen in the shortened recovery time for the Pc ground-state bleach in dyad **2**. The lifetimes of the Q_y states in dyad **1** and model Pc **4** have the same value (3 ns), whereas for dyad **2** the lifetime is reduced by a factor of 10 to 300 ps. When the conjugation length of the carotenoid is further increased (dyad **3**) the carotenoid becomes an even stronger quencher, the lifetime of the Q_y state being 56 ps. Fig. 2 *B*–*D* shows the results (see below).

Dyad 1. The results of a global analysis of the time-resolved data taken on dyad **1** are presented as evolution-associated difference spectra (EADS) in Fig. 2*B*. Four kinetic components are needed for an adequate description: the first, appearing at time 0 and evolving into the second in 100 fs, is mainly the consequence of cross-phase modulation and coherent artifacts and is not shown. The second EADS (Fig. 2*B*, red line) has a lifetime of 1.25 ps and features ground-state bleach in the Q_x band of Pc (610 nm), ground-state bleach and stimulated emission in the Q_y band of

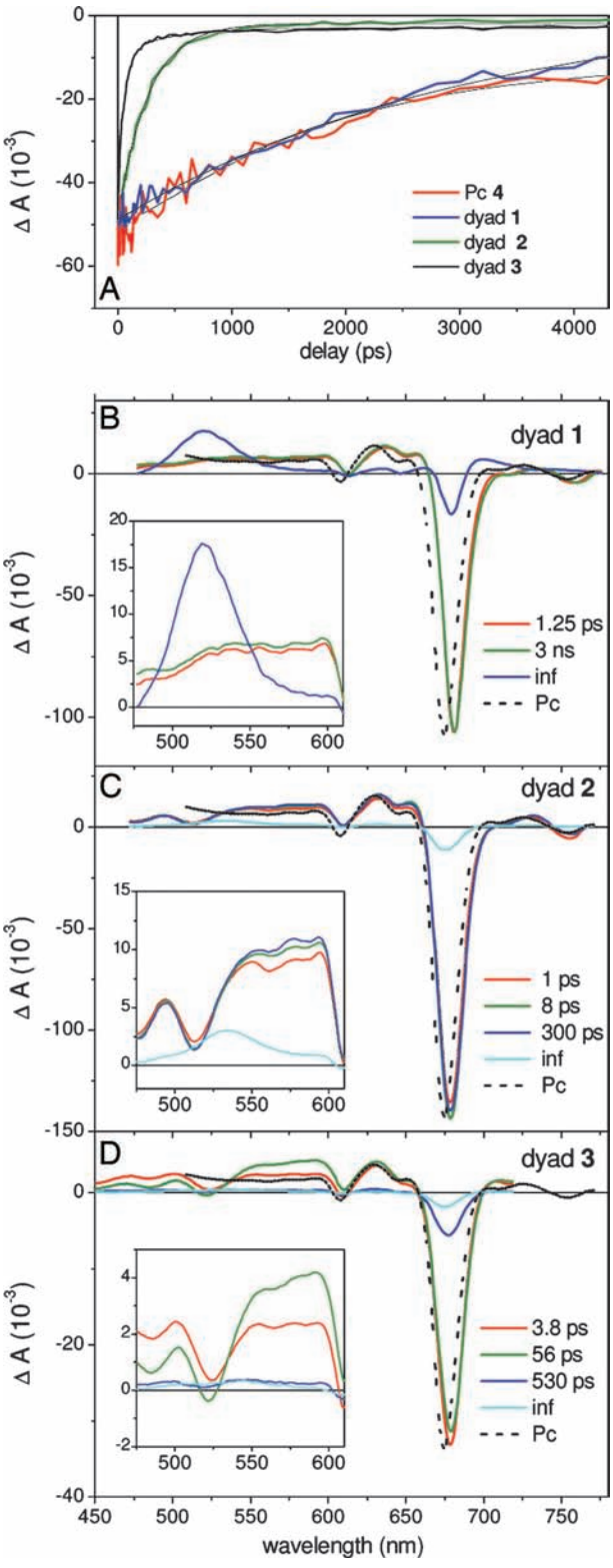

Fig. 2. Kinetic traces and global analysis of the time-resolved data. (*A*) Kinetic traces with excitation and detection at 680 nm for model Pc **4** (red line), dyad **1** (blue line), dyad **2** (green line), and dyad **3** (magenta line) in THF, along with the result of the global analysis fit (thin solid line). (*B*) EADS that follow from a global analysis of data for dyad **1**. (*Inset*) An expanded view of the EADS in the spectral region from 475 to 620 nm. (*C*) The same as for *B* for dyad **2**. (*D*) The same as for B for dyad **3**. The difference spectra corresponding to the vibrationally relaxed, fully solvated Q_y state for model Pc **4**, as determined from a global analysis, are also shown in *B*–*D* as black dashed lines.

Pc (680 nm), stimulated emission from Q_y (≈750 nm), and a broad, flat excited-state absorption from 480 to 600 nm. It evolves to the next EADS (Fig. 2*B*, green line), involving minor spectral changes, including a slight red shift of the Q_y bleach/stimulated emission signal near 680 nm, which is probably caused by solvation processes. The third EADS evolves into the nondecaying fourth EADS (Fig. 2*B*, blue line) in 3 ns. At this stage the Pc transient signals have greatly decreased. The spectrum presents a new absorption band near 515 nm corresponding to a carotenoid triplet excited state, as observed previously in a carotenoid–Si–Pc triad containing the same carotenoid (21). This feature is absent in the previous EADS and appears after most Pc has returned to the ground state. This observation suggests that carotenoid triplet formation is preceded by singlet to triplet intersystem crossing in Pc, followed by rapid triplet–triplet energy transfer between Pc and the carotenoid. The signal in the Q_y region of Pc has the typical shape of a band shift, as previously observed in the Si-Pc triads (21). When comparing the shape and amplitude of the first two EADS (Fig. 2*B*, red and green lines) with the spectrum corresponding to the vibrationally relaxed and fully solvated excited state of model Pc **4** (Fig. 2*B*, dashed black line), apart from an overall spectral shift and a more pronounced excited-state absorption shoulder at 655 nm in the dyad, there are only minor differences. Furthermore, the lifetime of the Q_y state of dyad **1** (3 ns) differs only marginally from the excited-state lifetime for model Pc **4**, meaning that the carotenoid in dyad **1** is incapable of quenching the Pc excited singlet state.

Dyad 2. Fig. 2*C* shows the EADS for dyad **2**. Five components are needed for a satisfactory fit. The first component, appearing at time 0 and evolving into the second spectrum in 100 fs, is again not shown. The second EADS (Fig. 2*C*, red line) has a lifetime of 1 ps and is similar to the corresponding EADS in dyad **1**. However, it also presents a small negative feature near 515 nm superimposed on the broad excited-state absorption signal that is absent in the spectra of model Pc **4** and dyad **1**. This phenomenon, highlighted in the Fig. 2*C Inset*, occurs in the ground-state absorption region of the covalently linked carotenoid and appears to be a band shift, possibly in combination with a small bleach of the carotenoid ground-state absorption, and results from excitation of Pc. This feature is similar to that observed previously in photosynthetic light-harvesting complexes (LHCs), where it was assigned to a change of the local electric field of the carotenoid and excitonic coupling between Chl and the optically allowed S_2 state of the carotenoid (24, 25). The second EADS evolves into the third EADS (Fig. 2*C*, green line) in 1 ps, with only minor changes in the shape and amplitude of the spectrum. There is a slight increase of the signal near 680 nm and a very small increase of the excited-state absorption in the 550- to 600-nm region. The evolution to the fourth EADS (Fig. 2*C*, blue line) occurs in 8 ps. This EADS is almost identical to the previous one apart from a very small decrease of the Q_y bleach. The fourth EADS evolves into the nondecaying fifth EADS (Fig. 2*C*, cyan line) in 300 ps. Now the Pc bleach and excited-state features have almost disappeared. The nondecaying EADS is characterized by a small residual bleach in the Q_y region and a small, broad, positive signal in the 500- to 580-nm region, corresponding to carotenoid triplet, and possibly Pc triplets. A crucial difference between these results and those of dyad **1** is the lifetime of the Pc singlet excited state. This value, 300 ps for dyad **2**, is 10 times shorter than in dyad **1** and model Pc **4**, meaning that the carotenoid of dyad **2** acts as a strong, effective quencher of Pc singlet excited states.

Dyad 3. The EADS for dyad **3** are presented in Fig. 2*D*. Again, the first EADS, with a lifetime of 100 fs, is not shown. The second EADS (Fig. 2*D*, red line) displays Q_x and Q_y bleach at 610 and 680 nm, respectively, and excited-state absorption features similar to those observed for dyads **1** and **2**. At 525 nm there is a negative-going feature, similar to that observed for dyad **2** but red-shifted by ≈10 nm. As in dyad **2**, we assign it to a band-shift/ground-state bleach of the carotenoid ground-state absorption upon excitation of Pc. The second EADS evolves into the third EADS (Fig. 2*D*, green line) in 3.8 ps. In the third EADS, a sizeable increase of the positive signal in the region above 540 nm is observed, as well as a small decrease of the Q_y bleach. In the region below 540 nm the third EADS shows a growth and blue shift of the negative feature, and, as mentioned above, an increase of the absorption at wavelengths >540 nm, as highlighted in Fig. 2*D Inset*. With a 56-ps time constant, this EADS evolves into the fourth one (Fig. 2*D*, blue line); the Q_y bleach and the excited-state absorption have dramatically decreased and most of Pc is now in its ground state. The remaining signal decays in 530 ps to the nondecaying component characterized by a small population of a long-lived, presumably triplet, species. In dyad **3** the Pc singlet lifetime is strongly quenched compared with dyads **1** and **4**. The decay of the Pc singlet excited state, as measured by Q_y bleach recovery, is biexponential with most of the excited states disappearing in 56 ps and a small fraction in 530 ps.

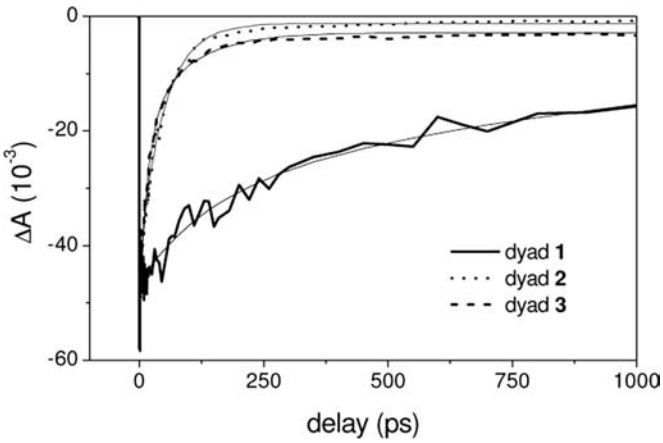

Fig. 3. Kinetic traces with excitation and detection at 680 nm for dyad **1** (solid line), dyad **2** (dotted line), and dyad **3** (dashed line) in acetone. The gray lines denote the result of a global analysis.

A closer look at the evolution from the second to the third EADS (Fig. 2*D*, red to green curve, in 3.8 ps) suggests that the increase of negative-going amplitude in the region <540 nm may correspond to depopulation of the carotenoid ground state, whereas the increase of the signal >540 nm must originate from the absorption of a species different from the Pc Q_y state (Fig. 2*D*, dashed black line). It will be later identified as a carotenoid excited state. This species appears to rise on a picosecond time scale and coexists from then on with the Pc Q_y state. This behavior suggests that the carotenoid state is slowly populated and quickly depopulated. Such a state may act as a quencher because its lifetime is far shorter than the intrinsic lifetime of the Pc Q_y state. For dyad **2**, similar phenomena appear to occur (Fig. 2*C Inset*) but are much less pronounced.

Solvent Polarity Dependence of Pc Singlet-Excited-State Quenching. To gain more insight into the quenching mechanism, we carried out experiments with dyads dissolved in acetone and DMSO. THF is of moderate polarity, with a static dielectric constant $\varepsilon_0 = 7.58$ and an index of refraction $n_D = 1.405$, whereas acetone ($\varepsilon_0 = 20.6$, $n_D = 1.356$) and DMSO ($\varepsilon_0 = 40.5$, $n_D = 1.478$) are of distinctly high polarity. Fig. 3 shows the kinetic traces and corresponding global analysis fits recorded at 680 nm for dyads

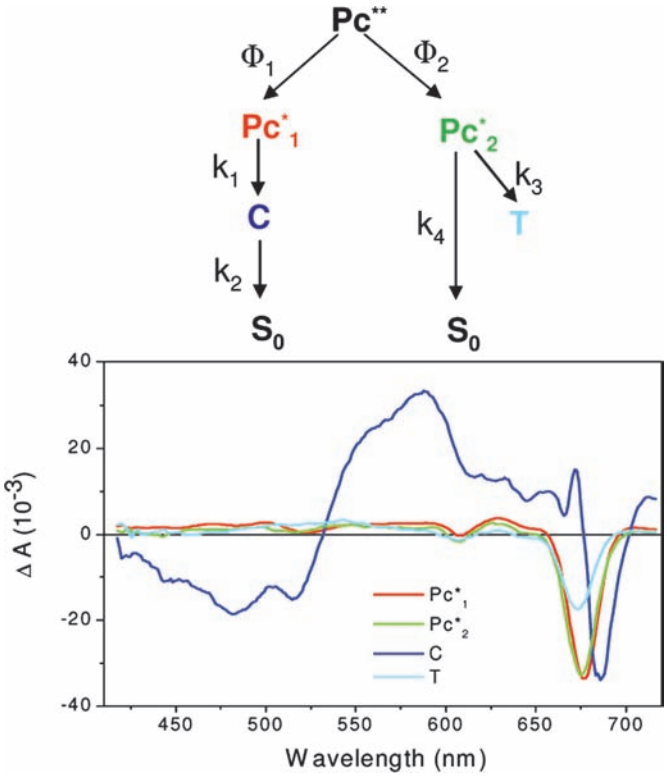

Fig. 4. Target analysis of the time-resolved data. (*Upper*) Kinetic model used in target analysis of time-resolved data on dyads **2** and **3**. (*Lower*) SADS from the target analysis for dyad **3** in THF. See text for details.

1–**3** in acetone. In all three systems the Q_y state has a shorter lifetime than it does in THF (Fig. 2*A*). Dyad **1** decayed monoexponentially with a time constant of 600 ps. Dyad **2** displayed a biexponential decay with time constants of 30 ps (75% amplitude) and 120 ps (25% amplitude), whereas dyad **3** showed a decay with 16 ps (65%) and 90 ps (35%). A similar scenario was found in DMSO (results not shown). Thus, in polar solvents the quenching becomes faster. The results from a global analysis on dyad **3** in acetone are shown in Fig. 6, which is published as supporting information on the PNAS web site.

Target Analysis: Identification of the Quenching Species. The sequential data analysis allows extraction of intrinsic lifetimes, but the spectra generally represent a mixture of transient species. Therefore, despite providing strong evidence for the presence of a transient species other than singlet-excited Pc, sequential analysis alone cannot provide a definitive spectral signature of such a species. To identify the relevant molecular states, we globally analyzed the time-resolved data with a target analysis, wherein the data are described in terms of a kinetic scheme, enabling the estimation of the spectral signatures, and lifetimes, of the "pure" molecular species (26). Our goal is to identify the carotenoid state that is responsible for quenching the singlet excited state of Pc.

The biexponential decay of Q_y in the case of dyad **3** observed in THF and acetone may stem from an inhomogeneity of the dyad ground-state population in which one species is more strongly quenched than the other. To account for the biexponentiality the target analysis model requires two independent Pc excited-state populations.

The kinetic model is depicted in Fig. 4 *Upper* and consists of five compartments: The first, **Pc****, corresponds to an unrelaxed Pc excited state that decays in <100 fs into two independent Pc excited-state populations, $\mathbf{Pc_1^*}$ and $\mathbf{Pc_2^*}$ (target analysis cannot distinguish this case from the case of two unrelaxed Pc excited-state species prepared initially). A fraction Φ_1 relaxes to $\mathbf{Pc_1^*}$, whereas a fraction Φ_2 relaxes to $\mathbf{Pc_2^*}$. $\mathbf{Pc_1^*}$ evolves to **C**, which represents a carotenoid state, with a rate constant k_1. **C** decays entirely to the ground state with a rate constant k_2. In this model the carotenoid state **C** is slowly populated and quickly depopulated and therefore attains a low transient concentration. $\mathbf{Pc_2^*}$ decays with rate constant k_3 to a long-lived mix of Pc and carotenoid triplet states **T**, in competition with decay to the ground state with a rate constant k_4.

Fig. 4 *Lower* shows the species-associated difference spectra (SADS) resulting from target analysis for dyad **3** in THF. The estimated rate constants and branching ratios are summarized in Table 1. The spectrum corresponding to **Pc**** is not shown; 82% of **Pc**** decays to $\mathbf{Pc_1^*}$ (Fig. 4 *Lower*, red line), whereas 18% decays to $\mathbf{Pc_2^*}$ (Fig. 4 *Lower*, green line). $\mathbf{Pc_1^*}$ decays to **C** (Fig. 4 *Lower*, blue line) with a rate constant of $(56\ \text{ps})^{-1}$, which in turn decays to the ground state with a rate constant $(3.8\ \text{ps})^{-1}$. $\mathbf{Pc_2^*}$ decays to **T** (Fig. 4 *Lower*, cyan line) with a rate constant of $(840\ \text{ps})^{-1}$ and to the ground state with a rate constant of $(1.3\ \text{ns})^{-1}$. The SADS (Fig. 4) of $\mathbf{Pc_1^*}$ shows bleaching of the Q_x and Q_y bands and a broad excited-state absorption from 520 to 600 nm. Compared with the EADS with a lifetime of 56 ps in Fig. 2*D* (green line), the carotenoid bleach feature near 520 nm and absorption feature near 550 nm have largely disappeared, indicating that the separation of Pc and carotenoid signals was successful. The small carotenoid band-shift/ground-state bleach remains present in the $\mathbf{Pc_1^*}$ SADS, consistent with its instantaneous occurrence in the sequential analysis.

The SADS of state **C** has the typical shape of the $S_1 \rightarrow S_n$ transient absorption spectrum of carotenoids (1). The negative features at wavelengths <530 nm correspond to ground-state bleaching of the strongly allowed S_2 state, with vibronic features at 480 and 520 nm. The excited-state absorption region >530 nm is typical for the S_1 state with a maximum at 580 nm and a pronounced shoulder near 550 nm. The strong bleach in the 680- to 690-nm region is an artifact and forms no part of the carotenoid S_1 spectrum. It results from relaxation processes of Pc that take place on the ps time scale and are independent from the quenching phenomenon, but could not be separated from the carotenoid dynamics in the target analysis procedure. In reality, this feature represents a small red shift of the Pc bleach, also observed in model Pc **4** (data not shown), and is artificially expanded by the target analysis. The results for dyad **2** and **3** in acetone are shown in Fig. 7, which is published as supporting

Table 1. Rate constants for dyad 3 in THF and dyads 2 and 3 in acetone as derived from the target kinetic model depicted in Fig. 4

Compound, solvent	Φ_1	Φ_2	k_1	k_2	k_3	k_4
Dyad **3**, THF	0.82	0.18	$(56\ \text{ps})^{-1}$	$(4\ \text{ps})^{-1}$	$(840\ \text{ps})^{-1}$	$(1.3\ \text{ns})^{-1}$
Dyad **2**, acetone	0.75	0.25	$(30\ \text{ps})^{-1}$	$(4\ \text{ps})^{-1}$	$(526\ \text{ps})^{-1}$	$(179\ \text{ps})^{-1}$
Dyad **3**, acetone	0.54	0.46	$(17\ \text{ps})^{-1}$	$(4.8\ \text{ps})^{-1}$	$(303\ \text{ps})^{-1}$	$(130\ \text{ps})^{-1}$

Φ_1 and Φ_2 are population fractions at the branching point.

information on the PNAS web site. We attempted to apply the target analysis to dyad **2** dissolved in THF, but found that the transient concentration of excited-state carotenoid species **C** was too low to reliably estimate its spectral shape and dynamics.

The polarity dependence of the quenching suggests that electron transfer from the carotenoid to the Pc moiety could be responsible for the quenching process. To test this possibility we extensively probed the 850- to 980-nm region, but did not find any signature of a carotenoid radical ion (see Fig. 8, which is published as supporting information on the PNAS web site). In all systems, including model **4**, we found the same scenario: a relatively flat spectrum decaying with the same lifetime as the Q_y state of Pc, confirming that the signal in this region is entirely caused by Pc excited-state absorption.

By showing that the SADS of the quenching species strongly resembles that of the well known S_1 difference spectrum of carotenoids (1), target analysis provides good evidence for the essential role of the carotenoid S_1 excited state as an energy acceptor in the quenching process. However, because energy transfer to or from the S_1 state should not depend markedly on solvent polarity (1), simple energy transfer involving the unperturbed carotenoid S_1 state is unlikely to be solely responsible for the Pc excited-state quenching. To characterize the putative perturbation to S_1, we performed transient absorption measurements on a model for the carotenoid from dyad **2**, where Pc was replaced by a methyl ester (Fig. 1, model carotenoid **2′**), dissolved in solvents of different polarities. Fig. 9, which is published as supporting information on the PNAS web site, shows the EADS of the model carotenoid after internal conversion from S_2 in ≈100 fs and vibrational cooling in ≈500 fs, dissolved in DMSO (green curve), THF (blue curve), and hexane (red curve). Solvent polarity-dependent shape changes that cannot be ascribed to the unperturbed S_1 state are readily apparent. In hexane the spectrum looks like the well known difference spectrum associated with population of the S_1 state of carotenoids (1), but in THF a new band, characterized by a broad signal in the region >625 nm, is present. When the polarity is further increased (DMSO), this signal (>650 nm) becomes more prominent.

A similar dependence of spectral shape on solvent polarity was reported for several naturally occurring substituted carotenoids and assigned to the formation of an intramolecular charge transfer (ICT) state (23, 27). The ICT state is thought to arise from the presence of a carbonyl moiety in conjugation with the extended π-electron system; the carbonyl moiety accumulates electron density upon photoexcitation. The ICT and S_1 states may effectively behave as one state (27) or as distinct molecular states that equilibrate rapidly upon population from the optically allowed S_2 state (28). The carotenoids in this study also feature carbonyl groups. In model carotenoid **2′**, the presence of a charge transfer band coexisting with the S_1 state is clear. The spectral signature of the carotenoid state **C** as it follows from the target analysis (Fig. 4 *Lower*) and Fig. 7 shows a broad, flat excited-state absorption at wavelengths longer than ≈600 nm, which is consistent with the population of an ICT state in this system as well. Thus, the quenching state in the dyads most likely does not correspond to the pure S_1 state, but to a mixture of S_1 and ICT states. Note that because ICT and S_1 are closely linked, it is not possible to treat them as separate entities in the target analysis.

Discussion

A change in the conjugation length of carotenoids is a key characteristic of the process leading to the thermal dissipation of excess energy in PSII, where the activation of Chl singlet excited-state quenching is correlated with the conversion of violaxanthin (nine double bonds) into zeaxanthin (11 double bonds). Our results with artificial light-harvesting dyads show

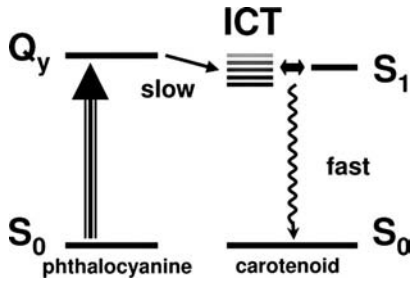

Fig. 5. Schematic representation of the proposed quenching process: the energy from the Q_y state of Pc is transferred to the carotenoid ICT state, which then equilibrates with the carotenoid S_1 state before relaxation to the ground state by internal conversion. An increase in solvent polarity leads to a lowering of the ICT energy (gray to black lines).

that a carotenoid of proper length can efficiently dissipate the Q_y energy of Pc by shortening its excited-state lifetime. In THF, a solvent of moderate polarity, an increase of the conjugation length by one double bond (dyad **1** to dyad **2**) turns the carotenoid from a nonquencher into a strong quencher. When the molecules are dissolved in the highly polar solvents acetone and DMSO, the quenching becomes stronger and even dyad **1** displays limited quenching. Target analysis has shown that the quenching in dyads **2** and **3** proceeds via a carotenoid S_1/ICT state. The solvent polarity dependence indicates that the ICT state modulates the process as shown in Fig. 5. The Q_y state of Pc transfers energy to the ICT state, which quickly equilibrates with S_1. Then, the carotenoid rapidly relaxes to the ground state on the time scale of several picoseconds by internal conversion. The increase in solvent polarity shifts the energy of the ICT state downward (Fig. 5, gray to black lines), making it more accessible from the Q_y state of Pc and increasing the quenching.

ICT states are not confined to carotenoids that have a carbonyl group in their conjugated system, as there is evidence for their occurrence in xanthophylls bound to natural photosynthetic LHCs, in particular LHCII, the main constituent of the PSII antenna (29). Instead of an internal electron withdrawing group (such as a carbonyl), the interaction with polar amino acids, inorganic cations such as Mg^{2+} or nearby pigments, resulting in a highly asymmetric environment of the molecule, may stabilize an ICT state. Also, geometric deformations of the polyene backbone have been proposed to play a role in lowering ICT states in carotenoids (30). Trimeric LHCII binds two luteins that are distinguishable by their steady-state absorption spectrum. A red-shifted lutein shows a particularly large Stark effect with a $|\Delta\mu|$ of 14.6 D (29), which corresponds to the transfer of ≈12% of an elementary charge along the conjugated backbone (31), demonstrating that electronic excited states in xanthophylls can be strongly coupled to ICT states. Interestingly, neither the second, blue-shifted lutein in trimeric LHCII, nor either of the two luteins in monomeric LHCII exhibited such a pronounced Stark effect. Additionally, it was shown that the red-shifted lutein assumed a distorted geometry in LHCII trimers, whereas the blue lutein assumes a relaxed conformation (32). These observations indicate that very specific carotenoid–protein or carotenoid–Chl interactions are responsible for the mixing between lutein electronic excited and ICT states, induced by conformational changes of the highly plastic LHCII protein.

It has been argued that the quenching of Chl excited states by zeaxanthin in PSII could not occur via the zeaxanthin S_1 state because the S_1 energies of violaxanthin and zeaxanthin in organic solvent and recombinant LHCII are not sufficiently different and lie below that of Chl *a* (6, 33, 34). However, *in vivo* light absorption and resonant Raman experiments on quenched PSII in leaves and chloroplasts indicated that zeaxanthin undergoes

dramatic spectroscopic changes upon induction of feedback deexcitation: its absorption maximum shifts to the red by at least 22 nm, and the molecule assumes a very specific, highly twisted conformation (35). To account for these phenomena, Ruban *et al.* (35) proposed that zeaxanthin is bound in a highly polarizing local environment, possibly arising from a strong electric field of a dipole or charge in the zeaxanthin vicinity. It seems plausible that such an extensive change of local environment, combined with a distortion of the polyene backbone, may bring down ICT states of zeaxanthin to couple with S_1, and thereby activate a quenching mechanism similar to that reported here for the model systems.

Conclusions

Our results with covalently linked carotenoid–Pc dyads show that carotenoids can efficiently quench tetrapyrrole singlet excited states by means of singlet energy transfer to low-lying, optically forbidden carotenoid excited states. The solvent polarity dependence and spectroscopic evidence point to the involvement of a carotenoid ICT state in the energy transfer process. Moreover, expanding the conjugated system of a carotenoid by only one double bond turns the carotenoid from a nonquencher into an effective quencher of Pc singlet excited states. In the antenna of PSII, a similar phenomenon may take place where the addition of two double bonds to the conjugated system of violaxanthin converts it to zeaxanthin, which may be a strong quencher. In other caroteno-tetrapyrrole constructs having structures and thermodynamics for photoinduced electron transfer distinctly different from those of dyads **1–3** electron transfer quenching of the tetrapyrrole Q_y state has been unequivocally assigned (21, 36). Having these two model systems in hand, it should be possible to establish the factors controlling the quenching mechanisms in natural photosynthesis.

Materials and Methods

Synthesis of the dyads is described in *Supporting Text*, which is published as supporting information on the PNAS web site. Femtosecond transient absorption spectroscopy was carried out with a spectrometer as described earlier (37). The excitation was tuned to 680 nm to selectively excite the Q_y state of Pc. The pulse energy was 100 nJ, corresponding to an excitation density of $\approx 10^{15}$ photons·pulse^{-1}·cm^{-2}. The data were globally analyzed (26) by using a kinetic model consisting of sequentially interconverting EADS, e.g., $1 \rightarrow 2 \rightarrow 3 \rightarrow \ldots$ in which the arrows indicate successive monoexponential decays of increasing time constants, which can be regarded as the lifetime of each EADS. The number of kinetic components corresponds to the minimum required to eliminate any correlated structure in the residuals. The first EADS corresponds to the time-zero difference spectrum. Because the EADS may reflect mixtures of molecular species, a target analysis was performed in which a specific kinetic scheme was applied. With this procedure, the SADS of pure molecular states were estimated. The instrument response function was fitted to a Gaussian of 120 fs (full width at half maximum), similar to the value obtained from the analysis of the induced birefringence in CS_2.

R.B. was supported by the Netherlands Organization for Scientific Research through the Earth and Life Sciences Council (NWO-ALW). J.T.M.K. was supported by the NWO-ALW through a VIDI fellowship. This work was supported by Department of Energy Grant FG02-03ER15393. This is publication 659 from the Arizona State University Center for the Study of Early Events in Photosynthesis.

1. Polivka, T. & Sundström, V. (2004) *Chem. Rev.* **104,** 2021–2071.
2. Frank, H. A. & Cogdell, R. J. (1996) *Photochem. Photobiol.* **63,** 257–264.
3. Griffiths, M., Sistrom, W. R., Cohenbazire, G. & Stanier, R. Y. (1955) *Nature* **176,** 1211–1214.
4. Robert, B., Horton, P., Pascal, A. A. & Ruban, A. V. (2004) *Trends Plant Sci.* **9,** 385–390.
5. Holt, N. E., Fleming, G. R. & Niyogi, K. K. (2004) *Biochemistry* **43,** 8281–8289.
6. Frank, H. A., Bautista, J. A., Josue, J. S. & Young, A. J. (2000) *Biochemistry* **39,** 2831–2837.
7. Muller, P., Li, X. P. & Niyogi, K. K. (2001) *Plant Physiol.* **125,** 1558–1566.
8. Kulheim, C., Agren, J. & Jansson, S. (2002) *Science* **297,** 91–93.
9. Horton, P., Ruban, A. V. & Walters, R. G. (1996) *Annu. Rev. Plant Physiol. Plant Mol. Biol.* **47,** 655–684.
10. Li, X. P., Gilmore, A. M., Caffarri, S., Bassi, R., Golan, T., Kramer, D. & Niyogi, K. K. (2004) *J. Biol. Chem.* **279,** 22866–22874.
11. Li, X. P., Björkman, O., Shih, C., Grossman, A. R., Rosenquist, M., Jansson, S. & Niyogi, K. K. (2000) *Nature* **403,** 391–395.
12. Frank, H. A., Cua, A., Chynwat, V., Young, A., Gosztola, D. & Wasielewski, M. R. (1994) *Photosynth. Res.* **41,** 389–395.
13. Dreuw, A., Fleming, G. R. & Head-Gordon, M. (2003) *Phys. Chem. Chem. Phys.* **5,** 3247–3256.
14. Fungo, F., Otero, L., Durantini, E., Thompson, W. J., Silber, J. J., Moore, T. A., Moore, A. L., Gust, D. & Sereno, L. (2003) *Phys. Chem. Chem. Phys.* **5,** 469–475.
15. Ma, Y. Z., Holt, N. E., Li, X. P., Niyogi, K. K. & Fleming, G. R. (2003) *Proc. Natl. Acad. Sci. USA* **100,** 4377–4382.
16. Holt, N. E., Zigmantas, D., Valkunas, L., Li, X. P., Niyogi, K. K. & Fleming, G. R. (2005) *Science* **307,** 433–436.
17. Pascal, A. A., Liu, Z. F., Broess, K., van Oort, B., van Amerongen, H., Wang, C., Horton, P., Robert, B., Chang, W. R. & Ruban, A. (2005) *Nature* **436,** 134–137.
18. Liu, Z. F., Yan, H. C., Wang, K. B., Kuang, T. Y., Zhang, J. P., Gui, L. L., An, X. M. & Chang, W. R. (2004) *Nature* **428,** 287–292.
19. Standfuss, R., van Scheltinga, A. C. T., Lamborghini, M. & Kühlbrandt, W. (2005) *EMBO J.* **24,** 919–928.
20. Gust, D., Moore, T. A. & Moore, A. L. (2001) *Acc. Chem. Res.* **34,** 40–48.
21. Kodis, G., Herrero, C., Palacios, R., Mariño-Ochoa, E., Gould, S., de la Garza, L., van Grondelle, R., Gust, D., Moore, T. A., Moore, A. L. & Kennis, J. T. M. (2004) *J. Phys. Chem. B* **108,** 414–425.
22. Mariño Ochoa, E. (2002) Ph.D. thesis (Arizona State University, Tempe).
23. Zigmantas, D., Hiller, R. G., Sharples, F. P., Frank, H. A., Sundstrom, V. & Polivka, T. (2004) *Phys. Chem. Chem. Phys.* **6,** 3009–3016.
24. Herek, J. L., Wendling, M., He, Z., Polivka, T., Garcia-Asua, G., Cogdell, R. J., Hunter, C. N., van Grondelle, R., Sundström, V. & Pullerits, T. (2004) *J. Phys. Chem. B* **108,** 10398–10403.
25. Gradinaru, C. C., van Grondelle, R. & van Amerongen, H. (2003) *J. Phys. Chem. B* **107,** 3938–3943.
26. van Stokkum, I. H. M., Larsen, D. S. & van Grondelle, R. (2004) *Biochim. Biophys. Acta* **1657,** 82–104.
27. Frank, H. A., Bautista, J. A., Josue, J., Pendon, Z., Hiller, R. G., Sharples, F. P., Gosztola, D. & Wasielewski, M. R. (2000) *J. Phys. Chem. B* **104,** 4569–4577.
28. Papagiannakis, E., Larsen, D. S., van Stokkum, I. H. M., Vengris, M., Hiller, R. G. & van Grondelle, R. (2004) *Biochemistry* **43,** 15303–15309.
29. Palacios, M. A., Frese, R. N., Gradinaru, C. C., van Stokkum, I. H. M., Premvardhan, L. L., Horton, P., Ruban, A. V., van Grondelle, R. & van Amerongen, H. (2003) *Biochim. Biophys. Acta* **1605,** 83–95.
30. Bautista, J. A., Connors, R. E., Raju, B. B., Hiller, R. G., Sharples, F. P., Gosztola, D., Wasielewski, M. R. & Frank, H. A. (1999) *J. Phys. Chem. B* **103,** 8751–8758.
31. Mathies, R. & Stryer, L. (1976) *Proc. Natl. Acad. Sci. USA* **73,** 2169–2173.
32. Ruban, A. V., Pascal, A., Lee, P. J., Robert, B. & Horton, P. (2002) *J. Biol. Chem.* **277,** 42937–42942.
33. Polivka, T., Herek, J. L., Zigmantas, D., Akerlund, H. E. & Sundström, V. (1999) *Proc. Natl. Acad. Sci. USA* **96,** 4914–4917.
34. Polivka, T., Zigmantas, D., Sundström, V., Formaggio, E., Cinque, G. & Bassi, R. (2002) *Biochemistry* **41,** 439–450.
35. Ruban, A. V., Pascal, A. A., Robert, B. & Horton, P. (2002) *J. Biol. Chem.* **277,** 7785–7789.
36. Hermant, R. M., Liddell, P. A., Lin, S., Alden, R. G., Kang, H. K., Moore, A. L., Moore, T. A. & Gust, D. (1993) *J. Am. Chem. Soc.* **115,** 2080–2081.
37. Gradinaru, C. C., Kennis, J. T. M., Papagiannakis, E., van Stokkum, I. H. M., Cogdell, R. J., Fleming, G. R., Niederman, R. A. & van Grondelle, R. (2001) *Proc. Natl. Acad. Sci. USA* **98,** 2364–2369.

IV. Palacios, Rodrigo E.; Kodis, Gerdenis; Herrero, Christian; Ochoa, Ernesto Marino; Gervaldo, Miguel; Gould, Stephanie L.; Kennis, John T. M.; Gust, Devens; Moore, Thomas A.; Moore, Ana L. **Tetrapyrrole Singlet Excited State Quenching by Carotenoids in an Artificial Photosynthetic Antenna.** Journal of Physical Chemistry B (2006), 110(50), 25411-25420.

Tetrapyrrole Singlet Excited State Quenching by Carotenoids in an Artificial Photosynthetic Antenna†

Rodrigo E. Palacios,‡ Gerdenis Kodis,‡ Christian Herrero,‡ Ernesto Mariño Ochoa,‡ Miguel Gervaldo,‡ Stephanie L. Gould,‡ John T. M. Kennis,§ Devens Gust,*,‡ Thomas A. Moore,*,‡ and Ana L. Moore*,‡

The Center for the Study of Early Events in Photosynthesis, Department of Chemistry and Biochemistry, Arizona State University, Tempe, Arizona 85287-1604, and Department of Biophysics, Division of Physics and Astronomy, Faculty of Sciences, Vrije Universiteit, 1081 HV Amsterdam, The Netherlands

Received: July 17, 2006; In Final Form: August 9, 2006

Two artificial photosynthetic antenna models consisting of a Si phthalocyanine (Pc) bearing two axially attached carotenoid moieties having either 9 or 10 conjugated double bonds are used to illustrate some of the function of carotenoids in photosynthetic membranes. Both models studied in toluene, methyltetrahydrofuran, and benzonitrile exhibited charge separated states of the type $C^{\bullet+}-Pc^{\bullet-}$ confirming that the quenching of the Pc S_1 state is due to photoinduced electron transfer. In hexane, the Pc S_1 state of the 10 double bond carotenoid-Pc model was slightly quenched but the $C^{\bullet+}-Pc^{\bullet-}$ transient was not spectroscopically detected. A semiclassical analysis of the data in hexane at temperatures ranging from 180 to 320 K was used to demonstrate that photoinduced electron transfer could occur. The model bearing the 10 double bond carotenoids exhibits biexponential fluorescence decay in toluene and in hexane, which is interpreted in terms of an equilibrium mixture of two isomers comprising s-cis and s-trans conformers of the carotenoid. The shorter fluorescence lifetime is associated with an s-cis carotenoid conformer where the close approach between the donor and acceptor moieties provides through-space electronic coupling in addition to the through-bond component.

Introduction

Carotenoids serve multiple functions in natural photosynthetic antennas and reaction centers including energy harvesting, photoprotection, and energy dissipation. The latter includes nonphotochemical quenching (NPQ), a process observed in green plants under high light conditions. NPQ is thought to protect the photosynthetic membranes from photooxidation, which could occur when the photon flux exceeds the capacity of the plant's photosynthetic processes.[1,2] Although NPQ has been studied for years, its intrinsic mechanisms are not well established. It seems to require the successive enzymatic conversion of violaxanthin (Vio) to antheraxanthin (Ant) and finally to zeaxanthin (Zea), carotenoids that contain 9, 10, and 11 conjugated double bonds, respectively. One possible molecular mechanism for NPQ involves the formation of a complex between chlorophyll *a* (Chl *a*) and zeaxanthin[3−5] in which the fluorescence of Chl *a* is quenched by electron transfer that forms a charge transfer (CT) state.[3,6−8] Studies on transgenic *Arabidopsis thaliana* have confirmed the formation of a carotenoid radical cation under conditions of active NPQ.[9] An increase in the rate of internal conversion and/or intersystem crossing or singlet energy transfer from the chlorophyll to the carotenoids are possible alternative mechanisms involving carotenoids in NPQ.

Artificial molecular constructs that serve as models for chlorophyll−carotenoid complexes (or heterodimers) have been constructed in order to explore the range of mechanisms that could be responsible for this quenching phenomenon. Fungo et al. have shown a correlation between porphyrin fluorescence quenching and the energy of the $C^{\bullet+}-P^{\bullet-}$ charge transfer state in a series of carotenoporphyrin dyads (C−P).[8] In certain carotenoporphyrins the formation of a charge transfer state was confirmed by transient absorption spectroscopy; the formation and decay of carotenoid radical species were observed.[10,11] In recent work we have reported a model system in which energy transfer to the attached carotenoid quenches the tetrapyrrole singlet state.[12]

Herein we report mechanistic studies of energy dissipation by carotenoids in artificial photosynthetic antennas that consist of a phthalocyanine (Pc) moiety to which a pair of carotenoids (C) have been covalently linked in axial positions. Triad **1** binds two carotenoids, each having nine conjugated carbon−carbon double bonds, whereas triad **2** bears two carotenoids, each with 10 carbon−carbon double bonds in conjugation. Varying the number of carbon−carbon conjugated double bonds leads to a difference in the oxidation potential of the carotenoids in **1** and **2** and, consequently, to a difference in the relative energies of the corresponding $C^{\bullet+}-Pc^{\bullet-}$ charge transfer states. The formation of such CT states through photoinduced electron transfer is explored in detail as a mechanism for quenching the phthalocyanine singlet excited state (Pc S_1).

Materials and Methods

Instrumental Techniques. *Steady-State Absorption and Fluorescence.* Ultraviolet−visible absorption spectra were measured on a Cary 500 UV-Vis-NIR spectrophotometer. Steady-state fluorescence emission spectra were measured using a

* To whom correspondence should be addressed.
† Part of the special issue "Arthur J. Nozik Festschrift".
‡ Arizona State University.
§ Vrije Universiteit.

10.1021/jp0645317 CCC: $33.50
Published on Web 09/20/2006 PAGE EST: 9.7

Photon Technology International MP-1 spectrofluorimeter and corrected. Excitation was produced by a 75 W xenon lamp and a single-grating monochromator. Fluorescence was detected at 90° to the excitation beam via a single-grating monochromator and an R928 photomultiplier tube having S-20 spectral response and operating in the single-photon-counting mode.

Transient Absorption Measurements. Femtosecond transient absorption measurements were carried out with an amplified Ti:sapphire laser system described earlier.[13] The laser pulse train was provided by a Ti:sapphire regenerative amplifier (Clark-MXR, model CPA-1000) pumped by a diode-pumped continuous wave solid-state laser (Spectra Physics, model Millennia V). The typical laser pulse was 100 fs at 790 nm, with a pulse energy of 0.9 mJ at a repetition rate of 1 kHz. Most of the laser energy (85%) was used to pump an optical parametric amplifier (IR-OPA, Clark-MXR). The excitation pulse was sent through a computer-controlled optical delay line. The remaining laser output (15%) was focused into a 1 cm flowing water cell to generate a white light continuum. The continuum beam was further split into two identical parts and used as the probe and reference beams. The probe and reference signals were focused onto two optical fiber bundles coupled to a spectrograph (Acton Research, model SP275). The spectra were acquired on a dual diode array detector (Princeton Instruments, model DPDA-1024).

Transient Emission Measurements. Fluorescence decay measurements were performed on $\sim 1 \times 10^{-5}$ M solutions by the time-correlated single photon counting method. The excitation source was a cavity-dumped Coherent 700 dye laser pumped by a frequency-doubled Coherent Antares 76s Nd:YAG laser. Fluorescence emission was detected at a magic angle using a single grating monochromator and microchannel plate photomultiplier (Hamamatsu R2809U-11). The instrument response time was ca. 60−90 ps, as verified by scattering from a Ludox AS-40 suspension. The spectrometer was controlled by software based on a LabView program from National Instruments. Low-temperature measurements were performed using an Oxford Optistat^{DN} liquid-nitrogen-cooled optical cryostat equipped with an Oxford ITC 601 temperature controller (accuracy ±0.1 K).

Synthesis. Triads **1** and **2** were prepared by coupling silicon tetra-*tert*-butylphthalocyanine dihydroxide (**5**) with the corresponding carotenoid acid chloride as previously described.[14−16]

Results

Conformation of Triad 2. The ring currents associated with phthalocyanines induce large changes in the ^{1}H NMR chemical shifts ($\Delta\delta$) of moieties directly attached to the macrocycle.[17−22] The direction and magnitude of such changes depend on the positions of the protons relative to the phthalocyanine plane. A combination of ^{1}H NMR data for **2** and **4** and semiempirical quantum chemical methods was used to gain insight into the three-dimensional structure of triad **2**. Experimental $\Delta\delta$ values were calculated from the difference between the observed carotenoid ^{1}H chemical shifts in triad **2** and the corresponding ^{1}H resonances in model carotenoid **4**.[14] The theoretical $\Delta\delta$ values for two partial models of **2** were estimated using silicon phthalocyanine ring current data[18,23] in combination with quantum chemical calculations (PM3) and crystal structure data for silicon carboxylatophthalocyanines.[24,25] In the fitting procedure described below for triad **2**, only the C6′−C7′ s-trans and s-cis conformations were considered; an extended structure (all trans configuration and all s-trans conformation) was assumed for the rest of the carotenoid backbone. The atom coordinates for the PM3-minimized C6′−C7′ s-trans and s-cis isomers (referred to simply as s-cis and s-trans) of model carotenoid **4′** (see Chart 1) were modified by changing the Si−O bond length and Si−O−C angle to match X-ray data.[24]

These coordinates were then plotted, designating the silicon atom as the origin, placing the abscissa in the phthalocyanine plane, and fixing the Si−O bond along the ordinate (Figure 1). The isoshielding lines were added to the plot, and the predicted $\Delta\delta$ values for the first nine magnetically distinct carotenoid protons contiguous to the silicon were recorded.[26]

The above information is presented in Figure 2, which shows the predicted $\Delta\delta$ values for the caroteniod s-cis (red circles) and s-trans (green triangles) conformations. Additionally, Figure 2 shows the predicted $\Delta\delta$ values for an s-[cis/trans] average (blue triangles) conformation, as well as the corresponding $\Delta\delta$ experimental values (black squares) as defined above.

A three-dimensional model of triad **2** was constructed by combining one s-trans conformer and one s-cis conformer of model carotenoid **4′** with a PM3 minimized model of **5**, as shown in Figure 3A. Manipulation of a three-dimensional model shows that rotation around the C6′−O single bond in the s-cis isomer yields a molecular conformation in which the carotenoid moiety lies within a few angstroms of the phthalocyanine plane (Figure 3B).

An analogous analysis of the three-dimensional structure of triad **1** indicates that the s-trans carotenoid conformation is predominant in this case. The formation of an s-cis folded conformation equivalent to the one described for **2** is not possible due to strong steric hindrance caused by the 19′ methyl group (see Chart 1).

Electrochemistry. The values for the oxidation and reduction potentials of **1**, **2**, **3**, **4**, and **5** from previous work[14] are summarized in Table 1. The carotenoid moieties of **1** and **2** are the species oxidized at 0.70 and 0.62 V, respectively. The difference in oxidation potential is also clearly seen in the model carotenoids; this difference is the origin of the lower energy of $C^{\bullet+}-Pc^{\bullet-}$ charge transfer state in **2** relative to **1**.

Steady-State Absorption. *Solvent Dependence.* Parts A and B of Figure 4 present the absorption spectra of triads **2** and **1**, respectively, in *n*-hexane (black line), toluene (red line), tetrahydrofuran (green line), and benzonitrile (blue line). The maxima of the phthalocyanine longest-wavelength absorption and shortest wavelength emission bands for triad **2** matched the corresponding maxima of triad **1** in all the solvents studied. This information together with the energy of the Pc S_1 state, calculated as the wavenumber average of the aforementioned maxima, is summarized in Table 2. Figure 4 shows that the energy of the carotenoid $S_0 \rightarrow S_2$ transition in **1** and **2** shifts to longer wavelengths and loses vibrational structure when the molecules are dissolved in solvents of increasing polarity. These effects were previously observed in other carotenoids and in the case of carbonyl-containing carotenoids are indicative of charge-transfer character in both the ground and excited states.[27]

Temperature Dependence. Figure 5 shows the corrected absorption spectrum for triad **2** in *n*-hexane at 190 K (black), 220 K (red), 260 K (green), 290 K (blue), and 320 K (cyan). The spectra were corrected for the volume change of the solvent upon cooling using the Rackett equation[28] and parameters obtained from the literature.[29] A 15 nm (0.078 eV) bathochromic shift is observed for the carotenoid longest-wavelength absorption band (associated with the $S_0 \rightarrow S_2$ electronic transition) in going from 320 to 190 K. In contrast to this, the phthalocyanine absorption bands do not show any significant shifts under the same conditions. The red shift in the carotenoid $S_0 \rightarrow S_2$ transition can be rationalized by considering that the dielectric

CHART 1: Structures of Triads 1 and 2, Model Carotenoids 3, 3′, 4, and 4′, and Phthalocyanine 5 Defining the Numbering for Relevant Carbon and Hydrogen Atoms

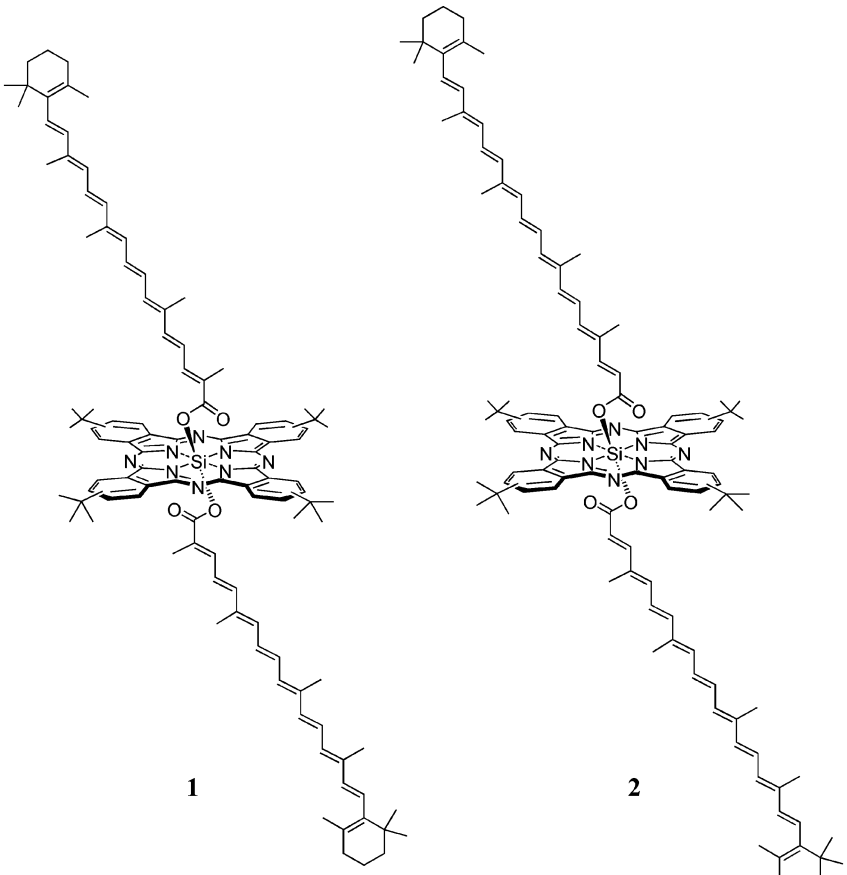

1 **2**

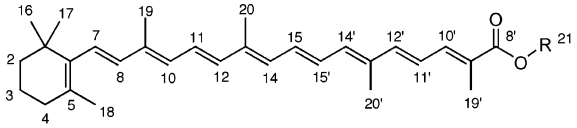

3 R = Me
3' R = $SiMe_3$

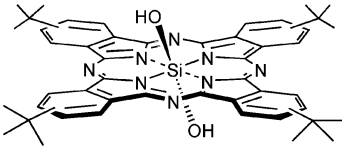

5

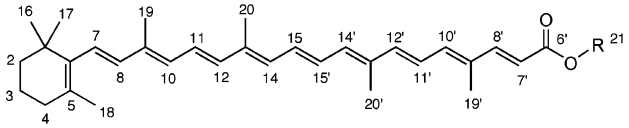

4 R = Me
4' R = $SiMe_3$

constant of *n*-hexane increases with decreasing temperature according to eq 8 (vide infra).

Phthalocyanine Singlet Excited State and $C^{\bullet+}-Pc^{\bullet-}$ Charge Transfer State Lifetimes. *Solvent Dependence.* Previous studies at room temperature indicate that the first excited singlet state lifetime of model phthalocyanine **5** is essentially independent of the solvent polarity.[16] However, the Pc singlet exited state lifetime in triads **1** and **2** is strongly dependent on the solvent dielectric constant and is generally quenched compared to the corresponding lifetime of model phthalocyanine **5**. In all the solvents studied except *n*-hexane, the origin of the observed quenching was assigned to the formation of a $C^{\bullet+}-Pc^{\bullet-}$ charge transfer state. This interpretation is based on the correspondence of the rise times of the $C^{\bullet+}$ and $Pc^{\bullet-}$ transient absorption ($\tau_{C^{\bullet+}}^{For}$ and $\tau_{Pc^{\bullet-}}^{For}$) and the decay of the phthalocyanine singlet excited state ($\tau_{^1Pc}^{Dec}$). Parts A and B of Figure 6 show the normalized near-infrared transient absorption spectra of triads **2** and **1**, respectively, in benzonitrile (black line), tetrahydrofuran (red line), and toluene (green line). For each spectrum the small band centered at ~980 nm is associated with the $Pc^{\bullet-}$ species whereas the broad large band at shorter wavelengths is associated with the $C^{\bullet+}$ radical cation.

In the case of triad **2** the Pc S_1 state was observed to exhibit a biexponential fluorescence decay in toluene and *n*-hexane. Table 3 shows the phthalocyanine singlet excited estate and the $C^{\bullet+}-Pc^{\bullet-}$ charge transfer state lifetimes for **1**, **2**, and **5** in

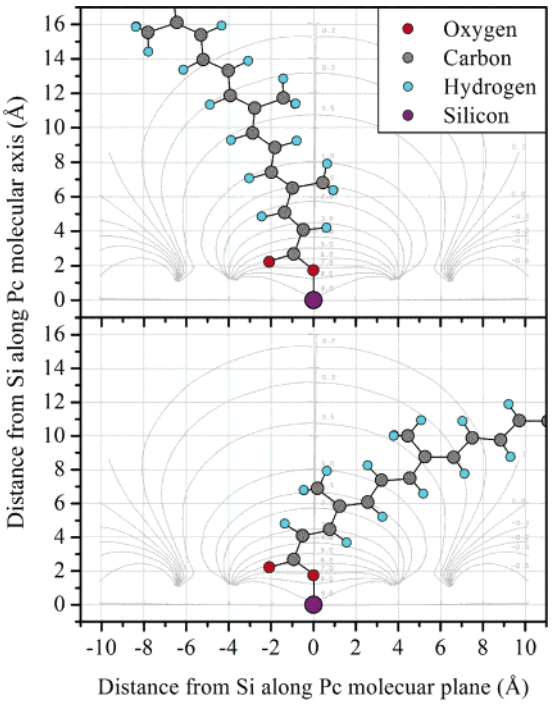

Figure 1. Atom coordinates for the PM3 minimized C6′−C7′ s-cis (upper panel) and s-trans (lower panel) conformations of model carotenoid **4′** superimposed over the phthalocyanine isoshielding lines (see text for details).

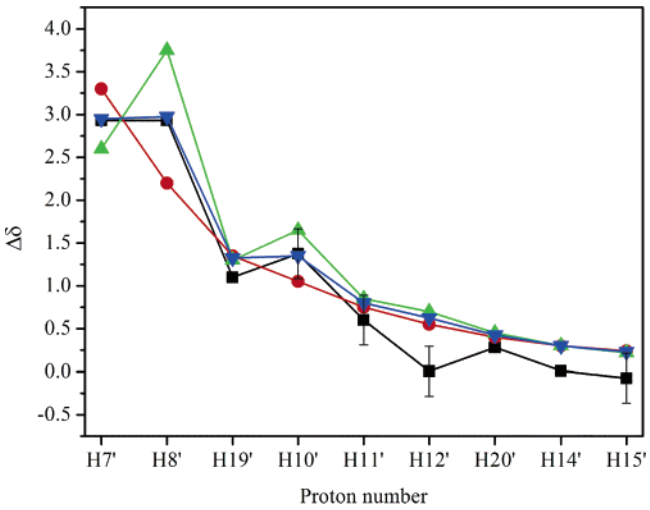

Figure 2. Predicted changes in chemical shift (Δδ) for the first nine magnetically distinct carotenoid protons adjacent to the silicon. Different conformations of triad **2** around C6′−C7′ are considered (see text for details): red circles, s-cis; green triangles, s-trans; blue triangles, s-[cis/trans] 50:50 average. The experimental Δδ (black squares) are shown for comparison.

different solvents. The data were taken from previously published work;[14,16] additionally, the lifetimes for **2** in toluene and tetrahydrofuran were measured.

Temperature Dependence. The temperature dependence of the fluorescence lifetime (τ_F) was measured in order to further investigate the nature of the Pc S_1 quenching in **2** in the nonpolar solvent *n*-hexane. A solution of **2** in *n*-hexane was excited at 615 nm, and the fluorescence decay at 689 nm was recorded at different temperatures in the 180−320 K range using the single photon timing technique. Two exponential components were necessary to satisfactorily fit the fluorescence decays at 200 K and above. The results are summarized in Table 4; the shorter component at each temperature is τ_{2a} and the longer component is τ_{2b}. Figure 7A shows the magnitude and amplitude of these components as a function of temperature, and Figure 7B shows some representative fluorescence decays.

Discussion

Structure and Biexponential Fluorescence Lifetime of Triad 2. Figure 3 illustrates that triad 2 can exist as several conformational isomers, and the NMR data suggest that at room temperature there are similar proportions of C6′−C7′ s-cis and s-trans carotenoid conformations. As seen in Figure 3A, the C6′−C7′ s-cis/trans conformations are significantly different in terms of the resulting orientation of the carotenoid moiety relative to the phthalocyanine plane. Indeed, further structural examination of **2** shows that rotation around the C6′−O single bond in the s-cis isomer yields a molecular conformation in which part of the carotenoid moiety lies within a few angstroms of the phthalocyanine plane (Figure 3B).[30] The short distance between the Pc and C π-systems allowed by this conformation predicts a significant increase of through space electronic coupling between the chromophores and therefore an increase in the rate of excited state quenching by photoinduced electron transfer. Considering that only one of the two carotenoids in **2** can undergo electron/energy transfer at a time, and assuming that the remaining carotenoid does not affect the process, two different fluorescence lifetimes are expected for triad **2**, corresponding to the isomeric forms of the polyene.[31] The data presented in Figure 7A are consistent with the presence of two isomers in equilibrium, **2b** and **2a** (eq 1), having different fluorescence lifetimes (**2b** is defined as the longer-lived isomer). Thus, the **2a** and **2b** isomers can be associated with the carotenoid s-cis and s-trans conformers, respectively. From Figure 7A insert, **2b** is favored over **2a** at low temperatures. Assuming that the isomer concentrations are proportional to the initial amplitudes of their respective fluorescence decays, a van't Hoff plot (Figure 8) yields the thermodynamic parameters $\Delta H^\circ = 2.7 \pm 0.2$ kcal/mol (0.12 ± 0.01 eV) and $\Delta S^\circ = 8.8 \pm 0.7$ cal/(K mol) for the equilibrium between **2b** and **2a**. These enthalpy and entropy differences are in reasonable agreement with experimental calculations for the s-trans/s-cis conformational forms in 1,3-butadiene that yield ΔH° and ΔS° values of 2.93 kcal/mol and 3.98 cal/(K mol), respectively.[32]

$$\mathbf{2b} \leftrightarrows \mathbf{2a} \tag{1}$$

$$\ln K = \ln \frac{[\mathbf{2a}]}{[\mathbf{2b}]} = -\frac{\Delta G^\circ}{RT} = \frac{\Delta S^\circ}{R} - \frac{\Delta H^\circ}{RT} \tag{2}$$

Additionally, an Arrhenius plot applied to the quenching of the observed fluorescence components (τ_{2a} and τ_{2b}) is shown in Figure 9. From this it can be concluded that in **2b** and **2a** the Pc singlet excited state is quenched by activated processes with Arrhenius activation energies of 0.171 and 0.096 eV, respectively. The significance of this observation will be discussed later.

Triad **1** displays a monoexponential fluorescence decay in all solvents studied, in agreement with NMR results which are consistent with a single s-trans isomer in solution. It is likely that steric considerations preclude the formation of an s-cis conformer, which could lead to biexponential fluorescence decay in triad **1**.

Exploring Electron Transfer (eT) as the Pc S_1 Quenching Mechanism. In polar solvents, the observed quenching of the Pc S_1 state of triads **1** and **2** is assigned to the formation a $C^{\bullet+}$−$Pc^{\bullet-}$ charge separated state. The effect of solvent and temper-

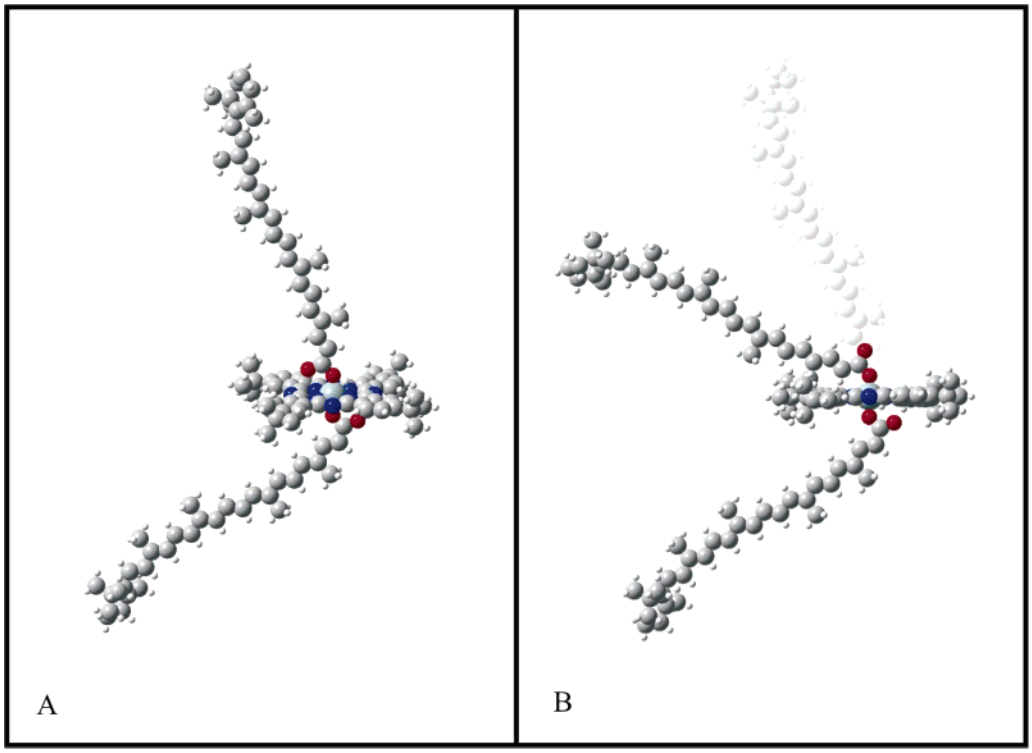

Figure 3. (A) Three-dimensional model of triad **2** depicting the C6′−C7′ s-cis/trans carotenoid conformations (see text for details). **(B)** Same as **(A)** showing a 180° rotation about the C6′−O single bond in the carotenoid s-cis conformation.

TABLE 1: Oxidation and Reduction Potentials of Triads 1 and 2 and Model Compounds vs SCE, Measured in Benzonitrile

compound	oxidation potential (eV)	reduction potential (eV)
1	0.70	−0.72
3	0.68	
2	0.62	−0.72
4	0.60	
5	1.04	−0.76

TABLE 2: Phthalocyanine Long Wavelength Absorption and Short Wavelength Emission Maxima for Triads 1 and 2 and the Corresponding Pc S_1 Energies

solvent	long wavelength absorption maxima (nm)	short wavelength emission maxima (nm)	Pc S_1 energy (eV)
n-hexane	684	685	1.81
toluene	692	698	1.78
tetrahydrofuran	689	696	1.79
benzonitrile	697	704	1.77

ature on the electron-transfer rate constant (k_{et}) involved in the formation of this state can be discussed in terms of eq 3[33,34] and similar equations[34,35] that have been developed for nonadiabatic electron-transfer reactions.

$$k_{et} = \frac{4\pi^2}{h\sqrt{4\lambda_s \pi k_B T}} |V|^2 \sum_{q=0}^{\infty} e^{-S} \frac{S^n}{n!} e^{-(\Delta G^\circ + \lambda_s + nh\nu)^2/4\lambda_s k_B T} \quad (3)$$

In eq 3, V is the electronic coupling matrix element, h is Planck's constant, k_B is Boltzmann's constant, T is the absolute temperature, λ_s is the outer-sphere (solvent) reorganization energy, ΔG° is the standard reaction free energy change, ν is the frequency of the effective vibrational mode, and S is the Huang−Rhys factor $\lambda_i/h\nu$, where λ_i is the total inner sphere reorganization energy. The summand n refers to the product's vibrational levels. For the systems studied here the first few terms in the sum provide an accurate evaluation of the rate constant. This treatment assumes that the molecular vibrational modes can be represented using a single effective high-frequency mode (ν). The low-frequency solute and solvent vibrational modes are treated classically.

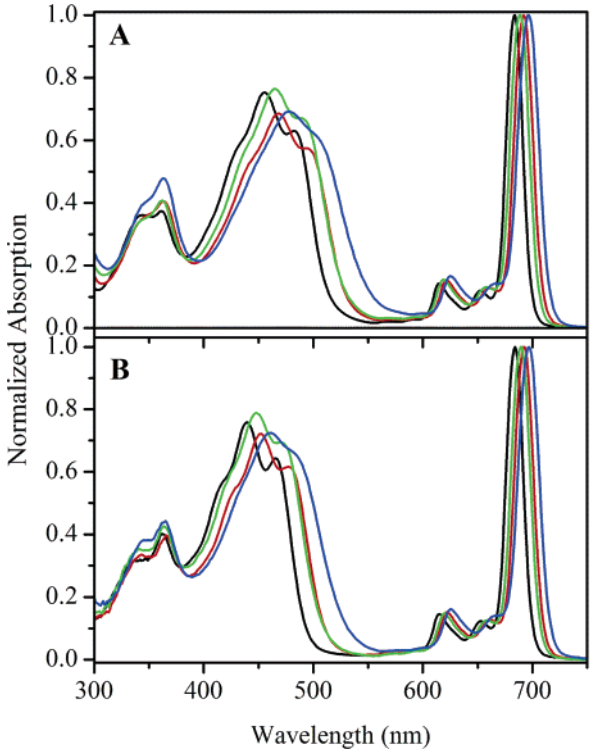

Figure 4. (A) Triad **2** absorption spectra in *n*-hexane (black line), toluene (red line), tetrahydrofuran (green line), and benzonitrile (blue line). **(B)** Same as **(A)** for triad **1**.

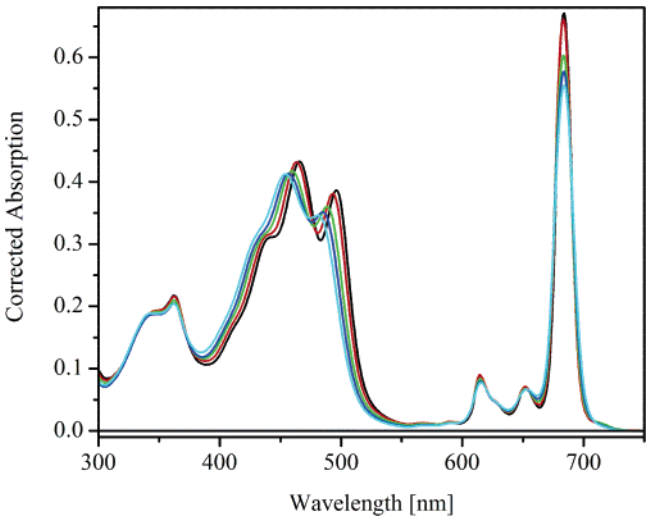

Figure 5. Corrected absorption spectra for triad **2** at 190 K (black line), 220 K (red line), 260 K (green line), 290 K (dark blue line), and 320 K (light blue line) in *n*-hexane. The absorption spectra were corrected for the change in solvent volume as described in the text.

Solvent Effect on the Electron-Transfer Rate. The influence of the solvent on the electron-transfer rate is given in principle by the dependence of V, λ_i, ν, $\Delta G°$, and λ_s on solvent parameters. In general, the parameters λ_i and $h\nu$ are taken to be solvent independent. Additionally, considering superexchange mediated by the Si−O bond linking the Pc and C moieties, the dominant source of donor/acceptor coupling in triads **1** and **2b**, V is assumed to be solvent independent and equal for these systems. Consequently, $\Delta G°$ and λ_s are responsible for the solvent dependency of k_{et}. To a first approximation, the reaction standard free energy ($\Delta G°$) and the outer-sphere reorganization energy (λ_s) can be written as a sum of two terms

$$\Delta G° = \Delta G_p° + \Delta G_n° \quad (4)$$

$$\lambda_s = \lambda_p + \lambda_n \quad (5)$$

The first terms in eqs 4 and 5 are related to the solute−solvent dipole interactions, while the second terms take into account higher order electrostatic interactions in addition to other interactions of nonelectrostatic nature between the solute and solvent. To a first approximation, the parameters $\Delta G_n°$ and λ_n for a given molecule can be considered to be constant for different solvents. Then, the solvent dependence of $\Delta G°$ and λ_s is given by $\Delta G_p°$ and λ_p, respectively. Models usually employed to calculate $\Delta G_p°$ as a function of the solvent treat the solute as an electrostatic charge distribution within a cavity that is immersed in a dielectric continuum; in general, these methods use as a starting point the Rhem and Weller equation

$$\Delta G_p° = (E_{Ox}{}^{D} - E_{Red}{}^{A})_{Ref} - E_{00} + C + S \quad (6)$$

where $E_{Ox}{}^{D}$ and $E_{Red}{}^{A}$ are the first oxidation and reduction potentials of the donor and acceptor, respectively, as measured electrochemically in a reference solvent of dielectric constant ϵ_{Ref}, and E_{00} is the energy of the donor first excited singlet state. The C and S terms are the Coulomb and solvation energy changes resulting from the electron-transfer reaction. The model employed here to calculate $\Delta G_p°$ uses a finite difference solution of the Poisson−Boltzmann equation (FDPB) to evaluate the Coulomb and solvation terms. Unlike other models, which use a highly idealized shape and charge distribution for the donor and acceptor, this model uses electronic structure calculations to account explicitly for molecular shape and charge distribution change upon electron transfer. The solvent is modeled as a continuum with a dielectric constant ϵ_s, and the solute is represented by a set of point charges placed into a cavity of dielectric constant ϵ_{IN}.

The first term in eq 5 is also usually estimated using continuum models. In this case, the FDPB equation for λ_p is given by

$$\lambda_p = \frac{1}{2}\sum_i \Delta q_i(\phi_i^{\epsilon_S} - \phi_i^{\epsilon_\infty}) \quad (7)$$

where Δq_i is the change in charge at site i when the electron is transferred from the donor to the acceptor. $\phi_i^{\epsilon_S}$ and $\phi_i^{\epsilon_\infty}$ are the electrostatic potentials calculated with the charge distribution given by Δq_i and the solvent dielectric constant equal to the solvent static and optical dielectric constants, respectively. More details of this model are provided elsewhere.[36−38]

Effect of Temperature on the Electron-Transfer Rate. The effect of temperature on k_{et} is seen explicitly in eq 3. The parameters V, λ_i, and ν are usually considered to be temperature independent. As in previous models for $\Delta G°$ and λ_s, the "nondipolar" terms, $\Delta G_n°$ and λ_n, can be considered temperature independent to a first approximation. The temperature dependence of $\Delta G°$ and λ_s is then given by the "dipolar" terms, $\Delta G_p°$ and λ_p, by means of the static (ϵ_s) and optical (ϵ_∞) dielectric constants. For the particular case of *n*-hexane, the dependence of ϵ_s and ϵ_∞ on the temperature is well described by eqs 8[39,40] and 9,[41] respectively, and the relationship $\epsilon_\infty = n^2$. Consequently, $\Delta G_p°$ can be calculated as a function of the temperature by applying eq 8 and the thermodynamic cycle described in the Supporting Information. For *n*-hexane ϵ_s and ϵ_∞ are formally the same, so λ_p is equal to zero (see eq 7). As a result, the temperature dependence on ϵ_∞ need not be considered.

$$\epsilon_s(T) = 2.11 + (1.26 \times 10^{-4})T - (2.98 \times 10^{-6})T^2 \quad (8)$$

$$n(T) = n^{293} - 0.0004(T - 293) \quad (9)$$

The corresponding refractive indexes at the specific temperature and 293 K are $n(T)$ and n^{293}.

Calculating the Electron-Transfer Rate as a Function of the Solvent. Previous experiments with artificial reaction centers indicate that in general the use of polar solvents favors the photoinduced electron-transfer process by lowering the energy of charge separated state relative to that of the initial excited state.[42] This stabilization effect is lost (or is substantially decreased) by the use of nonpolar solvents, in some cases by as much as 0.9 eV.[43] The electrochemical potentials for **2** in benzonitrile (without considering Coulombic effects) locate the $C^{\bullet+}-Pc^{\bullet-}$ state 0.47 eV below the $C-{}^1Pc$ state. Thus, assuming a 0.5 eV loss in stabilization in *n*-hexane, the formation of the $C^{\bullet+}-Pc^{\bullet-}$ state in **2** from the $C-{}^1Pc$ state would be slightly endergonic. Consequently, a putative $C^{\bullet+}-Pc^{\bullet-}$ charge transfer state in *n*-hexane would be characterized by slow formation relative to the rate of charge recombination, and under these circumstances, the maximum transient concentration of $C^{\bullet+}-Pc^{\bullet-}$ could be small enough to escape detection by transient absorption methods. Therefore, failure to observe the characteristic ion signals in the transient absorption experiment on **1** and **2** in *n*-hexane does not rule out the formation of the charge transfer state. On this basis, and assuming that the quenching of the longest fluorescence lifetime component of **2** in *n*-hexane (τ_{2b}) is due to photoinduced electron transfer, k_{et} can be

TABLE 3: Phthalocyanine Singlet Excited State and $C^{\bullet+}-Pc^{\bullet-}$ Charge Transfer State Lifetimes[a]

	triad **2**		triad **1**		model **5**
solvent[b]	$\tau^{1}{}_{Pc}{}^{Dec}$ or $\tau_{C^{\bullet+}}{}^{For}$	$\tau_{C^{\bullet+}}{}^{Dec}$	$\tau^{1}{}_{Pc}{}^{Dec}$ or $\tau_{C^{\bullet+}}{}^{For}$	$\tau_{C^{\bullet+}}{}^{Dec}$	$\tau^{1}{}_{Pc}{}^{Dec}$ [d]
n-hexane	3.49 ± 0.15 ns[c,d]		5.60 ± 0.11 ns[d]		5.23 ± 0.08 ns
toluene	1.22 ± 0.10 ns[c,d]	16 ± 2 ps	2.84 ± 0.10 ns[d]	20 ± 2 ps	5.65 ± 0.10 ns
THF	4.3 ± 0.5 ps	27 ± 3 ps	6.2 ± 0.6 ps[e]	25 ± 3 ps	6.11 ± 0.12 ns
PhCN	2.2 ± 0.3 ps	17 ± 2 ps	2.5 ± 0.2 ps	10 ± 1 ps	5.40 ± 0.10 ns

[a] Measured using the transient absorption pump−probe technique, unless otherwise noted. [b] THF is tetrahydrofuran and PhCN is benzonitrile. [c] Two fluorescence lifetimes were observed, the longer lifetime is reported here and is assigned to conformer **2b**. [d] Measured using the single photon counting technique. [e] Measured using the fluorescence up-conversion technique.

TABLE 4: Phthalocyanine Singlet Excited-State Lifetimes of Triad 2 in *n*-Hexane as a Function of Temperature[a]

temp (K)	τ_{2a} (ns)	τ_{2b} (ns)	χ^2
180		6.70 (100)	1.04
190		6.57 (100)	1.04
200	2.25 (3.5)	6.47 (96.5)	1.07
210	2.46 (8.0)	6.34 (92.0)	1.05
220	2.86 (14.5)	6.16 (85.6)	1.02
230	2.71 (20.5)	5.94 (79.5)	1.03
240	2.53 (26.0)	5.66 (74.0)	1.03
250	2.01 (26.5)	5.19 (73.5)	1.00
260	1.86 (32.1)	4.87 (67.9)	1.02
270	1.66 (37.3)	4.54 (62.7)	1.02
280	1.50 (42.0)	4.22 (58.0)	1.03
290	1.26 (43.7)	3.78 (56.3)	1.03
300	1.18 (49.2)	3.49 (50.8)	1.02
310	1.05 (52.3)	3.13 (47.7)	1.01
320	0.93 (55.2)	2.81 (44.8)	1.00

[a] Measured using the single photon timing technique, see text for details. Initial percentage amplitudes shown in parentheses.

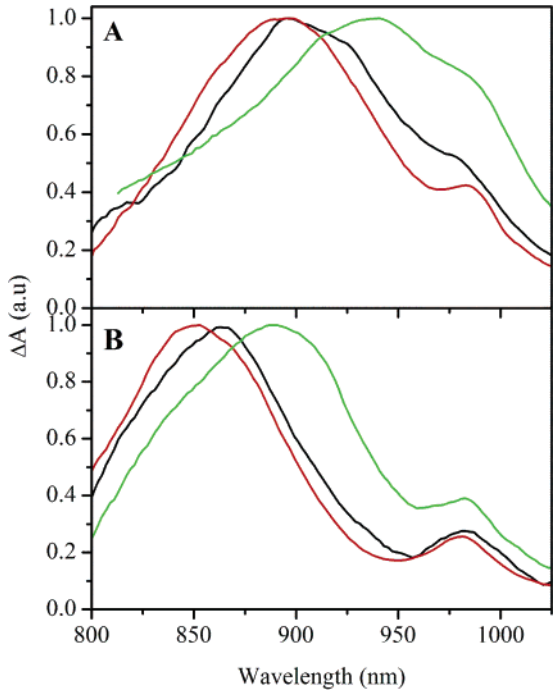

Figure 6. (A) Normalized near-infrared transient absorption spectra of triad **2** in benzonitrile (black line), tetrahydrofuran (red line), and toluene (green line). (B) Same as (A) for triad **1**. For each solvent, the excitation was tuned to match the energy of the phthalocyanine long-wavelength absorption band (see Table 2). The spectra were recorded at the time delay corresponding to the maximum intensity of the transient absorption signal.

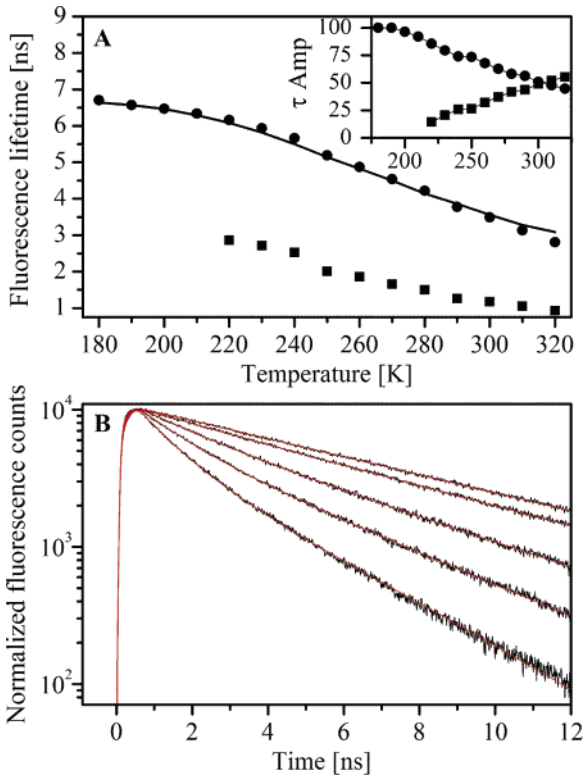

Figure 7. (A) Decay components obtained from the biexponential fit of the fluorescence decay of a deoxygenated ~10 μM solution of triad **2** in *n*-hexane at different temperatures. The excitation and emission wavelengths were 615 and 689 nm, respectively. The shorter component at each temperature is τ_{2a} (squares) and the longer component is τ_{2b} (circles). Lifetimes with amplitudes lower than 9% were excluded. The inset shows τ_{2a} and τ_{2b} initial percentage amplitudes, Amp**2a** (squares) and Amp**2b** (circles), respectively, as a function of temperature. The solid curve is the calculated fluorescence lifetime assuming electron transfer as the quenching mechanism; see discussion section for details. (B) Normalized fluorescence decays at 190, 220, 260, 290, and 320 K from top to bottom. The red smooth line is an exponential fit using the corresponding lifetimes from Table 4.

calculated for **2** in *n*-hexane at room temperature by replacing τ in eq 10 with the corresponding value for τ_{2b}. The unquenched fluorescence lifetime (τ_F°) in eq 10 is taken to be 6.70 ns, which is the longest value obtained at low temperatures. In an analogous way, the experimental electron-transfer rate constants for **1** and **2** are calculated in different solvents by using the corresponding Pc S_1 decay and $C^{\bullet+}$ formation lifetimes from Table 3; the results are summarized in Table 5. As mentioned above, triad **2** showed biexponential fluorescence decay in toluene and *n*-hexane; the values reported in Table 3 are the longest component for each solvent.

$$k_{et} = \frac{1}{\tau} - \frac{1}{\tau_F^\circ} \tag{10}$$

Substituting the expressions for ΔG° and λ_s given by eqs 4 and 5 into eq 3 and calculating ΔG_p° and λ_p with the continuum

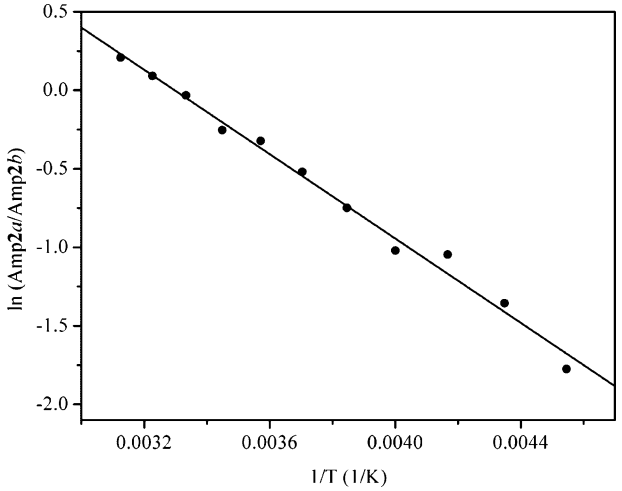

Figure 8. Natural logarithmic ratio of Amp**2a** and Amp**2b** (see Figure 7 panel A caption) as a function of the reciprocal of the absolute temperature (circles). Amplitudes lower than 9% were excluded from this analysis. The solid line represents the best linear fit to the data.

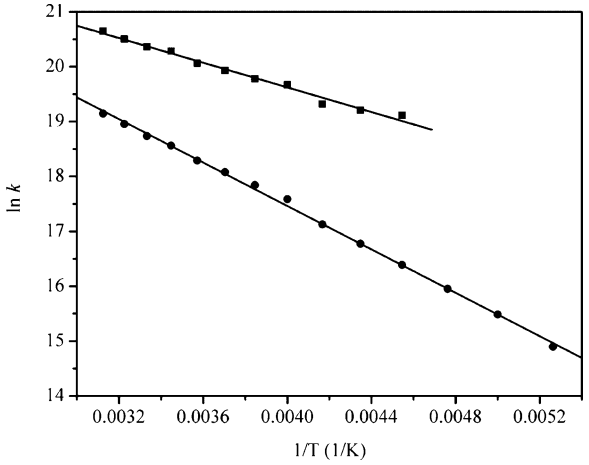

Figure 9. Arrhenius plot for the fluorescence quenching process in **2a** (squares) and **2b** (circles). The rate constants used to create the plot were calculated by subtracting 1/6.7 ns from the corresponding $1/\tau_{\mathbf{2a}}$ and $1/\tau_{\mathbf{2b}}$ values at each temperature. Lifetimes with initial amplitudes lower than 9% were excluded from this analysis.

FDPB model (see Supporting Information), five parameters are needed to calculate k_{et} for triads **1** and **2** in different solvents; V, λ_i, $h\nu$, ΔG_n°, and λ_n; $h\nu$ and λ_i can be considered equal for **1** and **2**.[44] Because in typical organic systems vibrational frequencies in the range of 1300−1600 cm^{-1} constitute a dominant fraction of the reorganization energy changes in the high-frequency modes, $h\nu$ is set to be 1600 cm^{-1} in the following analysis. As mentioned before, ΔG_n° and λ_n for a given molecule can be regarded as constant for different solvents yielding the following system of eight equations and six unknowns.

$$k_j^m = \frac{4\pi^2}{h\sqrt{4(\lambda_n^m + \lambda_j^m)\pi k_B T}} \times |V|^2 \sum_{q=0}^{\infty} e^{-(\lambda_i/h\nu)} \frac{\left(\frac{\lambda_i}{h\nu}\right)^n}{n!} e^{-[(\Delta G_n^m + \Delta G_j^m) + (\lambda_n^m + \lambda_j^m) + nh\nu]^2/4(\lambda_n^m + \lambda_j^m)k_B T} \quad (11)$$

$$m = 1, 2 \quad \text{and} \quad j = 1, 2, 3, 4$$

The values 1 and 2 for the superscript m refer to triads **1** and **2**, respectively; the values 1, 2, 3, and 4 for the subscript j correspond to the solvents *n*-hexane, toluene, tetrahydrofuran, and benzonitrile in that order. The rate constants k_j^m are taken from Table 5, and the values for ΔG_j^m and λ_j^m are calculated using the previously described continuum model and summarized in Table 2 of the Supporting Information. Applying the calculated ΔG_j^m and λ_j^m values in eq 11, a set of six parameters ($V = 194$ cm^{-1}, $\lambda_i = 0.490$ eV, $\Delta G_n^1 = 0.024$ eV, $\Delta G_n^2 = 0.075$ eV, $\lambda_n^1 = 0.144$ eV, $\lambda_n^2 = 0.195$ eV) is obtained that yields k_j^m values within the experimental error for all the solvents studied except toluene (vide infra). These theoretical k_j^m values are summarized in Table 5.

Although to a first approximation λ_n was considered to be the same for all the solvents, its value is expected to be slightly different for different solvents. In the particular case of toluene and *n*-hexane the nondipolar term, λ_n, is the predominant component of the solvent reorganization energy. Consequently, slight variations in λ_n will significantly affect the electron transfer rate in these two solvents. While a slightly different λ_n is also expected for tetrahydrofuran and benzonitrile, the effect is likely to be masked by the predominant contribution of λ_p to the total solvent reorganization energy in these solvents. Regarding the data in toluene, in both triads **1** and **2** the systematic red shift of the carotene $S_0 \rightarrow S_2$ transition and radical cation absorption maxima as a function of increasing solvent polarity is disrupted by toluene. Thus, differences in the experimental and theoretical electron-transfer rates in toluene for both triads might be related to their anomalous behavior in this solvent. For our purposes, the set of parameters chosen to solve the system of equations was the one that best fitted the observed quenching in *n*-hexane at the expense of a poor fit in toluene.

Calculating Electron Transfer as a Function of the Temperature. The Arrhenius analysis of the quenching of **2** in *n*-hexane (Figure 9) indicates that the Pc S_1 state is quenched by an activated process. Assuming that this quenching process is electron transfer, the fluorescence lifetime of **2** in *n*-hexane can be calculated as a function of temperature by combining eqs 10 and 11, and using the parameters V, λ_i, ΔG_n^2, and λ_n^2 obtained in the previous section. Additionally, ΔG_1^2 values were calculated at different temperatures by considering the temperature dependence of ϵ_S (eq 8) and using the thermodynamic cycle described in the Supporting Information. The result of this calculation is shown as a solid line in Figure 7. The longer component of the observed fluorescence lifetime, which is associated with the s-trans carotenoid, was chosen for this analysis for two reasons: (a) The relative amplitude of this component varies from 45 to 100% over the temperature range studied (compared to 55 to 0% for the shorter component) which means that the fluorescence lifetime of $\tau_{\mathbf{2b}}$ is in general, and especially at low temperatures, more accurately determined than that of $\tau_{\mathbf{2a}}$. (b) The shorter fluorescence lifetime, $\tau_{\mathbf{2a}}$, is associated with the s-cis carotenoid conformer where the close distance and relative orientation between chromophores is such that donor/acceptor coupling mediated through the Si−O bond, as assumed in the previous section, is likely augmented by through space interactions.

Quenching of the Tetrapyrrole Excited State by Electron Transfer or Energy Transfer? Our results show that in these systems the addition of a double bond to the carotenoid moiety has a marked effect on its ability to quench the phthalocyanine

TABLE 5: Experimental[a] and Theoretical Rate Constants[b] for the Formation of the $C^{\bullet+}-Pc^{\bullet-}$ Charge Transfer State in Triads 1 and 2

	triad **2**		triad **1**	
solvent[c]	experimental	theoretical	experimental	theoretical
n-hexane	0.13 ± 0.01	0.13	0.03 ± 0.01	0.02
toluene	0.67 ± 0.06	9.06	0.20 ± 0.01	4.10
tetrahydrofuran	230 ± 25	207	160 ± 15	161
benzonitrile	450 ± 50	480	400 ± 30	380

[a] Calculated applying eq 10 and using data from Table 3. [b] Expressed as ns^{-1}.

excited singlet state. The addition of a double bond to the carotenoid moiety has two effects relevant to this observation: Its oxidation potential is lowered, and the energies of its electronic excited states are lowered.

To definitively assign a quenching mechanism either to photoinduced electron transfer or to energy transfer, it is necessary to observe the product of the quenching, either a CT species or, presumably, the S_1 excited state of the carotenoid. Triads **1** and **2** demonstrate that with adequate driving force provided by a solvent-stabilized intermolecular CT state, electron-transfer quenching is observed and occurs on the picosecond time scale. Triad **1** is not quenched in nonpolar solvents, consistent with the expected endergonic nature of photoinduced electron transfer. Triad **2** in nonpolar solvents demonstrates modest quenching that is too slow to permit accumulation of a concentration of either the CT species or the carotenoid S_1 species that is adequate for detection. However, our theoretical treatment predicts photoinduced electron transfer in nonpolar solvents on the time scale of the observed quenching.

Carotenoid−phthalocyanine dyads having much less driving force for electron transfer (~0.20 V due to the presence of a phthalocyanine moiety with more negative reduction potential), and with substantial structural differences from those reported herein, quench the fluorescence of the phthalocyanine by energy transfer. In these dyads the carotenoid radical cation is not detected and the signature spectrum of the carotenoid S_1 species is observed.[12]

The fact that the tetrapyrrole singlet state can be selectively quenched by tuning the number of conjugated carbon−carbon double bonds of the attached carotenoids is reminiscent of the nonphotochemical quenching process observed in green plants. The preferential quenching of chlorophyll fluorescence in the presence of zeaxanthin is associated with either its lower oxidation potential or its lower S_1 level compared to violaxanthin. It is reasonable that the oxidation potential of violaxanthin is higher than that of zeaxanthin due to its shorter conjugation length and the presence of two electron-withdrawing oxygen atoms.[45] Theoretical calculations by Dreuw et al. support this view, indicating that the ionization potential of the xanthophyll cycle carotenoids vary in the following order: violaxanthin > antheraxanthin > zeaxanthin.[6] This in turn would make the Zea−Chl *a* charge transfer state lower in energy than that of the corresponding CT state involving violaxanthin and antheroxanthin.

Conclusions

Triad **2** features two carotenoid pigments of 10 conjugated carbon−carbon double bonds, each linked axially through a Si atom to a phthalocyanine tetrapyrrole. This construct illustrates important aspects of the photophysics associated with the carotenoid−chlorophyll interaction in photosynthetic membranes. Structural studies of triad **2** are consistent with the presence of an equilibrium mixture of two isomers in *n*-hexane and toluene solutions comprising the C6′−C7′ s-cis (**2a**) and s-trans (**2b**) conformers of the carotenoid. The s-cis isomer could yield a "folded" conformation in which the through-bond electronic coupling promoting photoinduced electron transfer in the s-trans isomer, **2b**, and in triad **1**, is augmented by through-space coupling in **2a**. Because increased electronic coupling and concomitant faster photoinduced electron transfer is expected for the s-cis isomer, the faster (τ_{2a}) and slower (τ_{2b}) components of the biexponential decay of the Pc fluorescence of **2** could be associated with the s-cis and s-trans conformers, respectively.

In all the solvents studied except *n*-hexane, the observation of the $C^{\bullet+}-Pc^{\bullet-}$ species confirms that the quenching mechanism of the Pc S_1 state in triads **1** and **2** is photoinduced electron transfer. To determine whether the modest quenching of **2** found in *n*-hexane could also be due to photoinduced electron transfer, and model the temperature dependence of the quenching, a semiclassical expression for the electron-transfer rate was employed to obtain a set of parameters that fits the experimental electron-transfer rates for **1** and **2b** in different solvents. These parameters were then used to calculate the electron-transfer rate of **2b** in *n*-hexane as a function of the temperature. The good agreement of these calculations with the temperature-dependent fluorescence decay of **2b** supports the possibility that the formation of the $C^{\bullet+}-Pc^{\bullet-}$ charge transfer state is responsible for the observed temperature-dependent quenching in *n*-hexane. Because the calculations depend on similar electronic coupling between the chromophores in **1** and **2**, the behavior of **2a** was not simulated.

This report focuses on the role of photoinduced electron transfer in quenching tetrapyrrole excited singlet states and defines critical parameters controlling the process. Evidence is presented that electron transfer from the 10 double bond carotenoid moiety to the excited tetrapyrrole is the mechanism of tetrapyrrole fluorescence quenching even in nonpolar solvents.

In another series of models consisting of different tetrapyrroles attached to the same carotenoids reported herein, although with different geometric arrangements, we have not been able to detect radical ions even though strong quenching of the tetrapyrrole fluorescence was observed.[12] Transient absorption studies provided good evidence that the quenching of the S_1 state of the tetrapyrrole proceeds through energy transfer from the excited Pc to the optically forbidden S_1 of the carotenoid and that this state is coupled to an intramolecular charge-transfer state. Thus, both model studies suggest the association of either inter- or intramolecular charge-transfer species involving carotenoids during the process of excess energy dissipation in photosystem II.

Acknowledgment. This work was supported by a grant from by the U.S. Department of Energy (DE-FG02-03ER15393). We thank Dmitry Matyushov for his advice on the theoretical calculations. This is publication 668 from the ASU center for the Study of early Events in Photosynthesis.

Supporting Information Available: Calculation of driving force and reorganization energy by the continuum model (FDPB) is described. This material is available free of charge via the Internet at http://pubs.acs.org.

References and Notes

(1) Gilmore, A. M. *Physiol. Plant.* **1997**, *99*, 197−209.

(2) Horton, P.; Ruban, A. V.; Walters, R. G. *Annu. Rev. Plant Physiol. Plant Mol. Biol.* **1996**, *47*, 655−684.

(3) Holt, N. E.; Fleming, G. R.; Niyogi, K. K. *Biochemistry* **2004**, *43*, 8281−8289.

(4) Ma, Y.-Z.; Holt, N. E.; Li, X.-P.; Niyogi, K. K.; Fleming, G. R. *Proc. Natl. Acad. Sci. U.S.A.* **2003**, *100*, 4377−4382.

(5) van Amerongen, H.; van Grondelle, R. *J. Phys. Chem. B* **2001**, *105*, 604−617.

(6) Dreuw, A.; Fleming, G. R.; Head-Gordon, M. *Phys. Chem. Chem. Phys.* **2003**, *5*, 3247−3256.

(7) Dreuw, A.; Fleming, G. R.; Head-Gordon, M. *J. Phys. Chem. B* **2003**, *107*, 6500−6503.

(8) Fungo, F.; Otero, L.; Durantini, E.; Thompson, W. J.; Silber, J. J.; Moore, T. A.; Moore, A. L.; Gust, D.; Sereno, L. *Phys. Chem. Chem. Phys.* **2003**, *5*, 469−475.

(9) Holt, N. E.; Zigmantas, D.; Valkunas, L.; Li, X.-P.; Niyogi, K. K.; Fleming, G. R. *Science (Washington, DC, U.S.)* **2005**, *307*, 433−436.

(10) Gould, S. L.; Kodis, G.; Palacios, R. E.; de la Garza, L.; Brune, A.; Gust, D.; Moore, T. A.; Moore, A. L. *J. Phys. Chem. B* **2004**, *108*, 10566−10580.

(11) Hermant, R. M.; Liddell, P. A.; Lin, S.; Alden, R. G.; Kang, H. K.; Moore, A. L.; Moore, T. A.; Gust, D. *J. Am. Chem. Soc.* **1993**, *115*, 2080−2081.

(12) Berera, R.; Herrero, C.; van Stokkum, I. H. M.; Vengris, M.; Kodis, G.; Palacios, R. E.; van Amerongen, H.; van Grondelle, R.; Gust, D.; Moore, T. A.; Moore, A. L.; Kennis, J. T. M. *Proc. Natl. Acad. Sci. U.S.A.* **2006**, *103*, 5343−5348.

(13) Freiberg, A.; Timpmann, K.; Lin, S.; Woodbury, N. W. *J. Phys. Chem. B* **1998**, *102*, 10974−10982.

(14) Kodis, G.; Herrero, C.; Palacios, R.; Marino-Ochoa, E.; Gould, S.; de la Garza, L.; van Grondelle, R.; Gust, D.; Moore, T.; Moore, A.; Kennis, J. *J. Phys. Chem. B* **2004**, *108*, 414−425.

(15) Marino-Ochoa, E. Synthesis and photophysics of carotenophthalocyanine artificial photosynthetic antennas. Ph.D. dissertation, Arizona Sate University, 2002.

(16) Marino-Ochoa, E.; Palacios, R.; Kodis, G.; Macpherson, A.; Gillbro, T.; Gust, D.; Moore, T.; Moore, A. *Photochem. Photobiol.* **2002**, *76*, 116−121.

(17) Esposito, J. N.; Sutton, L. E.; Kenney, M. E. *Inorg. Chem.* **1967**, *6*, 1116−1120.

(18) Janson, T. R.; Kane, A. R.; Sullivan, J. F.; Knox, K.; Kenney, M. E. *J. Am. Chem. Soc.* **1969**, *91*, 5210−5214.

(19) Kane, A. R.; Yalman, R. G.; Kenney, M. E. *Inorg. Chem.* **1968**, *7*, 2588−2592.

(20) Maskasky, J. E.; Kenney, M. E. *J. Am. Chem. Soc.* **1973**, *95*, 1443−1448.

(21) Maskasky, J. E.; Mooney, J. R.; Kenney, M. E. *J. Am. Chem. Soc.* **1972**, *94*, 2132−2133.

(22) Sutton, L. E.; Kenney, M. E. *Inorg. Chem.* **1967**, *6*, 1869−1872.

(23) Koyama, T.; Suzuki, T.; Hanabusa, K.; Shirai, H.; Kobayashi, N. *Inorg. Chim. Acta* **1994**, *218*, 41−45.

(24) Silver, J.; Frampton, C. S.; Fern, G. R.; Davies, D. A.; Miller, J. R.; Sosa-Sanchez, J. L. *Inorg. Chem.* **2001**, *40*, 5434−5439.

(25) Silver, J.; Sosa-Sanchez, J. L.; Frampton, C. S. *Inorg. Chem.* **1998**, *37*, 411−417.

(26) For the case of the methyl protons 19′ and 20′ an average position was estimated assuming free rotation around the C9′−C19′ and C13′−C20′ single bonds.

(27) Polivka, T.; Sundstroem, V. *Chem. Rev. (Washington, DC, U.S.)* **2004**, *104*, 2021−2071.

(28) Rackett, H. G. *J. Chem. Eng. Data* **1970**, *15*, 514−517.

(29) Lide, D. R., *CRC Handbook of Chemistry and Physics*, 84th ed.; CRC Press LLC: Boca Raton, FL, 2003; p 2616.

(30) In principle the presence of the s-cis "folded" conformation should be evident in the NMR data; however, if its lifetime were shorter that the integration time of the NMR experiment, its detection would be precluded. Consequently the lack of evidence for the presence of this "folded" conformation in the NMR data does not rule out its existence.

(31) This analysis is valid provided that the interconversion of the isomers is slow on the time scale of the fluorescence lifetime. Since the fluorescence decay and s-cis/trans isomerization processes considered here are in the order of a few nanoseconds and tenths of microseconds, respectively, this condition is easily met.

(32) Saltiel, J.; Sears, D. F., Jr.; Turek, A. M. *J. Phys. Chem. A* **2001**, *105*, 7569−7578.

(33) Barbara, P. F.; Meyer, T. J.; Ratner, M. A. *J. Phys. Chem.* **1996**, *100*, 13148−13168.

(34) Jortner, J. *J. Chem. Phys.* **1976**, *64*, 4860−4867.

(35) Jortner, J. *J. Am. Chem. Soc.* **1980**, *102*, 6676−6686.

(36) Kurnikov, I. V.; Zusman, L. D.; Kurnikova, M. G.; Farid, R. S.; Beratan, D. N. *J. Am. Chem. Soc.* **1997**, *119*, 5690−5700.

(37) Liu, Y.-P.; Newton, M. D. *J. Phys. Chem.* **1995**, *99*, 12382−12386.

(38) Sharp, K. A.; Honig, B. *Annu. Rev. Biophys. Biophys. Chem.* **1990**, *19*, 301−332.

(39) Wohlfarth, C., *Static Dielectric Constants of Pure Liquids and Binary Liquid Mixtures*; Springer-Verlag: Berlin, Heidelberg, New York, 1991; Vol. 6, p 521.

(40) Obtained by fitting the experimental data (213−333.2 K range) from ref 39 with a second-order polynomial function.

(41) Riazi, M. R.; Enezi, G. A.; Soleimani, S. *Chem. Eng. Commun.* **1999**, *176*, 175−193.

(42) It is important to note that lower polarity is associated with smaller λ so in principle, $-\Delta G^\circ$ could come closer to λ and increase k_{et}.

(43) Wasielewski, M. R.; Johnson, D. G.; Svec, W. A.; Kersey, K. M.; Minsek, D. W. *J. Am. Chem. Soc.* **1988**, *110*, 7219−7221.

(44) A rigorous analysis predicts different internal reorganization energies for **1** and **2**; however the similar dimension and structure of their carotenoid moieties suggest that taking λ_i to be equal for both systems is a reasonable approximation.

(45) Niedzwiedzki, D.; Rusling, J. F.; Frank, H. A. *Chem. Phys. Lett.* **2005**, *415*, 308−312.

V. Berera, Rudi; van Stokkum, Ivo H. M.; Kodis, Gerdenis; Keirstead, Amy E.; Pillai, Smitha; Herrero, Christian; Palacios, Rodrigo E.; Vengris, Mikas; van Grondelle, Rienk; Gust, Devens; Moore, Thomas A.; Moore, Ana L.; Kennis, John T. M. **Energy transfer, excited-state deactivation and exciplex formation in artificial carotene-phthalocyanine light-harvesting antennas.** Journal of Physical Chemistry B (2007), 111(24), 6868-6877.

Energy Transfer, Excited-State Deactivation, and Exciplex Formation in Artificial Caroteno-Phthalocyanine Light-Harvesting Antennas†

Rudi Berera,‡ Ivo H. M. van Stokkum,‡ Gerdenis Kodis,§ Amy E. Keirstead,§ Smitha Pillai,§ Christian Herrero,§ Rodrigo E. Palacios,§ Mikas Vengris,‡ Rienk van Grondelle,‡ Devens Gust,*,§ Thomas A. Moore,*,§ Ana L. Moore,*,§ and John T. M. Kennis*,‡

Department of Biophysics, Division of Physics and Astronomy, Faculty of Sciences, Vrije Universiteit, Amsterdam 1081 HV, The Netherlands, and Department of Chemistry and Biochemistry and the Center for the Study of Early Events in Photosynthesis, Arizona State University, Tempe, Arizona 85287-1604

Received: February 5, 2007; In Final Form: March 20, 2007

We present results from transient absorption spectroscopy on a series of artificial light-harvesting dyads made up of a zinc phthalocyanine (Pc) covalently linked to carotenoids with 9, 10, or 11 conjugated carbon−carbon double bonds, referred to as dyads **1**, **2**, and **3**, respectively. We assessed the energy transfer and excited-state deactivation pathways following excitation of the strongly allowed carotenoid S_2 state as a function of the conjugation length. The S_2 state rapidly relaxes to the S* and S_1 states. In all systems we detected a new pathway of energy deactivation within the carotenoid manifold in which the S* state acts as an intermediate state in the $S_2 \rightarrow S_1$ internal conversion pathway on a sub-picosecond time scale. In dyad **3**, a novel type of collective carotenoid−Pc electronic state is observed that may correspond to a carotenoid excited state(s)−Pc Q exciplex. The exciplex is only observed upon direct carotenoid excitation and is nonfluorescent. In dyad **1**, two carotenoid singlet excited states, S_2 and S_1, contribute to singlet−singlet energy transfer to Pc, making the process very efficient (>90%) while for dyads **2** and **3** the S_1 energy transfer channel is precluded and only S_2 is capable of transferring energy to Pc. In the latter two systems, the lifetime of the first singlet excited state of Pc is dramatically shortened compared to the 9 double-bond dyad and model Pc, indicating that the carotenoid acts as a strong quencher of the phthalocyanine excited-state energy.

Introduction

Carotenoids are ubiquitous pigments in nature where they serve a number of functions. In photosynthetic systems they act mainly as light harvesters and photoprotectors.[1] They absorb light in the blue-green region of the spectrum and transfer the energy to neighboring chlorophylls.[2] In this spectral region chlorophylls display very little absorption; photosynthesis thus relies on carotenoids to optimize the absorption cross-section. Concerning the photoprotective role, carotenoids can scavenge injurious singlet oxygen and limit its sensitization by quenching chlorophyll triplet states.[1] Carotenoids are also involved in the thermal dissipation of excess energy in photosystem II (PSII) via the process of nonphotochemical quenching, and there is evidence that they can directly quench the singlet excited state of chlorophylls via either energy or electron transfer.[3,4]

All the aforementioned properties originate from the extraordinary excited-state manifold of carotenoids. The strong absorption in the visible region is due to the strongly allowed $S_0 \rightarrow S_2$ transition. Hidden below the S_2 state is another singlet state, electronic dipole forbidden and known as S_1.[5−7] In recent years it has become clear that this two excited-state levels representation is incomplete: additional electronic states that lie below S_2 have been theoretically predicted;[5] experimental evidence for some of them has been presented by several workers.[8−12]

The S* state was discovered some years ago in spirilloxanthin, both in solution and bound to the light-harvesting (LH1) complex of *Rhodospirillum rubrum*.[9] It is characterized by an excited-state absorption (ESA) band blue-shifted with respect to that of the $S_1 \rightarrow S_n$ absorption but red-shifted with respect to the optically allowed $S_0 \rightarrow S_2$ transition. In spirilloxanthin bound to LH1, the S* state is a precursor for the formation of the carotenoid triplet state on the picosecond time scale via the singlet fission mechanism. In later work, S* was found in various carotenoids bound to light-harvesting (LH) complexes of other species of purple bacteria,[11,13,14] in some carotenoids in solution,[15] and in artificial LH constructs.[16] S* is involved in energy transfer from carotenoid to chlorophyll (Chl) or other tetrapyrroles in many of these systems. In all cases, S* and S_1 were formed in parallel by internal conversion (IC) from S_2 and evolved independently, decaying on the picosecond time scale by either IC, energy transfer, or, in the case of S*, triplet formation. Despite its common occurrence, the electronic nature of S* has remained rather elusive. It was proposed that it corresponds to the theoretically predicted, optically dark, $^1B_u^-$ state[9] or to excited dark states in geometrically distorted carotenoids.[17] Alternatively, it was suggested that S* corresponds to a hot ground state.[18]

In recent years advances in chemical synthesis have made it possible to synthesize artificial light-harvesting antennas capable of mimicking many of the functions carried out by their natural counterparts.[16,19,20] These systems mimic light-harvesting, energy transfer, electron transfer, and photoprotective functions of natural photosynthesis. The study of model systems is of increasing interest for several reasons: the simplicity of the

† Part of the special issue "Norman Sutin Festschrift".

* Authors to whom correspondence should be addressed. E-mail: gust@asu.edu; tmoore@asu.edu; amoore@asu.edu; john@nat.vu.nl.

‡ Vrije Universiteit.

§ Arizona State University.

10.1021/jp071010q CCC: $37.00
Published on Web 05/16/2007

systems, typically made up of a very small number of chromophores, allows one to establish the basic photophysical and photochemical mechanisms underlying the behavior of the natural systems. Of more practical interest would be the incorporation of these systems into nanodevices, where they could function in light-harvesting, photoprotection, and energy transduction.

In this report we describe our studies of the photophysics of a series of three dyads made up of a zinc phthalocyanine (Pc) covalently linked to a carotenoid with 9, 10, or 11 conjugated double bonds. We determined the energy transfer and energy deactivation pathways following excitation of the carotenoid moiety to its strongly allowed S_2 state. We report a previously unobserved pathway of energy deactivation within the carotenoid, where the S* state acts as an intermediate in the $S_2 \rightarrow S_1$ IC pathway. In dyad **3**, a novel type of collective carotenoid−Pc electronic state is observed that may correspond to a carotenoid excited state(s)−Pc Q exciplex. In dyad **1** a multiphasic carotenoid to Pc energy transfer process is observed, assigned to contributions from the carotenoid S_2 and S_1 excited states as well as a minor contribution from the hot S_1−S* excited state. As the conjugation length of the carotenoid is increased to 10 and 11 double bonds in dyad **2** and dyad **3**, respectively, the hot S_1 and S_1 energy transfer deactivation channels are precluded.

Materials and Methods

The synthesis of the compounds has been previously described.[4] Femtosecond transient absorption spectroscopy was carried out with a setup described in detail earlier.[21] The output of a 1 kHz amplified Ti:sapphire laser system (Coherent-BMI α1000) was used to drive a home-built non-collinear optical parametric amplifier. The excitation wavelength was tuned to 475 nm to selectively excite the S_2 state of the carotenoid moiety. The pulse width was 100 fs, and the energy was 100 nJ per pulse. A white light continuum, generated by focusing amplified 800 nm light on a 1 mm CaF_2 crystal, served as a probe beam. The pump and probe were focused on a 1 mm path length cuvette, and to avoid sample degradation and exposure of the sample to multiple laser shots, the cuvette was mounted on a shaker. The polarization between pump and probe was set to the magic angle (54.7°).

The data were first analyzed globally using a sequential model with increasing lifetimes.[22] The data are thus described by a small number of lifetimes and evolution-associated difference spectra (EADS). Each EADS corresponds in general to a mixture of states and does not portray the spectrum of a pure state. To extract spectra of pure states a target analysis model was also applied to our data.[22]

The fluorescence up-conversion measurement was carried out by employing laser pulses of 100 fs at 800 nm generated from an amplified, mode-locked Ti:sapphire kilohertz laser system (Millennia/Tsunami/Spitfire, Spectra Physics). Part of the laser pulse energy (gate pulse) was sent through an optical delay line and mixed with the sample fluorescence in a 1 mm β-barium borate (BBO) crystal. The remainder of the pulse energy was used to pump an optical parametric amplifier (Spectra Physics) to generate excitation pulses. Up-converted UV light was sent through a double monochromator and recorded by a photomultiplier tube (PMT) coupled to a box car integrator (SR250, Stanford Research Systems). The absorption spectra were measured before and after each experiment to confirm sample stability.

Results and Discussion

Figure 1A shows the structures of the compounds. The absorption spectra of dyads **1**, **2**, and **3** as well as model Pc **4** dissolved in tetrahydrofuran (THF) are shown in Figure 1B. Transient absorption experiments were performed on dyads **1**, **2**, and **3** with excitation of the carotenoid moiety at 475 nm and broadband detection with a white light continuum.

Dyad 2. Because dyad **2** exhibits the simplest behavior of the three systems studied, it will be discussed first. Figure 2A shows the EADS for dyad **2** in THF, whereas Figures 2B−D show kinetic traces at selected wavelengths. Nearly identical results were obtained for dyad **2** in dioxane as shown in Figure 1 of the Supporting Information. **(**For spectroscopic studies in different solvents see ref 4.**)** Five components are needed to satisfactorily fit the data. The first EADS (black line) appears at time zero and represents population of the optically allowed S_2 state of the carotenoid. It presents a region of negative signal at wavelengths below 570 nm originating from the carotenoid ground-state bleach, stimulated emission in the 570−600 nm region, and a band-shift-like signal in the Pc Q region around 680 nm due to perturbation of Pc by the proximate excited carotenoid.

The first EADS decays in 58 fs into the second EADS (red line). This EADS presents the carotenoid ground-state bleach below 520 nm and carotenoid ESA between 520 and 650 nm. This ESA originates from both the S* state, absorbing mainly in the 550 nm region, and the S_1 state (around 570 nm) of the carotenoid populated from S_2 via IC. In the region around 680 nm the ground-state bleach of the Pc Q-band is observed as well as a vibronic band at 610 nm. These bleaches on this time scale are prima facie evidence for carotenoid S_2 to Pc energy transfer. The signal above 700 nm is due to carotenoid ESA.

The second EADS evolves into the third EADS (green line) in 840 fs. As before, in the region below 510 nm the carotenoid ground-state bleach is seen. The carotenoid excited-state region shows an interesting phenomenon: the signal below 555 nm has decreased concomitantly with an increase of the signal above this wavelength. This behavior is suggestive of an IC process within the carotenoid where the S_1 state (ESA to the red of that of S*) is populated from the S* state and was further investigated by target analysis (vide infra). Figures 2B and 2C show the kinetic traces for dyad **2** recorded at 550 and 570 nm, respectively, along with the corresponding fits from global analysis. The 550 nm data represent the decay of the S* $\rightarrow S_n$ ESA, and the 570 nm data represent the evolution of the $S_1 \rightarrow S_n$ ESA. Within the first picosecond the two traces clearly show different dynamics in that the decrease in amplitude for the 550 nm trace (Figure 2B) is accompanied by an increase of the amplitude at 570 nm, further confirming the S* $\rightarrow S_1$ IC process. The fact that the Pc Q bleach at 680 nm (Figure 2D) does not increase with the decay of S* (Figure 2B) or S_1 (Figure 2C) supports the conclusion that neither the S* state nor the S_1 state is transferring energy to Pc in this system. Furthermore, energy transfer from S* would repopulate the carotenoid ground state, and that is not observed. The ground-state bleach below 510 nm is similar in the second and third EADS.

The fourth EADS (blue line) appears after 8.1 ps. The structured carotenoid ESA above 510 nm has disappeared as well as the carotenoid ground-state bleach below 500 nm implying that the carotenoid S_1 state has now decayed to the ground state. In the 520 nm region the spectrum presents a band-shift-like signal that is absent in the spectrum of the relaxed, fully solvated model Pc excited state (not shown) but previously

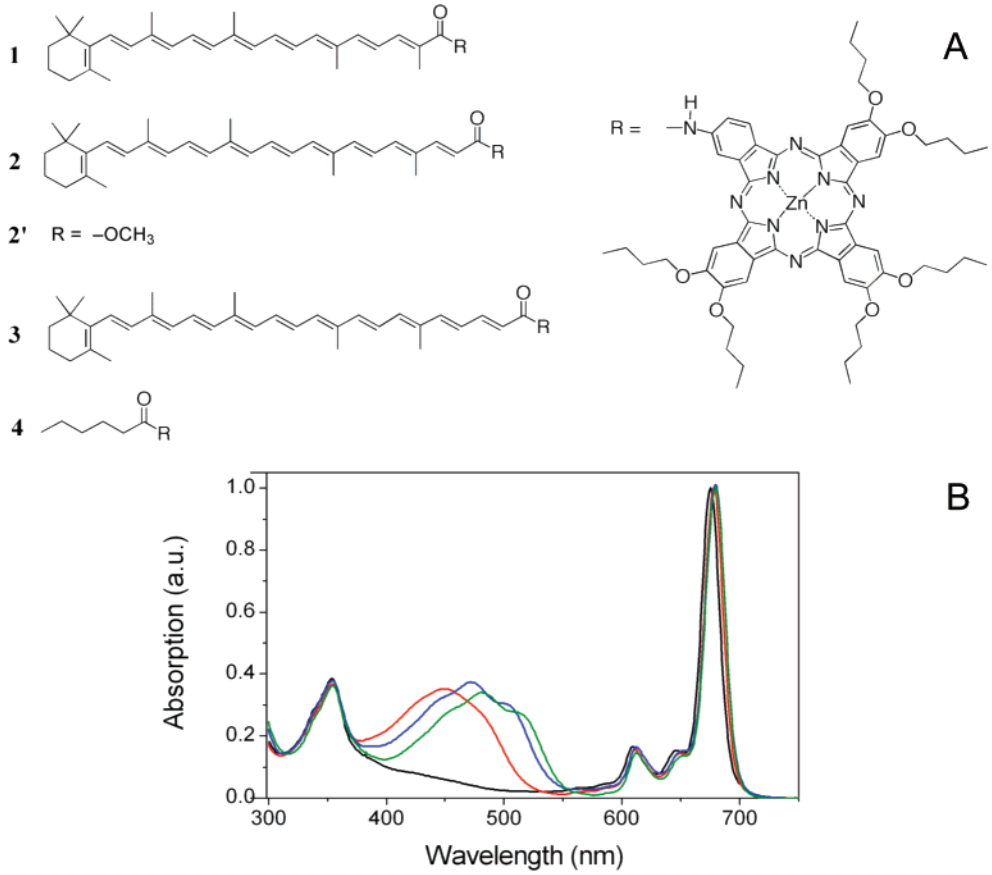

Figure 1. (A) Molecular structures of the dyads and reference carotenoid. A zinc phthalocyanine is covalently linked to a carotenoid with 9 conjugated carbon−carbon double bonds (dyad **1**), 10 carbon−carbon double bonds (dyad **2**), and 11 carbon−carbon double bonds (dyad **3**). Model carotenoid **2′** has a terminal methyl ester group instead of a phthalocyanine. (B) Absorption spectra in THF for dyads **1** (red line), **2** (blue line), and **3** (green line) and model Pc **4** (black line).

observed in the same dyad with excitation in the Pc Q state.[4] Similar phenomena were observed in photosynthetic light-harvesting complexes and assigned to a change of the local electric field of the carotenoid and excitonic coupling between Chl and the optically allowed carotenoid S_2 state.[23,24] In the Pc bleach region (680 nm) there is no detectable increase of the bleach, indicating that the carotenoid S_1 state is incapable of energy transfer to Pc.

A comparison of the S_1 lifetime (8.1 ps) for dyad **2** with the S_1 lifetime (12 ps) of the model carotenoid **2′**[4,16] reveals that the lifetime of the carotenoid (Car) S_1 state in the dyad is shorter. In light of the absence of any energy transfer from the S_1 state, this observation suggests that specific Car−Pc interactions lead to a shortening of the S_1 lifetime in the dyad. Possibly, the vibronic coupling between the carotenoid ground and the S_1 state has been enhanced by covalent linkage of Pc, leading to an enhanced rate of IC to the ground state. Note that in recombinant light-harvesting complex II (LHCII) with altered carotenoid pigments a similar phenomenon was observed.[25]

The fifth EADS (cyan line) appears in 268 ps and does not decay on the time scale of the experiment. We observe that by now the Pc Q bleach has almost disappeared and at the same time a broad ESA between 480 and 570 nm with low amplitude has appeared. The shape of this non-decaying EADS is likely to be due to a mixture of long-living species, e.g., Pc and carotenoid triplets. It is interesting to note that the lifetime of the Pc Q state (268 ps) is dramatically shorter compared to the lifetime of the Pc Q state in dyad **1** and model Pc (3 ns) meaning that the 10 double-bond carotenoid acts as an effective quencher of the Q state of Pc.[4] The low amplitude of the fifth EADS also indicates that the yield of the triplet species is minuscule; the quenching process primarily yields the ground state.

Target Analysis of Dyad 2: Characterization of a S* → S_1 IC Process. The sequential analysis of the data allows one to extract the intrinsic lifetimes of the processes, but the spectra portrayed by such an analysis are not in general pure spectra of molecular species but rather represent a mixture of the latter. To provide further evidence of the S* → S_1 IC process in the systems, we applied a target analysis of the data collected on dyad **2**, employing a specific kinetic model. The model is depicted in Figure 3A and consists of five compartments. The first compartment corresponds to the carotenoid S_2 state. It decays to the S* state by a fraction Φ_1 and to the S_1 state by a fraction Φ_2. A fraction Φ_3 transfers energy to give the Pc excited state, Pc*. The S* state decays to the ground state with rate constant k_1 and undergoes IC to the S_1 state with rate constant k_2. The S_1 state decays entirely to the ground state (GS) with a rate constant k_3. The fourth compartment corresponds to the excited Pc, Pc*, which transfers energy back to the S_1 state with a rate constant k_4, decays to the ground state with a rate constant k_5, and undergoes intersystem crossing (ISC) to the triplet state with a rate constant k_6.

The species-associated difference spectra (SADS) obtained from the target analysis are displayed in Figure 3B; the estimated rate constants and branching fractions are summarized in Table 1. The SADS corresponding to S_2 is not shown. The S_2 state decays to the S* state (red SADS) with $\Phi_1 = 15\%$ and to the S_1 state (green SADS) with $\Phi_2 = 25\%$ and by energy transfer to Pc with $\Phi_3 = 60\%$. S* decays to the ground state with a rate constant k_1 $(4\ \text{ps})^{-1}$ and to the S_1 state with a rate

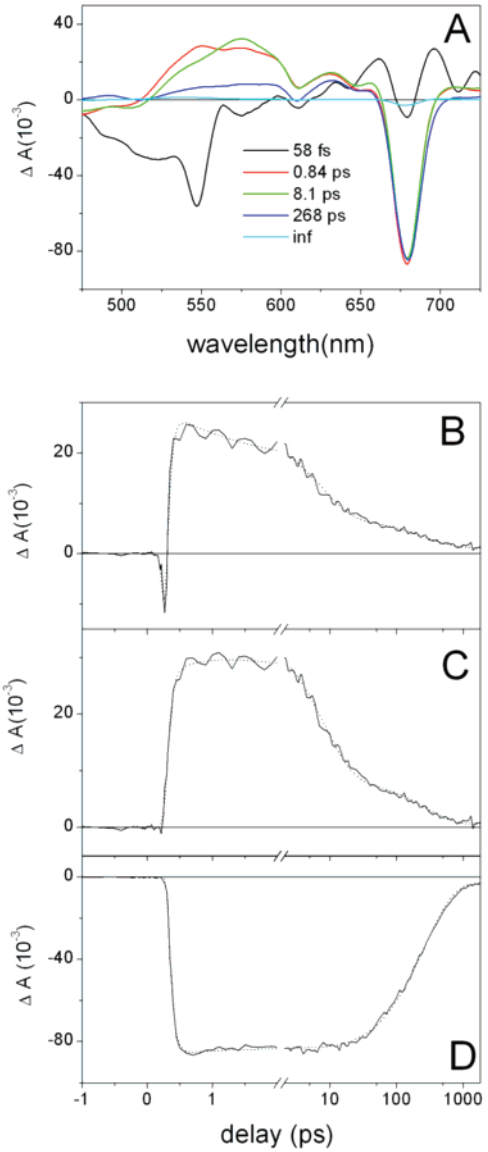

Figure 2. (A) Evolution-associated difference spectra that follow from a global analysis of data for dyad **2** in THF with excitation at 475 nm. (B) Kinetic trace with excitation at 475 nm and detection at 550 nm for **2** (solid line), along with the result of the global analysis fit (dotted line). (C) Same as panel B with detection at 570 nm. (D) Same as panel B with detection at 680 nm.

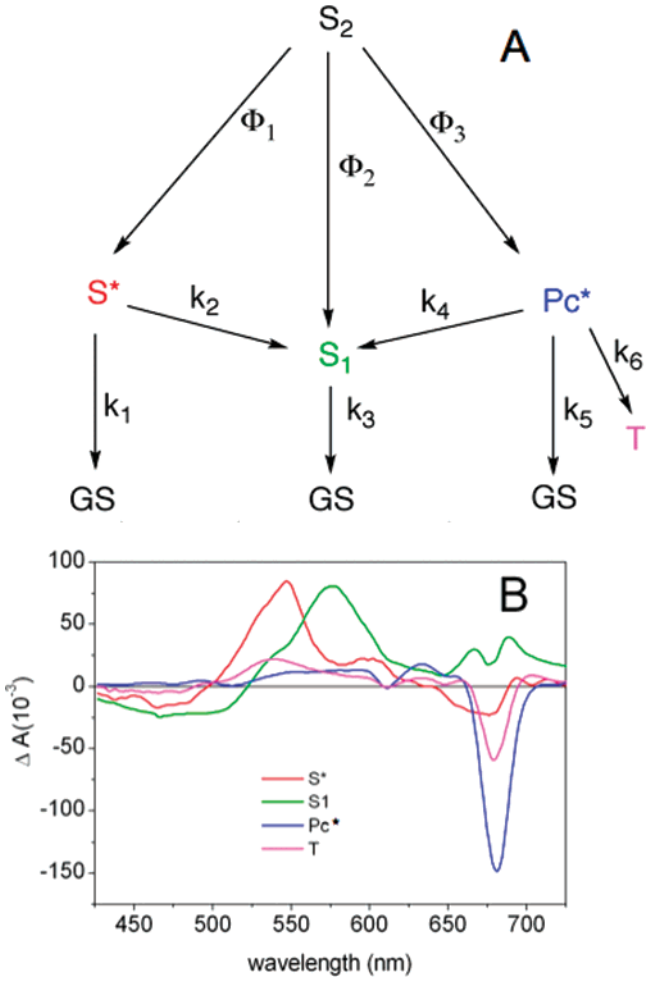

Figure 3. (A) Kinetic model used in the target analysis of the time-resolved data on dyad **2** (B) Species-associated difference spectra from the target analysis for dyad **2** in THF. See text for details.

constant k_2 (4 ps)$^{-1}$. The S_1 state decays to the ground state with a rate constant k_3 (8.3 ps)$^{-1}$. The Pc Q singlet excited state (blue SADS) transfers energy to the carotenoid with a rate constant k_4 (416 ps)$^{-1}$, decays to the ground state with a rate constant k_5 = (830 ps)$^{-1}$, and undergoes ISC to the triplet state (cyan line) with a rate constant k_6 = (2.5 ns)$^{-1}$.

The SADS representing S* (red line) has the typical shape of the S* → S_n absorption for a 10 double-bond carotenoid[11] with a peak at 547 nm, a tail above 575 nm, and a ground-state bleach below 497 nm. The SADS representing S_1 (green line) has the typical shape of the S_1 → S_n absorption: it peaks at 577 nm and displays a tail above 610 nm. Below 522 nm it shows a ground-state bleach. A comparison of the shapes of the two SADS with the rather broad and flat shape of the second EADS of dyad **2** (Figure 2A) shows that the separation of the spectral features of the two states has been successful. The SADS corresponding to excited Pc, Pc* (blue line), has the typical shape of Pc in the Q state[4] with bleaches at 680 and 610 nm, and a flat ESA below 600 nm. We conclude that the target analysis adequately describes the spectral evolution of dyad **2** and provides good evidence that the S* state undergoes IC to the S_1 state.

Dyad 3. Figure 4A shows the EADS for dyad **3**, with kinetic traces shown in Figures 4B−D. Six components are needed for a good fit of the data as demonstrated by the strongly multiphasic character of the traces, especially in the 660−670 and 690−700 nm regions (see Figure 2 in the Supporting Information for a study in acetone). The first EADS (black line) appears at time zero and is associated with the carotenoid S_2 state. It evolves into the second EADS (red line) in 43 fs. At this stage the S_2 state has decayed to the S* and S_1 states as displayed by the broad ESA in the 525−620 nm region. Around 680 nm, the appearance of a large bleach signal is observed, corresponding partly to the Q state of Pc, indicating that energy transfer from the carotenoid S_2 state to Pc has occurred (and partly population of a putative exciplex has taken place, vide infra).

The third EADS (green line) appears after 1.4 ps. This EADS shows a decrease of ESA corresponding to the S* state and a concomitant increase of the signal in the 580−620 nm region. As for dyad **2**, we assign this evolution to the decay of the S* state partly by IC to the ground state and partly by IC to the S_1

TABLE 1: Yields at Branching Points and Rate Constants for Dyad 2 in THF Obtained from Target Analysis

Φ_1	Φ_2	Φ_3	k_1	k_2	k_3	k_4	k_5	k_6
15%	25%	60%	$(4\ \text{ps})^{-1}$	$(4\ \text{ps})^{-1}$	$(8.3\ \text{ps})^{-1}$	$(416\ \text{ps})^{-1}$	$(830\ \text{ps})^{-1}$	$(2.5\ \text{ns})^{-1}$

state. Unlike the case with dyad **2**, the third EADS displays a decrease of the Pc Q bleach around 680 nm with respect to the second EADS. The evolution to the fourth EADS (blue line) takes place in 5.7 ps. It shows both carotenoid features with a bleach region below 540 nm and a considerably decreased carotenoid excited-state absorption in the 540 to 650 nm region. The decreased carotenoid ESA indicates that the carotenoid S_1 state has decayed to the ground state. Concomitant with the decay of the S_1 state, the fourth EADS features a further decrease of the Pc Q bleach.

The fifth EADS (cyan line) appears in ~18 ps and has a lifetime of 90 ps. It displays Pc Q bleach in the 680 nm region and relatively flat excited-state absorption below 650 nm and

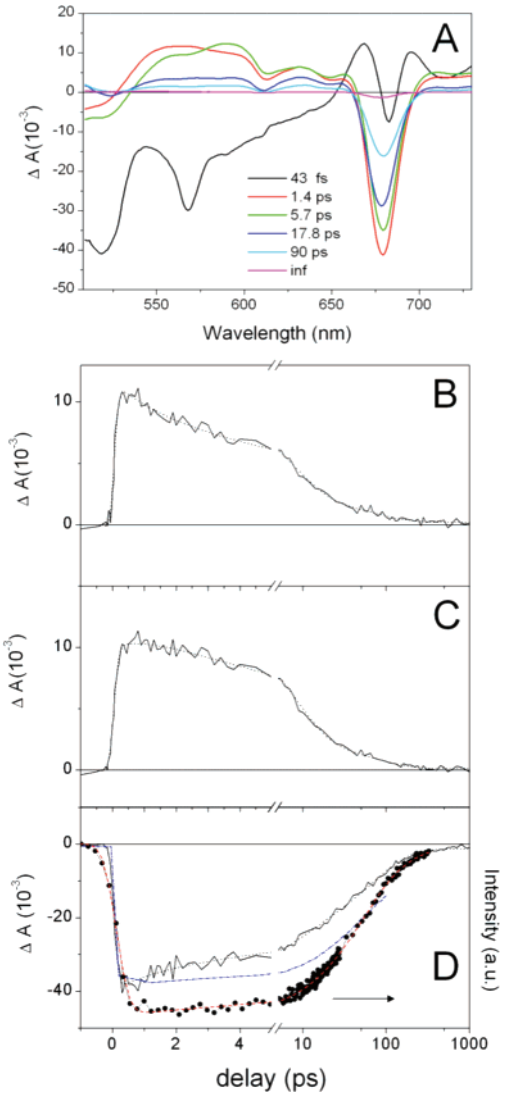

Figure 4. (A) Evolution-associated difference spectra that follow from a global analysis of data for dyad **3** in THF with excitation at 475 nm. (B) Kinetic trace with excitation at 475 nm and detection at 550 nm (solid line), along with the result of the global analysis fit (dotted line). (C) Same as panel B with detection at 590 nm. (D) Same as panel B with detection at 680 nm. The blue dash−dotted line denotes a kinetic trace with excitation and detection at 680 nm. Closed circles and the red dashed line show Pc fluorescence decay kinetics and a two exponential fit with 50 ps (80%, major component) and 220 ps lifetimes, respectively.

corresponds to the singlet excited state of Pc. The final EADS (magenta line) has a very low amplitude and corresponds to long-living triplet states. The lifetime of the Pc Q state, 90 ps, is shorter than that of Q in dyad **2**, and it is dramatically shortened compared to those of dyad **1** and model Pc, which implies that the carotenoid acts a strong quencher of the Q state of Pc, as noted previously.[4] Similar results were obtained for dyad **3** dissolved in acetone (Figure 2 in the Supporting Information).

A most intriguing observation of this experiment is that part of the carotenoid excited state(s) appears to decay together with the Pc Q state, mainly with a time constant of 18 ps. To investigate whether these decay processes are coupled, an experiment was carried out with excitation and detection in the Q state of Pc at 680 nm (Figure 4D, blue dash−dotted line). As can be seen from the kinetic traces in the 1−10 ps time frame, a picosecond decay component that is present upon excitation at 475 nm does not appear upon direct excitation of Pc at 680 nm. To further investigate this phenomenon a fluorescence up-conversion experiment was performed with selective excitation to the carotenoid S_2 state at 480 nm and Pc fluorescence detection at 700 nm (Figure 4D, closed circles and red dashed line). The fluorescence kinetics do not show the fast decay component that is present in the transient absorption experiment upon carotenoid excitation.

We conclude that the concomitant decay of the carotenoid excited-state absorption and the Pc ground-state bleach is not fortuitous and must arise from a collective, nonfluorescent excited state containing both carotenoid and Pc character. A carotenoid excited state is the obligatory precursor of this state. Tentatively, this collective excited state can be assigned to an exciplex[26] formed by the carotenoid in the S_1 and/or S* state and Pc in the ground state. The occurrence of the putative exciplex and its spectral and temporal properties are investigated by applying a target analysis, as described below.

Target Analysis of Dyad 3: Identification of a Carotenoid−Pc Exciplex. For a better understanding of the photophysics of dyad **3**, a target analysis has been applied with the kinetic model depicted in Figure 5A consisting of six compartments. The excited carotenoid S_2 state decays in parallel to the S* (fraction Φ_1) and S_1 (fraction Φ_2) states as well as to a Car−Pc Q exciplex (denoted as EXC) with a fraction Φ_3. The S_2 state also transfers energy to the Pc moiety (fraction Φ_4). The S* state besides decaying to the ground state with a rate constant k_3 undergoes internal conversion to populate the S_1 state (rate constant k_1). The S_1 state decays to the ground state with a rate constant k_3. The excited Pc is quenched by energy transfer to the carotenoid S_1 state with a rate constant k_2, as observed earlier,[4] and partly decays to the long-living state denoted T, which corresponds to a mixture of Pc and carotenoid triplet states.

The SADS obtained from the kinetic model are displayed in Figure 5B, while the fractions and rate constants are reported in Table 2. The black SADS corresponds to the initially excited carotenoid S_2 state. The red SADS corresponds to the S* state with a ground-state bleach below 520 nm and excited-state absorption in the 520−600 nm region. Moreover, it shows a small negative signal in the Pc Q region. The SADS of the S_1 state is in green and features carotenoid ground-state bleach below 540 nm and excited-state absorption between 540 and

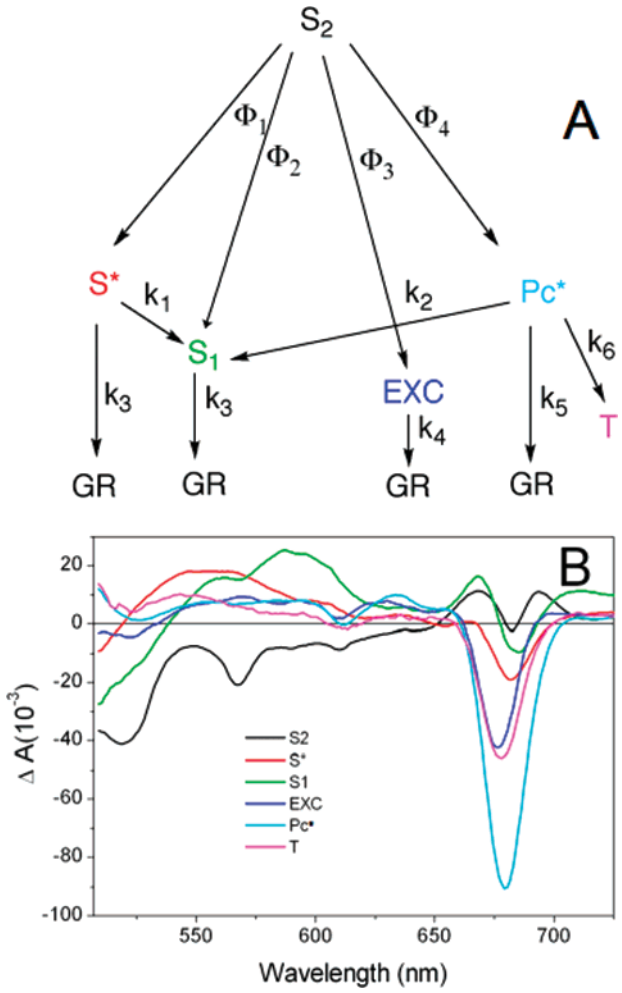

Figure 5. (A) Schematic representation of the excited-state energy transfer and IC pathways in dyad **3** upon excitation of the carotenoid moiety at 475 nm. EXC denotes an exciplex state between the carotenoid excited state(s) and the Pc Q state. See text for details. (B) Species-associated difference spectra from the target analysis for dyad **3** in THF. See text for details.

640 nm. In the Pc absorption region the spectrum shows a band-shift-like signal. The Pc excited state (cyan line) displays a bleach around 680 nm as well as a region of relatively flat excited-state absorption. The long-lived component (magenta line) corresponds to a mixture of carotenoid and Pc triplet states with the typical carotenoid $T_1 \rightarrow T_n$ excited-state absorption in the 480−560 nm region and Pc Q bleach around 680 nm.

The blue SADS corresponds to the putative carotenoid−Pc exciplex. It displays carotenoid bleach below 530 nm and carotenoid excited-state absorption between 530 and ~730 nm. In the Pc Q region the spectrum displays bleaches. Thus, a mixture of Pc and carotenoid signals constitutes the SADS of the exciplex, consistent with the assignment to a carotenoid excited state−Pc Q exciplex. It is interesting to note that the exciplex bleach in the Pc Q region is blue-shifted with respect to the negative signal that results from the Pc singlet excited state (cf. cyan line). This observation indicates that stimulated emission from Pc does not contribute to the spectral shape and amplitude of the exciplex, consistent with our finding that the exciplex is non-emissive.

The occurrence of the exciplex upon relaxation from the S_2 state may arise from excitonic interaction between the Pc Q states and the intense $S_1/S^* \rightarrow S_n$ absorption of the carotenoid. Indeed, the $S_1/S^* \rightarrow S_n$ absorption of the 11 double-bond carotenoid of dyad **3** is nearly in resonance with the vibronic band of the Pc Q transition near 610 nm, as can be observed in the third EADS in Figure 4A. (The vibronic Q bleach at 610 nm is nearly superimposed on the $S_1/S^* \rightarrow S_n$ ESA.) In dyads **1** and **2**, the spectral overlap of the carotenoid $S_1 \rightarrow S_n$ absorption with the vibronic Q-band is less extensive, which qualitatively explains the absence of such an exciplex in these systems. Moreover, the long carotenoid of dyad **3** (11 double bonds) is expected to be more flexible than the carotenoids of dyads **1** and **2**, which may lead to specific conformational changes of the carotenoid, as detected for caroteno-SiPc triads,[27] and this could favor exciplex formation with the Pc Q state. The longer carotenoid could also have a stronger charge-transfer character of the S_1 state and promote further charge shift to Pc and exciplex formation; a carbonyl group in the carotenoid moiety of the dyads confers a partial charge-transfer character to the S_1 state.[28]

It should be noted that the Pc Q bleach signals in the EADS of Figure 4A are made up of two components. These negative signals arise from both the population (and decay) of the Pc excited singlet state due to energy transfer from the carotenoid and from the exciplex formation, which depletes the ground state of Pc as well. The picosecond time scale decay of the bleach, the exciplex decay, correlates with the relaxation of the carotenoid S_1/S^* state. Because only ground-state Pc molecules are involved in the exciplex formation, the picosecond time scale decay of the Pc Q bleach does not constitute an additional decay pathway of the Pc excited state initially formed by energy transfer in dyad **3**.

Dyad 1. The results from a global analysis of the data for dyad **1** are shown in Figure 6A. Figures 6B−D show kinetic traces at selected wavelengths for dyad **1**. Six components are needed for a satisfactory fit of the data. The first EADS (black line) appears at time zero and represents population of the optically allowed S_2 state of the carotenoid. It presents a region of negative signal below 570 nm originating from the carotenoid ground-state bleach and stimulated emission and a band-shift-like signal in the Pc Q region around 680 nm. It evolves in 37 fs into the second EADS (red line), which is characterized by ESA in the 480−600 nm region. The second EADS is assigned to a mixture of the vibrationally hot S_1 state and the S* state. The hot S_1 ESA is expected to have a maximum around 560 nm while that of the S* state is around 525 nm.

The second EADS also displays strong bleach at 680 nm corresponding to the Pc Q state and a dip at 610 nm that originates from a vibronic band of the Pc Q state superimposed on the ESA of both the Pc and the carotenoid moieties. The presence of the bleach in the Pc ground-state absorption region indicates that the carotenoid S_2 state is active in transferring energy to Pc. The evolution to the third EADS (green line) takes place in 500 fs. It corresponds to a decrease of ESA at the red side of the S_1 absorption, which may be assigned to vibrational cooling of the S_1 state.[29,30] Moreover, an increase of the Pc Q bleach at 680 nm is observed that is likely to originate from energy transfer from the hot S_1 state and possibly the S* state to Pc. (Note that the third EADS overlaps with the fourth EADS,

TABLE 2: Yields at Branching Points and Rate Constants for Dyad 3 in THF Obtained from Target Analysis

Φ_1	Φ_2	Φ_3	Φ_4	k_1	k_2	k_3	k_4	k_5
30%	12%	34%	24%	$(1.4\text{ps})^{-1}$	$(102\text{ps})^{-1}$	$(5.7\text{ps})^{-1}$	$(18\text{ps})^{-1}$	$(750\text{ps})^{-1}$

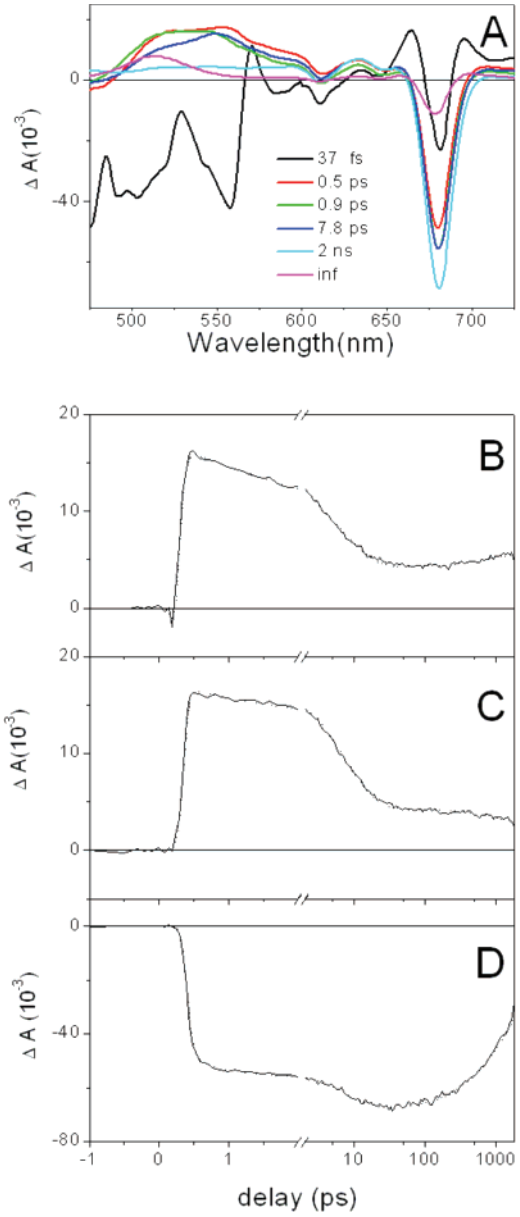

Figure 6. (A) Evolution-associated difference spectra that follow from a global analysis of data for dyad **1** in THF with excitation at 475 nm. (B) Kinetic trace with excitation at 475 nm and detection at 520 nm for dyad **1** (solid line), along with the result of the global analysis fit (dotted line). (C) Same as panel B with detection at 560 nm. (D) Same as panel B with detection at 680 nm.

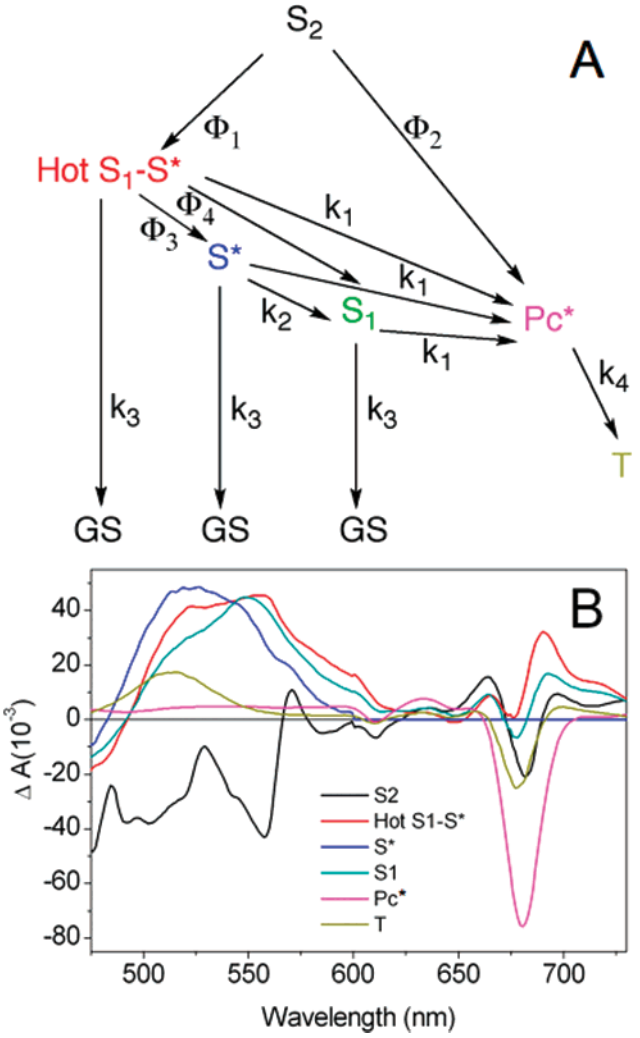

Figure 7. (A) Kinetic model used in the target analysis of the time-resolved data on dyad **1** (B) Species-associated difference spectra from the target analysis for dyad **1** in THF. See text for details.

blue line, in the Pc Q region and is not visible.) The next EADS (blue line) appears after 900 fs and has a lifetime of 7.8 ps. The signal in the 500−540 nm region, where the main contribution to the spectrum is given by S*, has decreased, whereas the signal in the 540−620 nm region, where the absorption is mainly due to S_1, has slightly increased, indicating decay of S* in about 0.9 ps, partly by IC to S_1, as observed for dyads **2** and **3** on similar time scales.

The evolution to the fifth EADS (cyan line) takes place in 7.8 ps. At this stage the carotenoid ESA has decayed, and the fifth EADS corresponds very well to that of the excited Pc Q state with a flat ESA in the 450−600 nm region.[4] Around 680 nm, the bleach presents a sizable increase with respect to the previous EADS, which implies that the carotenoid S_1 state has transferred energy to Pc. Figure 6D shows the kinetic trace recorded at 680 nm corresponding to the maximum of the Pc Q absorption. The ultrafast rise of the bleach corresponding to the carotenoid $S_2 \rightarrow$ Pc energy transfer is followed by two slower rises corresponding to hot S_1−S* → Pc and $S_1 \rightarrow$ Pc energy transfer. The carotenoid to Pc energy transfer in dyad **1** is reminiscent of several natural light-harvesting antennas where high carotenoid to chlorophyll energy transfer efficiency is obtained by employing a multiphasic Car to Chl energy transfer.[2,11,21,31−33]

The final EADS (magenta line) appears after 2 ns and represents the component that does not decay on the time scale of the experiment. It features the typical carotenoid triplet ESA in the 475−550 nm region as well as a bleach/band-shift-like signal in the Pc Q region. Thus, the carotenoid triplet state rises directly upon decay of the singlet excited state of Pc. This observation implies that triplet−triplet energy transfer from Pc to the carotenoid occurs much faster than the ISC process in Pc, which effectively occurs in 2 ns. A similar phenomenon was observed recently in carotenoid-SiPc triads.[16]

Target Analysis of Dyad 1. To quantify the yields of the various energy transfer and energy deactivation pathways in dyad **1** we carried out a target analysis with the kinetic model depicted in Figure 7A.

The initially excited S_2 state partly relaxes to the hot S_1−S* state with a fraction Φ_1 and transfers energy to the phthalocyanine moiety (fraction Φ_2). From the hot S_1−S* state the S* and S_1 states are populated in parallel with fractions Φ_3 and

TABLE 3: Yields at Branching Points and Rate Constants for Dyad 1 in THF Obtained from Target Analysis

Φ_1	Φ_2	Φ_3	Φ_4	k_1	k_2	k_3	k_4
31%	69%	70%	30%	$(11\ ps)^{-1}$	$(1.1\ ps)^{-1}$	$(25\ ps)^{-1}$	$(1.98\ ns)^{-1}$

Φ_4, respectively. The hot S_1-S^* state relaxes to the ground state with a rate constant k_3 and transfers energy to Pc with a rate constant k_1. The S* state internally converts into the S_1 state with a rate constant k_2, contributes to energy transfer to Pc with a rate constant k_1, and relaxes to the ground state with a rate constant k_3. The S_1 state transfers energy to Pc with a rate constant k_1 and relaxes to the ground state (rate constant k_3). From the excited Pc a long-lived mixture of carotenoid and Pc triplets is populated with a rate constant k_4.

Figure 7B depicts the SADS obtained from the kinetic model while the fractions and rate constants are reported in Table 3. The black SADS corresponds to the initially excited carotenoid S_2 state with a ground-state bleach below 560 nm. The hot S_1-S^* state (red SADS) shows a ground-state bleach below 500 nm and excited-state absorption associated with both the S* and the S_1 states. It relaxes in 0.5 ps (fixed in the analysis) to the S* state (blue SADS) and S_1 state (green SADS). The S* state displays excited-state absorption blue-shifted with respect to S_1 and a ground-state bleach below 490 nm. The S_1 state displays the typical $S_1 \rightarrow S_n$ excited-state absorption and a ground-state bleach below 500 nm. For both states the excited-state absorption regions are blue-shifted with respect to the hot S_1-S^* state.

The Pc excited state (magenta SADS) displays the Pc Q bleach at 677 nm and a vibronic band at 610 nm as well as a region of relatively flat excited-state absorption. The long-lived component shows the typical carotenoid $T_1 \rightarrow T_n$ excited-state absorption in the 480−560 nm region and some residual Pc Q bleach meaning that the spectrum corresponds to a mixture of carotenoid and Pc triplet states.

S* → S_1 Internal Conversion. The experiments on dyad **2** indicate that upon excitation of the optically allowed carotenoid S_2 state the S* and S_1 states are rapidly populated. Interestingly, the S* state, besides relaxation to the ground state, undergoes IC to the S_1 state. The similar evolution in the global analysis suggests that the same process is present in all three dyads. This is the first report of such an IC pathway in carotenoids and gives us more insight into the still mysterious nature of the S* state. Showing that S* can act as an intermediate state in the $S_2 \rightarrow S_1$ IC pathway establishes unequivocally the singlet excited-state nature of the S* state. Furthermore, the IC process allows us to locate S* above S_1 in these particular cases.

To investigate the role of the covalent linkage to Pc in the carotenoid excited-state dynamics, we performed a transient absorption measurement on carotenoid **2′**, a model for the carotenoid of dyad **2**, where Pc has been replaced by a methyl ester. The results from a global analysis of the time-resolved data are shown in Figure 8. Three components are needed for a good fit of the data: the first spectrum (black line) appears at time zero and corresponds to carotenoid S_2 state. It evolves into the second EADS (red line) in 125 fs. This spectrum has the typical shape of the hot S_1 state and vibrationally relaxes in 440 fs.[29,30] The S_1 state (green EADS) relaxes to the ground state in 11.8 ps. This evolution suggests that in the model carotenoid either the S* state is not populated or it is not distinguishable from the S_1 state; i.e., the two present the same dynamics. Thus, the presence of the covalently linked Pc in the dyad must be responsible for some specific interaction with the carotenoid leading to the separation of the S* and S_1 states

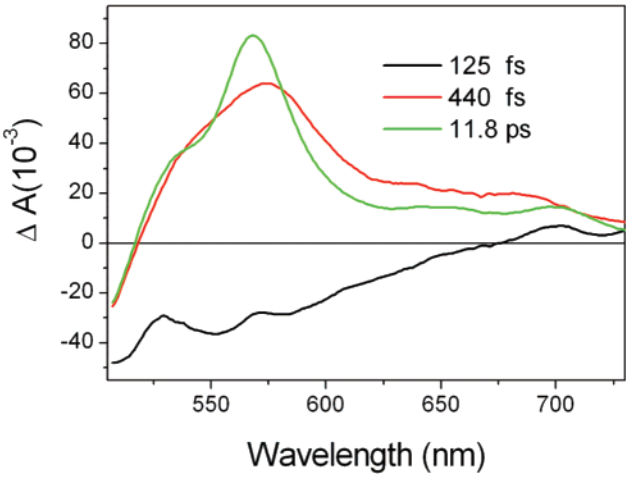

Figure 8. Evolution-associated difference spectra that follow from a global analysis of data for model carotenoid **2′** in THF with excitation at 475 nm.

TABLE 4: Carotenoid to Phthalocyanine Energy Transfer Efficiency from the Various Excited States

	dyad **1**	dyad **2**	dyad **3**
S_2	69%	60%	24%
hot S_1/S* and S*	<4%	0%	0%
S_1	20%	0%	0%

and to the ensuing IC process. Possibly, the presence of the covalently linked Pc leads to some distortion or twisting of the carotenoid, which could be responsible for the occurrence of the S* state in the dyad and not in the model carotenoid. Interestingly, twisting or distortion of the carotenoid backbone has been shown to influence the properties of S* in spirilloxanthin and spheroidene, where the extent of S* formation and ultrafast triplet formation from the S* state depends upon the degree of the deformation.[11,13]

The IC pathways available to S* thus depend on how the carotenoid is bound in a specific system. In bacterial LH complexes and caroteno-SiPc triads, S* and S_1 evolve independently, which was explained by high energetic barriers between these states.[9,16] In the Car−Pc dyads studied herein, S* rapidly internally converts to S_1 on a sub-picosecond time scale, indicating a nearly barrierless transition. These observations indicate that in the various carotenoid-binding systems a large variation exists in the energy landscapes of the S* and S_1 potential energy surfaces. Very likely, these potential energy surfaces are strongly dependent on the exact geometry of the carotenoid and its specific interaction with nearby pigments. It is conceivable that S* and S_1 actually represent distinct local minima on the same potential energy surface and that it may not be appropriate to refer to them as separate electronic states.[34]

Car to Pc Energy Transfer and Vice Versa. Our study shows that the carotenoid to phthalocyanine energy transfer can be tuned by changing the conjugation length of the carotenoid. (For a summary of the results, see Table 4.) The efficiency of energy transfer to Pc from the optically allowed carotenoid S_2 state is similar for dyads **1** and **2** and amounts to 69% and 60%, respectively. This number is significantly higher than that observed in caroteno-SiPc triads where the same carotenoids have been axially linked to the central silicon atom of Pc. In these systems, the energy transfer efficiency from the S_2 state was found to be ∼35%.[16,35] It is probable that the orientation of the transition dipole moments is more favorable for a dipole-coupling-based energy transfer mechanism in the dyads than in the triads, where the angle between the chromophores is close

to 90°. In addition a stronger electronic coupling by electron exchange terms is expected for the dyads, due to the partial conjugation provided by the amide bond, which is not present in the ester linkage of the caroteno-SiPc triads.

In dyad **1**, the carotenoid to Pc energy transfer is extremely efficient (>90%). Energy transfer from both the S_2 state and the optically forbidden, low-lying carotenoid state(s) is required to reach such a high efficiency. The addition of one double bond to the conjugation length of the carotenoid (dyad **2**) reduces the contribution from the low-lying S_1 state and leads to a drop in the energy transfer efficiency. It is likely that the carotenoid S_1 state energy, which is energetically above that of the Q state of Pc in dyad **1**, is lowered upon the extension of the conjugation length of the carotenoid so that the spectral overlap with the Pc Q state diminishes significantly. Indeed, in triads made up of the same carotenoids and a SiPc, the spectral overlap was estimated to diminish by a factor of 3 upon addition of one double bond to a 9 double-bond carotenoid.[16] This trend was corroborated by the study of the Pc Q state quenching in the same dyads reported herein where the addition of one double bond to the conjugation length, from dyad **1** to dyad **2**, turns the carotenoid S_1 state from an energy donor to the Pc Q excited state into a quencher of the Pc Q state.[4] This demonstrates the "molecular gear" mechanism in a model system, which has long been speculated to take place in plants.[36,37] Upon addition of another conjugated double bond to the carotenoid (dyad **3**), the S_1 state of the carotenoid becomes an even stronger quencher of the Pc Q excited state. Moreover, as described in this report for dyad **3**, the carotenoid excited state(s) appears to form an exciplex with the Pc ground state. This interaction could be fine-tuned by the local environment to lead to energy or electron transfer; experiments designed to test this and to look for similar states in natural systems are underway. Another factor possibly affecting the yield of S_1 energy transfer is the shorter intrinsic S_1 lifetime as the energy of the S_1 state is lowered. This IC follows roughly the energy gap law; typically, the S_1 lifetime of an 11 double-bond carotenoid is ~5 times shorter than that of a 9 double-bond carotenoid. It should be noted that the conjugated system of the carotenoid moiety in the dyads contains a carbonyl group, which confers a partial charge-transfer character to the S_1 state. This partial charge-transfer character has been shown to be responsible for the strong solvent polarity dependence of the Pc excited-state quenching by the carotenoid[4] and in principle could also affect the energy transfer efficiency from the S_1 state as was recently shown in similar systems.[38]

In contrast to many bacterial LH antennas and artificial caroteno-SiPc triads, the carotenoid S* state does not transfer energy to Pc in dyad **2** or **3**. Given that in the former systems energy transfer from S* occurred on the 5 ps to tens of picoseconds time scales, the absence of energy transfer from S* in dyads **2** and **3** most likely follows from the fast (sub-picosecond) IC rates to S_1 and S_0, which successfully compete with energy transfer.

LHCs of oxygenic photosynthetic organisms display trends in energy transfer characteristics similar to those observed here. In LHCII, CP43 and CP47 from plants and photosystem I (PSI) from cyanobacteria, the majority of excitations originating from carotenoids are transferred to Chl through the carotenoid S_2 state.[21,32,39−41] Energy transfer from the S_1 state was found to be dependent on the conjugation length of the carotenoid, with lutein and possibly neoxanthin being able to transfer efficiently from S_1,[21,32,42] whereas β-carotene could only partly transfer from S_1 in PSI[41,43] and not at all in CP47, CP43, and the PSII reaction center.[40,44]

Conclusions

By applying ultrafast time-resolved spectroscopy and rigorous spectro-temporal analysis, we have uncovered previously unobserved energy relaxation pathways and a novel type of collective carotenoid−phthalocyanine excited state in caroteno-phthalocyanine dyads. In dyads **1**, **2**, and **3**, which have a phthalocyanine covalently linked to a carotenoid with 9, 10, and 11 conjugated carbon−carbon double bonds, respectively, rapid internal conversion and energy transfer processes take place upon excitation of the carotenoid moiety at 475 nm. In all dyads we observed internal conversion from the optically allowed S_2 state to the optically forbidden S_1 and S* states. Remarkably, internal conversion from S* to S_1 occurs on a sub-picosecond time scale in all three dyads. This phenomenology contrasts with all previous observations of S* in carotenoids and carotenoid-based LH systems, where S* was found to evolve independently from all other carotenoid excited states.

In dyad **3**, we have characterized a novel type of collective carotenoid−phthalocyanine excited state, which we tentatively assign to a carotenoid−Pc exciplex. The exciplex is only observed in transient absorption upon excitation of the carotenoid and is non-emissive, and we therefore propose that it arises from population of the optically forbidden S* and/or S_1 states, which excitonically couple with the Pc ground-state absorption through their strong $S_1/S^* \rightarrow S_n$ transition.

Finally, the results on dyads **1**, **2**, and **3** show that the carotenoid S_2 and S_1 energy levels must be matched to that of phthalocyanine for an optimal light-harvesting function. Dyad **1** exhibits a light-harvesting function at near unity through energy transfer from the optically allowed S_2 state and the optically forbidden S_1 state to phthalocyanine. In dyad **2**, efficient energy transfer from S_2 occurs, but energy transfer from S_1 is precluded, presumably as a result of unfavorable energetics. In dyad **3**, energy transfer efficiency from the 11 double-bond carotenoid to the phthalocyanine is low. The carotenoid S_1 state does not transfer energy, and the energy transfer quantum yield from S_2 is only ~24%. Remarkably, S* does not appear to contribute significantly in the energy transfer process in any of the three dyads, which is likely related to its rapid internal conversion to the S_1 state.

The findings reported herein bear on the suggestion of a "molecular gear" mechanism controlling energy transfer between chlorophylls and carotenoids in plants.[36,37] While dyad **1** demonstrates S_1 to phthalocyanine energy transfer, in dyads **2** and **3** energy flows the other way − from the phthalocyanine to the carotenoid S_1. The switch in energy flow with the change in conjugation length in a model system demonstrates the "molecular gear" mechanism in a model dyad system.

Acknowledgment. R.B. was supported by The Netherlands Organization for Scientific Research through the Earth and Life Sciences Council (NWO-ALW). J.T.M.K. was supported by NWO-ALW via a VIDI fellowship. The work was supported by the U. S. Department of Energy (Grant No. FG02-03ER15393). This is publication 673 from the ASU Center for the Study of Early Events in Photosynthesis.

Supporting Information Available: Selected spectroscopic data in different solvents, a set of kinetic traces, and time-gated spectra with fits obtained from the global analysis of the time-resolved data for the three dyads. This material is available free of charge via the Internet at http://pubs.acs.org.

References and Notes

(1) Frank, H. A.; Cogdell, R. J. *Photochem. Photobiol.* **1996**, *63*, 257.
(2) Polivka, T.; Sundstrom, V. *Chem. Rev.* **2004**, *104*, 2021.

(3) Holt, N. E.; Zigmantas, D.; Valkunas, L.; Li, X. P.; Niyogi, K. K.; Fleming, G. R. *Science* **2005**, *307*, 433.

(4) Berera, R.; Herrero, C.; van Stokkum, I. H. M.; Vengris, M.; Kodis, G.; Palacios, R. E.; van Amerongen, H.; van Grondelle, R.; Gust, D.; Moore, T. A.; Moore, A. L.; Kennis, J. T. M. *Proc. Natl. Acad. Sci. U.S.A.* **2006**, *103*, 5343.

(5) Tavan, P.; Schulten, K. *Phys. Rev. B* **1987**, *36*, 4337.

(6) Hudson, B. S.; Kohler, B. E. *Chem. Phys. Lett.* **1972**, *14*, 299.

(7) Starcke, J. H.; Wormit, M.; Schirmer, J.; Dreuw, A. *Chem. Phys.* **2006**, *329*, 39.

(8) Sashima, T.; Nagae, H.; Kuki, M.; Koyama, Y. *Chem. Phys. Lett.* **1999**, *299*, 187.

(9) Gradinaru, C. C.; Kennis, J. T. M.; Papagiannakis, E.; van Stokkum, I. H. M.; Cogdell, R. J.; Fleming, G. R.; Niederman, R. A.; van Grondelle, R. *Proc. Natl. Acad. Sci. U.S.A.* **2001**, *98*, 2364.

(10) Cerullo, G.; Polli, D.; Lanzani, G.; De Silvestri, S.; Hashimoto, H.; Cogdell, R. J. *Science* **2002**, *298*, 2395.

(11) Papagiannakis, E.; Kennis, J. T. M.; van Stokkum, I. H. M.; Cogdell, R. J.; van Grondelle, R. *Proc. Natl. Acad. Sci. U.S.A.* **2002**, *99*, 6017.

(12) Larsen, D. S.; Papagiannakis, E.; van Stokkum, I. H. M.; Vengris, M.; Kennis, J. T. M.; van Grondelle, R. *Chem. Phys. Lett.* **2003**, *381*, 733.

(13) Papagiannakis, E.; Das, S. K.; Gall, A.; van Stokkum, I. H. M.; Robert, B.; van Grondelle, R.; Frank, H. A.; Kennis, J. T. M. *J. Phys. Chem. B* **2003**, *107*, 5642.

(14) Wohlleben, W.; Buckup, T.; Herek, J. L.; Cogdell, R. J.; Motzkus, M. *Biophys. J.* **2003**, *85*, 442.

(15) Billsten, H. H.; Pan, J. X.; Sinha, S.; Pascher, T.; Sundstrom, V.; Polivka, T. *J. Phys. Chem. A* **2005**, *109*, 6852.

(16) Kodis, G.; Herrero, C.; Palacios, R.; Marino-Ochoa, E.; Gould, S.; de la Garza, L.; van Grondelle, R.; Gust, D.; Moore, T. A.; Moore, A. L.; Kennis, J. T. M. *J. Phys. Chem. B* **2004**, *108*, 414.

(17) Papagiannakis, E.; van Stokkum, I. H. M.; Vengris, M.; Cogdell, R. J.; van Grondelle, R.; Larsen, D. S. *J. Phys. Chem. B* **2006**, *110*, 5727.

(18) Wohlleben, W.; Buckup, T.; Hashimoto, H.; Cogdell, R. J.; Herek, J. L.; Motzkus, M. *J. Phys. Chem. B* **2004**, *108*, 3320.

(19) Gust, D.; Moore, T. A.; Moore, A. L. *Acc. Chem. Res.* **2001**, *34*, 40.

(20) Berera, R.; Moore, G. F.; van Stokkum, I. H. M.; Kodis, G.; Liddell, P. A.; Gervaldo, M.; van Grondelle, R.; Kennis, J. T. M.; Gust, D.; Moore, T. A.; Moore, A. L. *Photochem. Photobiol. Sci.* **2006**, *5*, 1142.

(21) Gradinaru, C. C.; van Stokkum, I. H. M.; Pascal, A. A.; van Grondelle, R.; van Amerongen, H. *J. Phys. Chem. B* **2000**, *104*, 9330.

(22) van Stokkum, I. H. M.; Larsen, D. S.; van Grondelle, R. *Biochim. Biophys. Acta* **2004**, *1657*, 82.

(23) Gradinaru, C. C.; van Grondelle, R.; van Amerongen, H. *J. Phys. Chem. B* **2003**, *107*, 3938.

(24) Herek, J. L.; Wendling, M.; He, Z.; Polivka, T.; Garcia-Asua, G.; Cogdell, R. J.; Hunter, C. N.; van Grondelle, R.; Sundstrom, V.; Pullerits, T. *J. Phys. Chem. B* **2004**, *108*, 10398.

(25) Polívka, T.; Zigmantas, D.; Sundström, V.; Formaggio, E.; Cinque, G.; Bassi, R. *Biochemistry* **2002**, *41*, 439.

(26) Birks, J. B. *Rep. Prog. Phys.* **1975**, *38*, 903.

(27) Palacios, R. E.; Kodis, G.; Herrero, C.; Ochoa, E. M.; Gervaldo, M.; Gould, S. L.; Kennis, J. T. M.; Gust, D.; Moore, T. A.; Moore, A. L. *J. Phys. Chem. B* **2006**, *110*, 25411.

(28) Zigmantas, D.; Hiller, R. G.; Sharples, F. P.; Frank, H. A.; Sundstrom, V.; Polivka, T. *Phys. Chem. Chem. Phys.* **2004**, *6*, 3009.

(29) Billsten, H. H.; Zigmantas, D.; Sundström, V.; Polivka, T. *Chem. Phys. Lett.* **2002**, *355*, 465.

(30) de Weerd, F. L.; van Stokkum, I. H. M.; van Grondelle, R. *Chem. Phys. Lett.* **2002**, *354*, 38.

(31) Zigmantas, D.; Hiller, R. G.; Sundström, V.; Polívka, T. *Proc. Natl. Acad. Sci. U.S.A.* **2002**, *99*, 16760.

(32) Croce, R.; Muller, M. G.; Bassi, R.; Holzwarth, A. R. *Biophys. J.* **2001**, *80*, 901.

(33) Zhang, J. P.; Fujii, R.; Qian, P.; Inaba, T.; Mizoguchi, T.; Koyama, Y.; Onaka, K.; Watanabe, Y.; Nagae, H. *J. Phys. Chem. B* **2000**, *104*, 3683.

(34) Niedzwiedzki, D. M.; Sullivan, J. O.; Polivka, T.; Birge, R. R.; Frank, H. A. *J. Phys. Chem. B* **2006**, *110*, 22872.

(35) Marino-Ochoa, E.; Palacios, R.; Kodis, G.; Macpherson, A. N.; Gillbro, T.; Gust, D.; Moore, T. A.; Moore, A. L. *Photochem. Photobiol.* **2002**, *76*, 116.

(36) Frank, H. A.; Cua, A.; Chynwat, V.; Young, A.; Gosztola, D.; Wasielewski, M. R. *Photosynth. Res.* **1994**, *41*, 389.

(37) Frank, H. A.; Cua, A.; Chynwat, V.; Young, A.; Gosztola, D.; Wasielewski, M. R. *Biochim. Biophys. Acta* **1996**, 243.

(38) Polivka, T.; Pellnor, M.; Melo, E.; Pascher, T.; Sundstrom, V.; Osuka, A.; Naqvi, K. R. *J. Phys. Chem. C* **2007**, *111*, 467.

(39) Holt, N. E.; Kennis, J. T. M.; Dall'Osto, L.; Bassi, R.; Fleming, G. R. *Chem. Phys. Lett.* **2003**, *379*, 305.

(40) Holt, N. E.; Kennis, J. T. M.; Fleming, G. R. *J. Phys. Chem. B* **2004**, *108*, 19029.

(41) de Weerd, F. L.; Kennis, J. T. M.; Dekker, J. P.; van Grondelle, R. *J. Phys. Chem. B* **2003**, *107*, 5995.

(42) Walla, P. J.; Yom, J.; Krueger, B. P.; Fleming, G. R. *J. Phys. Chem. B* **2000**, *104*, 4799.

(43) Wehling, A.; Walla, P. J. *J. Phys. Chem. B* **2005**, *109*, 24510.

(44) de Weerd, F. L.; Dekker, J. P.; van Grondelle, R. *J. Phys. Chem. B* **2003**, *107*, 6214.

VI. Herrero, Christian; Lasalle-Kaiser, Benedikt; Leibl, Winfried; Rutherford, William A.; Aukauloo, Ally. **Artificial systems related to light driven electron transfer processes in PSII**. Coordination Chemistry Reviews. *In press*.

Available online at www.sciencedirect.com
ScienceDirect
Coordination Chemistry Reviews 252 (2008) 456–468
COORDINATION CHEMISTRY REVIEWS
www.elsevier.com/locate/ccr

Review

Artificial systems related to light driven electron transfer processes in PSII

Christian Herrero [a,b], Benedikt Lassalle-Kaiser [a], Winfried Leibl [b], A. William Rutherford [b], Ally Aukauloo [a,b,*]

[a] *Laboratoire de Chimie Inorganique, ICMMO, Bât. 420, UMR 8182, Université de Paris-Sud XI, F-91405 Orsay, France*
[b] *iBiTeC-S, CEA Saclay, Bât. 532, 91191 Gif-sur-Yvette Cedex, France*

Received 15 May 2007; accepted 1 September 2007
Available online 7 September 2007

Contents

Abstract

The water oxidising enzyme, photosystem II, performs one of the most important reactions for life on Earth. Today, in the context of finding renewable sources of energy as alternatives for fossil fuels, the four-electron oxidation of water using light energy stands as one of the most challenging reactions for scientists to understand and reproduce. Mastering this reaction is considered to be a key step towards the use of water and sunlight to produce renewable hydrogen. It is therefore not only timely but also urgent to understand the mechanism of this enzyme so that this understanding can be used to design artificial catalysts. A chemical catalyst that shares the property of the enzyme in its ability to oxidize water with a low overpotential, could greatly improve the efficiency of water electrolysis and photolysis. Here we briefly describe aspects of the enzyme focusing on the essential cofactors involved in the light driven oxidation of water and provide an overview of the work done to produce a biomimetic photocatalyst for water oxidation. The development of such a device can be conceptualized as the association of two chemical modules, a photoactive unit and a catalytic unit. The candidate of choice for the photoactive unit, at least on a proof-of-principle basis, is $[Ru(bpy)_3]^{2+}$. This is due to its robustness, its synthetic flexibility and its unique photophysical properties. The elusive manganese catalyst acting as the catalytic site is dealt with in the previous chapters of this issue. In this review we discuss the different challenges that must be met to develop a synthetic system for water photolysis. These include (1) efficient light absorption by a sensitizer, (2) development of a stable charge separating device, (3) vectorial

Abbreviations: Bpy, 2,2′-bispyridine; CB, conduction band; CPET, concerted proton electron transfer; DFT, density functional theory; EDTA, ethylenediaminetetraacetate; EPR, electron paramagnetic resonance; ET, electron transfer; His, histidine; MLCT, metal to ligand charge transfer; MV, methylviologen; NMR, nuclear magnetic resonance; OEC, oxygen evolving complex; P_{680}, pigment absorbing at 680 nm; PD1, protein D1; PhD1, pheophytin in protein D1; PQ, plastoquinone; PSII, photosystem II; PTZ, phenothiazine; SCE, saturated calomel electrode; TEA, triethylamine; TD-DFT, time-dependent density functional theory; TW, terawatt; Tyr, tyrosine.

* Corresponding author at: Laboratoire de Chimie Inorganique, ICMMO, Bât. 420, UMR 8182, Université de Paris-Sud XI, F-91405 Orsay, France.
E-mail address: aukauloo@icmo.u-psud.fr (A. Aukauloo).

0010-8545/$ – see front matter
doi:10.1016/j.ccr.2007.09.002

electron flow to/from, (3a) a donor site that must be capable to accumulate charges for consequent catalytic reactions, and (3b) an acceptor system that allows a multi-electron process.

Keywords: Energy; PSII; Electron transfer; Biomimetic models; Photocatalyst

1. Introduction

One of the most pressing challenges society is facing today is the transition to a new energy scenario. Increases in world population and the rise of emerging economies have projected an increase in energy consumption from 13 TW today to 30 TW by 2050 [1–3]. If we couple the fact that 86% of this energy comes from fossil fuels to the fact that CO_2 levels are the highest they have been for the past 650,000 years, it is clear that the burn rate that will be needed in 40 year's time is unacceptable. In order to fill the gap of needed energy we must look for complementary sources that will be reliable enough to meet the demand and sustainable enough so their use will not be deleterious to life on earth. Obviously, solar power presents itself as the most promising source of renewable energy available. The goal of artificial photosynthesis is to harness this energy to drive the production of high-energy chemicals from low energy source compounds.

Nature has given us the guidelines for such a process. During photosynthesis, absorption of light by phototrophic organisms initiates a series of energy and electron transfer processes that lead to the oxidation of water (Eq. (1)) to reducing equivalents that can then drive the reduction of CO_2 into higher carbohydrates (Eq. (2)).

$$2H_2O + 4h\nu \rightarrow O_2 + 4H^+ + 4e^- \quad (1)$$

$$nCO_2 + 2ne^- + 2nH^+ \rightarrow (CH_2O)_n \quad (2)$$

$$2H^+ + 2e^- \rightarrow H_2 \quad (3)$$

Artificial photosynthesis, thus, aims to imitate the above-mentioned processes of light absorption, catalysis, and energy conversion. Photo-driven water oxidation to generate reactive species is in itself a very hard task, but only half of the goal. The long-standing project has been to reuse the electrons and protons generated to drive the production of high energetic fuels such as H_2 (Eq. (3)), or reduced forms of carbon (Eq. (2)). Over the last two decades several advances have been made in this field. Examples of light induced long-lived charge-separated states [4–7], electron transfer from chromophores to catalytic sites [8,9] and water oxidation catalysis by chemical or electrochemical means [10–17] have been reported in the literature. Nevertheless, little success has been attained when trying to combine all these required processes into one complex. In the following, we present a review of the work done up to date in the field of molecular artificial photosynthesis by briefly describing the essential cofactors involved in natural systems and drawing parallels between these components and the synthetic equivalents that could be used as their artificial counterparts. While nature might provide us hints for a solution, trying to chase its mechanism too closely might impede the development of alternative methods which could perform better in an artificial system. The pursuit of such a monumental task will serve to advance the knowledge of the mechanisms at work in the natural systems as well as lead to significant improvements within each of the disciplines involved in the research process.

2. Map of the redox-active cofactors of PSII and their role

The water oxidising enzyme is a membrane-spanning, pigment-containing protein made up of several subunits. It reduces plastoquinone to plastoquinol on one side of the membrane ($PQ + 2e^- + 2H^+ \rightarrow PQH_2$) and at the other side it oxidizes water, producing molecular oxygen ($2H_2O \rightarrow 4e^- + 4H^+ + O_2$). The first of these processes is a two-electron, two-proton reaction while the second is a four-electron oxidation of two molecules of water, producing four protons and a molecule of oxygen. Since the chlorophyll photochemistry is a high quantum yield, univalent charge separating process, the enzyme must interface the one-electron processes with the multi-electron chemistry occurring at each side of the enzyme. The enzyme is often conceptualized as being made up of two parts: (1) a photochemical charge separating device which produces a reductant and a strong oxidant on opposite sides of the membrane, and (2) a catalytic device in which the oxidising power is accumulated in the form of increases in the valence of a cluster of manganese ions. A view of the main cofactors is given in Fig. 1 and the sequence of electron transfer processes after a photonic excitation of the chlorophylls is indicated.

1. Light induced charge separation: charge separation takes place between pigment molecules very rapidly after excitation of the chlorophylls in the enzyme (step 1 in Fig. 1). A radical pair is detected a few picoseconds after excitation and this appears to be made up of a chlorophyll (P_{D1} in Fig. 1) cation and a pheophytin (Ph_{D1} in Fig. 1) anion.
2. The pheophytin anion radical rapidly donates an electron to a quinone (Q_A) thereby stabilising the charge-separated state.
3. The highly oxidising chlorophyll cation extracts an electron from a tyrosine residue (Tyr_Z). The tyrosine's phenolic carbonyl group loses a proton as the tyrosyl radical forms.
4. The neutral tyrosyl radical then goes on to oxidize the Mn ions of the Mn complex (designated OEC, oxygen evolving complex, in Fig. 1).
5. The semiquinone anion formed is further stabilized by a lateral electron transfer step to a second quinone, Q_B.

The final state formed after the excitation of the enzyme by one photon contains a semiquinone (Q_B^-) and a high valence form of the Mn cluster. This state is stable for tens of seconds at room temperature and contains more than half of the energy

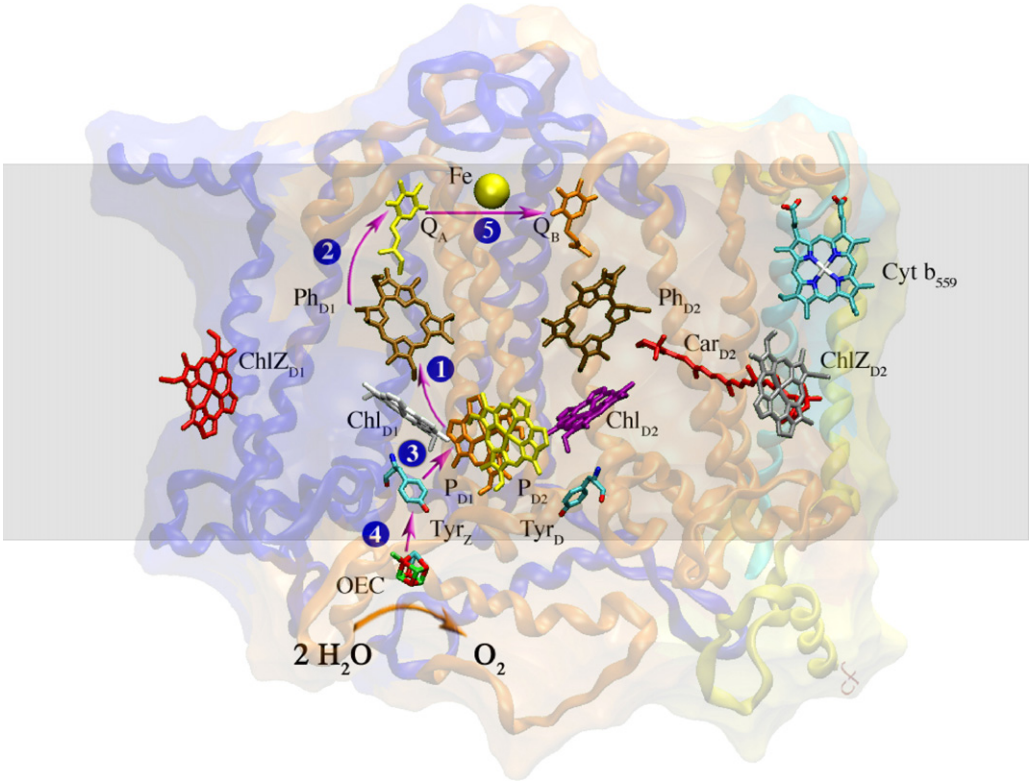

Fig. 1. Map of the main cofactors of PSII. The arrows show the electron transfer steps and the numbers indicate the order in which they occur.

(approx. 1 eV) of the absorbed photon. In order to complete the reduction of plastoquinone, a second turnover must occur. In order to oxidize water, a total of four photochemical events must take place, with each one resulting in an increase in the manganese cluster's valence.

3. Chemistry at the water oxidizing complex

The core complex of PSII described above contains six chlorophyll *a*'s and 2 β-carotene pigments [4,18]. In order to increase the collection of light, several antenna proteins containing a large number of chromophores are associated with the core complex to harvest light of various wavelengths. These antenna systems are capable of funnelling the photon energy through a series of energy transfer steps to the primary electron donor P_{680} which is probably made up by the four excitonically coupled chlorophyll molecules of the PSII core (P_{D1}, P_{D2}, Chl_{D1}, Chl_{D2} in Fig. 1). After excitation of P_{680}, a charge-separated state is created and a chain of well-positioned and optimally tuned redox cofactors makes up a pathway for efficient transfer of the electrons away from the oxidized primary donor P_{680}^+ (probably P_{D1} in Fig. 1). The efficiency of this process is virtually independent of the oxidation state of the Mn cluster, giving us an idea of how evolution has resulted in a high level of sophistication of the natural enzyme, which is capable of controlling the electron transfer away from the active catalytic site even if the latter is in a high valence state. The resulting P_{680}^+ is then reduced to its initial state upon oxidation of a tyrosine residue. Interestingly, recent crystallographic data [18,19] show that the phenolic oxygen of the tyrosine (Tyr_Z) is hydrogen bonded to the imidazole ring of a histidine residue (His_{191}). Babcock et al. [20,21] suggested that rather than being a simple intermediate in an electron transfer process as had been previously thought, the tyrosyl radical might act as a hydrogen atom abstractor. This would require proximity between the substrate water and the tyrosyl radical and the evacuation of the tyrosine's proton away from the active site. While the crystal structure confirmed that the distance between the tyrosine and the Mn cluster would allow H-bonding between the phenolic oxygen and a putative Ca-bonded water, there was no obviously discernible H-bonding pathway for proton evacuation [18,19]. Given the ambiguities in the structural model and the H atom transfer mechanism, a direct role for the tyrosyl radical in water oxidation has not been ruled out.

The manganese cluster, known as the oxygen evolving complex (OEC) catalyses the water oxidation reaction. It is composed of four manganese ions, bridged by oxo ligands. Calcium chloride and carbonate ions are known to be present at the OEC but their roles are unclear yet. The mechanism for the removal of four electrons and four protons from two substrate water molecules is still subject to speculations [22]. The main obstacle to the understanding of this mechanism is the lack of knowledge concerning the structure of the OEC. Recent X-ray diffraction structures [18,19] are impeded by lack of resolution and by reduction of the high valence Mn ions back to Mn^{II} by the X-ray beam [23]. A different proposal has incorporated the use of both theoretical modelling and X-ray absorption techniques [24]. New theoretical proposals based on experimental findings are providing possible scenarios for the functioning of the OEC

[25]. While the electronic structure of the different S-states, substrate binding, calcium/chloride binding, and function of amino acid side chains are still a matter of debate, it is widely admitted that the substrate waters undergo deprotonation as the valence state of the Mn cluster increases [26], compensating for charge accumulation and preventing large increases in the redox potential. Different possible pathways for the eventual formation of the oxygen–oxygen bond have been proposed (see previous chapters).

4. Construction of an artificial photosynthesis device

The most basic molecular device relevant to natural photochemical processes should be composed of a photosensitiser linked to an electron donor on one side and to an electron acceptor on another side. This triad should undergo the following steps:

1. $D–S–A \rightarrow D–S^*–A$ Light absorption by antenna system or sensitiser
2. $D–S^*–A \rightarrow D–S^+–A^-$ Electron transfer to an acceptor
3. $D–S^+–A^- \rightarrow D^+–S–A^-$ Electron transfer from donor (charge-separated state)

Triads have been published which show long lifetimes for a charge-separated state and multi-electron cascades have been observed [27,28]. These examples show that transformation of light energy into chemical energy in the form of a charge-separated state can be achieved. The next step towards water decomposition would require the coupling of the pertinent reduction and oxidation catalysts to a triad. The basic requirements for such a particular photocatalytic system to work are the following: (i) directionality of the electron transfer process for each individual charge separation step, (ii) tuning of the electronic coupling between the donor/acceptor and the photosensitiser in order to maximise electron transfer efficiency, (iii) a long-lived charge-separated state and (iv) catalysts (donor/acceptor) capable of storing oxidising/reducing equivalents.

Coupling two catalytic reactions involving the same number of electrons on a single molecule requires the rates for the catalytic reactions to be faster than the recombination rates. This challenge is even harder when the two reactions performed do not involve the same number of electrons. Decomposition of water belongs to the latter case. This reaction would require coupling a $2e^-$ reduction reaction (H^+ reduction) to a $4e^-$ oxidation reaction (H_2O oxidation). After accumulation of two charges, protons would be reduced, while the oxidation of water would still require two other oxidizing equivalents. In order to maintain the efficiency of the early photophysical events independent of the redox state of the catalysts, the charges accumulated have to be compensated for. Another point of importance is the condition under which a reaction is conducted, which might be different for the oxidation and the reduction sides.

These obstacles can partly be solved by designing a photochemical cell in which the oxidation and reduction reactions are separated. In such a system we could imagine the oxidation catalyst (Cat_{ox}) linked by a photosensitiser to an anode and a reduction catalyst (Cat_{red}) grafted to a cathode [29] (see Fig. 2). Through an electrical connection between both electrodes, the electrons from the oxidation half-cell could be transferred to the reduction half-cell, while protons would move in the opposite direction through a selective membrane. Of course, the four requirements (i–iv) mentioned above for the efficiency of a photoactive molecular catalyst still hold true for both components of such a photochemical cell. However, the use of two separated compartments with the catalysts bound to a surface prevents the intermolecular short-circuit reactions between i) the photocatalysts and ii) the photocatalysts and the reaction products. Another advantage of fixing the photocatalysts, notably the oxidation half, to an electrode resides in the properties of large bandgap semiconductor surfaces like TiO_2. These offer very fast injection rates for electrons from the excited state of attached chromophores in their conduction band [30] (see Section 4.3) contributing to the necessary control of directionality of electron transfer.

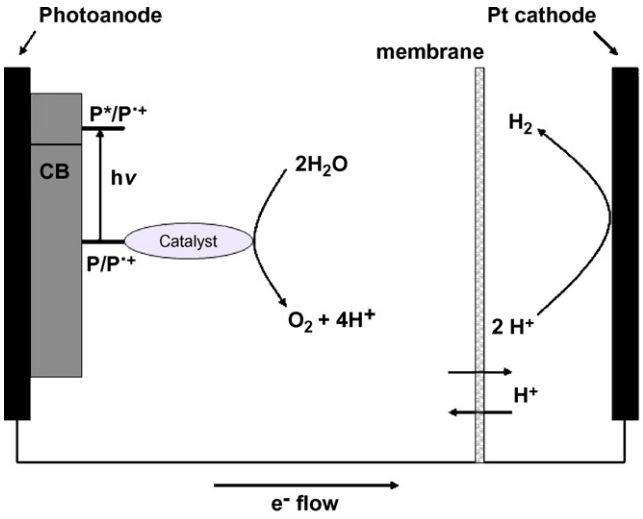

Fig. 2. Schematic of a water-splitting photochemical cell.

Examples of such devices have been developed with porphyrin-sensitised photoanodes [31,32], which drive oxidation of sugar via a natural enzyme, delivering sufficient reducing potential for H_2 production at a platinum electrode [33]. As far as we know, the use of a synthetic molecular photocatalyst has not been reported yet for such a system.

Following, we will review the research done in the field of each of the molecular constituents used in artificial photosynthesis devices: antennas, photoactive chromophores, acceptor groups and donor groups including manganese complexes. We will present the progress made in order to connect some of these modules together on the way to photodecomposition of water.

4.1. Antennas

The development of synthetic antenna systems is an active field [34–36], this for obvious reasons of collecting and harvesting solar energy in an efficient manner. The role of an antenna is to increase the absorption cross-section of the complex and, through a series of energy transfer steps, funnel that energy to a reaction centre where a charge-separated state is initiated. The solar spectrum has a maximum intensity just below 500 nm [37] and extends well into the infrared region where a photon with

$\lambda = 1000$ nm still has 1.2 eV energy. In nature, the efficient geometrical arrangement of the pigments is related to the tertiary structure of the PSII antenna subunits (light-harvesting complexes) [38]. In artificial photosynthesis this spatial arrangement is not easily achievable. The distance between the pigments to be used, their respective angle, and electronic coupling, must be engineered by the covalent bonds that unite them. Two mechanisms are responsible for energy transfer processes. Förster energy transfer occurs in cases where the distance between the chromophores is larger than their transition dipole strength, the dipoles have sufficient strength, and the lifetime of the emitting chromophore is sufficiently long. Dexter energy transfer takes place when the chromophores are brought into van der Waals contact and there is orbital overlap between them. Systems such as carotenoid–tetrapyrrole triads [39], diads [40,41], and (phenylethynyl) anthracene–porphyrin–fullerene heptads [42] have been shown to combine large absorption spectral range (350–700 nm), high extinction coefficients ($10^5\ M^{-1}\ cm^{-1}$), and quantum yields for energy transfer of close to 100% [43]. Different approaches, such as the use of dendrimers [44] or self-assembled π-stacked arrays [36,45] have also been reported in the literature. However, the connection of antenna pigments to a photochemically active chromophore to trigger a catalytic reaction has not been realised yet.

4.2. Photoactive chromophore

Several types of molecules have been used as photosensitisers, going from tetrapyrrole [6,7,46] systems to transition metal complexes (Ru, Re, Ir, Os) [44,47,48]. Synthetic porphyrin derivatives have been widely used to mimic the natural chlorophyll pigments in order to convert light energy into chemical energy [49]. However, their syntheses are long and tedious, therefore preventing their common utilisation as the photoactive module. Another well-known chromophore is the $[Ru(bpy)_3]^{2+}$ complex [50–52]. This complex is robust and can be easily prepared, therefore making it a better candidate. It presents an absorption band in the region around 450 nm corresponding to a metal to ligand charge transfer (MLCT) band with an extinction coefficient of about $13{,}000\ M^{-1}\ cm^{-1}$ [53]. Upon irradiation in the MLCT band, the input light energy is converted into a $1(d\pi^6) \rightarrow 1(d\pi^5\pi^*)$ excited state, which in turn relaxes to form the lowest triplet state (^{3}MLCT) in less than a picosecond [54–56]. This state is sufficiently long-lived to allow reductive or oxidative electron transfer processes to occur before regeneration of the ground state [57]. The oxidation potential of $[Ru(bpy)_3]^{3+}$ is around 1.2 eV [51,55] which is close to that of the primary donor of PSII, P_{680}^+ [58,123], therefore making it a suitable candidate to reproduce the oxidation reactions performed by the natural system.

Two different proposals describe the nature of the triplet state of the parent ruthenium(II) trisbipyridine complex [44]. On one hand, a localised description where the metal promoted electron is present on only one bipyridine moiety, on the other, a delocalised view where the excited electrons are extended on all three bipyridines. A recent DFT study [59] described the electronic properties of the ground and excited states of the $[Ru(bpy)_3]^{2+}$ complex. The lowest triplet state calculated $^3A_2$, as represented in Fig. 3, was the symmetric $[Ru^{III}(bpy^{[\bullet -]1/3})_3]^{2+}$.

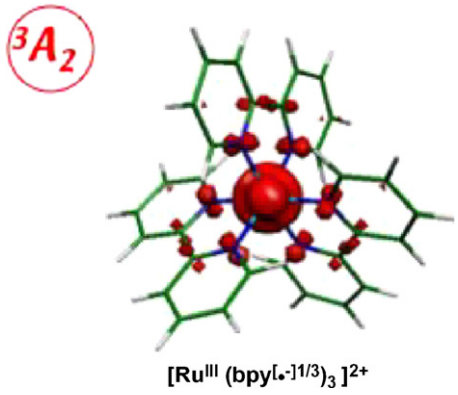

Fig. 3. Spin density distribution map of $[Ru(bpy)_3]^{2+}$ in the $^3A_2$ state.

In the computational methodology used, no asymmetry was introduced in the bipyridine ligands that could alter the transition moments. This calculated electronic snapshot may result from the statistical mean of three equivalent and equiprobable situations in which the electron is localised on one of the ligands. However, the computed data for the singlet state $^2A_1$ of the oxidized species after relaxation are in agreement with experimental data.

Synthetic methods are available [52,60] for the modification of the bipyridine ligands surrounding the ruthenium atom. In this manner it is possible to obtain mono and di-substituded ligands with either electron donating or withdrawing groups [53,60,61], as well as synthetic handles either for further synthesis [47,52,62,63] or for grafting [55,63–65] onto surfaces. Oxidation potentials for this group of molecules range from 1.20 to 1.40 V versus SCE, depending on the nature and number of substitutions [53,55,60].

These structural changes on the ligand allow the modulation of the photophysical properties of the complex. For instance, direct changes in the relative energies of the dπ and π* orbital levels observed as bathochromic shifts of up to 50 nm [48,53,60,66] are achieved by the addition of ester or carboxylate groups to the bipyridine ligands. The emission lifetimes of these compounds are also affected by substitution patterns on the bipyridines [53,60,67,68]. Electron withdrawing substituents diminish the fluorescence lifetimes and intensities by as much as 70% compared to the parent $[Ru(bpy)_3]^{2+}$ [55,60]. For all the above-mentioned reasons, we will focus in this review on the derivatives of the $[Ru(bpy)_3]^{2+}$ complex as the photoactive chromophore unit.

4.3. Acceptor side

A vectorial electron flow is established in PSII, that moves electrons coming from the excited P_{680}* pigment away from the catalytic oxidative site. Pheophytin and quinones are the main cofactors that drive the electrons in order to stabilize the charge-separated state. An important issue in the development of artificial photosynthesis devices is to borrow features of this type to control the directionality of electron transfers. Current work

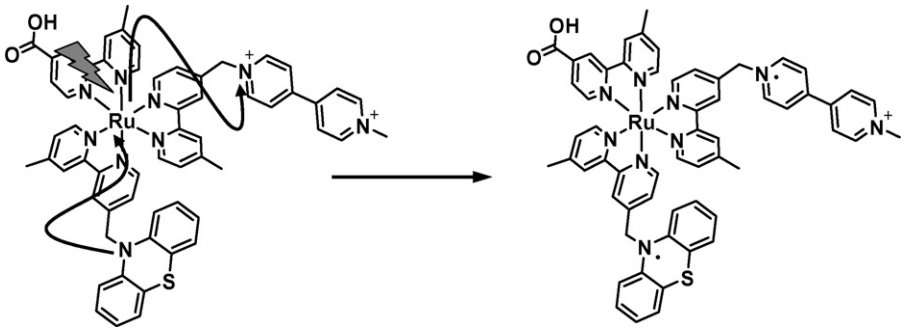

Fig. 4. Meyer's chromophore–quencher system.

in this field utilises external electron acceptors as the recipients of the first electron transfer. The more commonly utilized external electron acceptors are methyl viologen (MV) and cobalt(III) pentamine. The main disadvantage of external acceptors is the fact that the electron transfer rate is limited by diffusion. In order to overcome this problem, acceptors have been covalently linked to sensitisers [4,69–71]. Meyer et al. [72] have described an elegant example termed chromophore–quencher to illustrate the feasibility of controlling the directionality of a photo-induced electron transfer within a molecular assembly in solution. The synthetic strategy involved the linking of an acceptor (MV) and a donor (10-methylphenothiazine, PTZ) to the periphery of the bipyridine ligands, thus developing the synthesis of trisheteroleptic ruthenium(II) complexes. In order to be operational, the thermodynamics of each component must be adjusted so as to provide a free energy gradient to drive the electron in the right direction. In the case of the donor–chromophore–acceptor complex, as shown in Fig. 4, upon irradiation in the MLCT band, the primary excited electron transfer occurs to the appended MV^{2+} ($k \sim 6 \times 10^{10}\ s^{-1}$) and is followed by a rapid intramolecular PTZ to Ru(III) electron transfer ($k \sim 1 \times 10^{10}\ s^{-1}$) leading to the formation of the redox charge-separated state described as oxidized $PTZ^{\bullet+}$ and reduced $MV^{\bullet+}$. Back electron transfer occurs on the range of $\sim 10^6\ s^{-1}$.

Recently a ruthenium dimer bridged by a fused aromatic system containing two phenanthrolines at each end together with two pyrazines and a quinone was reported [73]. It was shown that the central part of the ligand acts as a reversible reservoir for four electrons upon irradiation in the visible region and in presence of a sacrificial electron donor (triethylamine) (Fig. 5). Experimental facts tend to support that the first UV–visible spectral modification corresponds to a two-electron reduction process leading to the formation of the doubly reduced form of the quinone fragment, followed by two consecutive one electron transfers. More importantly, each electron transfer step is coupled with the protonation of the reduced species.

Other examples of suitable electron acceptors are perylenes [74] and fullerenes [75–77]. The latter show first reduction potentials similar to those of the biomimetic quinones, and additionally, the ability to accept multiple electrons (accumulation), rapid charge separation rates and low reorganization energies. Diads and triads involving C_{60} modules have been reported to have up to ~1 μs lifetimes [49,77].

The more challenging case is where the acceptor is itself a catalyst. Systems comprising heterobinuclear ruthenium–platinum [9] and ruthenium–palladium [8] have been described. These compounds photocatalyse the reduction of protons into molecular hydrogen using light ≥390 nm, albeit low quantum yields and turnover numbers. The Ru–Pd complex is capable of reducing diphenylacetylene to *cis*-stilbene under mild conditions (25 °C, 470 nm). Although the mechanism is not fully understood, it is clear that the reaction is photo-induced and that the palladium is responsible for the catalytic activity. These examples of photocatalised reduction reactions are of utmost importance since they would be a potential couple to the water oxidation reaction.

One last example of an electron acceptor module consists of solid-state semiconducting materials. In recent years the use of nanocrystalline TiO_2-based systems has received much attention [78–80]. Grätzel's group has studied the photo-injection of elec-

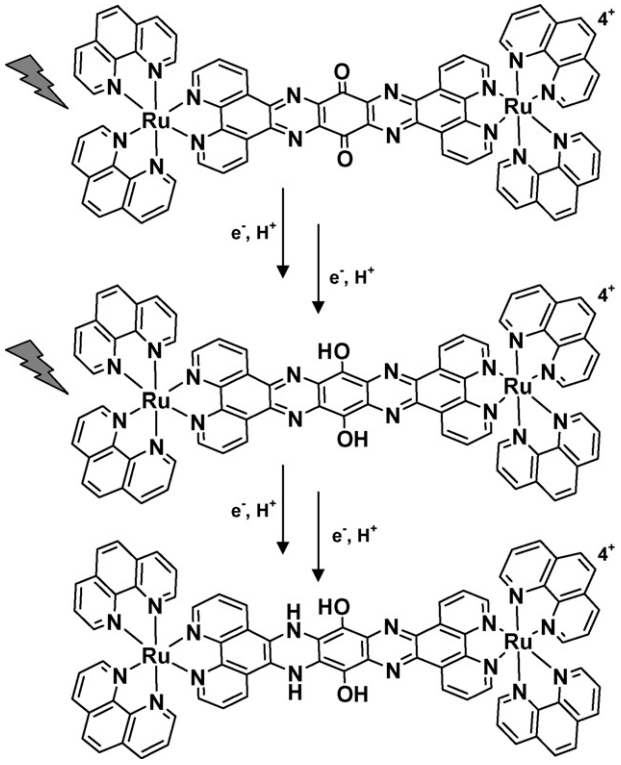

Fig. 5. Example of photo-induced sequential $2e^-$, $2H^+$ transfers.

trons into TiO_2 from the excited state of ruthenium polypyridyl complexes [81]. The resulting oxidized species can be reduced by a redox couple, which in a generic Grätzel cell is an electrolyte such as I^-/I_3^-, or by electrons coming from a catalytic centre. The advantages of such systems rely in the large surface area of the materials increasing the absorption by orders of magnitude (antenna effect), and the extremely fast rates of electron injection compared to the back electron transfer rates. These properties make the use of such materials is an interesting alternative to external electron acceptors in solution.

4.4. Donor side

The oxidized P_{680}^+ is reduced by Tyr_z, which in turn oxidizes the OEC. To date, the precise structure of the manganese cluster is not known, therefore preventing the elucidation of the water oxidation mechanism. The literature contains examples of anthracenes [42,82] carotenoids [35,46,83], metallated porphyrins [7,41] or transition metal complexes [84,85] used as electron donors. In the following sections, we will concentrate on examples more closely related to the natural systems. We will give an overview of the progress made into ruthenium systems linked to Tyr_z synthetic equivalents and manganese complexes. Finally, we will discuss the common issues between the oxidation of water by a (manganese) catalyst and the photogeneration of a charge-separated state by a ruthenium chromophore.

4.4.1. Phenol group

In the natural system, electron transfer processes are often accompanied by proton transfer processes. This observation is most important in the PSII system where a $4e^-$ oxidation is coupled to a 4 proton transfer in order to produce molecular oxygen. In PSII, the coupling of both these processes is initiated at Tyr_z, which not only reduces the photooxidised P_{680}, but is also involved in PCET processes [86] that prevent excessive charge accumulation from making the reaction too endergonic, and has even been thought to intervene in the abstraction of protons from the substrate water molecules [20,21]. This charge compensation process allows the OEC to rock within 300 mV between its four-oxidation states, therefore avoiding oxidation potentials that could not be achievable by P_{680} [58,87,123]. The chemical basis for this proton/electron transfer lies within the chemical properties of the phenol moiety. In aqueous solution, the pK_a of a phenol changes from 10 to −2 upon oxidation, with the corollary that these processes will happen concurrently. Whether these steps occur via proton first, electron first, or as a concerted process has been recently investigated by several groups [88–94].

From a synthetic point of view, phenol groups are widely used in the design of multidentate ligands [95,96] for their good ability to bind to a wide variety of metal ions and also for stabilising high oxidation state manganese ions [97–100]. There are several examples in the literature describing the oxidation of phenols by photochemical means, both as terminal groups [79,101,102] and as coordinated ligands [103–105].

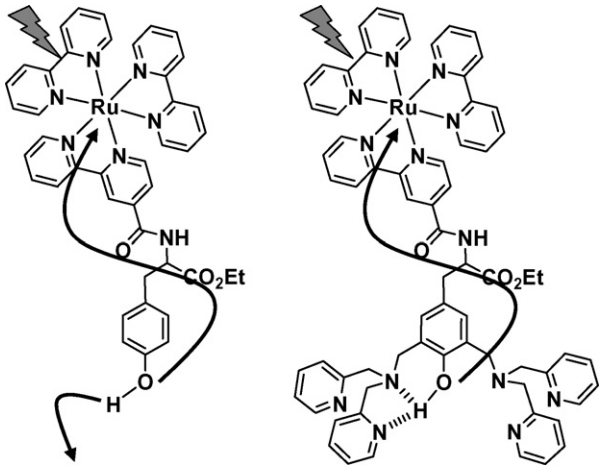

Fig. 6. Ruthenium–tyrosine complexes: free pending phenol (left); coordinating cavity (right).

A synthetic model where a tyrosine was covalently linked to a ruthenium(II) trisbipyridine complex through an amide group was reported [101] (see Fig. 6). The phenol ring was used as a molecular platform to prepare a biscompartmental coordinating cavity (Fig. 6). Prior to metallation of the coordinating cavities, photophysical measurements displayed an emission decay similar to that of the parent $[Ru(bpy)_3]^{2+}$ complex, insinuating that the tyrosine does not quench the excited state of ruthenium and also that the nature of the molecular link does not alter the intrinsic properties of the ruthenium(II) complex. Flash photolysis experiments performed by irradiating at 460 nm in presence of MV^{2+} in water, resulted in the bleaching of the MLCT band of the Ru(II) chromophore at 450 nm (formation of Ru(III)) with concomitant formation of the $MV^{\bullet+}$ radical. The longer lifetime of the $MV^{\bullet+}$ radical compared to that of the recovery of Ru(II) confirmed an intramolecular electron transfer process from the tyrosine to the photogenerated Ru(III). Interestingly, the rate of electron transfer was found to be two orders of magnitude faster in the case where the –OH fragment of the phenol ring was in hydrogen bond to the nitrogen atoms of the pending dipyridyl amine ligand. This behaviour was explained by an increase of electron density on the phenol ring upon hydrogen bonding. This assertion led to a series of studies on the implication of synthetic phenols in CPET processes, when hydrogen bonded to a nearby base [88–94].

Experiments using the above molecule grafted to colloidal TiO_2 in solution showed also the ability to photooxidize the tyrosine moiety using TiO_2 as the electron acceptor instead of an external equivalent [79]. Low yields were explained by the large electron transfer back reaction from TiO_2 to ruthenium, but the ability to use nanoparticles as electron acceptors is promising towards the development of photochemical cells.

A recent synthetic model mimicking the Tyr_Z/His_{191} pair has been reported [102] (Fig. 7). In solution, the existence of a hydrogen bond between the phenol and imidazole groups is supported by ^1H NMR study. Photoexcitation electron transfer studies were realised upon irradiation at 450 nm in presence of MV^{2+} as an electron acceptor. The transient absorption spectrum is dominated by the strong absorption of $MV^{\bullet+}$ and the extinction of

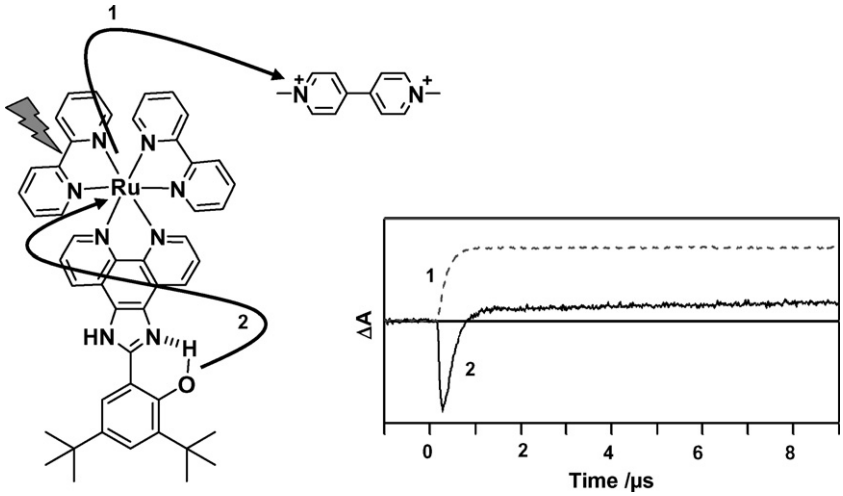

Fig. 7. Tyrosine–histidine couple mimic with its transient absorption spectrum. (1) Formation of methylviologen radical (605 nm) and (2) recovery of Ru(II) MLCT (450 nm).

the MLCT band, indicating the generation of a Ru(III) species. The kinetics shows a recovery of the reduced state of the chromophore within 500 ns (Fig. 7). This is much faster than the decay of $MV^{\bullet+}$, occurring in about 200 μs, meaning that the reduction of Ru(III) to Ru(II) is due to an electron transfer from an electron donating group on the ligand i.e. the phenol. Confirmation of the photooxidation of the phenol group comes from the EPR spectrum of an irradiated sample in presence of an irreversible electron acceptor.

As mentioned above, phenol groups have been used as coordinating groups in a large number of family of ligands [95,96]. An example of such a coordinating cavity is the salophen core [106], being defined by two imino nitrogen atoms and two oxygen atoms coming from phenol groups. A heteroditopic ligand holding both a phenanthroline end and a salophen cavity was synthesised and fixed to the ruthenium(II) ion through the phenanthroline appendix [105] (see Fig. 8). Upon excitation in the MLCT band at 450 nm, a quenching of the MLCT triplet excited state of the ruthenium(II) complex was evidenced (>95% as compared to $[Ru(bpy)_3]^{2+}$). This phenomenon was attributed to an intramolecular electron transfer process, which resulted in the formation of an extremely long-lived charge-separated state of 30 μs. Theoretical data support that both the lowest singlet and triplet states originate mainly from intra-ligand charge transfers within the extended π-ligand. The calculated spin density map of the triplet state indicates that it results from an electron transfer from the $N=CC_6H_4$–OH fragments to the binding phenanthroline moiety (Fig. 8). Therefore, this triplet cannot be considered as the usual charge-separated state in ruthenium(II) polypyridine type complexes. The electron transfer studies upon irradiation at 355 nm in the presence of an irreversible electron scavenger ($[Co^{III}(NH_3)_5Cl)]^+$) lead to the formation of a phenoxyl type radical as evidenced from the EPR spectrum (signal at $g = 2.004$). This suggests that a Ru(III) intermediate is generated that can be reductively quenched by a phenol group. The insertion of a copper ion in the coordinating cavity resulted in a complete extinction of the luminescence and no significant electron transfer process was observed under irradiation in presence of external electron acceptors. The authors explained this phenomenon by a strong electronic coupling between the two metal ions.

4.4.2. Manganese complexes

The outstanding challenge in artificial photosynthesis research is to power a water oxidation catalyst by a photoactive chromophore. Manganese complexes known to perform the four-electron water oxidation reaction are scarce [11–13,16] and intensive efforts are still needed to discover robust molecular

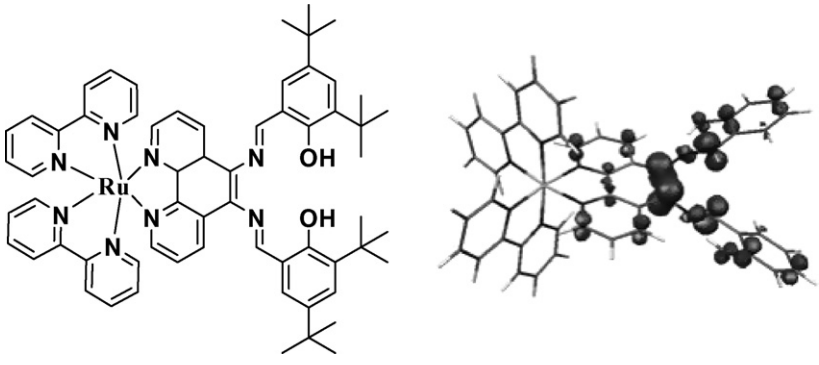

Fig. 8. Structure of a ruthenium bound to a salophen cavity (left), and calculated spin density map of the lowest triplet state (right).

catalysts working at modest overpotential (see previous chapters in this issue). In this section we will discuss about the first attempts in building a molecular system bearing a ruthenium(II) chromophore and a mono- or polynuclear manganese complex as the donor component.

The first published work on a molecule containing a sensitiser covalently linked to a manganese complex dates back to 1997 [107]. It was shown that upon photoexcitation of a binuclear Ru–Mn complex, the ruthenium chromophore could donate an electron to an external acceptor and consequently oxidize a coordinated manganese ion with rate constants ~50 ns to 10 μs. On the up side, this first work proved the fact that upon light absorption, a chain reaction of ET events could be initiated, on the down side, it already outlined the difficulties intrinsic to manganese chemistry. First, de-coordination phenomena were reported, and biphasic decays corresponding to mono and bimetallic complexes were observed. Additionally, insertion of a manganese ion to a ruthenium complex led to significant quenching of the excited state of the chromophore. The process, identified as energy transfer from ruthenium to manganese, was reported by Abrahamsson et al. [108] and showed that, within this family of molecules, when the metal-to-metal distances were smaller than 10 Å the ruthenium complex was very difficult to photooxidize due to its very short excited state lifetime (~10 ns). Additionally, this work also showed that chemical modifications in the ligands around the ruthenium could lower this quenching process. The authors found the reorganization energy for the Mn^{II}/Mn^{III} transition to be high, 1.4–2.0 eV, while typical values for electron transfer reactions in polar media are around 1.0 eV. These conclusions pointed out the inherent problems of using Mn^{II} as an electron donor. Therefore, a higher oxidation state of manganese and/or an electron relay intermediate might be needed.

An elegant example by Burdinski et al. [104] presented for the first time the photooxidation of both a $Ru_3(Mn^{II})_3$ complex, and a ligand coordinated to a Mn^{IV} ion via three phenolate groups. In the first case, each manganese(II) ion could be oxidized by one electron only, showing the need for charge compensation. In the second case, one electron could be removed from a phenolate group. This last example raises the issue of the oxidation site in phenolate-containing manganese complexes, which has been barely addressed so far [109,110].

Magnusson et al. [111] showed how a Ru–Tyr molecular dyad was used to power the light driven oxidation of a dinuclear $Mn_2^{III–III}$ complex. In this study, it was shown that the observed one electron transfer process could parallel the first electron transfer sequence in PSII. Indeed, upon light absorption, a chain reaction of ET could be achieved whereby the Ru(III) species, obtained in presence of an electron acceptor, was quenched through an intermolecular ET leading to the formation of the tyrosyl radical. Conclusive evidence that the tyrosyl radical was sufficiently oxidising to abstract one electron from the dinuclear $Mn_2^{III–III}$ came from monitoring the EPR spectrum from the starting silent $Mn_2^{III–III}$ to the formation of a typical 18 lines spectrum for the mixed valence mono-μ-oxo $Mn_2^{III–IV}$ dimer [99]. Time-resolved EPR measurements for the decay of the generated tyrosyl radical in presence and absence of the manganese complex confirmed the results. Furthermore, photo-induced intermolecular ET studies between the parent $[Ru(bpy)_3]^{2+}$ complex and the dinuclear $Mn_2^{III–III}$ compound in the same experimental conditions lead to more oxidized forms of the manganese complex. This example shows that a phenol group can act as an electron relay, by tuning the oxidation potential applied to the manganese complex (Fig. 9).

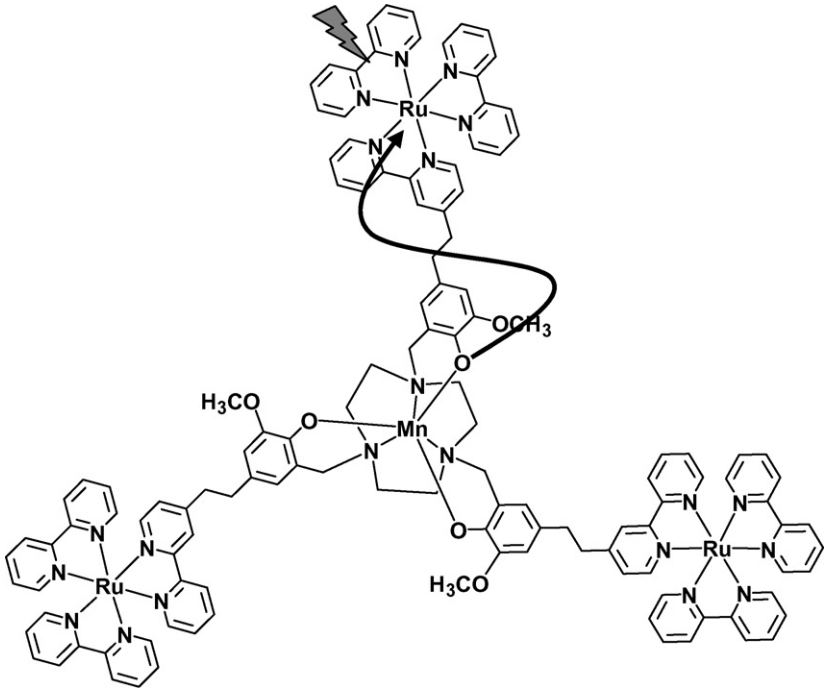

Fig. 9. Light driven oxidation of manganese bound phenolate group.

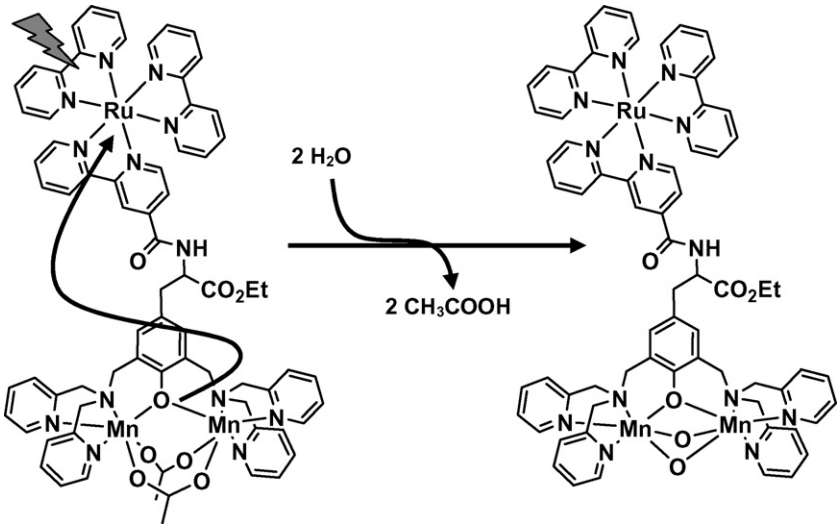

Fig. 10. Intramolecular photo-induced electron transfers from a dinuclear Mn^{II} to Mn^{II} complex, followed by ligand exchange reaction.

Phenolate-bridged bimetallic manganese complexes have yielded up to date the most promising results in the field. Huang et al. [103,112,113] showed that multi-electron transfer steps could be observed from a dimanganese complex to a $[Ru(bpy)_3]^{2+}$ unit, whether it was covalently linked or not. The intermolecular ET experiments involve the exchange of the initial acetate ligands in the manganese complexes to water molecules, which coordinate as μ-oxo bridges [112] (see Fig. 10). The exchange process was later studied itself by X-ray absorption spectroscopy on the ruthenium-free dinuclear manganese complexes [114].

To conclude, no example has been reported where oxidation of water is driven by a photosensitiser covalently linked to a catalyst. Manganese(II) has shown to be reluctant to ET, mainly because of high reorganization energy on going from Mn^{II} to Mn^{III} [107,108]. Phenolate containing ligands have shown to be efficient electron relays [104,111]. It is to be noted that out of all the artificial OEC systems that have been reported to undergo oxidation of water, there have been no attempts to link them to photoactive centres.

5. Discussion

Of all the components required for a molecular artificial photosynthesis device described above, the catalytic part is the most elusive. As already mentioned, the lack of efficient water oxidizing catalysts is an obstacle to the design of an all-in-one system. However, lessons can already be drawn from the examples shown above, concerning the issues that overlap water oxidizing/reducing catalysts and charge separating units.

Attempts to tackle the subject of charge build-up and compensation are closer to serendipity than design. Ligand exchange reactions have been observed, where bridging acetates are replaced by μ-oxo bridges [112]. These oxo-bridged adducts of manganese complexes are thermodynamically stable and are very unlikely to perform O–O bond formation. The PSII machinery keeps the oxidation potential of the OEC to a reasonable level thanks to CPET, and produces highly reactive oxo ligands (bridging or not), most likely stabilized by secondary sphere interactions. In order to reproduce these features, catalysts with a scaffold providing basic groups in the secondary sphere should be developed [115–117]. They should also be capable of holding the metal ions at such a distance [118] that collapse into oxo-bridged unreactive polynuclear complexes is not possible.

The electronic coupling between the sensitiser and the donor side (manganese catalyst) has been nicely laid out by the use of different phenol groups. Intermolecular ET from $Mn_2^{II,II}$ [112] and $Mn_2^{III,III}$ [111,112] complex has been shown to be possible. However, there is no example of a ruthenium–manganese system with a non-coordinated Tyr_z equivalent. Such a compound would be of great help for confirming or discarding the H atom abstraction mechanism proposed for water oxidation in the natural system.

Another point of crucial importance, which has not been given sufficient attention, is the conditions under which the catalytic reactions occur most efficiently. First, this has to be taken into account in the tuning of the electronic properties of the catalysts themselves and second, the groups and linkages used should be chosen among those which do not suffer damage under such particular conditions. Therefore, basic principles for designing robust and efficient catalysts [119] should also be applied to the whole architecture of a molecular artificial photosynthesis device, in order to prevent the molecule from auto-oxidation phenomena [120].

6. Conclusion

Work in the field of artificial photosynthesis is still in its infancy. While there have been vast improvements in the knowledge of the structure [18,19,24] and functioning of the natural system [121], there is still no definite answer to these issues. On the chemistry side, individual problems have been thoroughly studied and the basic science seems to be understood (except for water oxidation). Problems arise when trying to com-

bine all these aspects into a functioning system. Efficient light absorption, generation of a charge-separated state both sufficiently long-lived to allow subsequent reactions, and energetic enough to make them happen, sequential multiple electron transfer, substrate binding to catalytic centres, and catalysis must be all harnessed in one complex in order for this to work. As in any multi-step process, the loss of efficiency at any given step constitutes a burden to the rest of the process. On top of these requirements, there are additional demands placed on the synthetic process of the system. Besides the perennial needs of stability and high yield synthesis, one must take in consideration the ability to have/use different templates for the catalytic centres, the different substitution patterns for the optimization of the system and the different linkages between these modules. To date, complexes that try to encompass all these processes are few. Whether for reduction or oxidation models, ruthenium bispyridine complexes are the main candidates for sensitization. On the reduction side, catalytic production of H_2 has been reported but with limited turnovers [8,9]. On the oxidation part, no successful complex has been found, and none of the structures that have shown activity by chemical or electrochemical means [10–17] have been tried in a light powered complex [122]. A new approach seems to have emerged with the use of surfaces, which allows to short-cut many complications. Photochemical cells have been set up and showed good results [30], but the case was only applied to the oxidation of sugar. Again, the rate-limiting step to the achievement of artificial photosynthesis seems to be the finding of an efficient water oxidizing complex.

Acknowledgements

The authors would like to thank their colleagues at Saclay and Orsay for past and on-going collaborations: A. Boussac, M. Sjödin, A. Quaranta, T. Moore, A. Moore, G. Blondin, M.-F. Charlot, E. Anxolabéhère-Mallart, P. Millet, P. Dorlet, S. Un, Y. Pellegrin, F. Lachaud. We would particularly like to thank Dr. C. Fufezan for providing Fig. 1. This work is funded in part by the EU through the STRP network Solar-H, CNRS Energy Program, ANR HYPHO, ANR PhotobioH_2, Biohydrogen program of the DSV CEA and the Conseil Général d'Essonne.

References

[1] N.S. Lewis, D.G. Nocera, Proc. Natl. Acad. Sci. U.S.A. 103 (2006) 15729.
[2] Intergovernmental Panel on Climate Change, Climate Change 2007, The Physical Science Basis, 2007.
[3] N. Armaroli, V. Balzani, Angew. Chem. Int. Ed. 46 (2007) 52.
[4] M.R. Wasielewski, Chem. Rev. 92 (1992) 435.
[5] D. Gust, T.A. Moore, A.L. Moore, N. Alisdair, Macpherson, A. Lopez, J.M. DeGraziano, I. Gouni, E. Bittersmann, G.R. Seely, F. Gao, R.A. Nieman, X.C. Ma, L.J. Demanche, S.-C. Hung, D.K. Luttrull, S.-J. Lee, P.K. Kerrigan, J. Am. Chem. Soc. 115 (1993) 11141.
[6] D.M. Guldi, H. Imahori, K. Tamaki, Y. Kashiwagi, H. Yamada, Y. Sakata, S. Fukuzumi, J. Phys. Chem. A 108 (2004) 541, 548.
[7] H. Imahori, J. Phys. Chem. B 108 (2004) 6130.
[8] S. Rau, B. Schäfer, D. Gleich, E. Anders, M. Rudolph, M. Friedrich, H. Görls, W. Henry, J.G. Vos, Angew. Chem. Int. Ed. 45 (2006) 6215.
[9] H. Ozawa, M.-A. Haga, K. Sakai, J. Am. Chem. Soc. 128 (2006) 4926.
[10] S.W. Gersten, G.J. Samuels, T.J. Meyer, J. Am. Chem. Soc. 104 (1982) 4829.
[11] J. Limburg, J.S. Vrettos, L.M. Liable-Sands, A.L. Rheingold, R.H. Crabtree, G.W. Brudvig, Science (1999) 283.
[12] W. Ruettinger, M. Yagi, K. Wolf, S. Bernasek, G.C. Dismukes, J. Am. Chem. Soc. 122 (2000) 10353.
[13] Y. Shimazaki, T. Nagano, H. Takesue, B.-H. Ye, F. Tani, Y. Naruta, Angew. Chem. Int. Ed. 43 (2004) 98.
[14] T. Wada, K. Tsuge, K. Tanaka, Inorg. Chem. 40 (2001) 329.
[15] M. Yagi, M. Kaneko, Chem. Rev. 101 (2001) 21.
[16] A.K. Poulsen, A. Rompel, C.J. McKenzie, Angew. Chem. Int. Ed. 44 (2005) 6916.
[17] F. Liu, T. Cardolaccia, B.J. Hornstein, J.R. Schoonover, T.J. Meyer, J. Am. Chem. Soc. 129 (2007) 2446.
[18] B. Loll, J. Kern, W. Saenger, A. Zouni, J. Biesiadka, Nature 438 (2005) 1040.
[19] J. Barber, K. Ferreira, K. Maghlaoui, S. Iwata, Phys. Chem. Chem. Phys. 6 (2004) 4737.
[20] C.W. Hoganson, G.T. Babcock, Science (1997) 277.
[21] K.L. Westphal, C. Tommos, R.I. Cukier, G.T. Babcock, Curr. Opin. Plant Biol. 3 (2000) 236.
[22] A.W. Rutherford, A. Boussac, Science 303 (2004) 1782.
[23] J. Yano, J. Kern, K.-D. Irrgang, M.J. Latimer, U. Bergmann, P. Glatzel, Y. Pushkar, J. Biesiadka, B. Loll, K. Sauer, J. Messinger, A. Zouni, V.K. Yachandra, Proc. Natl. Acad. Sci. U.S.A. 102 (2005) 12047.
[24] J. Yano, J. Kern, K. Sauer, M.J. Latimer, Y. Pushkar, J. Biesiadka, B. Loll, W. Saenger, J. Messinger, A. Zouni, V.K. Yachandra, Science 314 (2006) 821.
[25] E.M. Sproviero, J.A. Gascon, J.P. McEvoy, G.W. Brudvig, V.S. Batista, J. Chem. Theory Comput. 2 (2006) 1119.
[26] J. Lavergne, W. Junge, Photosynth. Res. 38 (1993) 279.
[27] M. Falkenström, O. Johansson, L. Hammarström, Inorg. Chim. Acta 360 (2007) 741.
[28] D. Gust, T.A. Moore, S.-J. Lee, E. Bittersmann, D.K. Luttrull, A.A. Rehms, J.M. DeGraziano, X.C. Ma, F. Gao, R.E. Belford, T.T. Trier, Science 248 (1990) 199.
[29] M. Grätzel, Acc. Chem. Res. 14 (1981) 376.
[30] M. Grätzel, Inorg. Chem. 44 (2005) 6841.
[31] A. Brune, G. Jeong, P.A. Liddell, T. Sotomura, T.A. Moore, A.L. Moore, D. Gust, Langmuir 20 (2004) 8366.
[32] L.d.l. Garza, G. Jeong, P.A. Liddell, T. Sotomura, T.A. Moore, A.L. Moore, D. Gust, J. Phys. Chem. B 107 (2003) 10252.
[33] M. Hambourger, A. Brune, D. Gust, A.L. Moore, T.A. Moore, Photochem. Photobiol. Sci. 81 (2005) 1015.
[34] D. Gust, T.A. Moore, A.L. Moore, Acc. Chem. Res. 34 (2001) 40.
[35] T.A. Moore, A.L. Moore, D. Gust, Phil. Trans. R. Soc. Lond. B 357 (2002) 1481.
[36] M.R. Wasielewski, J. Org. Chem. 71 (2006) 5051.
[37] H. Neckel, D. Labs, Solar Phys. 90 (1984) 205.
[38] J.L. Herek, W. Wohlleben, R.J. Cogdell, D. Zeidler, M. Motzkus, Nature 417 (2002) 533.
[39] S.L. Gould, G. Kodis, P.A. Liddell, R.E. Palacios, A. Brune, D. Gust, T.A. Moore, A.L. Moore, Tetrahedron 62 (2006) 2074.
[40] D.I. Schuster, P. Cheng, P.D. Jarowski, D.M. Guldi, C. Luo, L. Echegoyen, S. Pyo, A.R. Holzwarth, S.E. Braslavsky, R.M. Williams, G. Klihm|, J. Am. Chem. Soc. 126 (2004) 7257.
[41] D. Kuciauskas, S. Lin, G.R. Seely, A.L. Moore, T.A. Moore, D. Gust, T. Drovetskaya, C.A. Reed, P.D.W. Boyd, J. Phys. Chem. 100 (1996) 15926.
[42] G. Kodis, Y. Terazono, P.A. Liddell, J. Andreasson, V. Garg, M. Hambourger, T.A. Moore, A.L. Moore, D. Gust, J. Am. Chem. Soc. 128 (2006) 1818.
[43] G. Kodis, C. Herrero, R. Palacios, E.M. Ochoa, S. Gould, L.d.l. Garza, R.v. Grondelle, D. Gust, T.A. Moore, A.L. Moore, J.T.M. Kennis, J. Phys. Chem. B 108 (2004) 414.
[44] V. Balzani, A. Juris, M. Venturi, Chem. Rev. 96 (1996) 759.
[45] C. Roger, M.G. Muller, M. Lysetska, Y. Miloslavina, A.R. Holzwarth, F. Wurthner, J. Am. Chem. Soc. 128 (2006) 6542.

[46] S.L. Gould, G. Kodis, R.E. Palacios, L.d.l. Garza, A. Brune, D. Gust, T.A. Moore, A.L. Moore, J. Phys. Chem. B 108 (2004) 10566.
[47] F.R. Keene, Coord. Chem. Rev. 166 (1997) 121.
[48] V. Balzani, A. Juris, Coord. Chem. Rev. 211 (2001) 97.
[49] F. Hauke, S. Atalick, D.M. Guldi, A. Hirsch, Tetrahedron 62 (2006) 1923.
[50] T.J. Meyer, Pure Appl. Chem. 58 (1988) 1193.
[51] M. Hang, V. Huynh, D.M. Dattelbaum, T.J. Meyer, Coord. Chem. Rev. 249 (2005) 457.
[52] L. Spiccia, G.B. Deacon, C.M. Kepert, Coord. Chem. Rev. 248 (2004) 1329.
[53] P.A. Anderson, F.R. Keene, T.J. Meyer, J.A. Moss, G.F. Strouse, J.A. Treadway, J. Chem. Soc., Dalton Trans. (2002) 3820.
[54] N.H. Damrauer, G. Cerullo, A.T. Yeh, T.R. Boussie, C.V. Shank, J.K. McCusker, Science 275 (1997) 54.
[55] D.P. Rillema, C.B. Blanton, R.J. Shaver, D.C. Jackman, M. Boldaji, S. Bundy, L.A. Worl, T.J. Meyer, Inorg. Chem. 31 (1992) 1600.
[56] J.V. Caspar, T.J. Meyer, J. Am. Chem. Soc. 105 (1983) 5583.
[57] H.D. Gafney, A.W. Adamson, J. Am. Chem. Soc. 94 (1972) 8238.
[58] I. Vass, S. Styring, Biochemistry 30 (1991) 830.
[59] M.-F. Charlot, Y. Pellegrin, A. Quaranta, W. Leibl, A. Aukauloo, Chem. Eur. J. 12 (2006) 796.
[60] B.-Z. Shan, Q. Zhao, N. Goswami, D.M. Eichhorn, D.P. Rillema, Coord. Chem. Rev. 211 (2001) 117.
[61] L.D. Ciana, I. Hamachi, T.J. Meyer, J. Org. Chem. 54 (1989) 1731.
[62] N. Garelli, P. Vierling, J. Org. Chem. 57 (1992) 3046.
[63] D.G. McCafferty, B.M. Bishop, C.G. Wall, S.G. Hughes, S.L. Mecklenberg, T.J. Meyer, B.W. Erickson, Tetrahedron 51 (1995) 1093.
[64] C.G. Garcia, J.F.d. Lima, N.Y.M. Iha, Coord. Chem. Rev. 196 (2000) 219.
[65] G. Sprintschnik, H.W. Sprintschnik, P.P. Kirsch, D.G. Whitten, J. Am. Chem. Soc. 99 (1977) 4947.
[66] P.A. Andenon, G.F. Strouse, J.A. Treadway, F.R. Keene, T.J. Meyer, Inorg. Chem. 33 (1994) 3863.
[67] J.-P. Collin, R. Kayhanian, J.-P. Sauvage, G. Calogero, F. Barigelletti, A.D. Ciancand, J. Fischerc, Chem. Commun. (1997) 775.
[68] S. Fanni, T.E. Keyes, C.M. O'Connor, H. Hughes, R. Wang, J.G. Vos, Coord. Chem. Rev. 208 (2000) 77.
[69] D. Gust, A.L. Moore, A.L. Moore, Acc. Chem. Res. 34 (1996) 40.
[70] E. Danielson, M. Elliott, J.W. Merkert, T.J. Meyer, J. Am. Chem. Soc. 109 (1987) 2519.
[71] T.A. Moore, D. Gust, P. Mathis, J.-C. Mialocq, C. Chachaty, R.V. Bensasson, E.J. Land, D. Doizi, P.A. Liddell, W.R. Lehman, G.A. Nemeth, A.L. Moore, Nature 307 (1984) 630.
[72] K.A. Maxwell, M. Sykora, J.M. DeSimone, T.J. Meyer, Inorg. Chem. 39 (2000) 71.
[73] (a) R. Konduri, H. Ye, F.M. MacDonnell, S. Serroni, S. Campagna, K. Rajeshwar, Angew. Chem. Int. Ed. 41 (2002) 3185;
(b) M.-J. Kim, R. Konduri, H. Ye, F.M. MacDonnell, F. Puntoriero, S. Serroni, S. Campagna, T. Holder, G. Kinsel, K. Rajeshwar, Inorg. Chem. 41 (2002) 2471.
[74] M. Borgström, N. Shaikh, O. Johansson, M.F. Anderlund, S. Styring, B. Åkermark, A. Magnuson, L. Hammarström, J. Am. Chem. Soc. 127 (2005) 17504.
[75] P.A. Liddell, J.P. Sumida, A.N. MacPherson, L. Noss, G.R. Seely, K.N. Clark, A.L. Moore, T.A. Moore, D. Gust, Photochem. Photobiol. Sci. (1994) 60.
[76] D.M. Guldi, C. Luo, T.D. Ros, M. Prato, E. Dietel, A. Hirsch, Chem. Commun. (2000) 375.
[77] D. Kuciauskas, P.A. Liddell, S. Lin, S.G. Stone, A.L. Moore, T.A. Moore, D. Gust, J. Phys. Chem. B 104 (2000) 4307.
[78] M. Morisue, N. Haruta, D. Kalita, Y. Kobuke, Chem. Eur. J. 12 (2006) 8123.
[79] R. Ghanem, Y. Xu, J. Pan, T. Hoffmann, J. Andersson, T. Polıvka, T. Pascher, T. Styring, L. Sun, V. Sundström, Inorg. Chem. 41 (2002) 6258.
[80] F. Liu, G.J. Meyer, Inorg. Chem. 44 (2005) 9305.
[81] M. Grätzel, Nature 414 (2001) 338.
[82] J.R. Schoonover, D.M. Dattelbaum, A. Malko, V.I. Klimov, T.J. Meyer, D.J. Styers-Barnett, E.Z. Gannon, J.C. Granger, W.S. Aldridge, J.M. Papanikolas, J. Phys. Chem. A (2005) 109.
[83] S.N. Smirnov, P.A. Liddell, I.V. Vlassiouk, A. Teslja, D. Kuciauskas, C.L. Braun, A.L. Moore, T.A. Moore, D. Gust, J. Phys. Chem. A 107 (2003) 7567.
[84] T. Tsubomura, S. Enoto, S. Endo, T. Tamane, K. Matsumoto, T. Tsukuda, Inorg. Chem. 44 (2005) 6373.
[85] L. Sun, L. Hammarström, B. Åkermark, S. Styring, Chem. Soc. Rev. 30 (2001) 36.
[86] M. Sjödin, S. Styring, B. Åkermark, L. Sun, L. Hammarström, J. Am. Chem. Soc. 122 (2000) 3932.
[87] W. Ruttinger, G.C. Dismukes, Chem. Rev. 97 (1997) 1.
[88] J.M. Mayer, I.J. Rhile, Biochim. Biophys. Acta 1655 (2004) 51.
[89] J.M. Mayer, I.J. Rhile, J. Am. Chem. Soc. 126 (2004) 12718.
[90] F. Thomas, O. Jarjayes, H. Jamet, S. Hamman, E. Saint-Aman, C. Duboc, J.-L. Pierre, Angew. Chem. Int. Ed. (2004) 594.
[91] I.J. Rhile, J.M. Mayer, Angew. Chem. Int. Ed. 44 (2005) 1598.
[92] L. Benisvy, R. Bittl, E. Bothe, C.D. Garner, J. McMaster, S. Ross, C. Teutloff, F. Neese, Angew. Chem. Int. Ed. (2005) 5314.
[93] C. Costentin, M. Robert, J.-M. Savéant, J. Am. Chem. Soc. 128 (2006) 4552.
[94] M. Sjödin, T. Irebo, J.E. Utas, J. Lind, G. Merényi, B. Åkermark, L. Hammarström, J. Am. Chem. Soc. (2006).
[95] A.L. Gavrilova, B. Bosnich, Chem. Rev. 104 (2004) 349.
[96] S. Mukhopadhyay, S.K. Mandal, S. Bhaduri, W.H. Armstrong, Chem. Rev. (2004) 3981.
[97] I.J. Hewitt, J.-K. Tang, N.T. Madhu, R. Clérac, G. Buth, C.E. Ansona, A.K. Powell, Chem. Commun. (2006) 2650.
[98] A. Neves, S.M.D. Erthal, I. Vencato, A.S. Ceccato, Y.P. Mascarenhas, O.R. Nascimento, M. Hörner, A.A. Batista, Inorg. Chem. 31 (1992) 4749.
[99] O. Horner, E. Anxolabéhère-Mallart, M.-F. Charlot, L. Tchertanov, J. Guilhem, T.A. Mattioli, A. Boussac, J.J. Girerd, Inorg. Chem. 38 (1999) 1222.
[100] S.K. Chandra, P. Basu, D. Ray, S. Pal, A. Chakravorty, Inorg. Chem. 29 (1990) 2423.
[101] A. Magnuson, H. Berglund, P. Korall, L. Hammarström, B. Åkermark, S. Styring, L. Sun, J. Am. Chem. Soc. 119 (1997) 10720.
[102] F. Lachaud, A. Quaranta, Y. Pellegrin, P. Dorlet, M.-F. Charlot, S. Un, W. Leibl, A. Aukauloo, Angew. Chem. Int. Ed. 117 (2005) 1560.
[103] L. Sun, M.K. Raymond, A. Magnuson, D. LeGourriérec, M. Tamm, M. Abrahamsson, P.H. Kenéz, J. Martensson, G. Stenhagen, L. Hammarström, S. Styring, B. Åkermark, J. Inorg. Biochem. 78 (2000) 15.
[104] D. Burdinski, K. Wieghardt, S. Steenken, J. Am. Chem. Soc. 121 (1999) 10781.
[105] Y. Pellegrin, A. Quaranta, P. Dorlet, M.-F. Charlot, W. Leibl, A. Aukauloo, Chem. Eur. J. 11 (2005) 3698.
[106] E.M. McGarrigle, D.G. Gilheany, Chem. Rev. 105 (2005) 1563.
[107] L. Sun, H. Berglund, R. Davydov, T. Norrby, L. Hammarström, P. Korall, A. Börje, C. Philouze, K.E. Berg, A. Tran, M. Andersson, G. Stenhagen, J. Martensson, M. Almgren, S. Styring, B. Åkermark, J. Am. Chem. Soc. 119 (1997) 6996.
[108] M.L.A. Abrahamsson, H. Berglund Baudin, A. Tran, C. Philouze, K.E. Berg, M.K. Raymond-Johansson, L. Sun, B. Åkermark, S. Styring, L. Hammarström, Inorg. Chem. 41 (2002) 1534.
[109] B. Adam, E. Bill, E. Bothe, B. Goerdt, G. Haselhorst, K. Hildenbrand, A. Sokolowski, S. Steenken, T. Weyhermüller, K. Wieghardt, Chem. Eur. J. 3 (1997) 308.
[110] J. Müller, A. Kikuchi, E. Bill, T. Weyhermüller, P. Hildebrandt, L. Ould-Moussa, K. Wieghardt, Inorg. Chim. Acta 297 (2000) 265.
[111] A. Magnuson, Y. Frapart, M. Abrahamsson, O. Horner, B. Åkermark, L. Sun, J.-J. Girerd, L. Hammarström, S. Styring, J. Am. Chem. Soc. 121 (1999) 89.
[112] P. Huang, J. Högblom, M.F. Anderlund, L. Sun, A. Magnuson, S. Styring, J. Inorg. Biochem. 98 (2004) 733.
[113] P. Huang, A. Magnuson, R. Lomoth, M. Abrahamsson, M. Tamm, L. Sun, B. vanRotterdam, J. Park, L. Hammarström, B. Åkermark, S. Styring, J. Inorg. Biochem. 91 (2002) 159.
[114] A. Magnuson, P. Liebisch, J. Högblom, M.F. Anderlund, R. Lomoth, W. Meyer-Klaucke, M. Haumann, H. Dau, J. Inorg. Biochem. 100 (2006) 1234.

[115] A.S. Borovik, Acc. Chem. Res. 38 (2005) 54.
[116] S.-Y. Liu, D.G. Nocera, J. Am. Chem. Soc. 127 (2005) 5278.
[117] J.P. Collman, R.R. Gagne, C.A. Reed, W.T. Robinson, G.A. Rodley, Proc. Natl. Acad. Sci. U.S.A. 71 (1974) 1326.
[118] Y. Deng, C.J. Chang, D.G. Nocera, J. Am. Chem. Soc. 122 (2000) 410.
[119] C.J. Elsevier, J. Reedijk, P.H. Walton, M.D. Ward, J. Chem. Soc., Dalton Trans. (2003) 1869.
[120] T.J. Collins, Acc. Chem. Res. 35 (2002) 782.
[121] J.P. McEvoy, G.W. Brudvig, Chem. Rev. 106 (2006) 4455.
[122] H. Wolpher, P. Huang, M. Borgström, J. Bergquist, S. Styring, L. Sun, B. Åkermark, Catal. Today 98 (2004) 529.
[123] F. Rappaport, M. Guergova-Kuras, P.J. Nixon, B.A. Diner, J. Lavergne, Biochemistry 41 (2002) 8518.

VII. **Herrero, Christian; Quaranta, Annamaria; Leibl, Winfried; Fallahpour, Reza; Aukauloo, Ally.** Photoinduced Oxidation of a Manganese Terpyridine Complex. Laser Flash Photolysis and EPR studies. ***In preparation***.

Photoinduced Oxidation of a Manganese Terpyridine Complex. Laser Flash Photolysis and EPR studies.

Christian Herrero[1,2], Annamaria Quaranta[2], Winfried Leibl[2], Wlliam A. Rutherford[2], Reza Fallahpour[3], Ally Aukauloo[1,2]

[1] *Institut de Chimie Moléculaire et des Matériaux d'Orsay, UMR-CNRS 8182, Université de Paris-Sud, F-91405 Orsay, France. E-mail: aukauloo@icmo.u-psud.fr*

[2] *Laboratoire de Photocatalyse et Biohydrogène, CEA, iBiTecS, URA2096, Gif-sur-Yvette, F-91191, France.*

Abstract

We develop synthetic molecular mimics with the final goal to perform the water oxidation reaction carried out by Photosystem II. The supramolecular complexes contain modules that are able to undergo light-induced charge separation, electron transfer, and accumulation of oxidising/reducing equivalents, simulating therefore the main events of photosynthesis. A prototypal model contains a photoactive component covalently linked through a spacer to a cavity where a metal ion is located. The photosensitiser used is a $[Ru(bipy)_3]^{2+}$ (bipy = 2,2'-bipyridine) analogue, a counterpart to P_{680}, which absorbs light in the visible region (450 nm) via a MLCT state, and triggers an electron transfer process by interaction with a sacrificial electron acceptor. The resulting Ru^{III} species has a reversible oxidation potential of 1.3 V *vs.* SCE, comparable to that of $P680^+$, and is capable in principle of oxidizing a Mn cluster and ultimately water. In this paper, the charge accumulator unit is a Mn complex with terpyridine

coordination cavity, precursor of Mn di μ-oxo dimers which have been reported to catalyse the oxidation of water into molecular oxygen. To date this reaction has been driven by the addition of highly oxidising agents, it is our aim to power this reaction using light energy. Electrochemical and photophysical studies coupled to EPR data are reported in order to characterize the light driven intramolecular electron transfer processes.

Introduction

Photosynthesis deals with the capture of sunlight and its conversion to chemical energy. In order to accomplish this Nature has developed two photosystems, PSII and PSI that use sunlight to oxidize water and to provide the reducing equivalents (NADPH) needed to fix carbon dioxide in the form of sugars. In what is known as the donor side of the photosynthetic electron transfer chain, PSII provides the system with the necessary reducing equivalents by stripping four electrons and four protons from water and releasing oxygen as a by-product. From a conceptual point of view, this enzyme can be considered as made up of a photoactive part and a catalytic unit. It's functioning is triggered when a photon strikes the photosynthetic antenna, and, after a cascade of energy transfer processes, the excitation energy reaches the primary donor ($P_{680} \rightarrow P_{680}^{*}$), where P680 is a Chl species. This excited chromophore donates an electron to a nearby pheophytin, a process which yields the highly oxidizing radical cation P_{680}^{+} (1.30 V *vs* SCE), which is capable of oxidising a nearby tyrosine, which in turn oxidises the manganese cluster known as Oxygen Evolving Complex (OEC). After four such cycles ($S_0 \rightarrow S_4$), the manganese cluster stores enough oxidising equivalents to transform water into molecular oxygen. Interest in the above mentioned processes have driven the research field of artificial photosynthesis which aims to use light and water as the sole ingredients needed in order to provide alternate, clean sources of energy. A minimalist synthetic model of PSII

would therefore be composed of a photoactive chromophore and a molecular catalyst for water oxidation, with the energy needed to power the catalyst coming from light, and the source of electrons being water.

Several manganese-based complexes have been reported to catalyse water oxidation. Amongst these, manganese cubanes[1], di μ-oxo manganese terpyridines[2], di-manganese polypyridil complexes[3], and face to face Mn oxo porphyrins[4]. All these molecules need large excesses of very strong external oxidizing agents in order to work, and in most cases the mechanisms as well as the origin of the oxygen atoms involved in O_2 formation are unknown. It would be very interesting from an artificial photosynthesis point of view to link any of these working catalysts to a chromophore that could provide the oxidative power needed to drive these reactions, and thus replacing the chemical oxidants. There have been several attempts to link ruthenium chromophores to different manganese containing ligands[5-10]. And although to date none of these complexes has been shown to be an active water oxidation catalyst, very important advances have been achieved towards the improvement of synthetic techniques, intermediate identification, and the understanding of the metal-metal interactions.

In this paper we report the synthesis of Ruthenium-Manganese constructs based on published water oxidation catalysts. The architecture of these molecules is made up of a ruthenium-based chromophore covalently linked to a terpyridine ligand through an imidazole linkage. The photosensitizer acts as the P_{680} counterpart, capable of harvesting light and triggering an electron transfer cascade. The Ru^{III} species resulting from oxidative quenching of the MLCT state is capable of initiating the processes leading to the oxidation of a Mn^{II} atom which is lodged in a terpyridine cavity.

The resulting Ruthenium-Terpyridine-$MnCl_2$ complex is a building block from which to build upon in order to arrive towards the ($terpy_2Mn_2$ (III-IV) di μ-oxo) complexes. These molecules resemble a higher oxidation state in the Kok S-cycle, and in principle, could be

photochemically driven towards the high oxidation states of manganese state needed to oxidize water.

2. Experimental

2.1. Synthesis and characterisation

The organic skeleton of the target molecule presents two potential metal binding sites. These include i) a 1,10-phenanthroline group designed for binding ruthenium , and ii) a 2,2':6',2''-terpyridine cavity where a second metal, in this case manganese is inserted. Pheneanthroline groups are used fortheir known ability to leave the ligand field around ruthenium unperturbed and therefore not change the photochemical properties of the chromophore. Terpyridines present a typical metal binding domain with three near co-planar nitrogen donor atoms (N_3) in which metal atoms can be coordinated, as well as serve as building blocks for the higher oxidation state manganese clusters mentioned above.

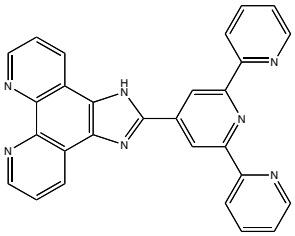

Given these two potential coordinating sites of our target ligand, the synthetic pathway whereby the ligand is prepared prior to metallation was discarded to avoid undiscriminating metallation processes. In order to circumvent this problem, we have used a synthetic procedure where a metal complex serves as a starting molecular platform from where we can initiate the synthetic build-up of the target molecules. The main synthetic requirement is a highly inert complex that will undergo neither demetallation nor ligand exchange under the reaction conditions. In this sense, low spin ruthenium(II) complexes are good candidates.

Therefore ruthenium(II) heterolyptic cores ($[Ru(bpy)_2(phendione)]^{2+}$, and [Ru(ethyl ester-$bpy)_2(phendione)]^{2+}$ complexes) were prepared, containing either bipyridines or ester modified bipyridines, with a coordinated phendione ligand serving as the synthetic handle. These complexes were then reacted with 4'-formyl terpyridine in refluxing acetic acid and in presence of an excess of ammonium acetate. After purification through column chromatography, the target mononuclear ruthenium(II) salts were isolated in good yields. Insertion of the manganese(II) ion in the terpyridine cavity was performed following modified literature procedures[11].

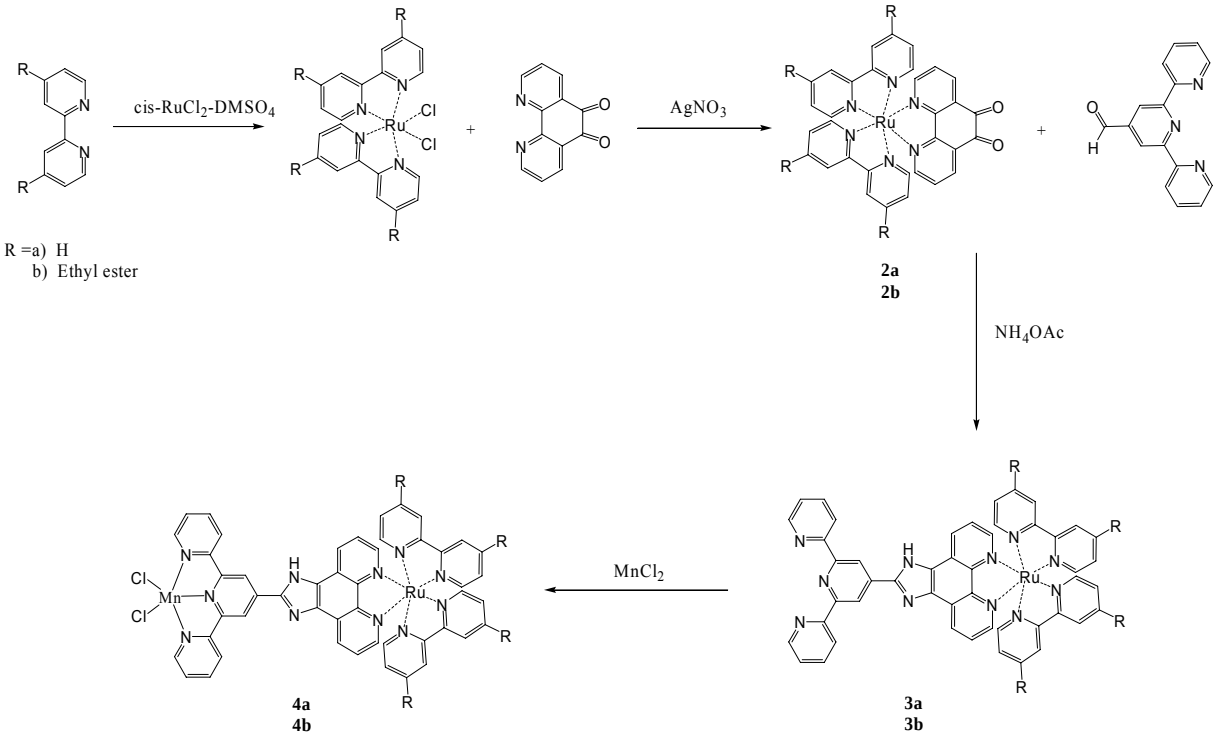

The bipyridine ligands as well as the Ru (bipyridine$_2$) Cl_2 were synthesised following modified literature procedures.

Ruthenium Phendione (2a). 484 mg of Ru-bipyridine dichloride (1 mmol, 1 eq) were reacted with 338 mg of silver nitrate (2 mmol, 2 eq) in methanol for 2 hours. The solution was filtered in order to remove the silver salt, and the filtrate was evaporated under reduced pressure. The solid was re-dissolved in ethanol and one equivalent of phendione (1) (210 mg,

1 mmol) was added. The solution was refluxed in the dark for three hours. At this time the solvent was evaporated, the remaining solid re-dissolved in a minimum amount of methanol, and the desired compound was precipitated by drop wise addition of a saturated aqueous solution of sodium hexafluorophosphate (275 mg, 44%). H^1 NMR. (400 MHz, δ, DMSO): 8.85 (d, J= 8.0 Hz, 4H, H_4), 8.54 (d, *J*=7.68 Hz, 2H, H_c), 8.21-8.16 (m, 4H, H_3), 7.94 (d, *J*=5.6 Hz, 2H, H_a), 7.75-7.74 (dd, *J*=8.9 Hz, 4H, H_1), 7.70-7.68 (dd, J = 5.7 Hz, 2H, H_B), 7.57-7.52 (m, 4H, H_2). MS (ESI) = 312.1 $[M]^{2+}$, 624.1 $[M]^+$, 769.1 $[M+PF_6]^+$.

[Ru[((ethyl ester)$_2$ bpy)$_2$Phendione]$^{2+}$ (2b). Synthesis of this compound was done following the above procedure using 4, 4' diethyl ester bipyridine. (65% yield).H^1 NMR. (400 MHz, δ, DMSO): 9.34 (d, J= 8.0 Hz, 4H, H_4), 8.58 (d, *J*=7.68 Hz, 2H, H_C), 8.00-7.92 (m, 4H, H_1.H_2), 7.80 (d, *J*=5.6 Hz, 2H, H_A), 7.70-7.68 (dd, J = 7.6 Hz, 2H, H_B), 4.45 (q, J = 7.1 Hz, 8 H, *CH_2*-H), 1.39 (t, J = 7.5 Hz, 12H, *CH_3*-H)**.** MS (ESI) = 456.1 $[M]^{2+}$, 912.2 $[M]^+$.

Ru-Im-Tpy (3a). Ru-phen-terpy (3) was synthesised as follows. 83.78 mg of terpyridine-4' carbaldehyde (.321 mmol, 1 eq) were reacted with 200 mg Ru-phendione (2) (321 mmoles, 1 eq) in 10 mls acetic acid. The mixture was heated to 80°C for thirty minutes. At this time 495 mg of dry ammonium acetate (6.42 mmol, 20 eq) were added and the reaction mixture was heated in the dark at 100°C for 12 hours. The solvent was evaporated under reduced pressure and redisolved in a minimum amount of MeOH. An aqueous solution of $NaPF_6$ was added dropwise and the resulting precipitate was filtered, washed with cold MeOH and dried under vacuum. The reaction afforded 224 mg of product, 81% yield.

H^1 NMR. (400 MHz, δ, DMSO): 9.39 (s, 2H, terpy-H), 9.27 (d, *J*=8.3 Hz, 2H, terpy-H), 8.91-8.87 (m, 4H, bpy-H), 8.87 (d, *J*=8.0 Hz, 2H, phen-H), 8.76 (d, *J*=7.5 Hz, 2H, terpy-H), 8.26-8.19 (m, 4H, bpy-H), 8.15-8.08 (m, 4H, bpy-H), 8.07 (t, *J*=7.5 Hz, 2H, terpy-H), 8.01 (dd, *J*=8.7, 8.3 Hz, 2H, phen-H), 7.67 (t, *J*=7.2 Hz, 2H, terpy-H), 7.65-7.58 (m, 4H, bpy-H),

7.32 (d, *J*=7.8 Hz, 2H, phen-H). ESI-MS yields mono charged peaks at 1011.1 m/z, $[M\text{-}PF_6^-]^+$, 864.2 m/z, $[M\text{-}H]^+$, and a doubly charged peak at 432.7 m/z, $[M\text{-}H]^{2+}$.

Ru-Im-Tpy-Mn (4a). Compound 3 (52 mg, 0.060 mmol, 1 eq) was dissolved in a minimal amount of acetonitrile. To this solution, 75 mg of $MnCl_2$ (0.60 mmol, 10 eq) dissolved in a minimal amount of MeOH were added and the solution was stirred in the dark under an Ar atmosphere at room temperature. The precipitate formed was filtered, washed with MeOH and ether. The resulting red/orange powder was redissolved in MeOH and precipitated by adding a couple drops of a saturated aqueous NH_4PF_6 solution. This mixture was filtered, washed with MeOH and ether, and dried under vacuum. The reaction yielded 46 mg of product. (77 % yield). ESI-MS = 955 $[M\text{-}Cl]^+$.

Ester Ru-Im-Tpy (3b). Synthesis of this compound was done by reacting terpyridine-4' carbaldehyde and 2b following the same procedure as for 3a.

H^1 NMR. (400 MHz, δ, DMSO):9.34 (m, 4H, bpy-H), 9.20 (m, 2H, terpy-H), 8.84 (d, J= 5.58 Hz, 2H, Phen-H), 8.75 (d, J=7.75 Hz, 2H, terpy-H), 8.65 (m, 4H, bpy-H), 8.26 (d, J= 7.72 Hz, 2H, Terpy-H), 8.11 (m, 2H, terpy-H), 7.97(m, 2H, phen-H), 7.87 (s, 4H, bpy-H), 7.73(t, J = 7.53 Hz, 2H, phen-H), 7.51(m, 2H, terpy-H), 4.45 (q, J = 7.1 Hz, 8 H, CH_2-H), 1.39 (t, J = 7.5 Hz, 12H, CH_3-H). ESI-MS = 576.2 $[M]^{2+}$.

Ester–Ru-Im-Tpy-Mn (4b). The same procedure as for compound (4a). (64 % yield). ESI-MS = 1242.0 $[M\text{-}Cl]^+$.

Material and methods

Acetonitrile and methanol (Aldrich,) were HPLC grade. Methylviologen (Aldrich) and $[Co^{III}(NH_3)_5]^{3+}$(Aldrich) were used as received. Tetrabutyl ammonium perchlorate (Aldrich)

was used as electrolyte in electron transfer experiments as well as for electrochemical measurements.

Physical Measurements: Absorption spectra were recorded on a Specord 210 (Analytic Jena) spectrophotometer. Values for the molar extinction coefficients (ε, M^{-1} cm^{-1}) were obtained from Beer-Lambert plots by varying the sample concentration between 10 and 250 μM. Linear regressions were obtained for all samples in this concentration range.

Luminescence spectra were recorded on a Varian Cary Eclipse spectrofluorimeter. Samples were purged with Argon for 10 minutes prior to measurements. Luminescence quantum yields (Φ_L) were obtained for optically-matched, diluted ($A(\lambda_{exc}) < 0.1$) solutions with excitation at 460 (MLCT maximum) and 532 nm (laser excitation wavelengths) by averaging different measurements and using $[Ru(bpy)_3]^{2+}$ as reference (ref). Emission lifetimes were measured using a frequency-doubled nanosecond Nd/YAG laser (532 nm, duration 7 ns, 2 $mJcm^{-2}$, Quantel). The detection wavelengths were selected by interference filters (610 or 650 nm, ~10 nm width) and signals were detected with a micro channel plate photomultiplier tube (R2566U, Hamamatsu) and recorded by a digital oscilloscope (TDS 744 A, Tektronix). For flash-absorption transients the measuring light was provided by a 450 W xenon lamp equipped with a pulsing unit. The wavelength was selected with a monochromator (Czerny-Turner) placed after the 10 x 10 mm sealed cuvette containing the sample. The sample was excited at 90° to the measuring beam by a flash from a frequency-tripled Nd/YAG laser (Surelite, Continuum) equipped with an OPO (SLOPO, Continuum). Excitation was set at 460 nm (duration 5 ns, 2 mJ cm^{-2}). Absorbance changes were detected with a silicon photodiode and signals were amplified by a wideband preamplifier (model 5185, EG&G) before recording by a digital oscilloscope (TDS 3034B, Tektronix).

Cyclic voltammetry was performed with a potentiostat-galvanostat using a 3 mm^2 surface glassy carbon electrode. Acetonitrile was distilled prior to each experiment and the

solution (1 mM for the complexes, 0.1 M of tetrabutyl ammonium perchlorate introduced in an Argon purged electrochemical cell. The experiments were performed at room temperature using a glassy carbon electrode as the working electrode, a platinum wire as the counter electrode, and a $Ag/AgClO_4$ (0.01 M) electrode in acetonitrile as the reference electrode (+0.292 V vs. SCE).

Mass Spectra were recorded on a Finnigan MAT95S in a mixture of CH_2Cl_2/MeOH/H_2O (1/1/1).

Nuclear magnetic resonance experiments were performed on a Bruker 400 …..

X-band electron paramagnetic resonance spectra were recorded on a Bruker 300 spectrometer at 5° K with the following parameters: microwave 3 mW, modulation amplitude 25 G, time constant 80 ms, and modulation frequency 100 kHz. Photodriven oxidation of **4a** and **4b** were performed by mixing the required Ruthenium compounds (0.5 mL, 1 mM) with $[Co(NH_3)_5Cl]Cl_2$ (2.5 mL, 20 mM) resulting in solutions 0.17 mM in Ruthenium complex and 17 mM in electron acceptor. The samples were degassed with Argon and the solutions were placed under illumination with a 250 W lamp for 10 min with both infrared and UV (400 nm) cut off filters. After this time 100 μL aliquots were transferred in an EPR tube which was immediately immersed into liquid nitrogen for further analysis.

3. Results and Discussion

3.1. Electrochemistry. The redox potentials for compounds **3a** and **4a** (also noted as Ru-Im-Tpy and Ru-Im-Tpy-Mn respectively in the text) and **3b** and **4b** (also noted as Ester-Ru-Im-Tpy and Ester-Ru-Im-Tpy-Mn respectively in the text) were obtained in CH_3CN and 0.1 M $TBAPF_6$ and are given in Table 1. All samples exhibit typical cyclic voltammogram of

ruthenium(II) polypyridine type complexes. Compound **3a** shows two oxidation waves Figure 1). First, a one-electron oxidation around 1.30V vs SCE attributed to $Ru^{III/II}$ couple, followed by another oxidation wave at 1.25V that is attributed to the oxidation of the imidazole moiety. On the cathodic side there are three one-electron reductions from -1.41 to -1.96 V corresponding to the sequential reduction of the bipyridines coordinated to the ruthenium atom. The ester modified compound **3b** exhibits a one electron oxidation for the RuII/RuIII process at 1.51 V, no wave for the oxidation of the imidazole, and three one electron reductions spanning from -1.01 to -1.73 V. The shift towards more positive values for this compound (~200 mV) can be explained by the electron withdrawing property of the ester groups which renders the ruthenium harder to oxidise and concomitantly the bipyridine groups more prone to reduction. It is to be noted that in this case a Ru(III) intermediate with higher oxidizing power can be generated. Upon insertion of manganese, the resulting bimetallic complexes **4a-4b**, show an additional quasi-reversible peak at 1.09 and 1.11V vs. SCE respectively. This wave is assigned to the one electron oxidation of the Mn(II) ion, and seems to be independent of the electrochemical behaviour of the ruthenium centre as only a 2 mV difference is observed for the manganese oxidation process between the two bimetallic derivatives (4a and 4b)

Insert Figure 1 here

Table 1 : Electrochemical Data for complexes **3a-4a** and **3b-4b**.

3.2. Spectroscopic characterisation

The UV-visible absorption spectra of **3a-b** and **4a-b** in acetonitrile (Figure 2) show that the spectral morphology of the Ru-Im-Tpy complex is comparable to the one of the parent $[Ru(bpy)_3]^{2+}$ compound in that both the π-π* transitions at around 280 nm and the double-hump metal to ligand charge-transfer (MLCT) transitions peaking at 450 nm are present. Additionally a broad band at 320 nm is observed for the Ru-Im-Tpy complex, which can be assigned to an intra ligand charge-transfer transition. Insertion of Mn(II) ion in the terpyridine cavity modifies the absorption spectrum. The ligand centred band at 280 nm is strongly reduced while a new band is observed at 350 nm. This band probably originates also from charge-transfer transitions within the extended π-delocalised ligand but modified by the presence of the Mn(II) ion. The MLCT band at 450 nm is slightly reduced in intensity while tailing up to 600 nm. For the Ester-Ru-Im-Tpy derivative, the absorption spectrum exhibits a broad and red-shifted peak in the UV (308 nm), an enhanced charge-transfer band at 350 nm and more noticeably a broader and red-shifted MLCT band whose maximum occurs at 475 nm. Metallation of the terpyridine cavity with manganese leads to a strong reduction in intensity of the electronic absorption spectrum.

Insert Figure 2 here

The Ru-Im-Tpy luminescence excitation profile (Fig. 3a) reproduces the absorption spectrum in the region characterised by MLCT transitions (370 - 550 nm), whereas in the case of the dinuclear complex (Fig. 3b), the superposition of the excitation and the absorption spectra reveals pronounced differences in this region indicating the presence of other transitions close in energy not contributing to luminescence emission.

Insert Figure 3 here

Upon excitation at 460 nm in acetonitrile, Ru-Im-Tpy and Ru-Im-Tpy-Mn exhibit emission bands with maxima at 620 nm and 614 nm respectively as compared to 611 nm for the parent $[Ru(bpy)_3]^{2+}$ complex (Table 2). The Ester-Ru-Im-Tpy analogue exhibits a ~ 30 nm red shift of the emission band, with a maximum at 650 nm. The observed red-shift in the optical transitions, is a result of a decrease in the HOMO-LUMO gap, due to the electron withdrawing character of ester groups which lowers the energy of the π antibonding orbitals. (B.-Z. Shan et al, *Coord Chem Rev* 211 (2001) 117-144).

Insert Table 2??

In order to determine the emission quantum yields, reported in Table 2, the area underlying the curves was compared for the different compounds, using $[Ru(bpy)_3]^{2+}$ as reference. Data in methanol are also reported for comparison. Interestingly, complex **3a** exhibits an enhanced luminescence quantum yield as compared to $[Ru(bpy)_3]^{2+}$. The time-resolved luminescence decay data confirm the trend found by steady-state measurements. The recorded lifetimes for Ru-Im-Tpy and Ester-Ru-Im-Tpy are 1.65 μs and 1.60 μs respectively, nearly twice as long as the lifetime for $[Ru(bpy)_3]^{2+}$ (860 ns; in acetonitrile). These results indicate that one or more deactivating processes in competition with radiative decay are less favoured in these complexes than in $[Ru(bpy)_3]^2$.//can we be a bit more specific saying eg. that nonradiative desactivation via the MC state is less efficient most likely due to (partly?) the decreased level of the MLCT?// The photophysical behaviour is different when Mn(II) is present in the terpyridine cavity. Indeed, the emission lifetimes are biphasic for both Ru-Im-Tpy-Mn and ester-Ru-Im-Tpy-Mn complexes with a main, short-lived (50 -120 ns) and a small, long-lived

component (0.7-1 μs) in acetonitrile. The origin of these two emitting states//unlikely that there are two emitting states with the same energy (wavelength of emission). replace by "this biphasic behaviour"?// is unclear. It can probably be excluded that the long-lived components originate from impurities due to de-coordination of Mn from the Tpy cavity since the lifetimes do not correspond to the lifetime of parent molecules Ru-Im-Tpy and Ester-Ru-Im-Tpy. Further studies, for instance dependence on temperature and on solvent polarity, are in progress to elucidate the origin of the biphasic decay.

The transient absorption spectra upon excitation at 460 nm for complexes Ru-Im-Tpy and Ester-Ru-Im-Tpy are similar to those of $Ru(bpy)_3$ and characterised by a depletion of the MLCT ground state absorption band and by a weak absorption in the visible, extending in near IR region (data not shown). Due to the predominance of short lifetime of the excited state for the Ru/Mn dinuclear complexes, the detectable absorption transients were very weak.

3.3. Photoinduced electron transfer

The emission lifetime observed for Ru-Im-Tpy in presence of the electron acceptor MV^{2+} plotted as function of MV^{2+} concentration, gives a bimolecular rate constant of 2×10^9 M^{-1} s^{-1} (see Supplementary Information). In Figure 4, the kinetic traces of absorption changes at 450 and 605 nm are presented for the four complexes studied. These wavelengths are the spectroscopic probes for the recovery of the photogenerated Ru^{III} to Ru^{II} and the presence of the reduced state of the electron acceptor, $MV^{\bullet+}$, respectively.

Insert Figure 4 here

For Ru-Im-Tpy, the depletion signal at 450 nm exhibits a shorter lifetime than the methylviologen radical ($MV^{\bullet+}$), supporting the fact that the reduction of Ru^{III} to Ru^{II} is faster ($k = 5 \times 10^4\ s^{-1}$) than the re-oxidation of $MV^{\bullet+}$ to MV^{2+} (k=??). Thus the metal centred reductive process is due to an intramolecular electron transfer resulting in the oxidation of the imidazole ring. This scenario is also supported by the electrochemical data where a redox wave for the Im/Im^+ transition is observed prior the $Ru^{III/II}$ couple. //a work about the slow rate (compared to Ru-Imi-phenyl) proably related to the small driving force??//

Surprisingly, in the case of the Ester-Ru-Im-Tpy derivative, both kinetic traces at 450 and 605 nm decay simultaneously implying that both the oxidised Ru(III) and the methyl viologen radical recover to their initial oxidation states through a bi-molecular electron transfer process ($k = 8 \times 10^3\ s^{-1}$). The fact that no oxidation wave of the imidazole ring is observed on the cyclic voltammogram for the Ester-Ru-Im-Tpy complex supports this interpretation of absence of intramolecular electron transfer. As discussed before, this shift of the Im/Im^+ potential might be due to the inductive effect of the ester groups. As both the ligands//??// and the ruthenium moieties become more electron deficient, the imidazole group does as well, and therefore it is impossible for the Ru(III) to oxidise the ligand.//but the increase in Imi potential must be more important than the increase in Ru otherwise oxidation should still be possible//

To confirm these observations and to identify the seat of oxidation, EPR spectra in presence of an irreversible electron acceptor, $[Co^{III}(NH_3)_5]^{3+}$ were recorded. These experiments showed that upon illumination of the complex 3a, the resulting Ru(III) species is capable of oxidising the ligand. Proof for this process is the appearance of an organic radical-like signal around g = 2.01, and the concomitant appearance of a low field band due to the reduced Co(II) species. A similar experiment using 3b did not yield any indication of this process happening//but was CoII observed??//. //Are these experiments shown in a figure?? if not : data not shown, else make reference!//

For both dinuclear complexes 4a and 4b the reduction of the MV^{2+} electron acceptor is accompanied by an oxidation on the ligand (Fig. 4) and in this case, as indicated by the electrochemical data, Mn should be the locus of oxidation. In the case of 4a???, the formation of $MV^{\bullet+}$ is very fast (τ = 50 ns) and the initial spike due to the transition $[Ru^{III}L^{-}]^{2+} \rightarrow [Ru^{III}L]^{3+}$ could not be resolved on the long timescale.//I would put this in the figure legend or a footnote// For the complex 4b, oxidation of the ligand appears to be significantly faster than for complex 4a (k = 2 x 10^4 s^{-1} compared to k = 7 x 10^3 s^{-1}). The faster rate observed for the $Ru^{III}Mn^{II}$ -> $Ru^{II}Mn^{III}$ reaction in presence of the ester groups can be explained by the increased driving force which, taking the electrochemical data (Table 1) for a first approximation, is more favourable by about 200 mV in the case of 4b.

EPR measurements performed on the bimetallic Ru-Mn complexes (Fig. 5) show the change undergone by a mixture of cobalt(III) pentamine and 4a and 4b in the dark (blue line), and after exposure to light (red line). Mn(II) complexes are paramagnetic systems with spins 5/2 and exhibit characteristic EPR signals around g = 2.00. By contrast, the one-electron oxidised products, Mn(III) complexes, are diamagnetic and therefore silent under standard EPR conditions. On the contrary, Cobalt (III) compounds are EPR silent while their reduced counterparts exhibit strong transitions at low fields, and it is in this manner that we could follow the changes in the oxidation states of the bi-metallic complexes. The blue traces in Figure 5a and b show a strong band at g = 2.00 characteristic of Mn(II) for both compounds. After illumination of theses compounds with continuous light, the Mn(II) signal disappeared, with the concomitant appearance of a low field band corresponding to the reduced Co(II) species. (g = 4.44). We report this to be proof of restitution of the chromophore back to its original Ru(II) state by oxidation of the manganese ion. During the illumination period, no sign of appearance of multi-line signals arising from Mn-Mn dimer formation were observed.

Insert Figure 6 here

4. Conclusions

Several conclusions can be drawn from the work here presented. From a synthetic point of view, it is demonstrated that heteroleptic Ru moieties such as 2a and 2b can be used as synthetic building blocks for the development of supramolecular constructs. This becomes more important as the complexity of the molecules grows and we move towards bi-, or multi-metallic complexes because the amount of free coordination sites is reduced, and therefore consequent metallation processes become more selective. Furthermore, we have shown that the physical properties of the chromophores are easily modified by introduction of different substitution patterns on the bipyridine ligands of the ruthenium ion. In addition to modifying the electronic properties of the chromophore, such ester or carboxylic substitutions on the bpys may serve as anchoring groups for grafting of these molecules on surfaces, eg. nano crystalline TiO_2.

From the photochemical point of view, it is important to notice the strong quenching that the MLCT state on the ruthenium chromophore experiences upon insertion of manganese in the second site. This effect, previously described as an energy transfer process from ruthenium to manganese[7], very pronounced in the Ru-Im-Tpy-Mn compound 4a, can be reduced by addition of electron withdrawing groups (compound 4b). Increasing the metal-to-metal distance, by intercalating a phenyl group between the imidazole and the terpyridine bearing the manganese ion was found to be less efficient (data not shown). As far as electron transfer is concerned, we have evidenced by photophysical studies as well as by EPR experiments the

possibility to induce oxidation of Mn by the photoexcited Ruthenium chromophore in presence of an external electron acceptor

Acknowledgements

References

(1) Ruettinger, W.; Yagi, M.; Wolf, K.; Bernasek, S.; Dismukes, G. C. *Journal of the American Chemical Society* **2000**, *122*, 10353-10357.
(2) Limburg, J.; Vrettos, J. S.; Liable-Sands, L. M.; Rheingold, A. L.; Crabtree, R. H.; Brudvig, G. W. *Science* **1999**, *283*.
(3) Poulsen, A. K.; Rompel, A.; McKenzie, C. J. *Angewandte Chemie. Int. Ed* **2005**, *44*, 2-7.
(4) Shimazaki, Y.; Nagano, T.; Takesue, H.; Ye, B.-H.; Tani, F.; Naruta, Y. *Angewandte Chemie. Int. Ed* **2004**, *43*, 98 –100.
(5) Romain, S.; Baffert, C.; Dumas, S.; Chauvin, J.; Lepretre, J.-C.; Daveloose, D.; Deronzier, A.; Collomb, M.-N. *Dalton Trans.* **2006**, 5691–5702.
(6) Romain, S.; Lepretre, J.-C.; Chauvin, J.; Deronzier, A.; Collomb, M.-N. *Inorg Chem* **2007**, *46*, 2735−2743.
(7) Abrahamsson, M. L. A.; Baudin, H. B.; Tran, A.; Philouze, C.; Berg, K. E.; Raymond-Johansson, M. K.; Sun, L.; Akermark, B.; Styring, S.; Hammarstrom, L. *Inorganic Chemistry* **2002**, *41*, 1534−1544
.
(8) Huang, P.; H€ogblom, J.; Anderlund, M. F.; Sun, L.; Magnuson, A.; Styring, S. *Journal of Inorganic Biochemistry*
2004, *98*, 733-745.
(9) Huang, P.; Magnuson, A.; Lomoth, R.; Abrahamsson, M.; Tamm, M.; Sun, L.; Rotterdam, B. v.; Park, J.; Hammarstrom, L.; Akermark, B.; Styring, S. *Journal of InorganicBiochemistry* **2002**, *91*, 159-172.
(10) Burdinski, D.; Wieghardt, K.; Steenken, S. *Journal of the American Chemical Society* **1999**, *121*, 10781-10787.
(11) Chen, H.; Tagore, R.; Das, S.; Incarvito, C.; J. W. Faller; Crabtree, R. H.; Brudvig, G. W. *Inorg Chem* **2005**, *44*, 7661-7670.

Tables

Compound	$E_{1/2}$ $Ru^{III/II}$	$E_{1/2}$ Im/Im^{+}	$E_{1/2}$ $Mn^{III/II}$	$E_{1/2}$ Ligands	ΔG (eV)
Ru-Im-Tpy (3a)	1.33	1.25		-1.41, -1.61, -1.96	
Ru-Im-Tpy-Mn (4a)	1.30		1.09		-0.21
Ester-Ru-Im-Tpy (3b)	1.51			-1.01, -1.24, -1.73	
Ester-Ru-Im-Tpy-Mn (4b)	1.54		1.11		-0.43

Table 1

Table 2

Complex	Solvent[1]	λ_{max} / nm	Φ_L	A_1	τ_1 / ns	A_2	τ_2 / ns
$[Ru(bpy)_3]^{2+}$	ACN	610	0.059[2]	1	860	-	-
	MeOH	606	0.045[b]	1	740	-	-
	DMF		0.068[b]		860	-	-
Ru-Im-Tpy	ACN	618	0.073	1	1650	-	-
	MeOH	616	0.054	1	1400	-	-
	DMF	628			1370	-	-
ester-Ru-Im-Tpy	ACN	640	0.051	1	1600	-	-
	MeOH	647	0.0285	1	1140	-	-
Ru-Im-Tpy-Mn	ACN	617	0.003	0.85	50	0.15	1000
	MeOH	616	0.035	0.70	1200	0.30	40
ester-Ru-Im-Tpy-Mn	ACN	640	0.015	0.60	120	0.40	700
	MeOH	647	0.019	1	800	-	-0

[1] Donor Number (DN) for ACN ε = xx and DN= 14.1; for MeOH ε = xx and DN = 19/30; for DMF ε = xx and DN = 26.6 from Montalti *et al*, Handbook of Photochemistry, 2006.
[2] Balzani *et al.*, Coord. Chem. Rev., 1988

Figure legends

Figure 1 EC

Figure 2 UV-visible absorption spectra in acetonitrile for (a) $[Ru(bpy)_3]^{2+}$, Ru-Im-Terpy and Ru-Im-Terpy-Mn; and (b) $[Ru(bpy)_3]^{2+}$, ester-Ru-Im-Terpy and ester-Ru-Im-Terpy-Mn.

Figure 3 Absorption (gray) and luminescence excitation (black) spectra (emission wavelength: 610 nm) (a) for Ru-Im-Terpy and (b) Ru-Im-Terpy-Mn in acetonitrile.

Figure 4 Absorption kinetics at 605 nm (black) and at 450 nm (grey) in presence of MV^{2+} upon excitation at 460 nm. (a) RuTerpy (A_{460} = 0.39) + 10mM MV^{2+} in ACN/H_2O (90:10); (b) ester RuTerpy (A_{460} = 0.32) + 30 mM MV^{2+} in ACN/H_2O (70:30); (c) RuTerpyMn (A_{460} = 0.40) +100 mM MV^{2+} in ACN/H_2O (70:30); (d) ester RuTerpyMn (A_{460} = 0.42)+120 mM MV^{2+} in ACN/H_2O (60:40). Solution were purged with Argon for 15 minutes.

Figure 5 EPR

Figures

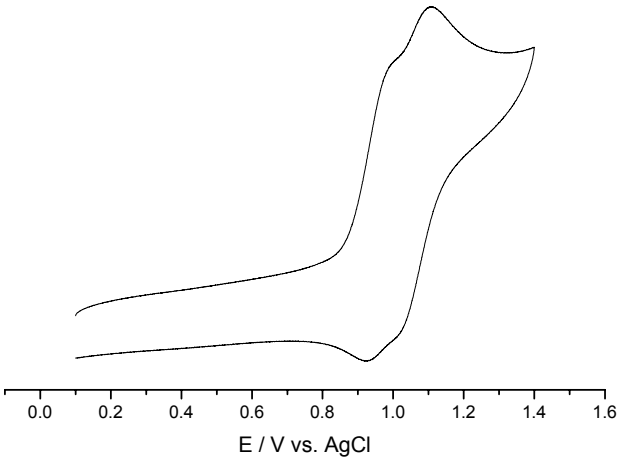

Figure 1

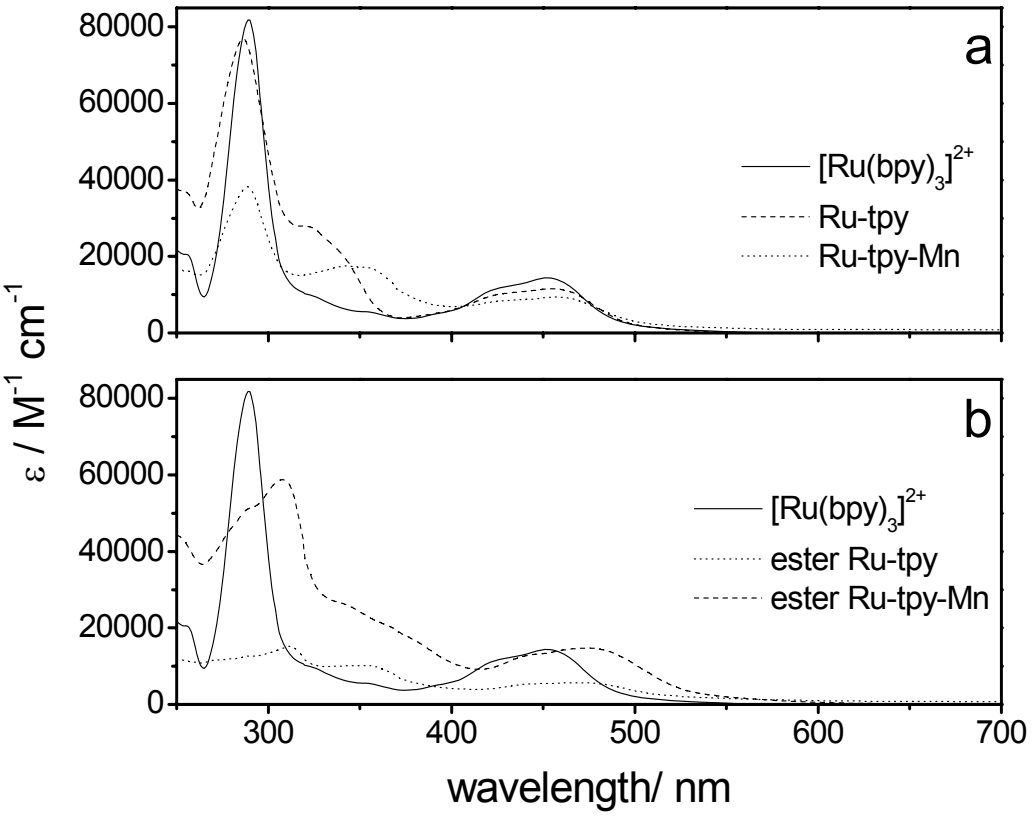
a
b
80000
60000
40000
20000
0
ε / M-1 cm-1
[Ru(bpy)3]2+
Ru-tpy
Ru-tpy-Mn
ester Ru-tpy
ester Ru-tpy-Mn
300
400
500
600
700
wavelength/ nm

Figure 2

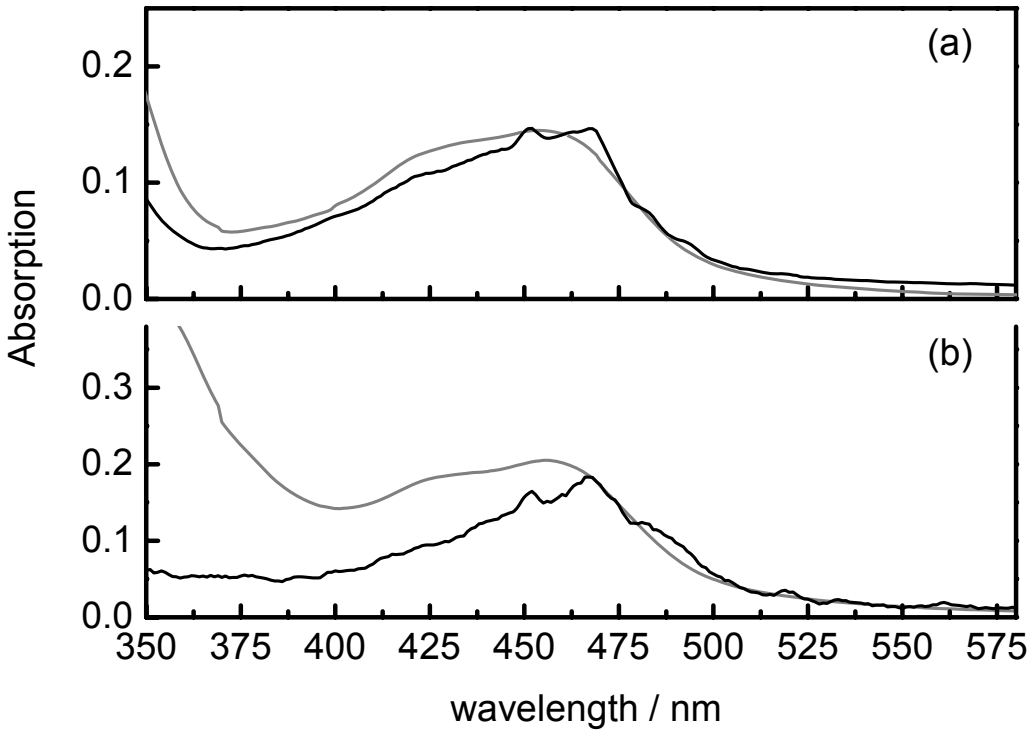
(a)
(b)
Absorption
0.0
0.1
0.2
0.3
350
375
400
425
450
475
500
525
550
575
wavelength / nm

Figure 3

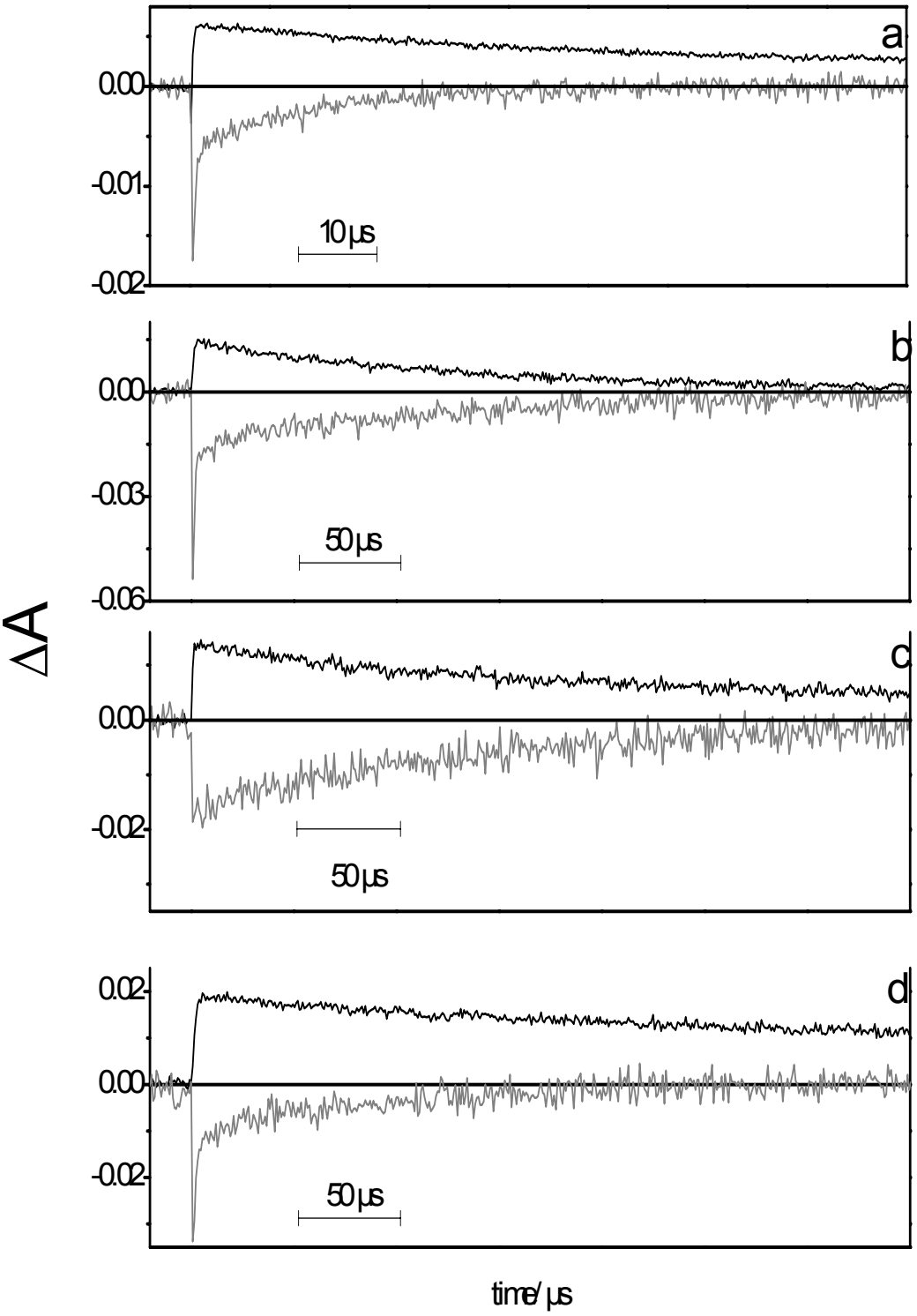
a
0.00
-0.01
-0.02
10 µs
b
0.00
-0.03
-0.06
50 µs
c
0.00
-0.02
50 µs
d
0.02
0.00
-0.02
50 µs
ΔA
time/ µs

Figure 4

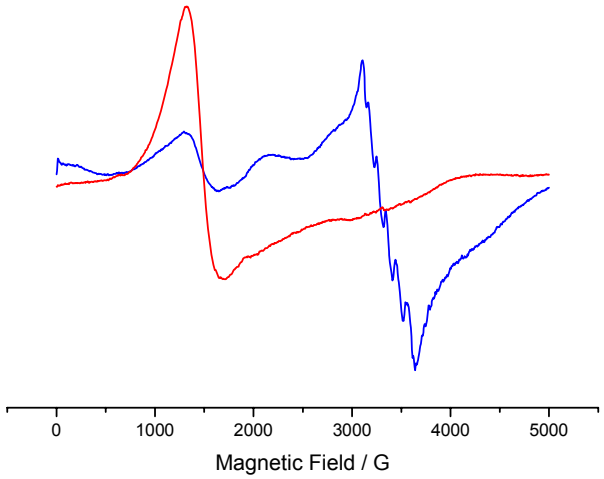
0
1000
2000
3000
4000
5000
Magnetic Field / G

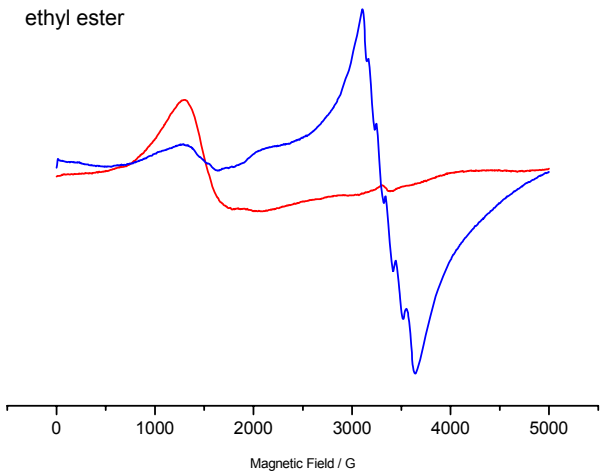
ethyl ester
0
1000
2000
3000
4000
5000
Magnetic Field / G

Fig. 5

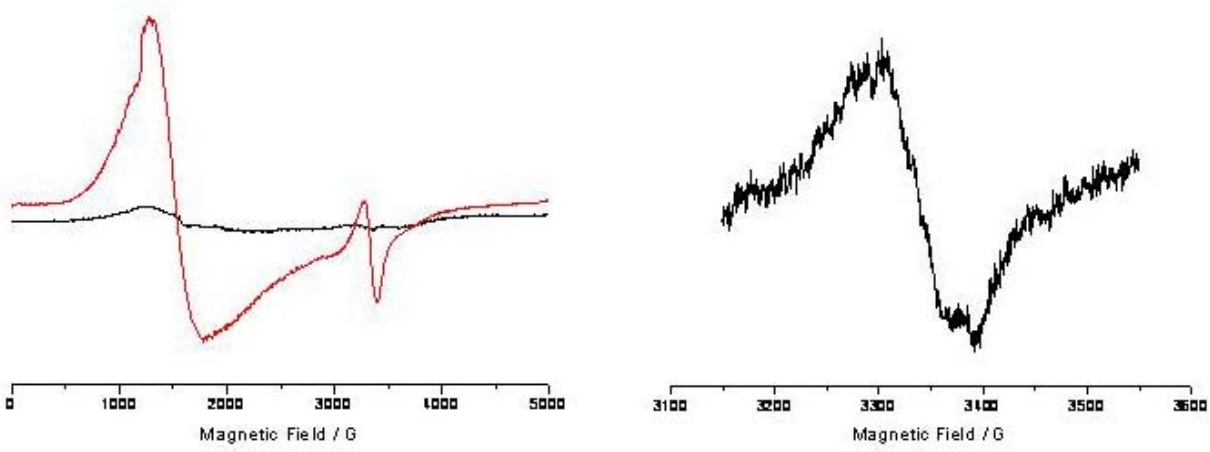
0
1000
2000
3000
4000
5000
Magnetic Field / G
3100
3200
3300
3400
3500
3600
Magnetic Field / G

Figure 6

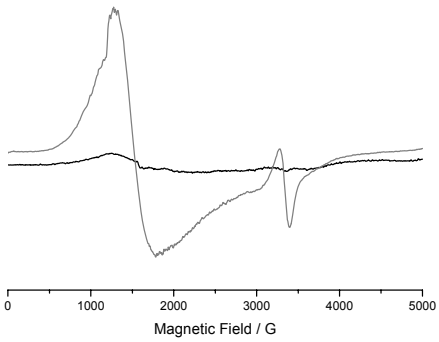
0
1000
2000
3000
4000
5000
Magnetic Field / G

Supplementary Information

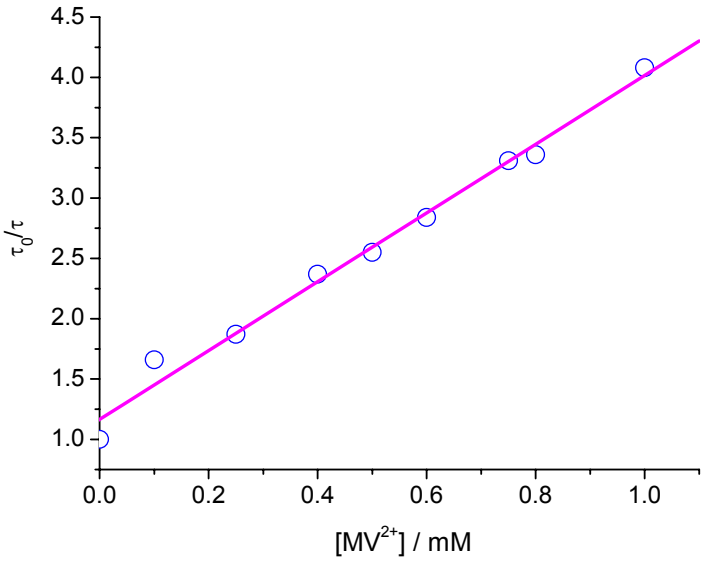

Stern-Vollmer Plot…..Rate constant for electron transfer between Ru-Tpy and MV2+

VIII. Quaranta, Annamaria; Lachaud, Fabien; Herrero, Christian; Guillot, Regis, Charlot, Marie-France; Leibl, Winfried; Aukauloo, Ally. **Influence of the Protonic State of an Imidazole-Containing Ligand on the Electrochemical and Photophysical Properties of a Ruthenium(II)–Polypyridine-Type Complex.** Chemistry. A European Journal. (2007), 13, 8201-8211.

DOI: 10.1002/chem.200700185

Influence of the Protonic State of an Imidazole-Containing Ligand on the Electrochemical and Photophysical Properties of a Ruthenium(II)–Polypyridine-Type Complex

Annamaria Quaranta,[a] Fabien Lachaud,[b] Christian Herrero,[a] Régis Guillot,[b] Marie-France Charlot,*[b] Winfried Leibl,*[a] and Ally Aukauloo*[a, b]

Abstract: The synthesis and characterisation of $[Ru(bpy)_2(PhenImHPh)]^{2+}$ where PhenImHPh represents the 2-(3,5-di-*tert*-butylphenyl)imidazo[4,5-*f*]-[1,10]phenanthroline ligand are described. The compounds issued from the three different protonic states of the imidazole ring $[Ru(bpy)_2(PhenImPh)]^{+}$ (**I**), $[Ru(bpy)_2(PhenImHPh)]^{2+}$ (**II**) and $[Ru(bpy)_2(PhenImH_2Ph)]^{3+}$ (**III**) were isolated and spectroscopically characterised. The X-ray structures of $[Ru(bpy)_2(PhenImPh)](PF_6)\cdot H_2O\cdot 6\,MeOH$, $[Ru(bpy)_2(PhenImHPh)](NO_3)_2\cdot H_2O\cdot 3\,MeOH$ and $[Ru(bpy)_2(PhenImH_2Ph)](PF_6)_3\cdot 5\,H_2O$ are reported. Electrochemical data obtained on these complexes indicate almost no potential shift for the $Ru^{III/II}$ redox couple. Therefore a Coulombic effect between the imidazole ring and the metal centre can be ruled out. The monooxidised forms of **I** and **II** have been characterised by EPR spectroscopy and are reminiscent of the presence of a radical species. The emission properties of the parent compound $[Ru(bpy)_2(PhenImHPh)]^{2+}$ were studied as a function of pH and both the lifetimes and intensities decreased upon deprotonation. Photophysical properties, investigated in the absence and presence of an electron acceptor (methylviologen), were distinctly different for the three compounds. Transient absorption features indicate that unique excited states are involved. Theoretical data obtained from DFT calculations in water on the three protonic forms are presented and discussed in the light of the experimental results.

Keywords: density functional calculations · imidazole · photophysical studies · protonic states · ruthenium

Introduction

Even after decades of intensive investigations, ruthenium(II)–polypyridine-type complexes (with $[Ru(bpy)_3]^{2+}$ as the prototype complex) are still opening new avenues in modern coordination chemistry and photochemistry. Indeed, the realms of this coordination metal complex core stem from its high chemical stability and its exceptional photophysical properties.[1,2] Domains extending from electron- and energy-transfer processes to molecular switches, are all based on the well known metal-to-ligand charge transfer (MLCT) transitions within this family of complexes.[3–8] A most important electronic feature of $[Ru(bpy)_3]^{2+}$ is that the lowest excited states are of metal-to-ligand charge transfer character. Upon irradiation in this absorption band, a long-lived excited state ($\approx$600 ns) is reached where the electronic distribution is best described as the presence of a Ru^{III} ion and one electron on the bpy ligands.[9–11] The fact that this state can be quenched through a bimolecular pathway, either by an electron acceptor to generate the highly oxidising Ru^{III} species or by an electron donor to give the formal reducing Ru^{I} form has prompted the use of $[Ru(bpy)_3]^{2+}$ complex as the promising candidate in the field of photoinduced electron transfer studies.[12–15] More sophisticated systems have been developed where this photoactive module was covalently linked to an electron acceptor or donor.

[a] Dr. A. Quaranta, C. Herrero, Dr. W. Leibl, Prof. Dr. A. Aukauloo
iBiTec-S, CEA Saclay, Bât. 532
91191 Gif-sur-Yvette Cedex (France)
E-mail: winfried.leibl@cea.fr
aukauloo@icmo.u-psud.fr

[b] F. Lachaud, Dr. R. Guillot, Dr. M.-F. Charlot, Prof. Dr. A. Aukauloo
Laboratoire de Chimie Inorganique
Institut de Chimie Moléculaire et des Matériaux
d'Orsay UMR CNRS 8182, Univ Paris-Sud
91405 Orsay Cedex (France)
E-mail: mcharlot@icmo.u-psud.fr

Supporting information for this article is available on the WWW under http://www.chemeurj.org/ or from the author.

These diads were elaborated to duplicate the early events in the conversion of light into chemical energy in the reaction centre of photosynthetic systems.[16] In doing so, chemists have overcome the diffusion limits between the donor and acceptor partners and have also gained a better control on the directionality of electron transfer from the donor to the acceptor side. Continuous research is devoted to fine tune both the intramolecular distance between the integrated modules and the nature of the organic spacer, which are crucial parameters for the control of electron transfer rates and understanding the pathways of the electron flow.

Our laboratory is involved in the development of molecular assemblies composed of a photoactive chromophore and a metal complex, the latter being capable of storing oxidative or reductive equivalents. En route towards these target systems, we have prepared and characterised different heteroditopic ligands.[17,18] Recently, we have reported on the synthesis of an imidazole–phenol containing ligand covalently linked to the $[Ru(bpy)_3]^{2+}$ chromophore as a biomimetic model of the His190/TyrZ pair of amino acid residues, which are involved in the catalytic cycle of light-driven water oxidation in photosystem II.[19] A photoinduced electron transfer to an external acceptor (MV^{2+}) was observed to generate the phenoxyl radical concomitantly to the reduction of the photogenerated Ru^{III}. Under identical experimental conditions, a rapid intramolecular reduction of the photogenerated Ru^{III} was evidenced for a related compound lacking the phenol function. It was suspected that in this case the imidazole ring fused to the phenanthroline was the electron donor site. As the imidazole ring is the connecting fragment in this organised assembly of components, we have been interested in elucidating the primary electrochemical and photophysical behaviour of the $[Ru(bpy)_2(PhenImHPh)]^{2+}$ (**II**) complex which contains only the lumophore and the spacer 2-[(3′,5′-di-*tert*-butylbenzene)]imidazo[4,5-*f*][1,10]-phenanthroline (PhenImHPh). Such a family of ligands has been used in the studies on the interaction between transition-metal complexes and DNA.[20–22]

In order to shed light on the influence of the protonic states of the imidazole ring on both the ground and excited states properties of the chromophore/spacer system, we have also isolated and characterised $[Ru(bpy)_2(PhenImPh)]^{+}$ (**I**) and $[Ru(bpy)_2(PhenImH_2Ph)]^{3+}$ (**III**); in the first compound, the secondary amino group is in the deprotonated state, while in the second the imino nitrogen of the imidazole ring is protonated (see below).

The parent compound $[Ru(bpy)_2(PhenImHPh)]^{2+}$ (**II**) and the corresponding deprotonated derivative, **I** and protonated form **III**, have been also characterised by X-ray diffraction technique. The photophysical properties for the three different protonic states were investigated in aqueous solutions at different pH and revealed distinct effects on functional properties of the ensemble. To rationalise the experimental results we will compare them with the theoretical data from DFT calculations obtained on the three water solvated protonic forms of $[Ru(bpy)_2(PhenImHPh)]^{2+}$.

Experimental and Theoretical Results

Synthesis: The ligand PhenImHPh was prepared following a well established imidazole synthetic procedure.[23] An equimolar mixture of phenanthrolinedione and 3,5-di-*tert*-butylbenzaldehyde were heated under reflux in glacial acetic acid containing an excess of ammonium acetate. The compound precipitated as a yellow powder upon cooling. Metathesis of the chloride ions from the $Ru(bpy)_2Cl_2$ source to nitrate ions was realised prior to metallation of the phenanthroline end of the ligand. A methanolic solution of the Ru^{II} salt was heated to reflux in the presence of the ligand. The target compound $[Ru(bpy)_2(PhenImHPh)](PF_6)_2$ was isolated upon addition of an excess of $NaPF_6$ in a concentrated solution of the reacting mixture and was purified by column chromatography on neutral alumina. The protonated form $[Ru(bpy)_2(PhenImH_2Ph)](PF_6)_3$ could be isolated by addition of a dilute solution of HNO_3 followed by an excess of $NaPF_6$ salt. The deprotonated form was isolated after treatment with sodium methoxide.

X-ray structures: The crystal structures of the three different protonated forms of the ruthenium complex were obtained. We summarise here the main crystallographic parameters. X-ray data revealed that the parent compound **II** is described with a chemical formula of $[Ru(bpy)_2(PhenImHPh)](NO_3)_2{\cdot}H_2O{\cdot}3\,MeOH$. An ORTEP view of the monomeric $[Ru(bpy)_2(PhenImHPh)]^{2+}$ unit is shown in Figure 1. ORTEP views of the cationic complexes $[Ru(bpy)_2(PhenImPh)]^{+}$ and $[Ru(bpy)_2(PhenImH_2Ph)]^{2+}$ are reported in the Supporting Information.

A selection of the bond lengths and angles for the units $[Ru(bpy)_2(PhenImPh)]^{+}$, $[Ru(bpy)_2(PhenImHPh)]^{2+}$ and $[Ru(bpy)_2(PhenImH_2Ph)]^{3+}$ are gathered in Table 1.

In all cases, the coordination sphere around the metal ion can be best described as a trigonally distorted octahedral geometry. The angles around the ruthenium centre deviate significantly from ideal octahedral geometry as a result of the constraints imposed by the five-membered chelate rings. The average Ru–N bond length is 2.058, 2.055 and 2.063 Å for **I**, **II** and **III**, respectively. These values fall within the same range as those found for $[Ru(bpy)_3]^{2+}$ (2.056 Å) and related compounds[24] supporting the fact that the protonic states of the ligand do not influence the coordinating properties of the latter to the ruthenium(II) centre. The torsional angle between the imidazole and the phenyl ring is found to be around 17 and 14° for **I** and **II**, respectively while it is 38.5° for **III**. The larger value, when compared with **I** and **II**, can be attributed to the steric hindrance between the protons on the nitrogen atoms of the imidazole and those on the phenyl rings. In the X-ray analysis of **III**, two types of water molecules of crystallisation are identified. Four molecules of water are not involved in the close interaction with either the cation or the anion. While three molecules of water are intercalated between the NH group of the imidazolium ring of two contiguous monomeric units leading to the existence of a hydrogen-bonding network between the

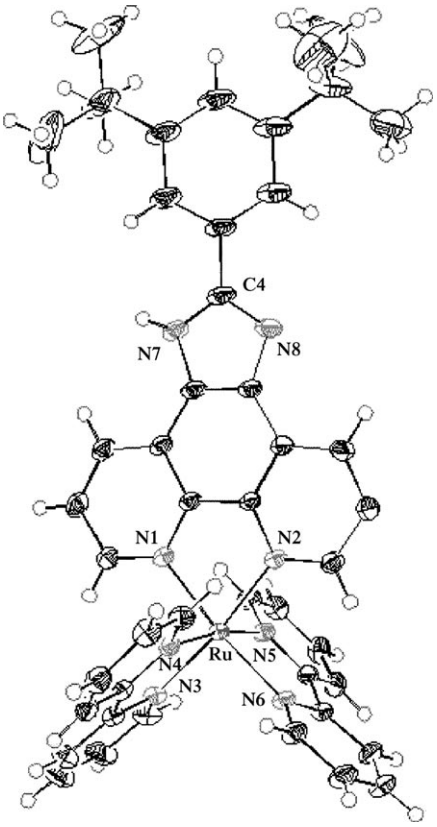

Figure 1. ORTEP drawing of $[Ru(bpy)_2(PhenImHPh)](NO_3)_2{\cdot}H_2O{\cdot}3MeOH$ with partial atom numbering.

Table 1. Selected bond lengths [Å] and angles [°] for complexes $[Ru(bpy)_2(PhenImPh)](PF_6){\cdot}H_2O{\cdot}6MeOH$ (**I**), $[Ru(bpy)_2(PhenImHPh)](NO_3)_2{\cdot}H_2O{\cdot}3MeOH$ (**II**) and $[Ru(bpy)_2(PhenImH_2Ph)](PF_6)_3{\cdot}5H_2O$ (**III**).

	I	II	III
Ru–N1	2.063	2.059	2.058
Ru–N2	2.063	2.068	2.068
Ru–N3	2.061	2.047	2.053
Ru–N4	2.055	2.054	2.070
Ru–N5	2.055	2.052	2.065
Ru–N6	2.061	2.054	2.064
C4–N7	1.352	1.355	1.351
C4–N8	1.352	1.364	1.338
N1-Ru-N2	80.0(8)	79.6(5)	79.5(2)
N3-Ru-N4	78.9(7)	78.5(5)	78.9(9)
N5-Ru-N6	78.9(7)	78.9(8)	78.1(0)

monomeric cationic species. The availability of hydrogen-bonding sites on each edge of the imidazolium ring (NH group) leads to saturation of hydrogen bonds in one dimension as shown in Figure 2.

The hydrogen bond length d(N-H-O_{w1}) is equal to 2.74(1) Å and is thus in the range of very strong hydrogen bonds.[25] The O_{w1}–O_{w3} and O_{w2} are also involved in hydrogen-bonding interaction with an average separation of 2.77 Å.[26] The N-H-O motifs are almost linear with N-H-O_{w1} and N-H-O_{w2} bond angles between 173 and 178°. However, the kink at the N-O-O angles (N-O_{w1}-O_{w3} and N-O_{w2}-O_{w3} 121.2(5) and 112.6(2)°, respectively) confers a zig–zag configuration to the one dimensional hydrogen-bonding network.

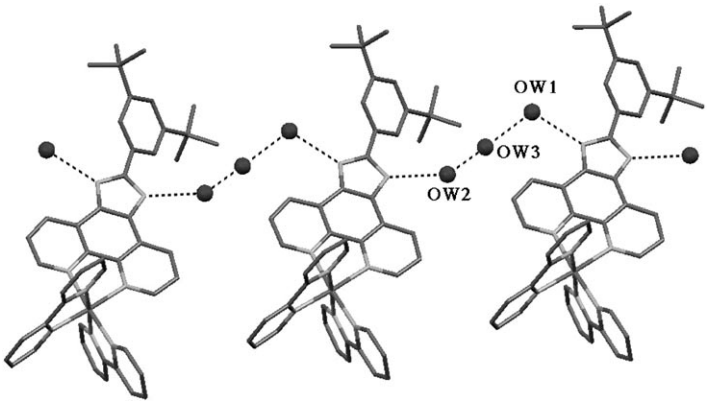

Figure 2. Hydrogen network bonding running between contiguous $[Ru(bpy)_2(PhenImH_2Ph)]$ entities and water molecules.

^{1}H NMR and UV-visible spectra: The protonation and deprotonation steps of the parent complex **II** were monitored by ^{1}H NMR spectroscopy (see Supporting Information). Not surprisingly, upon protonation, a deshielding of the signals for the imidazole containing ligand was observed while an upfield shift of these signals was perceptible upon deprotonation. A small effect was also depicted for the protons in *ortho*-position of the bpy ligands. The major shift (0.2 ppm) was observed for the aromatic proton in *para*-position to the imidazole ring from the deprotonated to the protonated state. This experimental fact suggests that there is no drastic electronic reshuffling upon these chemical processes.

The electronic absorption spectrum of **II** in an organic solvent such as acetonitrile is composed of three sets of bands, one intense band at high energy corresponding to the π–π* transitions of the bpy ligands and a double-humped band in the visible region corresponding to the MLCT transitions in analogy to the spectrum of the $[Ru(bpy)_3]^{2+}$ (Figure 3). However, the spectrum presents unique features like the band at around 340 nm and the shoulder to the MLCT band tailing up to 550 nm which may be attributed to transitions involving the PhenImHPh ligand.

The spectral features for the deprotonated form are similar to those of the parent compound. Nevertheless, we noticed a decrease of intensity of the π–π* transitions at high energy together with an increase in the intensity of the absorption band at 340 nm. It is worthwhile to note that the shoulder to the MLCT band still persists for the deprotonated state. In the case of the protonated state, two main changes are observed on the electronic absorption spectrum in that both bands at 340 nm and the shoulder at 500 nm decrease in intensity. From this experimental data, we can tentatively propose that those bands which fade upon protonation are assigned to the PhenImHPh ligand in the coordination sphere of the ruthenium centre.[27] Notably the absorption spectra are modified in protic solvents like water and

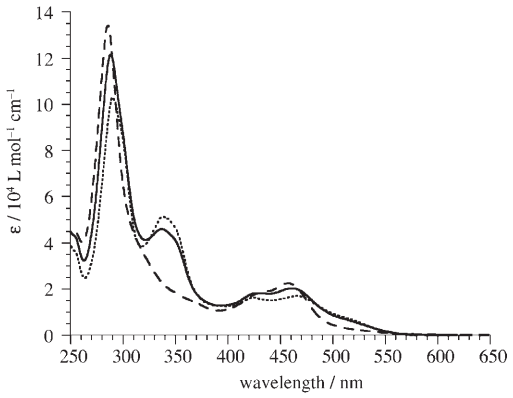

Figure 3. Absorption spectra in CH_3CN for complexes **I** (•••••), **II** (——) and **III** (-----).

methanol (see Supporting Information). The experimental observation is a decrease in intensity of both bands at 340 and 500 nm. This is also the case when methanol is added to a solution of **II** in acetonitrile. Thus it is more likely that the imidazole containing ligand is sensitive to protic solvents, probably due to the formation of hydrogen bonds between the imidazole and the molecules of solvent. Analogous modifications of the ground state absorption spectrum are observed in aqueous solution upon decrease of pH. The pK values of the imidazole ring (pK_1 3.1 ± 0.3, corresponding to deprotonation of the iminium fragment, and pK_2 8.7 ± 0.3, corresponding to deprotonation of the secondary amine) were obtained from titration experiments following the electronic spectral changes (see Supporting Information).

Electrochemistry: Electrochemical studies were performed on the chemically isolated forms of **I**, **II** and **III** in dichloromethane and the data are collected in Table 2.

Table 2. Half-wave potentials for the reduction (^{N}E) and oxidation (^{mi}E) of ligand PhenImHPh and complexes **I**, **II** and **III** in CH_2Cl_2.

Compound	^{II}E[a]	^{I}E[a]	^{i}E[a]	^{ii}E[a]	^{iii}E[a]
PhenImHPh			1.15[b]	1.64[b]	
I	−1.65[b]	−1.35	0.85	1.35[b]	1.43
II	−1.65[b]	−1.35	1.00[b]	1.36[b]	1.46
III	−1.65[b]	−1.35			1.46

[a] Determined by CV at 100 mV s^{-1}; $E=1/2$ ($E_{pa}+E_{pc}$) in V versus SCE in the presence of tetra-*n*-butylammonium perchlorate. [b] Irreversible.

The most surprising observation on the anodic side of the cyclic voltammograms of the three compounds (see Supporting Information) is that the redox potential of the $Ru^{III/II}$ couple is almost unaltered upon remote protonation or deprotonation of the imidazole unit. This result supports the fact that no significant Coulombic effect is exerted on the ruthenium ion by the charge carried on the imidazole ring. Two oxidative processes are observed at lower potentials than that of the $Ru^{III/II}$ redox couple for **I** and **II**. They are assigned to the oxidation of the imidazole–phenyl part of the ligand when compared with the redox behaviour of the ligand only (see Table 2). A shift of about 150 mV to less positive potential is observed for the first anodic wave when going from **II** to **I**, which was logically attributed to the more easy oxidation of the deprotonated imidazole ring. Under our experimental conditions, this wave gains in reversibility in the case of **I**. This observation is most likely due to the loss of the chemical step (proton release) following the one electron-abstraction process in case of compound **II**. An exhaustive one electron electrolysis was performed on **I** and **II** at around 1.0 and 1.2 V versus SCE, respectively. The reversibility of the redox process for compound **I** was justified by the observation of the same cyclic voltammogram trace before and after electrolysis. The X-band EPR spectrum of the frozen sample of the oxidised form of **I** and **II** indicates an isotropic signal centred at $g=2.0024$ in both cases (see Supporting Information) with a peak-to-peak through width of 0.78 mT. No hyperfine coupling is observed not even with the nitrogen atoms of the imidazolate ring.[28] This indicates that the spin density is not centred on the nitrogen atoms and is delocalised on a more extended π-skeleton. On the cathodic side of the cyclic voltammograms of the three complexes no noticeable change is observed at least for the first two reduction waves.

Photochemistry

Emission: The emission spectrum of **II** (between pH ≈3 and ≈9) exhibits a broad band with a maximum at 608 nm and a shoulder at 695 nm (Figure 4). The observed emission

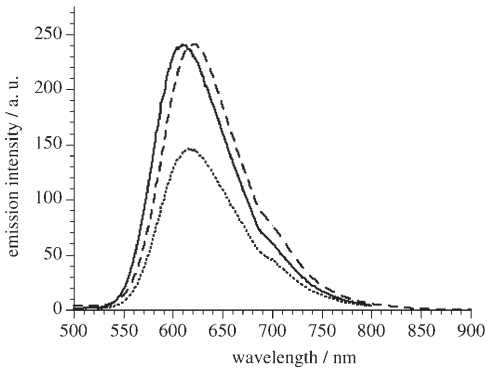

Figure 4. Emission spectra in aqueous solution at pH 2.0 (**III**, -----), 7.6 (**II**, ——) and 10.5 (**I**, •••••) in mixed buffer solutions. Excitation wavelength: 440 nm. Samples optically matched at 440 nm ($A_{440}=0.1$).

lifetime (τ_{em}), ≈800 ns, (see below for more detailed description of each component) is slightly longer than that of $[Ru(bpy)_3]^{2+}$, for which $\tau_{em}=620$ ns. Consistent with the longer lifetime, the emission quantum yield ($\Phi_{em}=0.054$) is higher than that of $[Ru(bpy)_3]^{2+}$ ($\Phi_{em}=0.042$).[29]

The protonation of the imidazole moiety to the protonic state **III** does not alter the emission quantum yield and lifetime, although a red-shift in the emission maximum ($\lambda_{max}=$ 622 nm at pH ≈2) is observed. From the inflection point in

an emission maximum wavelength versus pH plot (see Supporting Information) an apparent pK_1* value of 2.4 ± 0.3 was extracted. However, since a true thermodynamic acid–base equilibrium is not necessarily established within the lifetime of the excited state (<1 μs), the correct pK_1* value for the imidazole protonation in the excited state is calculated using Equation (1)[30] based on the Förster thermodynamic cycle:[31] and references therein

$$pK_1^* = pK_1 + \frac{0.625}{T}(\nu_B - \nu_A) \quad (1)$$

In Equation (1) ν_B and ν_A, the wavenumbers of the 0–0 transition in the base and acid forms, were evaluated as the intersection between the normalised absorption and emission spectra. A pK_1* value of 3.6 was obtained thus indicating that the excited state is a slightly weaker acid than the ground state (pK_1 3.1). Deprotonation of the imidazole to reach the protonic state **I** results in a red shift of the emission accompanied by a decrease in the emission quantum yield ($\Phi_{em}=0.032$) and lifetime (500 ns). The inflection point in the emission maximum wavelength versus pH plot gave an apparent pK_2* 8.9 ± 0.3, while the calculated Förster value is pK_2* 8.3, indicating that the excited state is a slightly weaker base than the ground state (pK_2 8.7).

A closer inspection of the emission kinetic traces obtained upon excitation at 440 nm with ns laser pulses shows a generally biphasic decay containing a minor fast phase whose amplitude relative to the slow phase is virtually independent of pH ($\approx$25%, not shown). The lifetime of this fast phase is $\approx$10 ns (close to time resolution) increasing to 30 ns for **III**. The lifetime of the slow phase decreases from 900 to 500 ns for increasing pH between pH 2 and 11, following a classical titration curve with an apparent pK_2* value of 8.2. The relative yield of the time resolved emission of the protonic state **I** (calculated as the sum of the product of the relative amplitudes and time constants for the different kinetic phases) falls to about 40% of the neutral state. The decrease in the emission yield indicates an apparent pK_2* of 9.0.

Transient absorption: The excited state transient kinetics obtained for the complex in its neutral and protonated forms at pH 7 (**II**) and 2 (**III**), respectively, exhibit a monoexponential decay in the investigated range (400–900 nm) with a lifetime $\tau=(900\pm50)$ ns. At pH 11.0 (**I**), the excited state of the complex in its deprotonated form has a lifetime of (600 ± 50) ns (see inset Figure 5). Those values are in good agreement with the emission lifetimes.

The transient difference absorption spectra taken at 230 ns after excitation for **I**, **II** and **III** (Figure 5) exhibit typical features related to the parent $[Ru(bpy)_3]^{2+}$, that is, a negative band centred at 460 nm due to depletion of the ground state MLCT absorption band, and a very weak transient absorption increase in the region 600–900 nm. For the protonic state **I**, the bleaching in the 400–500 nm region appears to be strongly reduced. However, this decrease in amplitude of the absorption changes at high pH is overestimated to some degree due to changes in sample concentration related to the degassing procedure.[32]

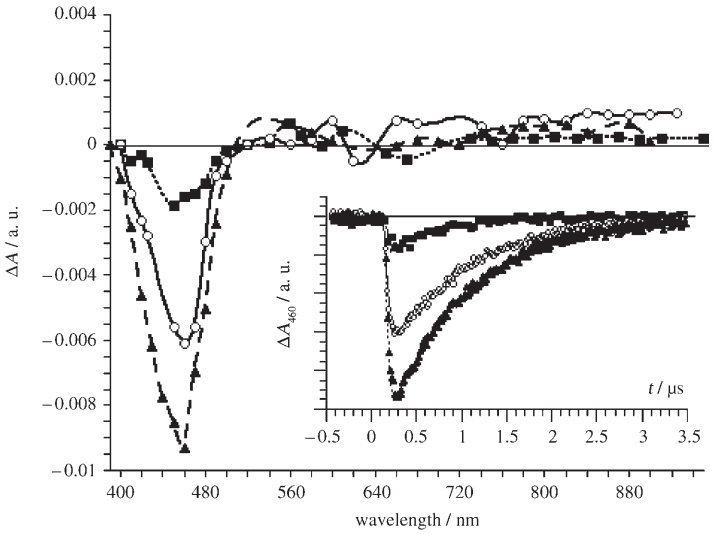

Figure 5. Transient absorption spectra in Argon purged aqueous solutions at pH 2 (10 mM citrate buffer), pH 7 (10 mM HEPES buffer) and pH 11 (10 mM CAPS buffer). Absorption changes taken 230 ns after laser pulse. Excitation wavelength: 440 nm. Samples optically matched at 440 nm ($A_{440}=0.3$); inset: kinetics at 460 nm at pH 2 (**III**, ▲), 7 (**II**, ○) and 11 (**I**, ■).

Photoinduced electron transfer in the presence of an external acceptor: In Figure 6, the kinetic traces of absorption changes at two different wavelengths, 460 and 605 nm are presented. These wavelengths are probes for the recovery of the photogenerated Ru^{III} to Ru^{II} and the presence of $MV^{\bullet+}$ respectively.

At pH 7, the depletion signal at 460 nm exhibits a much shorter lifetime than $MV^{\bullet+}$, indicating that the reduction of Ru^{III} to Ru^{II} is faster than re-oxidation of methyl viologen $MV^{\bullet+}$ to MV^{2+}. This gives evidence that the recovery of Ru^{II} involves a fast intramolecular electron transfer. The low intensity and very fast reappearance of the MLCT band at 460 nm at pH 11, indicates that Ru^{III} is almost not evidenced on this time scale in the deprotonated form of the

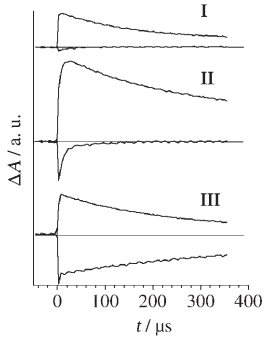

Figure 6. Absorption change kinetics for complexes **I**, **II** and **III** at 460 and 605 nm in Argon purged aqueous solutions in the presence of 10 mM MV^{2+}. Excitation wavelength: 532 nm. Samples optically matched at 532 nm; $A_{532}=0.3$.

imidazole containing ligand. The absorption at 605 nm indicates that methylviologen can still be efficiently reduced. However, the nature of the excited state(s) responsible for the reduction of MV^{2+} remains unclear. To characterise the species after electronic excitation of the Ru^{II} centre, MV^{2+} was replaced by $[Ru(NH_3)_6]^{3+}$, a reversible electron acceptor which is optically transparent in the visible region in both forms. Immediately after irradiation, the transient absorption spectrum collected (see Supporting Information) indicates an absorption band extending from 500 to above 600 nm which can be attributed to the formation of a neutral imidazolyl radical.[33] For **III**, the decay of the kinetic traces at 460 nm and 605 nm is very similar, supporting the fact that the recovery of the photogenerated Ru^{III} to Ru^{II} involves the re-oxidation of $MV^{\bullet+}$ through a bimolecular reaction, thus excluding any intramolecular electron transfer.

These experimental observations will be analysed in more details below in the light of theoretical data.

Theoretical results: We have performed DFT calculations for both the ground and selected excited states (see Charlot et al.[9] and more experimental details in the Experimental Section). As a prerequisite to these calculations the optimised geometric parameters for the ground singlet state S_0, the lowest triplet state T_1 and the lowest D_0 doublet state of the oxidised form were calculated at the (U)B3LYP/LanL2DZ level for the three complexes. They are given in the Supporting Information for states S_0 and T_1 of the three complexes.

DFT calculations realised on isolated molecules (see below) have allowed in many cases to bring conclusive information in rationalising the physical behaviour of coordination metal complexes.[9] However, the extension of these theoretical data from the gas phase to the experimental results in solution is often misleading. For instance, it has been shown that the medium tends to spread the accumulation of charges,[34] so that solvent effects may alter the electronic state of molecules bearing different charges in a dissimilar way. Indeed, electrostatic effects are often much less important for species placed in a solvent with a high dielectric constant than they are in the gas phase.[35] Recent theoretical work on ruthenium–polypyridine complexes have also pointed out the importance of solvent effects to improve the description of electronic spectra.[36–39] Henceforth, owing to the dissymmetry of charges in our molecular systems studied herein, we have analysed our chemical models in solution in the framework of a self-consistent reaction field method (SCRF). The polarizable continuum model (PCM)[40] was used. This approach places the solute in a cavity defined by the union of a series of interlocking atomic spheres within the solvent represented as a polarisable dielectric. All calculations were hence repeated in water. This choice was guided by the fact that all the photophysical experiments were realised in an aqueous solution. Notably the time-consuming geometry optimisations in a water medium was omitted for which convergence problems have been reported.[41] In the aim to clarify the photophysical properties observed for compounds **I**, **II** and **III**, we will focus in this paper on some of our theoretical results obtained for the named compounds in a water surrounding such as i) the relative energies of the different type of molecular orbitals in the ground state, ii) the nature of the low-lying excited singlet states and iii) the nature of the lowest triplet state and the singly oxidised forms. A more in detail analysis of the impact of the surrounding medium will be reported in a forthcoming paper.

Energy levels and molecular orbitals in the ground state: Some typical MOs of **II**, the parent compound for this study, are given in the Supporting Information. A comparison of the ground state MOs of the protonated (**III**) and deprotonated (**I**) complexes with compound **II** allows to establish a correlation between the orbitals of the three complexes (see Supporting Information). The striking evidence is the downshift in energy for all the orbitals located on the ligand upon protonation, that is, a decrease of the electronic density on this part of the molecule. In **I** the negative charge on the imidazole–phenyl fragment is responsible for a HOMO delocalised on L, while the HOMOs of **II** and **III** are d_π orbitals as mostly encountered in such complexes. For the same reason, the LUMO is a combination of the π_1* orbitals of the two bipyridines in **I** and **II** but is the ψ orbital of local *b* symmetry on phenanthroline in **III**.

The mean difference in energy between the set of d_π orbitals and the LUMO is nearly the same that is, 3.41, 3.45 and 3.38 eV for **I**, **II** and **III**, respectively, in comparison to 3.39 eV that we have calculated in the same manner in water for $[Ru(bpy)_3]^{2+}$. The HOMO–LUMO energy gap is 2.84 eV in **I**, 3.36 eV in **II** and 3.28 eV in **III**, the small gap for **I** resulting from the destabilisation of the HOMO on L.

Excited singlet states and electronic absorption spectra: The low-lying singlet excited states of the three complexes in their ground-state geometry were studied using time-dependent DFT (TDDFT) calculations, a method which describes these states in terms of monoexcitations from occupied to vacant MOs of the ground state. Our calculations indicate that for **I**, the lowest excited singlet state S_1 results essentially from a HOMO to LUMO monoexcitation and is hence a ligand-to-bipyridine charge transfer, abbreviated as LBCT. In contrast, S_2 to S_6 states involve either LBCT or charge shifts from the HOMO developed on the imidazole–phenyl part of the ligand to the vacant π orbitals of the phenanthroline moiety of the same ligand, that is, intraligand charge transfers (ILCT). In the case of **I**, MLCT states are encountered at higher energies. For **II**, S_1 results essentially from a charge transfer from d_π to π_1*(bpy) (referred to as MBCT) while for **III** S_1 is obtained by an excitation from the highest d_π MO toward ψ(phen) (MPCT).

Lowest triplet state and oxidised complexes: The lowest triplet state T_1 of each compound was investigated using spin-unrestricted UB3LYP/LanL2DZ calculations followed by geometry optimisation in vacuo. Single point calculations

using this geometry were then performed with the PCM model and water as medium. The same procedure was followed for the ground doublet state D_0 of the oxidised complexes. The theoretical outcomes are reflected by the spin density distributions and are reported in Figure 7 for the T_1 and D_0 states of the three complexes.

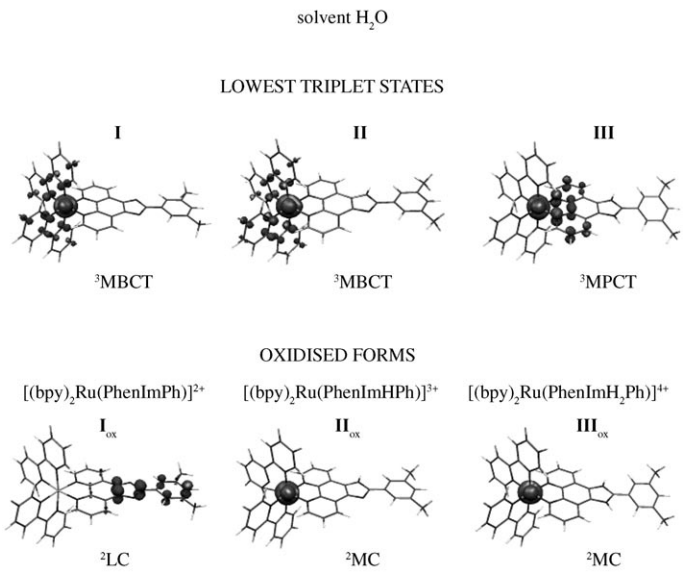

Figure 7. Spin density distribution for the lowest triplet state and the oxidised form of the three complexes calculated in water.

As depicted in Figure 7, all the T_1 states can be viewed as the distribution of one spin on the ruthenium while the other is spread over the two coordinated bipyridines in cases **I** and **II** or over the phenanthroline part of the ligand for **III**. These calculated triplet states resemble that of ruthenium–tris(bipyridine),[9] and can be qualified as the "charge-separated states" in which ruthenium is oxidised in Ru^{III} with partial reduction of the corresponding ligand(s). It is noteworthy that the protonic states of the ligand confer a directionality to the charge separated state: in **I** and **II** the T_1 state is directed from the metal to the bipy motifs (^{3}MBCT), while in **III** it is directed from the metal to the phenanthroline part of the protonated ligand (^{3}MPCT).

Our computed data for the monooxidised form of complex **I** show that almost one spin is localised essentially on the imidazole–phenyl moiety of the ligand and that ruthenium bears no spin (Figure 7). This supports the fact that the first electron abstraction has occurred on the deprotonated imidazole–phenyl part of the ligand (^{2}LC state) and not on the metallic ion which remains formally Ru^{II}. In contrast, for the singly oxidised complexes **II** and **III**, ruthenium bears one spin and oxidation is metal-centred (^{2}MC) as shown in Figure 7.

Discussion

The photophysical behaviour of compounds **I**, **II** and **III** after a flash excitation at 450 nm in the MLCT band show in all cases an emission band centred at around 610 nm. Our calculated lowest triplet states for all three compounds indeed show that they can be described as the charge separated state found for the prototype ruthenium tris(bipyridine) complex. The ruthenium ion is formally in a +III oxidation state characterised by the absence of MLCT transitions and absorption in the 400–460 nm region which is much weaker than the absorption of the ground state. Consequently, a bleaching is observed around 460 nm in the transient spectra (see Figure 5). As Ru^{III} possesses a local unpaired spin, spin-orbit coupling may produce a radiative luminescent decay from the lowest ^{3}MLCT state as observed in Figure 4 for the three complexes. However, other deactivation paths may be efficient or changes of protonation may occur.

On the basis of both experimental and theoretical results, we now propose different schematic pathways for the interpretation of the photoinduced electron transfer studies for compounds **I**, **II** and **III** in the presence of an external electron acceptor. The map for the different electronic and protonic states for compound **I** is shown in Scheme 1.

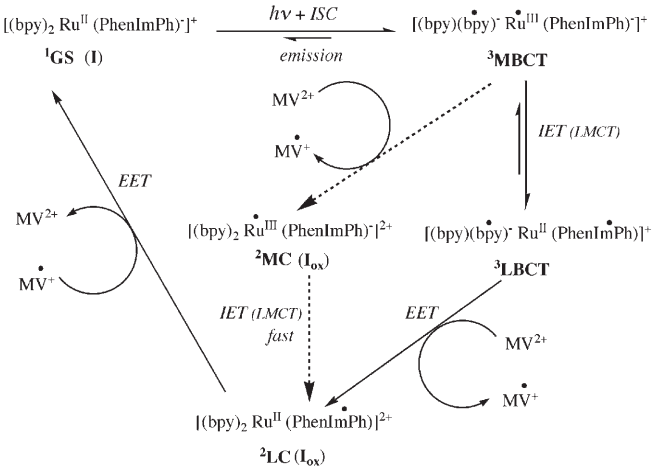

Scheme 1. *hν*: Laser excitation at $\lambda = 440$ nm; ISC: intersystem crossing (^{1}MLCT→^{3}MLCT); EET: external (bimolecular) electron transfer (redox reaction); IET: internal electron transfer.

After irradiation in absence of an external electron acceptor (*hν* step), the emitting ^{3}MBCT is reached. However, in the case of **I**, both the emission intensity at 610 nm (Figure 4) and the bleaching of the MLCT band at 450 nm are less pronounced (Figure 5) as compared to **II** and **III**. These experimental facts suggest the rapid recovery of a Ru^{II} centre. In effect, the oxidising power of the photogenerated Ru^{III} is sufficient to abstract one electron from the deprotonated imidazole part leading to a ^{3}LBCT state through a ligand-to-metal electron transfer. This redox reaction is thermodynamically favourable as confirmed by electrochemical studies. An equilibrium between ^{3}MBCT and ^{3}LBCT may be present in the medium.[42]

In the presence of MV^{2+}, electron density is removed from the high-lying π*(bpy) orbitals occupied in the ^{3}MBCT

state (EET) generating a ^{2}MC state of the oxidised complex (I_{ox}). Simultaneously equilibrium between the low lying triplets is shifted toward ^{3}LBCT. Therefore, these processes can account for the weak absorption changes (Figure 6) in contrast with the formation of a genuine Ru^{III} intermediate. After bimolecular charge shifts reaction between $[(bpy)(bpy^{\bullet})–Ru^{II}(PhenImPh^{\bullet})]^{+}$ and methylviologen, a ^{2}LC state in which the unpaired electron is localised on the deprotonated imidazole–phenyl is reached. An alternate pathway to this state is obtained following an intramolecular electron-transfer process from the deprotonated anionic form of the ligand to photogenerated ruthenium(III) centre, the ^{2}MC state. The X-band EPR data for the monooxidised species of **I** (see Supporting Information) confirm the nature of this oxidised state which is furthermore supported by DFT calculations.

The photoinduced electron pathways for compound **II** (i.e., at pH≈7) is given in Scheme 2.

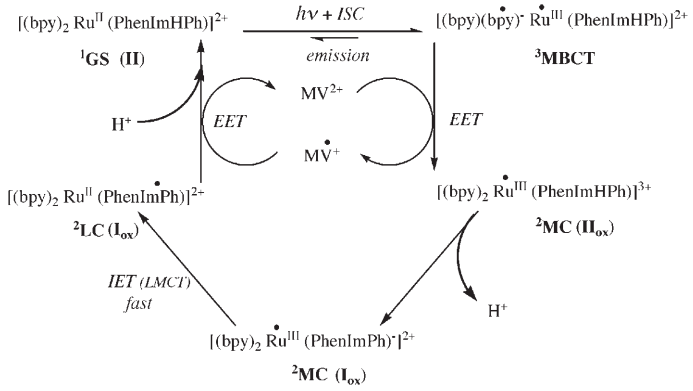

Scheme 2.

The lowest triplet ^{3}MBCT state is reached after light excitation. This state is responsible for the excited state luminescence (Figure 4) and the bleaching at 450 nm observed on the transient spectrum (Figure 5) at neutral pH in absence of an electron acceptor. In the presence of an electron acceptor (MV^{2+}), an electron is transferred from the bipyridines and the bleaching at 460 nm (Figure 6) evidences the formation of Ru^{III} intermediate in agreement with the calculated ground ^{2}MC state of the oxidised complex ($\mathbf{II}_{ox}$). This high valent metal Ru^{III} species ($[(bpy)_2Ru(PhenImHPh)]^{3+}$ on Scheme 2) must be highly polarising therefore enhancing the acidity of the imidazole ring. A subsequent deprotonation step in experimental pH conditions (pH≈7) leads to the oxidised I_{ox} complex $[(bpy)_2Ru(PhenImPh)]^{2+}$. As discussed above, the ground state of I_{ox} is a ^{2}LC state resulting from an internal electron transfer from the deprotonated imidazole fragment of the ligand to Ru^{III}. This proton coupled electron transfer process is most likely at the origin for the rapid recovery of the Ru^{II} MLCT absorption band (Figure 6). An imidazolyl-type radical was evidenced both by EPR spectroscopy and by transient absorption spectroscopy of **II** in the presence of a non-absorbing electron acceptor, $[Ru(NH_3)_6]^{3+}$ (see Supporting Information).

A stepwise proposal for the photodriven charge shifts of compound **III** (pH≈1) is given in Scheme 3.

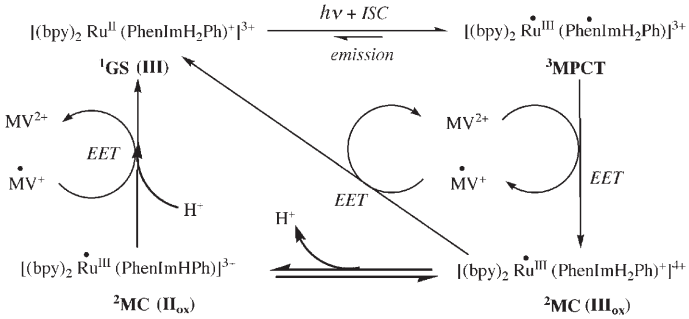

Scheme 3.

The computed lowest triplet state of the protonated complex is a ^{3}MPCT state and the emission properties of **III** are comparable to those of $[Ru(bpy)_3]^{2+}$. Upon irradiation in the presence of an electron acceptor, the charge accumulated on the phenanthroline moiety is transferred to the exogenous MV^{2+}. Both the formation of the $MV^{\bullet+}$ and the bleaching of the MLCT band account for this reaction (Figure 6). The concomitant regeneration of the Ru^{II} and MV^{2+} in this case (Figure 6) indicates that the Ru^{III} is not quenched through an intramolecular electron transfer. This is supported from the electrochemical data where no redox process is depicted before the $Ru^{III/II}$ couple in acidic medium. As can be noticed, the ^{2}MC state is described with a Ru^{III} containing centre and we propose here that a mono deprotonation of the imidazolium may occur under our experimental conditions. However, both oxidised ^{2}MC states (of $\mathbf{III}_{ox}$ or $\mathbf{II}_{ox}$) will experience a similar back electron transfer with $MV^{\bullet+}$ to return to the ground state, as demonstrated by the similar absorption change kinetics at 460 and 605 nm.

Conclusion

In this work, we have described the physical properties of a ruthenium–polypyridine-type complex holding a modified phenanthroline ligand fused with an imidazole ring. The combined electrochemical and photophysical studies supported by DFT calculations have allowed us to understand the electronic perturbations undergoing upon (de)protonation of the imidazole ring. We have shown how the protonic states of the imidazole ring modified drastically the photophysical properties and therefrom the pathways involved in the photoinduced electron transfer process. These results set the basis for future work on more elaborate systems using this chromophore/spacer as the molecular lynchpin to hold a putative metal complex catalyst.

Experimental Section

X-ray crystallography: X-ray diffraction data for $[Ru(bpy)_2(PhenImPh)](PF_6)\cdot H_2O\cdot 6\,MeOH$, $[Ru(bpy)_2(PhenImHPh)](NO_3)_2\cdot H_2O\cdot 3\,MeOH$ and $[Ru(bpy)_2(PhenImH_2Ph)](PF_6)_3\cdot 5\,H_2O$ were collected by using a Kappa X8 APPEX II Bruker diffractometer with graphite-monochromated $Mo_{K\alpha}$ radiation ($\lambda = 0.71073$ Å). The temperature of the crystal was maintained at the selected value (100 K) by means of a 700 series Cryostream cooling device to within an accuracy of ± 1 K. The data were corrected for Lorentz, polarization, and absorption effects. The structures were solved by direct methods using SHELXS-97[43] and refined against F^2 by full-matrix least-squares techniques using SHELXL-97[44] with anisotropic displacement parameters for all non-hydrogen atoms. Hydrogen atoms were located on a difference Fourier map and introduced into the calculations as a riding model with isotropic thermal parameters. All calculations were performed by using the Crystal Structure crystallographic software package WINGX.[45]

One NO_3^- anion of structure $[Ru(bpy)_2(PhenImHPh)](NO_3)_2\cdot H_2O\cdot 3\,MeOH$ appeared to be disordered. The occupancy factors were fixed in the ratio 50:50 for the N atom and one O atom, the two other O atoms being refined with an occupancy factor of 1.0. For this structure also, the hydrogen atom carried by nitrogen is disordered on the two sites with an occupancy rate of 0.5.

The crystal data collection and refinement parameters are given in Table S1 of the Supporting Information.

CCDC-609989, -609990, and -652213 contain the supplementary crystallographic data for this paper. These data can be obtained free of charge from The Cambridge Crystallographic Data Centre via www.ccdc.cam.ac.uk/data_request/cif.

Electrochemical measurements: The experiments were performed with an EGG PAR (model 273 A) electrochemical workstation. The solvents were distilled under nitrogen in the presence of dry calcium chloride and the solution (1 mmol L^{-1} for complexes and ligand and 0.1 mol L^{-1} of tetrabutylammonium perchlorate ($TBAClO_4$) introduced within an argon purged heart shaped cell. Cyclic voltammetry was performed using a glassy carbon electrode (3 mm in diameter) as working electrode, a platinum grid as the counter electrode and an $Ag/AgClO_4$ (0.01 M) electrode in acetonitrile as the reference ($E_{ref} = 0.3$ V/ECS). Electrolyses were carried out at controlled potentials in a three-electrode cell, using a platinum gauze as working electrode, a platinum grid as counter electrode and an $Ag/AgClO_4$ (0.01 M) in acetonitrile electrode as the reference. Low temperature electrolyses were run with 0.2 M of $TBAClO_4$.

UV-visible-NIR spectra: The spectra were recorded with a Varian Cary 5E spectrophotometer (200–1500 nm), with 1 cm quartz cells. Spectroelectrochemical data were obtained by combination of a three electrode thin cell (0.5 mm) mounted in a UV-visible-NIR spectrophotometer. IR spectra were performed with a Perkin–Elmer spectrum 1000 spectrometer, using KBr matrix pellets. NMR spectra were obtained with a Bruker spectrometer AV 360 (360 MHz). The solvents used were $CDCl_3$ or $[D_6]$DMSO. The ^{1}H NMR spectra are given in the Supporting information. EPR spectra were recorded on a X-band spectrometer Elexsys E500 (Bruker) at 100 K. Elemental analyses were performed at Services de Microanalyse, ICSN-CNRS, Gif-sur-Yvette. Mass spectra were recorded on a Finnigan Mat, Mat95S in a BE configuration at low resolution.

Photochemistry: In order to cover a large range of pH and to exclude effects of the buffer, several buffers were used (CAPS, TRIS, HEPES, MES, citrate) as well as their mixture. Steady-state emission spectra were recorded on a Varian Cary Eclipse Spectrofluorimeter upon excitation at 440 nm. All the solutions were optically matched with absorbances of 0.1 at excitation wavelength. Flash-absorption and emission transients were measured with setups of local design. All measurements were done at 296 K. For absorption transients the measuring light was provided by a 450 W xenon lamp. The wavelength was selected with a monochromator (Czerny-Turner) placed after the 10×10 mm, sealed cuvette containing the sample. The sample was excited at 90° to the measuring beam by a flash from a frequency-tripled Nd/YAG laser (Surelight, Continuum) equipped with an OPO. Excitation was set at 440 nm (duration 5 ns, ≈ 5 mJ cm^{-2}). Absorbance changes were detected with a silicon photodiode and signals were amplified by a wideband preamplifier (model 5185, EG&G) before recording by a digital oscilloscope (TDS 3034B, Tektronix). Solutions were purged with Argon for ≈ 20 minutes prior to measurements. A flow-through system was employed to avoid sample degradation due to prolonged exposure to light. For emission transients excitation was done by a flash from a frequency-doubled picosecond Nd/YAG laser (532 nm, duration 25 ps, ≈ 300 μJ cm^{-2}; continuum) or from a frequency-doubled nanosecond Nd/YAG laser (532 nm, duration 7 ns, 2 mJ/cm^2; Quantel). The detection wavelength was selected by interference filters and signals detected with a microchannel plate photomultiplier tube (R2566U, Hamamatsu) and a 7 GHz digitising oscilloscope (IN7000, Intertechnique) or by a digital oscilloscope (TDS 744 A, Tektronix).

Computation methods: Density Functional Theory calculations were carried out using Becke's three-parameter hybrid functional B3LYP[46,47] along with the valence double-ζ basis set LanL2DZ[48,49] including the Los Alamos effective core potential for heavy atoms. All the calculations were performed using the Gaussian 98[50] and Gaussian 03[51] software packages. For consistency reasons we used calculated geometries which were fully optimised in the ground state (closed-shell singlet S_0) for the three compounds. However, in order to decrease the computation time, the two *t*Bu groups on the phenyl ring, which present numerous degrees of freedom without influence on our problem, were replaced by two methyl groups. Starting from the closed-shell S_0 state, time-dependent density functional calculations (TDDFT)[52] were performed to determine the energies and character of the lowest excited singlets and triplets states *in the ground-state geometry*. As photophysical experiments, in absence as well as in the presence of an electron acceptor, may involve the lowest triplet state T_1 and the ground doublet state D_0 of the oxidised complex, these two states were completely studied using a different approach : spin-unrestricted calculations were performed and the corresponding geometries of T_1 and D_0 were fully optimised at the UB3LYP/LanL2DZ level, except for the oxidised form of **III**, a highly-charged (+4) complex for which convergence of the geometry optimisation was not achieved. We have checked that in the open-shell calculations the spin contamination from states of higher spin multiplicity is low by looking at the values of $<S^2>$ (typically 2.006 to 2.009 for a triplet state). The nature of these states was precised by analysis of the corresponding spin-orbitals and spin density distributions, as done by other authors, for instance ref. [53].

In a first step, all these calculations were performed on the isolated molecule (gas phase) and, in a second step, solvent effects were modelled in the framework of a self-consistent reaction field method (SCRF). Calculations on the gas-phase optimised geometries were performed with the polarized dielectric model (PCM)[40,54] using the integral equation formalism (IEF).[55,56] The selected solvent was water and all parameters were kept to their implemented Gaussian 03 values. No geometry optimisation was attempted in the solvent.

Materials: Ruthenium trichloride was purchased from the Aldrich Chemical Company. 2,2′-Bipyridine (bpy) and 1,10-phenanthroline (phen) were obtained from Janssen Chemical Company. 1,10-Phenanthroline-5,6-dione,[57] 3,5-di-*tert*-butylbenzaldehyde,[58] and $[Ru(bpy)_2Cl_2]$[59] were synthesised as described in the literature.

PhenImHPh: A 1:1 mixture of 5,6-phenanthrolinedione (420 mg, 2 mmol) and 3,5-di-*tert*-butyl-benzaldehyde (444 mg, 2 mmol) in AcOH together with an excess of NH_4OAc (3.1 g, 40 mmol) was heated to reflux. A yellow solid precipitates out upon cooling, which was isolated by filtration and washed with water and vacuum dried (610 mg, ≈75%). ^{1}H NMR ($[D_6]$DMSO, 360 MHz): δ = 13.70 (s, NH), 9.05 (d, 2H), 8.90 (d, 2H), 8.20 (d, 2H) 7.86 (m, 2H), 7.60 (s, 1H), 1.50 ppm (s, 18H); IR: $\tilde{\nu}$ = 3385 (NH), 2952, 2900, 2864 (CH), 1643 cm^{-1} (C=N Phen); ESI MS: *m*/*z* (%): 409.2 $[M+H]^+$.

Complex II: $[Ru(bpy)_2Cl_2]$ (242 mg, 0.5 mmol) was treated with $AgNO_3$ (170 mg, 1.0 mmol) in MeOH (5 mL) for 1 h. The AgCl precipitate was filtered off and the filtrate evaporated to dryness. Ligand PhenImHPh (204 mg, 0.5 mmol) was added to the ruthenium salt in MeOH (10 mL) and stirred under reflux for 3 h. The solvent was removed by rotary evap-

oration and the crude product was purified by column chromatography on neutral alumina (CH_2Cl_2/MeOH 90:10) to afford **II**$(NO_3)_2$ (353 mg, 72%) as an orange solid. The corresponding hexaflurophosphate salt was isolated upon addition of a saturated aqueous solution of $NaPF_6$ to a concentrated solution of **II**$(NO_3)_2$ in methanol. ^{1}H NMR ([D$_6$]DMSO, 360 MHz): δ = 9.05 (d, 2H), 8.90, 8.85 (d, 4H), 8.27 (d, 2H), 8.22 (t, 2H), 8.10 (t, 2H), 7.89 (d, 2H), 7.81 (d, 2H), 7.73 (dd, 2H), 7.59 (m, 4H), 7.39 (m, 3H), 1.38 ppm (s, 18H); IR: $\tilde{\nu}$ = 2951, 2902, 2863 (CH), 1623 (C=N), 1360 cm^{-1} (N=O, NO_3^-); UV λ_{max} (ε) = 240 (26500), 250 (sh, 22000), 287 (61500), 335 (23400), 430 (9500), 460 (10000), 520 nm (sh, 3000); ESI MS: *m*/*z* (%): 411.3 (100) $[M]^{2+}$; elemental analysis calcd (%) for $C_{47}H_{44}N_{10}O_6Ru\cdot 2H_2O$ (982.02): C 57.48, H 4.93, N 14.26; found: C 57.90, H 5.09, N 14.20.

Complex III: **II**$(NO_3)_2$ (67 mg, 0.07 mmol) was dissolved in methanol (3 mL). To this solution was added 1 M nitric acid (80 μL). This solution was stirred for an hour, and then concentrated under reduced pressure. The hexafluorophosphate salt was isolated upon addition of a saturated aqueous solution of $NaPF_6$ to give an orange powder (78 mg, 85%). ^{1}H NMR ([D$_6$]DMSO, 360 MHz): δ = 9.13 (d, 2H), 8.90, 8.86 (d, 4H), 8.23 (t, 2H), 8.18 (d, 2H), 8.13 (t, 2H), 8.03 (d, 2H), 7.9 (m, 4H), 7.6 (m, 5H), 7.37 (t, 2H), 1.43 ppm (s, 18H); IR: $\tilde{\nu}$ = 3104 (NH), 2952, 2900, 2864 (CH), 1624 cm^{-1} (C=N phen); UV: λ_{max} (ε) = 286 (67000), 430 (10000), 460 nm (11500); ESI MS: *m*/*z* (%): 411.2 (100) $[M]^{2+}$; elemental analysis calcd (%) for $C_{47}H_{45}F_{18}N_8P_3Ru\cdot 3H_2O$ (1311.92): C 43.03, H 3.92, N 8.54; found C 43.17, H 4.09, N 8.62.

Complex I: **II**$(NO_3)_2$ (67 mg, 0.07 mmol) was dissolved in acetonitrile (3 mL). An excess of sodium methoxide was added to this solution. The mixture was stirred for 2 h then filtered to remove undissolved material. The filtrate evaporated to dryness. The solid was dissolved in a small amount of methanol and precipitated with an excess of $NaPF_6$ salt (62 mg, 87%). ^{1}H NMR ([D$_6$]DMSO, 250 MHz): δ = 8.97 (d, 2H), 8.90, 8.86 (d, 4H), 8.27 (d, 2H), 8.22 (t, 2H), 8.16 (t, 2H), 7.89 (d, 2H), 7.71 (m, 4H), 7.60 (m, 4H), 7.36 (m, 3H), 1.40 ppm (s, 18H); IR: $\tilde{\nu}$ = 2954, 2900, 2866 (CH), 1629 cm^{-1} (C=N phen); UV: λ_{max} (ε) = 240 (23500), 250 (sh, 18000), 290 (55000), 337 (26000), 425 (9000), 460 (8000), 520 (sh, 3000); ESI MS: *m*/*z* (%): 411.3 (100) $[M]^{2+}$, 821.3 (21) $[M]^{+}$; elemental analysis calcd (%) for $C_{47}H_{43}F_6N_8PRu\cdot H_2O\cdot CH_3OH$ (1015.99): C 56.74, H 4.86, N 11.03; found C 56.80, H 4.92, N 11.20.

Acknowledgements

This work was supported by the CNRS (ANR Blanc HYPHO) and the European Commission (NEST STREP SOLAR-H contract No 516510). We thank the Centre Informatique National de l'Enseignement Supérieur at Montpellier (France) and the Institut du Développement et des Ressources en Informatique Scientifique at Orsay (France) for providing calculation means. C.H. is grateful to the International Chair of Blaise Pascal for a scholarship.

[1] V. Balzani, A. Juris, *Coord. Chem. Rev.* **2001**, *211*, 97–115.
[2] K. Kalyanasundaram, *Coord. Chem. Rev.* **1982**, *46*, 159–244.
[3] N. D. McClenaghan, Y. Leydet, B. Maubert, M. T. Indelli, S. Campagna, *Coord. Chem. Rev.* **2005**, *249*, 1336–1350.
[4] V. Balzani, A. Credi, M. Venturi, *Coord. Chem. Rev.* **1998**, *171*, 2–16.
[5] P. D. Beer, P. A. Gale, *Angew. Chem.* **2001**, *113*, 502–532; *Angew. Chem. Int. Ed.* **2001**, *40*, 486–516.
[6] S. Welter, K. Brunner, J. W. Hofstraat, L. De Cola, *Nature* **2003**, *421*, 54–58.
[7] B. Schlicke, L. De Cola, P. Belser, V. Balzani, *Coord. Chem. Rev.* **2000**, *208*, 267–275.
[8] R. Passalacqua, F. Loiseau, S. Campagna, Y.-Q. Fang, G. S. Hanan, *Angew. Chem.* **2003**, *115*, 1646–1649; *Angew. Chem. Int. Ed.* **2003**, *42*, 1608–1611.
[9] M.-F. Charlot, Y. Pellegrin, A. Quaranta, W. Leibl, A. Aukauloo, *Chem. Eur. J.* **2006**, *12*, 796–812.
[10] C. Daul, E. J. Baerends, P. Vernooijs, *Inorg. Chem.* **1994**, *33*, 3538–3543.
[11] J. K. McCusker, *Acc. Chem. Res.* **2003**, *36*, 876–887.
[12] C. R. Bock, J. A. Connor, A. R. Gutierrez, T. J. Meyer, D. G. Whitten, B. P. Sullivan, J. K. Nagle, *J. Am. Chem. Soc.* **1979**, *101*, 4815–4824.
[13] M. Kirch, J.-M. Lehn, J. P. Sauvage, *Helv. Chim. Acta* **1979**, *62*, 1345–1384.
[14] N. Kitamura, H.-B. Kim, S. Sumio, S. Tazuke, *J. Phys. Chem.* **1989**, *93*, 5750–5756.
[15] H.-B. Kim, N. Kitamura, Y. Kawanishi, S. Tazuke, *J. Phys. Chem.* **1989**, *93*, 5757–5764.
[16] F. Scandola, C. Choiorboli, M. T. Indelli, M. A. Rampi, *Vol. 3* (Ed.: V. Balzani), Wiley-VCH, Weinheim, **2001**, pp. 337–408.
[17] Y. Pellegrin, K. E. Berg, G. Blondin, E. Anxolabéhère-Mallart, W. Leibl, A. Aukauloo, *Eur. J. Inorg. Chem.* **2003**, 1900–1910.
[18] Y. Pellegrin, A. Quaranta, P. Dorlet, M.-F. Charlot, W. Leibl, A. Aukauloo, *Chem. Eur. J.* **2005**, *11*, 3698–3710.
[19] F. Lachaud, A. Quaranta, Y. Pellegrin, P. Dorlet, M.-F. Charlot, S. Un, W. Leibl, A. Aukauloo, *Angew. Chem.* **2005**, *117*, 1560–1564; *Angew. Chem. Int. Ed.* **2005**, *44*, 1536–1540.
[20] H. Xu, K.-C. Zheng, H. Deng, L.-J. Lin, Q.-L. Zhang, L.-N. Ji, *New J. Chem.* **2003**, *27*, 1255–1263.
[21] Y. Xiong, L.-N. Ji, *Coord. Chem. Rev.* **1999**, *185–186*, 711–733.
[22] L.-N. Ji, X.-H. Zou, J.-G. Liu, *Coord. Chem. Rev.* **2001**, *216–217*, 513–536.
[23] E. A. Steck, A. R. Day, *J. Am. Chem. Soc.* **1943**, *65*, 452–456.
[24] D. P. Rillema, D. S. Jones, C. Woods, H. A. Levy, *Inorg. Chem.* **1992**, *31*, 2935–2938.
[25] G. C. Pimentel, A. L. McClellan, *The hydrogen bond*, W. H. Freeman, San Francisco, **1960**, p. 260.
[26] M. C. Munoz, R. Ruiz, M. Traianidis, A. Aukauloo, J. Cano, Y. Journaux, I. Fernandez, J. R. Pedro, *Angew. Chem.* **1998**, *110*, 1933–1936; *Angew. Chem. Int. Ed.* **1998**, *37*, 1833–1836.
[27] J.-Z. Wu, Y. Guang, S. Chen, L. N. Ji, J.-Y. Zhou, Y. Xu, *Inorg. Chim. Acta* **1998**, *283*, 17–23.
[28] J. Abe, T. Sano, M. Kawano, Y. Ohashi, M. M. Matsushita, T. Iyoda, *Angew. Chem.* **2001**, *113*, 600–602; *Angew. Chem. Int. Ed.* **2001**, *40*, 580–582.
[29] D. M. Roundhill, *Photochemistry and photophysics of metal complexes*, Plenum Press, New York, **1994**, pp. 165–215.
[30] The equation is obtained assuming that the entropy changes accompanying protonation are the same in the ground and in the excited states.
[31] R. J. Crutchley, N. Cress, A. B. P. Lever, *J. Am. Chem. Soc.* **1983**, *105*, 1170–1178.
[32] We noticed a loss of solubility associated to the increase of solvent basicity. During the degassing procedure, especially at high pH, part of the complex adheres on the cuvette walls. The amplitude of signal might thus be affected due to a decreased bulk concentration of the compound. Due to the long measurement times to record the full spectrum, absorption change measurements are much more susceptible to be affected than measurements of emission spectra.
[33] R. H. Riem, A. McLachlan, G. R. Coraor, E. J. Urban, *J. Org. Chem.* **1971**, *36*, 2272–2275.
[34] M. K. Nazeeruddin, Q. Wang, L. Cevey, V. Aranyos, P. Liska, E. Figgemeier, C. Klein, N. Hirata, S. Koops, S. A. Haque, J. R. Durrant, A. Hagfeldt, A. B. P. Lever, M. Grätzel, *Inorg. Chem.* **2006**, *45*, 787–797.
[35] J. B. Foresman, Æ. Frisch in *Exploring chemistry with electronic structure methods*, Gaussian, Inc., Pittsburg, PA, **1996**, p. 237.
[36] J. E. Monat, J. H. Rodriguez, J. K. McCusker, *J. Phys. Chem. A* **2002**, *106*, 7399–7406.
[37] J. F. Guillemoles, V. Barone, L. Joubert, C. Adamo, *J. Phys. Chem. A* **2002**, *106*, 11354–11360.
[38] S. R. Stoyanov, J. M. Villegas, D. P. Rillema, *Inorg. Chem. Commun.* **2004**, *7*, 838–841.

[39] F. De Angelis, S. Fantacci, A. Sgamelotti, F. Cariati, D. Roberto, F. Tessore, R. Ugo, *Dalton Trans.* **2006**, 852–859.
[40] E. Cancès, B. Menucci, J. Tomasi, *J. Chem. Phys.* **1997**, *107*, 3032–3041.
[41] F. De Angelis, S. Fantacci, A. Selloni, *Chem. Phys. Lett.* **2004**, *389*, 204–208.
[42] Indeed, TDDFT calculations in water starting from T_1 (^{3}B symmetry) point out that T_2, lying 0.09 eV above T_1 is the ^{3}MBCT of ^{3}A symmetry corresponding to a promotion of d_π electrons to the second combination of π_1*(bpy) orbitals. T_2 has therefore exactly the same photophysical properties as T_1. In addition, T_3, a ^{3}LBCT state is calculated only 0.04 eV higher in energy.
[43] G. M. Sheldrick, *SHELXS-97*, University of Göttingen, Göttingen (Germany), **1990**.
[44] G. M. Sheldrick, *SHELXL-97*, University of Göttingen, Göttingen (Germany), **1997**.
[45] L. J. Farrugia, *J. Appl. Crystallogr.* **1999**, *32*, 837–838.
[46] A. D. Becke, *J. Chem. Phys.* **1993**, *98*, 5648.
[47] C. Lee, W. Yang, R. G. Parr, *Phys. Rev. B* **1988**, *37*, 785.
[48] T. H. Dunning Jr, P. J. Hay, *Mod. Theor. Chem.* **1976**, p. 1–28.
[49] P. J. Hay, W. R. Wadt, *J. Chem. Phys.* **1985**, *82*, 270–283.
[50] Gaussian 98, Revision A.11.3, M. J. Frisch, G. W. Trucks, H. B. Schlegel, G. E. Scuseria, M. A. Robb, J. R. Cheeseman, V. G. Zakrzewski, J. A. Montgomery, Jr., R. E. Stratmann, J. C. Burant, S. Dapprich, J. M. Millam, A. D. Daniels, K. N. Kudin, M. C. Strain, O. Farkas, J. Tomasi, V. Barone, M. Cossi, R. Cammi, B. Mennucci, C. Pomelli, C. Adamo, S. Clifford, J. W. Ochterski, G. A. Petersson, P. Y. Ayala, Q. Cui, K. Morokuma, P. Salvador, J. J. Dannenberg, D. K. Malick, A. D. Rabuck, K. Raghavachari, J. B. Foresman, J. Cioslowski, J. V. Ortiz, A. G. Baboul, B. B. Stefanov, G. Liu, A. Liashenko, P. Piskorz, I. Komaromi, R. Gomperts, R. L. Martin, D. J. Fox, T. Keith, M. A. Al-Laham, C. Y. Peng, A. Nanayakkara, M. Challacombe, P. M. W. Gill, B. Johnson, W. Chen, M. W. Wong, J. L. Andres, C. Gonzalez, M. Head-Gordon, E. S. Replogle, J. A. Pople, Gaussian, Inc., Pittsburgh PA, **2002**.
[51] Gaussian 03, Revision D.02, M. J. Frisch, G. W. Trucks, H. B. Schlegel, G. E. Scuseria, M. A. Robb, J. R. Cheeseman, J. A. Montgomery, Jr., T. Vreven, K. N. Kudin, J. C. Burant, J. M. Millam, S. S. Iyengar, J. Tomasi, V. Barone, B. Mennucci, M. Cossi, G. Scalmani, N. Rega, G. A. Petersson, H. Nakatsuji, M. Hada, M. Ehara, K. Toyota, R. Fukuda, J. Hasegawa, M. Ishida, T. Nakajima, Y. Honda, O. Kitao, H. Nakai, M. Klene, X. Li, J. E. Knox, H. P. Hratchian, J. B. Cross, V. Bakken, C. Adamo, J. Jaramillo, R. Gomperts, R. E. Stratmann, O. Yazyev, A. J. Austin, R. Cammi, C. Pomelli, J. W. Ochterski, P. Y. Ayala, K. Morokuma, G. A. Voth, P. Salvador, J. J. Dannenberg, V. G. Zakrzewski, S. Dapprich, A. D. Daniels, M. C. Strain, O. Farkas, D. K. Malick, A. D. Rabuck, K. Raghavachari, J. B. Foresman, J. V. Ortiz, Q. Cui, A. G. Baboul, S. Clifford, J. Cioslowski, B. B. Stefanov, G. Liu, A. Liashenko, P. Piskorz, I. Komaromi, R. L. Martin, D. J. Fox, T. Keith, M. A. Al-Laham, C. Y. Peng, A. Nanayakkara, M. Challacombe, P. M. W. Gill, B. Johnson, W. Chen, M. W. Wong, C. Gonzalez, J. A. Pople Gaussian, Inc., Wallingford CT, **2004**.
[52] M. E. Casida, C. Jamorski, K. C. Casida, D. R. Salahub, *J. Chem. Phys.* **1998**, *108*, 4439.
[53] J. M. Villegas, S. R. Stoyanov, W. Huang, L. L. Lockyear, J. H. Reibenspies, D. P. Rillema, *Inorg. Chem.* **2004**, *43*, 6383–6396.
[54] M. Cossi, G. Scalmani, N. Rega, V. Barone, *J. Chem. Phys.* **2002**, *117*, 43–54.
[55] B. Mennucci, J. Tomasi, *J. Chem. Phys.* **1997**, *106*, 5151–5168.
[56] J. Tomasi, B. Mennucci, E. Cancès, *J. Mol. Struct Theochem* **1999**, *464*, 211–226.
[57] W. Paw, R. Eisenberg, *Inorg. Chem.* **1997**, *36*, 2287–2293.
[58] E. Rose, B. Andrioletti, P. P. Ramasamy, *J. Porphyrins Phthalocyanines* **2002**, *6*, 602–606.
[59] B. P. Sullivan, T. J. Meyer, *Inorg. Chem.* **1978**, *17*, 3334–3341.

Received: February 2, 2007
Published online: July 16, 2007

